

**USE OF TIRE CHIP/SOIL MIXTURES TO LIMIT FROST HEAVE
AND PAVEMENT DAMAGE OF PAVED ROADS**

By

Brian K. Lawrence, Lihue Chen, and Dana N. Humphrey

Prepared For

The New England Transportation Consortium

June 2000

NETCR 12

Project 95-1

Prepared by

University of Maine

Department of Civil and Environmental Engineering

This report was sponsored by the New England Transportation Consortium, a cooperative effort of the Departments of Transportation and the Land Grant Universities of the six New England States, and the US Department of Transportation's Federal Highway Administration.

The contents of this report reflect the views of the authors who are responsible for the facts and the accuracy of the data presented herein. The contents do not necessarily reflect the official views or policies of the Departments of Transportation, and the Land Grant Universities of the six New England States, or the US Department of Transportation's Federal Highway Administration. This report does not constitute a standard, specification, or regulation.

ACKNOWLEDGMENTS

The authors wish to thank the members of the New England Transportation Consortium research advisory panel. Their input and guidance throughout the course of this project is gratefully acknowledged. Dr. Justin Poland from the University of Maine Department of Mechanical Engineering is thanked for his help in designing the thermal conductivity test apparatus. David Trefethen and Ron Brown from the University of Maine Facilities Management are thanked for their help in securing a site for the field trial. Owen J. Folsom Construction, Old Town, Maine is thanked for their help in constructing the field trial. Robert Eaton, Dick Roberts, and Dick Guyer from the U.S. Army Corps of Engineers Cold Regions Research and Engineering Laboratory are thanked for their help in installing the field instrumentation.

Technical Report Documentation Page

1. Report No. NETCR 12		2. Government Accession No. N/A		3. Recipient's Catalog No. N/A	
4. Title and Subtitle Use of Tire Chip/Soil Mixtures to Limit Frost Heave And Pavement Damage of Paved Roads				5. Report Date June 2000	
				6. Performing Organization Code N/A	
7. Author(s) Brian K. Lawrence, Lihue Chen, and Dana N. Humphrey				8. Performing Organization Report No. NETCR 12	
9. Performing Organization Name and Address Dept. of Civil and Environmental Engineering 5711 Boardman Hall University of Maine Orono, ME 04469-5711				10 Work Unit No. (TRAIS) N/A	
				11. Contract or Grant No. N/A	
				13. Type of Report and Period Covered Final	
12. Sponsoring Agency Name and Address New England Transportation Consortium 179 Middle Turnpike University of Connecticut, U-202 Storrs, CT 06269-5202				14. Sponsoring Agency Code NETC 95-1 A Study conducted in cooperation with the U.S. DOT	
				15 Supplementary Notes N/A	
16. Abstract This study consisted of two parts: (1) laboratory measurement of the thermal conductivity and permeability of tire chips and mixtures of tire chips and soil; and (2) constructing a field trial to investigate the use of tire chips to reduce frost penetration and improve drainage beneath paved roads. In the laboratory study, the samples were compressed under surcharges up to 18 kPa. Five types of tire chips, six tire chip/gravel mixtures, and one gravel sample were tested. The apparent thermal conductivity (K) of steel belted tire chips decreased from 0.32 to 0.20 W/m.°C as the density increased. The K of glass belted tire chips was slightly lower. The effect of moisture was small, increasing K by between 0.01 and 0.05 W/m.°C. K increased as the temperature gradient increased. The K of mixtures increased as the gravel content increased. The measured K of tire chips was very close to the value backcalculated from a field trial constructed in Richmond, Maine. The permeability of tire chips ranged from 26.3 cm/s for an uncompressed sample to 6.5 cm/s for a compressed sample. The permeability of mixtures decreased significantly as gravel content increased. The NETC field trial showed that tire chips reduced frost penetration by up to 47% and frost heave was reduced by up to 74%. The values of K measured in the laboratory were slightly higher than those backcalculated from the NETC field trail. Pavement performance measurements showed that 330 mm of soil cover over the tire chip layer would lead to premature cracking but that 483 mm of soil cover could be used with only a small effect on pavement life.					
17. Key Words tires, tire chips, tire shreds, waste tires, frost penetration, drainage, permeability, thermal conductivity, pavement performance			18. Distribution Statement No restrictions. This document is available to the public through the National Technical Information Service, Springfield, Virginia 22161.		
19. Security Classif. (of this report) Unclassified		20. Security Classif. (of this page) Unclassified		21. No. of Pages 331	21. Price N/A

Form DOT F 1700.7 (8-72)

Reproduction of completed page authorized

TABLE OF CONTENTS

ACKNOWLEDGEMENTS	i
TABLE OF CONTENTS	ii
LIST OF TABLES	vii
LIST OF FIGURES.....	ix
1. INTRODUCTION.....	1
1.1 BACKGROUND	1
1.2 OBJECTIVES OF STUDY.....	3
1.3 ORGANIZATION OF REPORT	4
2. LITERATURE REVIEW	7
2.1 INTRODUCTION.....	7
2.2 THERMAL PROPERTIES OF TIRE CHIPS	8
2.2.1 University of Alaska Fairbanks	10
2.2.2 Quebec Thermal Conductivity Measurements	12
2.2.3 Benson, et al. (1996) Thermal Conductivity Measurement	15
2.3 PERMEABILITY OF TIRE CHIPS	16
2.4 CASE HISTORIES	19
2.4.1 Richmond Maine	19
2.4.2 Saint-Joachim Quebec Test Sections	26
2.4.3 Georgia Vermont Road Base.....	29
2.5 PAVEMENT PERFORMANCE.....	34
2.5.1 Quebec Mechanical Properties Model.....	34
2.5.2 North Yarmouth and TWP31-MD Field Trials.....	36
2.6 SUMMARY	51
3. MATERIAL CHARACTERIZATION FOR LABORATORY TESTS.....	53
3.1 MATERIAL SOURCES	53
3.2 GRADATIONS	61
3.3 SPECIFIC GRAVITY	62
4. TESTING METHODOLOGY.....	65
4.1 INTRODUCTION.....	65
4.2 TESTING METHOD	66
4.3 APPARATUS.....	69
4.3.1 Sample container.....	69
4.3.2 Energy source	75
4.3.3 Data acquisition system.....	78

4.4 INTERPRETATION OF RESULTS	80
4.4.1 Calculation of thermal conductivity	80
4.4.2 Precision and bias	81
4.4.3 Summary of error analysis.....	89
5. TEST PROCEDURES	91
5.1 INTRODUCTION	91
5.2 DATA ACQUISITION SYSTEM.....	91
5.2.1 Hardware.....	91
5.2.2 Thermocouples	92
5.2.3 Attachment of thermocouples	92
5.3 THERMOCOUPLE CALIBRATION.....	92
5.4 TEST PROCEDURE	94
5.4.1 Sample preparation	94
5.4.2 Surcharge	96
5.4.3 Testing procedure.....	96
6. THERMAL CONDUCTIVITY TEST RESULTS.....	97
6.1 INTRODUCTION	97
6.2 DATA ANALYSIS	97
6.3 RESULTS.....	103
6.3.1 Gravel.....	106
6.3.2 Tire chips.....	108
6.3.2.1 Influence of density	109
6.3.2.2 Influence of water content.....	113
6.3.2.3 Influence of tire chip sizes	114
6.3.2.4 Influence of glass or steel belt content	114
6.3.2.5 Comparison with results from other laboratory studies	115
6.3.3 Tire chip/gravel mixtures	116
6.3.3.1 Influence of density.....	117
6.3.3.2 Influence of percent gravel in the mixture.....	117
6.3.3.3 Influence of water content.....	123
6.4 INFLUENCE OF TEMPERATURE GRADIENT.....	124
6.5 SUMMARY.....	125
7. COMPARISON WITH RICHMOND FIELD TRIAL	127
7.1 INTRODUCTION	127
7.2 CALCULATION PROCEDURE.....	127
7.3 COMPARISON WITH LABORATORY MEASURED THERMAL CONDUCTIVITY	136
8. LABORATORY PERMEABILITY TESTS.....	139
8.1 INTRODUCTION	139
8.2 APPARATUS	139
8.2.1 Permeameter body	140
8.2.2 Constant head tank	143

8.3 TESTING METHODOLOGY	144
8.4 RESULTS	147
8.5 SUMMARY	154
9. FIELD TRIAL LAYOUT AND CONSTRUCTION	159
9.1 INTRODUCTION	159
9.2 DESIGN	160
9.3 LAYOUT	164
9.4 MATERIALS	173
9.5 CONSTRUCTION	175
9.5.1 Excavation	175
9.5.2 Placement of Tire Chips and Tire Chip/Soil Mixtures.....	179
9.5.2.1 Filling Trench	180
9.5.2.2 Filling Roadbed	182
9.5.3 Placement of Subbase Course.....	183
9.5.4 Bituminous Pavement.....	187
9.6 INSTRUMENTATION & MONITORING.....	188
9.6.1 Settlement Plates.....	188
9.6.2 Thermocouples.....	191
9.6.3 Datalogger	194
9.6.4 Frost Free Benchmarks.....	195
9.6.5 Piezometers.....	195
9.7 SUMMARY	196
10. FROST PENETRATION	201
10.1 INTRODUCTION	201
10.2 FROST DEPTH.....	201
10.2.1	205
10.2.1 Frost Depth Versus Date.....	205
10.2.2 Maximum Depth of Frost Penetration.....	209
10.2.3 Temperature Profiles	211
10.3 FROST HEAVE	215
10.3.1 Comparison of Heave Between Sections.....	218
10.3.2 Frost Penetration into Subgrade and Frost Heave	220
10.4 BACKCALCULATION OF THERMAL CONDUCTIVITY	221
10.4.1 Volumetric Heat Capacity of Tire Chips and Tire Chip/Soil Mixtures	221
10.4.2 Backcalculation Methods.....	222
10.4.3 Comparison of Laboratory and Field Thermal Conductivities.....	227
10.4.4 Comparison with Richmond Field Trial.....	230
10.5 SUMMARY	231
11. PAVEMENT PERFORMANCE.....	235
11.1 INTRODUCTION	235
11.2 MEASUREMENT METHODS	235
11.2.1 Modified Benkelman Beam.....	235
11.2.2 Heavy Weight Deflectometer (HWD).....	236

11.3.2 Model of Pavement Deflections with KENLAYER	271
11.3.3 Layer Moduli	275
11.3.4 Pavement Strains.....	275
11.4 HWD TESTS	281
11.4.1 Results.....	281
11.4.2 Backcalculation of Young's Modulus	282
11.4.3 Comparison with Typical Values of Moduli	285
11.4.4 Comparison with KENLAYER Moduli.....	286
11.5 SUMMARY	287
12. SUMMARY, CONCLUSIONS, AND RECOMMENDATIONS.....	291
12.1 SUMMARY.....	291
12.2 CONCLUSIONS.....	302
12.3 DESIGN RECOMMENDATIONS	306
12.4 RECOMMENDATIONS FOR FURTHER RESEARCH.....	307
13. REFERENCES	309
APPENDIX A - FWD AND HWD TEST RESULTS.....	315

LIST OF TABLES

Table 2.1 Thermal properties of selected materials	9
Table 2.2 Description of test materials (after Shao, et al., 1995).....	11
Table 2.3 Thermal conductivities for rubber buffings (after Shao, et al., 1995)	11
Table 2.4 Thermal conductivities for granulated rubber (after Shao, et al., 1995).....	11
Table 2.5 Thermal conductivities for rubber chips (after Shao, et al., 1995).....	12
Table 2.6 Thermal conductivities for mixed materials (after Shao, et al., 1995).....	12
Table 2.7. Summary of reported permeabilities of tire chips.....	17
Table 2.8. Permeabilities of mixtures of tire chips and soil (after Ahmed, 1993).....	17
Table 2.9 Summary of test section configuration (after Humphrey and Eaton, 1995).....	21
Table 2.10 Deflections from FWD tests and structural numbers on TH 4, Georgia, Vermont (after Frascoia and Cauley, 1995).....	35
Table 2.11 Test section configuration for North Yarmouth test sections (after Nickels, 1995)	38
Table 2.12 Test section configuration for TWP31-MD test sections (after Nickels, 1995)	41
Table 2.13 Pavement deflections directly under wheel load in North Yarmouth (after Nickels, 1995)	46
Table 2.14 Pavement deflections directly under wheel load in TWP31-MD (after Nickels, 1995)	47
Table 2.15 Maximum tensile strains for North Yarmouth and TWP31-MD (after Nickels, 1995)	48
Table 3.1 Summary of apparent specific gravity of tire chips	64
Table 3.2 Specific gravity of tire chip/gravel mixtures	64
Table 6.1 Summary of test results for air dried samples	105
Table 6.2 Summary of test results for moist samples	106
Table 6.3 Temperature gradient influence - Pine State tire chips under full surcharge ...	124
Table 7.1 Estimated $K_{\text{tire-chips}}$	131
Table 7.2 Frost penetration depth in Richmond, Maine, project.....	135
Table 7.3 Summary of field and laboratory condition.....	137
Table 8.1 Summary of permeability results.....	148
Table 9.1 Laboratory index properties of cohesive subgrade material	163
Table 9.2 Summary of test section configuration.....	166
Table 9.3 Thickness of tire chip and tire chip/soil layers from settlement plate data.....	184
Table 9.4 Results of field density tests.....	186
Table 9.5 Results of stability and flow tests.....	188
Table 9.6 Groundwater elevations.....	196
Table 10.1 Summary of frost depths by section	211
Table 10.2 Temperature gradients of tire chip and tire chip/soil layers	214
Table 10.3 Values of c_m and c_v for tire chips and tire chip/soil mixtures	222
Table 10.4 Estimated $K_{\text{tc/soil}}$	224
Table 10.5 Input parameters for modified Berggren equation	226

Table 10.7 Comparison of field and laboratory thermal conductivities	229
Table 11.1 Centerline pavement deflections, April 1997.	250
Table 11.2 Gravel base temperature on Benkelman Beam test dates	251
Table 11.3 Centerline pavement deflections, August 1997.	258
Table 11.4 Radius of deflection basins	268
Table 11.5 KENLAYER input parameters	272
Table 11.6 Moduli calculated from KENLAYER	276
Table 11.7 Computation of strain at base of pavement in KENLAYER.....	276
Table 11.8 Failure criterion ratios from normalized strains in tire chip and tire chip/soil mixture sections	278
Table 11.9 Input parameters for MODCOMP4	282
Table 11.10 Backcalculated resilient moduli from MODCOMP4 for November test ...	283
Table 11.11 Backcalculated resilient moduli from MODCOMP4 for April test.....	284
Table 11.12 Typical values of Young's Modulus.....	285
Table 12.1 Tire chip properties recommended for design	306

LIST OF FIGURES

Figure 2.1 Results of thermal conductivity tests (after Dore, et al., 1995).....	13
Figure 2.2 Pavement structures used in model study (after Dore, et al., 1995).....	14
Figure 2.3 Calculated frost penetration (after Dore, et al., 1995).....	14
Figure 2.4 Calculated maximum heave (after Dore, et al., 1995).....	15
Figure 2.5 Hydraulic conductivities of mixtures of tire chips and clean sand (after Edil and Bosscher, 1992) (1 cm/s = 1.035x10 ⁶ ft/yr).....	18
Figure 2.6 Plan view of test site (after Humphrey and Eaton, 1995).....	21
Figure 2.7 Typical cross section (after Humphrey and Eaton, 1995).....	21
Figure 2.8 Location of instrumentation (after Humphrey and Eaton, 1995).....	23
Figure 2.9 Cross section showing thermocouple and resistivity gages (after Humphrey and Eaton, 1995).....	23
Figure 2.10 Maximum depth of frost penetration (after Humphrey and Eaton, 1995).....	24
Figure 2.11 Depth of frost penetration versus date (after Humphrey and Eaton, 1995).....	25
Figure 2.12 Temperature profile on February 16, 1994 (after Humphrey and Eaton, 1995).....	27
Figure 2.13 Frost heave (after Humphrey and Eaton, 1995).....	28
Figure 2.14 Profile of Saint-Joachim, Quebec test sections (after Rioux, 1994).....	30
Figure 2.15 Plan of Saint-Joachim, Quebec test sections (after Rioux, 1994).....	31
Figure 2.16 Cross sections of Saint-Joachim, Quebec test sections (after Rioux, 1994).....	31
Figure 2.17 Gradation of natural soil, sand, and gravel in Saint-Joachim, Quebec test sections (after Rioux, 1994).....	32
Figure 2.18 Frost penetration vs. time in Saint-Joachim, Quebec test sections (after Rioux, 1994).....	33
Figure 2.19 Total frost depth through January 26, 1994 for the Saint-Joachim test sections (after Rioux, 1994).....	33
Figure 2.20 Typical section of TH4, Georgia, Vermont: initial construction (after Frascoia and Cauley, 1995).....	35
Figure 2.21 Calculated deflection at surface of pavement (after Dore, et al., 1995).....	37
Figure 2.22 Calculated horizontal strain at base of layer (after Dore, et al., 1995).....	37
Figure 2.23 North Yarmouth longitudinal layout (after Nickels, 1995).....	39
Figure 2.24 North Yarmouth longitudinal layout (after Nickels, 1995).....	40
Figure 2.25 TWP31-MD longitudinal layout (after Nickels, 1995).....	42
Figure 2.26 TWP31-MD typical cross section (after Nickels, 1995).....	43
Figure 2.27 Maximum deflection basins from each section in North Yarmouth (after Nickels, 1995).....	44
Figure 2.28 Maximum deflection basins from each section in TWP31-MD (after Nickels, 1995).....	45
Figure 2.29 Normalized pavement deflection data for North Yarmouth and TWP31- MD (after Nickels, 1995).....	49

Figure 2.30 Normalized maximum asphalt tensile strains for North Yarmouth and TWP31-MD (after Nickels, 1995).....	50
Figure 3.1 Photograph of F&B glass belted tire chips	54
Figure 3.2 Photograph of F&B steel belted tire chips.....	54
Figure 3.3 Photograph of Palmer tire chips.....	55
Figure 3.4 Photograph of Pine State tire chips.....	55
Figure 3.5 Photograph of Sawyer tire chips.....	56
Figure 3.6 Photograph of gravel.....	57
Figure 3.7 Photograph of 67% Palmer/33% gravel.....	58
Figure 3.8 Photograph of 67% F&B steel belted/33% gravel.....	59
Figure 3.9 Photograph of 67% F&B glass belted/33% gravel.....	59
Figure 3.10 Photograph of 33% Palmer/67% gravel.....	60
Figure 3.11 Photograph of 33% F&B steel belted/67% gravel.....	60
Figure 3.12 Photograph of 33% F&B glass-belted/67% gravel.....	61
Figure 3.13 Gradation of tire chip samples.....	62
Figure 3.14 Gradation of gravel samples.....	63
Figure 4.1 Principal of operation of test apparatus.....	66
Figure 4.2 Comparison of one-sided mode and double-sided mode apparatus.....	68
Figure 4.3 Cross-section of the one-sided mode insulated-hot plate apparatus.....	70
Figure 4.4 Plan view of the apparatus.....	70
Figure 4.5 Picture showing side view of the apparatus.....	71
Figure 4.6 Picture showing the light bulbs of Heater #1.....	71
Figure 4.7 Picture of the apparatus under full surcharge.....	72
Figure 4.8 Illustration of guarded hot plate apparatus (after ASTM C177, 1992).....	75
Figure 4.9 Diagram of a heater.....	76
Figure 4.10 Picture of a heater.....	77
Figure 4.11 Energy source and measurement.....	77
Figure 4.12 Picture of the power supplies and multimeters used in the test.....	78
Figure 6.1 Spreadsheet Example: Palmer tire chips under half surcharge.....	98
Figure 6.2 K-value versus time.....	101
Figure 6.3 T ₃₋₄ versus time.....	102
Figure 6.4 T ₁₋₂ versus K-value.....	104
Figure 6.5 Gravel: apparent thermal conductivity versus density.....	107
Figure 6.6 Average apparent thermal conductivity for sand and gravel: unfrozen (after Andersland and Ladanyi, 1994).....	108
Figure 6.7 F&B glass belted tire chips: apparent thermal conductivity versus density....	110
Figure 6.8 F&B steel belted tire chips: apparent thermal conductivity versus density....	110
Figure 6.9 Palmer tire chips: apparent thermal conductivity versus density.....	111
Figure 6.10 Pine State tire chips: apparent thermal conductivity versus density.....	111
Figure 6.11 Sawyer tire chips: apparent thermal conductivity versus density.....	112
Figure 6.12 Apparent thermal conductivity versus density for tire chips.....	113
Figure 6.13 33% F&B glass belted/67% gravel mixture: apparent thermal conductivity versus density.....	118
Figure 6.14 67% F&B glass belted/33% gravel mixture: apparent thermal conductivity versus density.....	118

Figure 6.15 33% F&B steel belted/67% gravel mixture: apparent thermal conductivity versus density	119
Figure 6.16 67% F&B steel belted/33% gravel mixture: apparent thermal conductivity versus density	119
Figure 6.17 33% Palmer/67% gravel mixture: apparent thermal conductivity versus density.....	120
Figure 6.18 67% Palmer/33% gravel mixture: apparent thermal conductivity versus density.....	120
Figure 6.19 Comparison: apparent thermal conductivity versus density for air samples (no surcharge)	121
Figure 6.20 Comparison: apparent thermal conductivity versus density for air dried samples (9 kPa surcharge)	121
Figure 6.21 Comparison: apparent thermal conductivity versus density for air dried samples (18 kPa surcharge)	122
Figure 6.22 Comparison: apparent thermal conductivity versus density for air dried samples	122
Figure 6.23 Comparison: apparent thermal conductivity versus void ratio for air dried samples	123
Figure 6.24 Apparent thermal conductivity versus temperature gradient.....	125
Figure 7.1 Temperature vs. depth.....	129
Figure 7.2 Apparent thermal conductivity versus surcharge for air dried Pine State tire chips at a temperature gradient of about 42.8°C/m (23.5°F/ft)	136
Figure 8.1 Photograph of permeameter and constant head tank	140
Figure 8.2 Permeameter and constant head tank detail.....	141
Figure 8.3 Permeability versus percent gravel subbase aggregate.....	150
Figure 8.4 Permeability versus percent compression for 33% tire chips	151
Figure 8.5 Permeability versus percent compression for 67% tire chips	152
Figure 8.6 Permeability versus percent compression for tire chips.....	153
Figure 8.7 Permeability versus void ratio for 33% tire chips	155
Figure 8.8 Permeability versus void ratio for 67% tire chips	156
Figure 8.9 Permeability versus void ratio for tire chips	157
Figure 9.1 Plan view of full scale field trial.....	161
Figure 9.2 Boring logs next to trial road.....	162
Figure 9.3 Gradation curves of cohesive soil from borings, subgrade samples, and auger holes made for thermocouple installation.....	164
Figure 9.4 Longitudinal cross-section along centerline of road	165
Figure 9.5 Cross section of Section 1	167
Figure 9.6 Cross section of Section 2.....	168
Figure 9.7 Cross section of Section 3	169
Figure 9.8 Cross section of Section 4.....	170
Figure 9.9 Cross section of Section 5.....	171
Figure 9.10 Cross section of Control.....	172
Figure 9.11 Gradation curves of tire chips.....	174
Figure 9.12 Gradation curves of tire chip/soil mixtures.....	174
Figure 9.13 Gradation curves of MDOT subbase obtained from outside contractor	176

Figure 9.14 Gradation curves of MDOT Type D subbase aggregate available from previous NETC project (after Tweedie, et al., 1998)	176
Figure 9.15 Photograph of excavation of roadbed with hydraulic excavator	177
Figure 9.16 Photograph of excavation of trench with Case 580	178
Figure 9.17 Photograph of trench compaction with tractor and concrete block	181
Figure 9.18 Photograph of trench compaction with walk-behind compactor	181
Figure 9.19 Photograph of tire chips being spread over geotextile	182
Figure 9.20 Photograph of compaction of MDOT Type D subbase with vibratory roller	185
Figure 9.21 Settlement plate detail	189
Figure 9.22 Photograph of settlement plate before placement in roadbed	190
Figure 9.23 Photograph of thermocouple-dowel setup	192
Figure 9.24 Thermocouple pair positions beneath test sections	193
Figure 9.25 Plan location of piezometers and typical cross section	197
Figure 10.1 Cumulative freezing degree-days versus date	203
Figure 10.2 Average daily temperature versus date	204
Figure 10.3 Depth of frost penetration vs. date, Sections 1 through 3	206
Figure 10.4 Depth of frost penetration vs. date, Section 4	207
Figure 10.5 Depth of frost penetration vs. date, Section 5	208
Figure 10.6 Maximum depth of frost penetration	210
Figure 10.7 Temperature profiles on February 14, 1997	212
Figure 10.8 Average frost heave in individual wheel paths	217
Figure 10.9 Average frost heave vs. percent tire chips, Sections 1, 2, and 3	219
Figure 10.10 Average heave vs. frost penetration into subgrade	220
Figure 10.11 Thermal conductivity vs. percent tire chips	224
Figure 10.12 Laboratory thermal conductivity versus surcharge for moist tire chips and tire chip/soil mixtures	228
Figure 11.1 Modified Benkelman Beam used for pavement deflection measurements (after Nickels, 1995)	237
Figure 11.2 Plan view of test locations for Modified Benkelman Beam and HWD tests	238
Figure 11.3 Plan location of MBB probe between dual truck tires (after Nickels, 1995)	239
Figure 11.4 Photograph of MBB and dump truck on the test road	239
Figure 11.5 Photograph of Heavy Weight Deflectometer (HWD)	241
Figure 11.6 April pavement deflection basins for Section 1 with 483 mm (19 in.) of soil cover and 305 mm (12 in.) of 33% tire chip/67% soil	243
Figure 11.7 April pavement deflection basins for Section 2 with 483 mm (19 in.) of soil cover and 305 mm (12 in.) of 67% tire chip/33% soil	244
Figure 11.8 April pavement deflection basins for Section 3 with 483 mm (19 in.) of soil cover and 305 mm (12 in.) of tire chips	245
Figure 11.9 April pavement deflection basins for Section 4 with 483 mm (19 in.) of soil cover and 152 mm (6 in.) of tire chips	246
Figure 11.10 April pavement deflection basins for Section 5 with 330 mm (13 in.) of soil cover and 305 mm (12 in.) of tire chips	247

Figure 11.11	April pavement deflection basins for the Control Section with 635-mm (25-in.) thick aggregate subbase course	248
Figure 11.12	Average April pavement deflection basins for all sections	249
Figure 11.13	August pavement deflection basins for Section 1 with 483 mm (19 in.) of soil cover and 305 mm (12 in.) of 33% tire chip/67% soil	252
Figure 11.14	August pavement deflection basins for Section 2 with 483 mm (19 in.) of soil cover and 305 mm (12 in.) of 67% tire chip/33% soil	253
Figure 11.15	August pavement deflection basins for Section 3 with 483 mm (19 in.) of soil cover and 305 mm (12 in.) of tire chips	254
Figure 11.16	August pavement deflection basins for Section 4 with 483 mm (19 in.) of soil cover and 152 mm (6 in.) of tire chips	255
Figure 11.17	August pavement deflection basins for Section 5 with 330 mm (13 in.) of soil cover and 305 mm (12 in.) of tire chips	256
Figure 11.18	August pavement deflection basins for the Control Section with 635-mm (25-in.) thick aggregate subbase course.....	257
Figure 11.19	Average August pavement deflection basins for all sections.....	259
Figure 11.20	Comparison of measured April & August MBB deflection basins with deflection basins calculated by KENLAYER for Section 1.....	260
Figure 11.21	Comparison of measured April & August MBB deflection basins with deflection basins calculated by KENLAYER for Section 2.....	261
Figure 11.22	Comparison of measured April & August MBB deflection basins with deflection basins calculated by KENLAYER for Section 3.....	262
Figure 11.23	Comparison of measured April & August MBB deflection basins with deflection basins calculated by KENLAYER for Section 4.....	263
Figure 11.24	Comparison of measured April & August MBB deflection basins with deflection basins calculated by KENLAYER for Section 5.....	264
Figure 11.25	Comparison of measured April & August MBB deflection basins with deflection basins calculated by KENLAYER for the Control Section	265
Figure 11.26	Average centerline deflections vs. percent tire chips, April and August, 1997.....	267
Figure 11.27	Centerline deflection versus distance from edge drain, April 1997.....	269
Figure 11.28	Centerline deflection versus distance from edge drain, August 1997	270
Figure 11.29	Resilient modulus-deviator stress relationship for four types of subgrade (after Thompson and Elliot, 1985).....	273

1. INTRODUCTION

1.1 BACKGROUND

There are an estimated 850 million scrap tires stockpiled throughout the United States and an additional 253 million are discarded annually (Associated Press, 1996). Stockpiles of scrap tires are of major concern for two reasons: fire hazard and water-borne diseases. When large open tire piles burn, they release potentially harmful products of incomplete combustion (PICs) into the atmosphere and ground (Ryan, 1990). The introduction and spread of several mosquito species has been directly attributed to the presence of scrap tires. Cases of encephalitis have been traced to insects originating in scrap tire piles (Maine DEP, 1989). Landfilling of tires seems to avoid these two problems, but improperly buried tires can rise to the surface and disrupt the landfill cover.

In 1993 the EPA reported that of the approximately 242 million tires that were discarded annually, approximately 10 million were reused, 17 million were recycled, 27 million were used for energy, and 189 million were stockpiled, landfilled, or illegally dumped (EPA, 1993). Although the number of tires generated per year has increased since 1993, significantly fewer tires are being landfilled and more are being reused or recovered. By 1996 the annual replacement of tires had increased to 253 million and 95 percent of these were returned to tire retailers at the end of their useful life (Zimmer, 1996). Approximately 72 percent of these were recovered through various markets. Of these, approximately 136 million were used in energy recovery (cement kilns, paper/pulp mills, electricity generation), 15 million for civil engineering, and 14 million were exported for further use or retreading. Other uses are agriculture, products made from

crumb rubber, products made from stamped or cut pieces of tire, and other miscellaneous applications, which totaled 17.8 million tires. Only 70 million tires were landfilled.

The civil engineering applications for whole tires or tires shredded into tire chips include: artificial reefs, breakwaters, lightweight embankment fill, retaining wall backfill, landfill cell daily cover, septic system leach fields, and landfill leachate collection systems (Zimmer, 1996). The first use of tire chips in roadway construction was in Minnesota in the late 1980's (Geisler et al., 1989). Here the tire chips were used over compressible soils, such as peat, to reduce settlement in roadways. Tire chips have also been used as lightweight and conventional embankment fill beneath paved roads (Manion and Humphrey, 1992; Nickels and Humphrey, 1997). Research has been done to find the necessary amount of soil cover over tire chips to limit pavement deflections to acceptable levels (Nickels and Humphrey, 1997; Humphrey and Nickels, 1994). Tire chips were used in a highway embankment for the exit serving the Portland International Jetport on the Maine Turnpike (Scrap Tire News, 1997). Here tire chips were used as lightweight fill over a weak, compressible stratum.

Tire chips can be used as retaining wall backfill because the unit weight of tire chips is one-half to one-third the unit weight of conventional granular fill (Manion and Humphrey, 1992; Tweedie, et al., 1998). This reduces horizontal pressure on the wall. Tire chips have been used as a lightweight fill for a bridge abutment and as a compressible inclusion against the abutment walls of a rigid frame bridge (Whetten, et al., 1997; Cosgrove, 1998).

Tire chips show considerable promise as a subgrade insulation. The maximum depth of frost penetration in New England ranges from 1.27 to 2.54 m (50 to 100 in.) (U.S. Department of Commerce Weather Bureau Data). Tire chips have already been used successfully as subgrade insulation on a gravel surfaced road in Richmond, Maine (Humphrey and Eaton, 1993a, 1993b; Humphrey and Eaton, 1994; Humphrey and Nickels, 1994; Humphrey and Eaton, 1995). In addition, the high permeability of tire chips have enabled the Vermont Agency of Transportation to use them as a drainage layer for a gravel surfaced local road (Frascoia and Cauley, 1995). This significantly improved the drivability of the road during the spring melt.

This research (NETC Project 95-1) investigated the use of tire chips and tire chip/soil mixtures as subgrade insulation on secondary paved roads. Insulating properties of tire chips can reduce frost heave induced damage to paved roads. The free draining properties of tire chips can strengthen the subgrade and subbase during the spring thaw by allowing excess water to drain. The use of tire chips would also remove large quantities of whole tires from stockpiles.

1.2 OBJECTIVES OF STUDY

The purpose of this research was to continue the investigation started by Humphrey and Eaton (1995) on the use of tire chips as subgrade insulation materials in roadways. This study consisted of two phases: a laboratory investigation and a full scale field trial. The focus of the laboratory investigation was to determine the thermal conductivity and permeability of tire chips and tire chip/soil mixtures in the laboratory. The major goals of the laboratory phase were to determine: (1) the relationship between the thermal

conductivity of tire chips and their density and/or void ratio; (2) the influence of tire chips size, glass fabric or steel belt content on the thermal conductivity; and (3) the effect of soil content on the thermal conductivity of tire chip/soil mixtures.

The purpose of the field trial was to determine the feasibility of using tire chips and tire chip/soil mixtures as a subgrade insulation and drainage layer without adversely affecting the life of the pavement. The objectives of the field trial can be broken down into two parts. The first was to investigate the insulating qualities and drainage of tire chip and tire chip/soil mixtures placed directly above the subgrade. This included determining the field thermal conductivity of tire chips and tire chip/soil mixtures and comparing the results to the laboratory values and values determined from the Richmond Field Trial.

A second major goal of the field trial was to find a combination of parameters that would allow tire chips and/or tire chip/soil mixtures to be used for insulation without compromising pavement life. This included using less soil cover over the tire chips than previous investigations to better understand minimum cover requirements for tire chips in the subbase.

1.3 ORGANIZATION OF REPORT

This report contains twelve chapters and one appendix, organized as follows.

Chapter 2 is a literature review of laboratory testing of the thermal conductivity of tire chips and case histories of tire chips used as subgrade insulation. Available

information on the permeability of tire chips is also presented. There is also a brief discussion of cover requirements for tire chips to minimize pavement strains.

The properties of tire chips and soil used in this study are discussed in Chapter 3. This includes gradation, specific gravity and compacted unit weight.

In Chapter 4 a large-scale thermal conductivity measurement apparatus that was designed and constructed for this project is discussed in detail. The procedures used to conduct the thermal conductivity tests are presented in Chapter 5.

The results of the thermal conductivity tests are presented in Chapter 6. In Chapter 7, the laboratory measured values of thermal conductivity are compared with the results of a field trial in Richmond, Maine.

Chapter 8 presents the testing procedures and results for laboratory permeability tests on tire chips and tire chip/soil mixtures.

Chapter 9 describes the construction of the University of Maine field trial. It includes information on material properties, construction procedures, instrumentation, and settlement of tire chip and tire chip/soil layers.

Chapter 10 gives the results of frost penetration monitoring and frost heave for one winter. It also compares the results from this research to previous laboratory tests and results from the field trial in Richmond, Maine.

Chapter 11 gives the results of Benkelman Beam, Heavy Weight Deflectometer, and Falling Weight Deflectometer tests. A program named KENLAYER is used to model

pavement deflections and estimate tensile strains in the pavement. HWD data is used in MODCOMP4, a modulus backcalculation program, to calculate Young's Modulus for tire chip and tire chip/soil mixtures.

Chapter 12 summarizes the findings of this research and gives conclusions and recommendations for further research.

An appendix presents detailed results of Heavy Weight Deflectometer and Falling Weight Deflectometer tests conducted at the field trial.

2. LITERATURE REVIEW

2.1 INTRODUCTION

This chapter discusses the literature on the use of tire chips as drainage and insulation. There are few instances in the literature documenting the use of tire chips as subgrade insulation or drainage, however there are several studies documenting use of tire shreds in road construction and the engineering properties of tire shreds.

The first recorded use of tire chips as road fill was in Minnesota in 1986 (Geisler, et al., 1989) to improve a forest road. Several applications were tested, ranging from a single layer of whole tires tied into a mat to 0.9 m (3 ft) of tire chip fill. There have been several subsequent studies on the use of tire chips as fill (Eldin and Senouci, 1992; Humphrey and Sandford, 1993; Gharegrat, 1993; Humphrey, 1996; Humphrey and Nickels, 1997). The use of tire chips as retaining wall backfill has also been investigated (Humphrey et al., 1992, 1993; Tweedie, et al., 1998; Humphrey, et al., 1997).

Two studies on the basic engineering properties of tire chips were published in 1992 by the University of Maine (Manion and Humphrey, 1992; Humphrey et al., 1992). The following tire chip properties were investigated: gradation, specific gravity, compacted unit weight, compressibility, shear strength, and permeability. Compressibility tests showed that the moduli ranged from 0.8 to 1.2 MPa (112 to 181 psi) for tire chips compared to 10 to 172 MPa (1,500 to 25,000 psi) for soil (Humphrey, et al., 1992). Other studies on tire chips include: Bressette, (1984); Edil and Bosscher, 1992; Ahmed, 1993; Ahmed and Lovell, 1993; Edil and Bosscher, 1994; Cosgrove, 1995; Benda, 1995).

2.2 THERMAL PROPERTIES OF TIRE CHIPS

Tires are made from a mixture of vulcanized natural rubber and synthetic styrene and butadiene with embedded steel wire or glass fibers. The steel content in new steel belted radial passenger car tires is 9.8% to 12.5% by weight (Personal communication, Bill Jones, Cooper Tire Co., 1996). This percentage would be somewhat higher for discarded tires because some rubber was worn away during use, reducing the total weight of the tires. Tire chips that are available for use in civil engineering applications are generally made from steel belted tires and have steel belts protruding from the cut edges of the tire chips. Rubber is the major content in tires so the thermal properties of tire chips will largely depend on the properties of rubber. There is also air and moisture in the voids between tire chips, as well as the steel wire or glass fibers embedding in tire chips, thus the thermal properties of tire chips will also depend on the thermal properties of air, water, steel, and glass fibers.

The thermal conductivity of some common materials are listed in Table 2.1. The thermal conductivity of hard rubber is listed as $0.161 \text{ W/m}^{\circ}\text{C}$ ($0.093 \text{ Btu/hr}^{\circ}\text{Fft}$) (Brownell, 1989) and that of steel is $43 \text{ W/m}^{\circ}\text{C}$ ($25 \text{ Btu/hr}^{\circ}\text{Fft}$). This data will be helpful in understanding the factors that affect the thermal conductivity of tire chips and in judging the thermal conductivity of tire chips relative to other materials.

The thermal conductivity of tire chips have been measured in three laboratory studies (Shao, et al., 1994; Dore, et al., 1995; Benson, et al., 1996). The results of these studies are summarized in the following sections.

Table 2.1 Thermal properties of selected materials.

Material	Density	Heat Capacity	Thermal Conductivity	
	(kg/m ³)	(kJ/kg·°C)	(W/m·C)	(Btu/hr·ft·°F)
Air (10°C)	1.25	1.00	0.026	0.015
Polystyrene foam	30	1.25	0.036	0.021
Glass wool	64	0.84	0.042	0.024
Snow, loose	85	2.09	0.08	0.046
Snow, compacted	500	2.09	0.7	0.41
Ice (-40°C)	900	2.09	2.66	1.54
Ice (0°C)	900	2.09	2.21	1.28
Water (0°C)	999.87	4.2177	0.56	0.32
Water (10°C)	999.73	4.1922	0.58	0.33
Peat, dry	250	2.09	0.07	0.04
Clay, dry	1700	0.92	0.9	0.52
Sand, dry	2000	0.80	1.1	0.64
Wood				
plywood, dry	600		0.17	0.098
fir or pine, dry	500		0.12	0.069
Concrete	2500	0.67	1.7	0.98
Concrete, asphalt	2150		1.28	0.74
Rock, typical	2500	0.84	2.2	1.27
Quartz	2660	0.733	8.4	4.86
Granite			1.7-4.0	0.98-2.32
Shale			1.5	0.87
Steel	7500	0.50	43	24.9
Iron, ductile	7500		50	28.9
Copper	2800	0.42	375	217
^a Rubber (hard)	1200		0.161	0.093

After Andersland and Ladanyi (1994) unless otherwise noted. Values are representative; most materials have some variation with density and temperature.

^aValue is after Brownell (1989).

2.2.1 University of Alaska Fairbanks

The University of Alaska Fairbanks performed laboratory thermal conductivity tests on rubber buffings, granulated rubber, and rubber chips (Shao, et al., 1995). Almost all of the steel belts had been removed from rubber buffings and granulated rubber, and many steel belts were removed from the rubber chips. The materials tested are described in Table 2.2. Two types of thermal conductivity apparatuses were used. The samples were tested wetted and non-wetted in both frozen and unfrozen states. The frozen samples were tested in a two-sided mode guarded-hot-plate apparatus Dynatech Model TCFGM. The inner diameter of this apparatus was 200 mm (7.875 in.) and the sample thickness was 44 mm (1.73 in.). The two cold plates were set to -6°C (21°F) and the hot plate was set to approximately -4°C (24°F). The test apparatus used for thawed samples was an Anacon Model 88, a one-sided mode guarded-hot-plate apparatus. The inner diameter of this apparatus was 168 mm (6.625 in.) and the thickness was 45 mm (1.77 in.). The hot plate temperature was about 38°C (100°F), and the cold plate temperature was about 10°C (50°F).

Results of these tests are listed in Tables 2.3 through 2.6. The measured thermal conductivities for both frozen and unfrozen samples increased only slightly as water content increased and as density increased. Frozen samples also had higher conductivities than unfrozen samples. Densities are reported in relation to low, medium, and high compaction, but actual densities were not recorded.

Table 2.2 Description of test materials (after Shao, et al., 1995)

	Rubber Buffing	Granulated Rubber	Rubber Chip
Particle Sizes	80% passing #10 sieve	99% passing 1/4" sieve	80% passing 1" sieve
Processing Method	Re-Tread Buffing Machine	Granulator	Shredder

Table 2.3 Thermal conductivities for rubber buffings (after Shao, et al., 1995)

		moisture content	low compaction		high compaction	
			Btu/hr-ft. ^{°F}	W/m. ^{°C}	Btu/hr-ft. ^{°F}	W/m. ^{°C}
thawed samples	un-wetted	<1%	0.0563	0.0973	0.059	0.1020
	wetted	4-5%	0.0594	0.1026	0.0602	0.1040
frozen samples	un-wetted	<1%	0.0757	0.1308	0.0778	0.1344
	wetted	4-5%	0.0779	0.1346	0.0798	0.1379

Table 2.4 Thermal conductivities for granulated rubber (after Shao, et al., 1995)

	moisture content	low compaction		medium compaction		high compaction	
		Btu/hr-ft. ^{°F}	W/m. ^{°C}	Btu/hr-ft. ^{°F}	W/m. ^{°C}	Btu/hr-ft. ^{°F}	W/m. ^{°C}
thawed samples	<1%	0.0587	0.1014	0.0602	0.1040	0.0613	0.1059
	3%	0.0612	0.1058	0.0637	0.1101	0.0658	0.1137
frozen samples	<1%	0.0794	0.1372	0.0883	0.1526	0.0903	0.1560
	3%	0.0799	0.1381	0.0935	0.1616	0.0957	0.1654

Table 2.5 Thermal conductivities for rubber chips (after Shao, et al., 1995)

		moisture	low compaction		high compaction	
		content	Btu/hr-ft. [°] F	W/m. [°] C	Btu/hr-ft. [°] F	W/m. [°] C
thawed samples	un-wetted	2%	0.071	0.1227	0.0716	0.1237
	wetted	5%	0.0863	0.1491	0.095	0.1642
frozen samples	un-wetted	2%	0.0799	0.1381	0.0821	0.1419
	wetted	5%	0.0942	0.1628	0.0988	0.1707

Table 2.6 Thermal conductivities for mixed materials (after Shao, et al., 1995)

	50% granulated rubber / 50% rubber chip		50% granulated rubber / 50% rubber buffing		50% rubber chip / 50% rubber buffing	
	Btu/hr-ft. [°] F	W/m. [°] C	Btu/hr-ft. [°] F	W/m. [°] C	Btu/hr-ft. [°] F	W/m. [°] C
thawed samples	0.0648	0.1120	0.0602	0.1040	0.0658	0.1137
frozen samples	0.0806	0.1393	0.0771	0.1332	0.0785	0.1356

* The sample moisture content for the mixture was not reported.

2.2.2 Quebec Thermal Conductivity Measurements

Laboratory thermal conductivity tests were performed on a variety of alternative insulation materials by Dore, et al. (1995) including: tire chips (size range of 20 to 40 mm; 0.79 to 1.57 in.) with no removal of steel or polyester belts; and ground tire (size range of 1 to 4 mm; 0.039 to 0.15 in.). The measured values of K from these tests are shown in Figure 2.1. The measured thermal conductivity of dry tire chips was 0.38 W/m.[°]C (0.22 Btu/hr-ft.[°]F) and a dry 50% tire chip/50% ground tire mixture was 0.34 W/m.[°]C (0.22 Btu/hr-ft.[°]F). Dry and saturated unfrozen samples of ground tire had a thermal conductivity of about 0.31 W/m.[°]C (0.18 Btu/hr-ft.[°]F). These values are more than

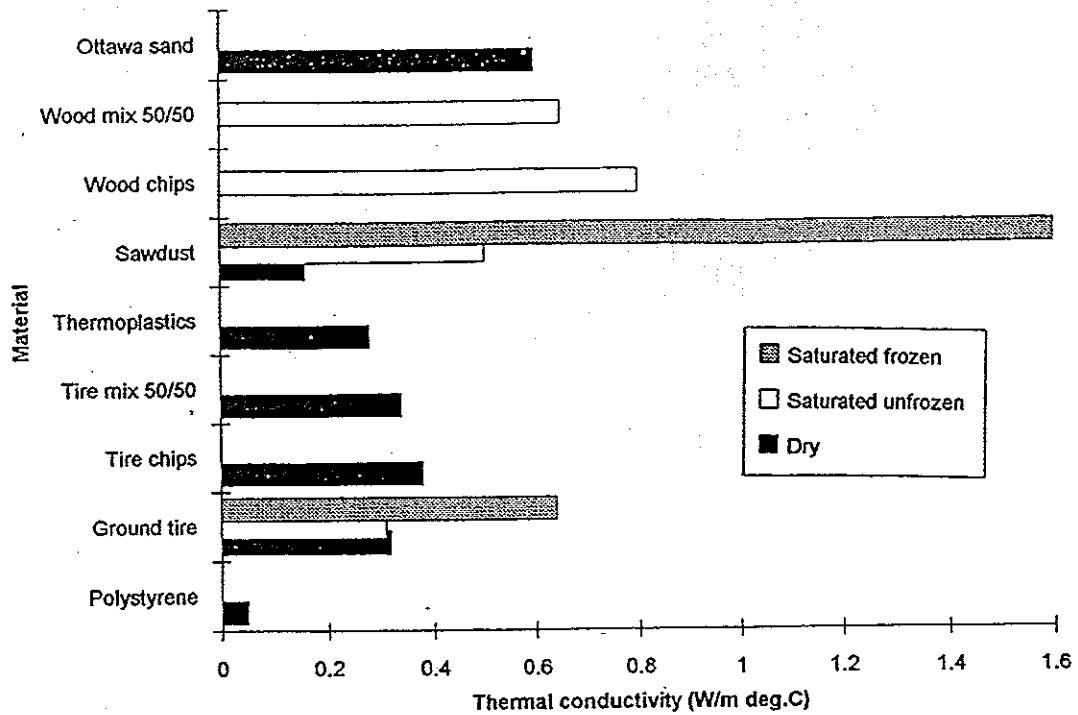


Figure 2.1 Results of thermal conductivity tests (after Dore, et al., 1995)

double those reported by Shao, et al. (1995). Saturated frozen samples of ground tire had an even higher thermal conductivity of $0.63 \text{ W/m}\cdot\text{C}$ ($0.36 \text{ Btu/hr}\cdot\text{ft}\cdot\text{F}$).

Dore, et al. (1995) used the measured thermal properties of tire chips and sawdust in a numerical bi-dimensional model developed by at Laval University to estimate frost penetration and heave of the 12 model pavement sections shown in Figure 2.2. Calculated frost penetration and maximum heave are shown in Figures 2.3 and 2.4, respectively. Frost penetration for sections with either tire chips or sawdust was expected to be reduced by 36 to 44 percent, and heave was expected to be reduced by 72 to 90 percent.

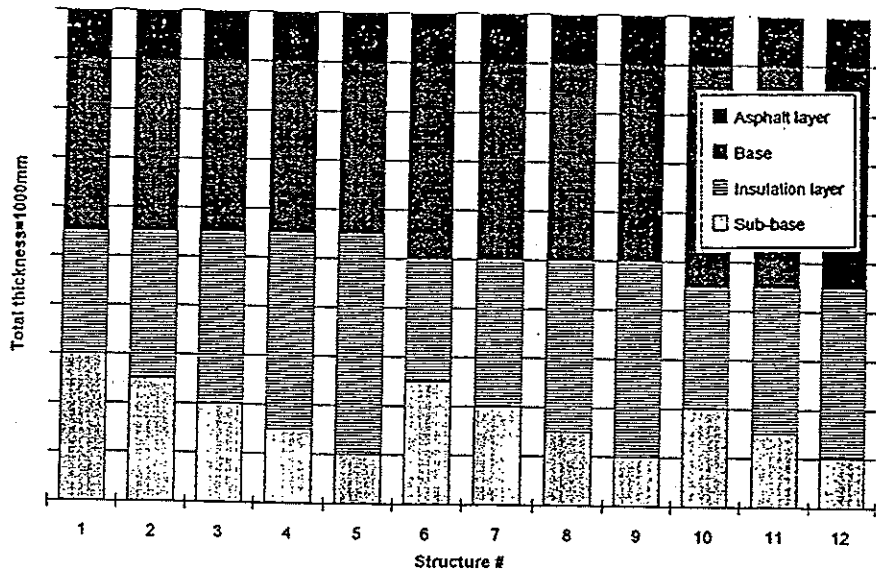


Figure 2.2 Pavement structures used in model study (after Dore, et al., 1995)

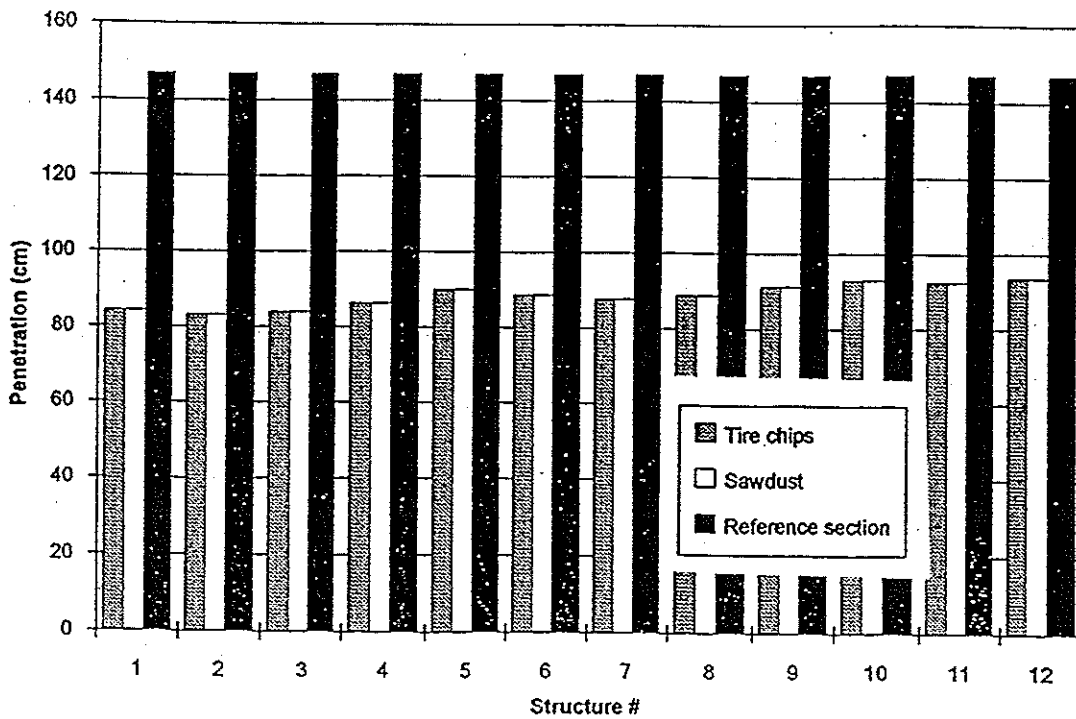


Figure 2.3 Calculated frost penetration (after Dore, et al., 1995)

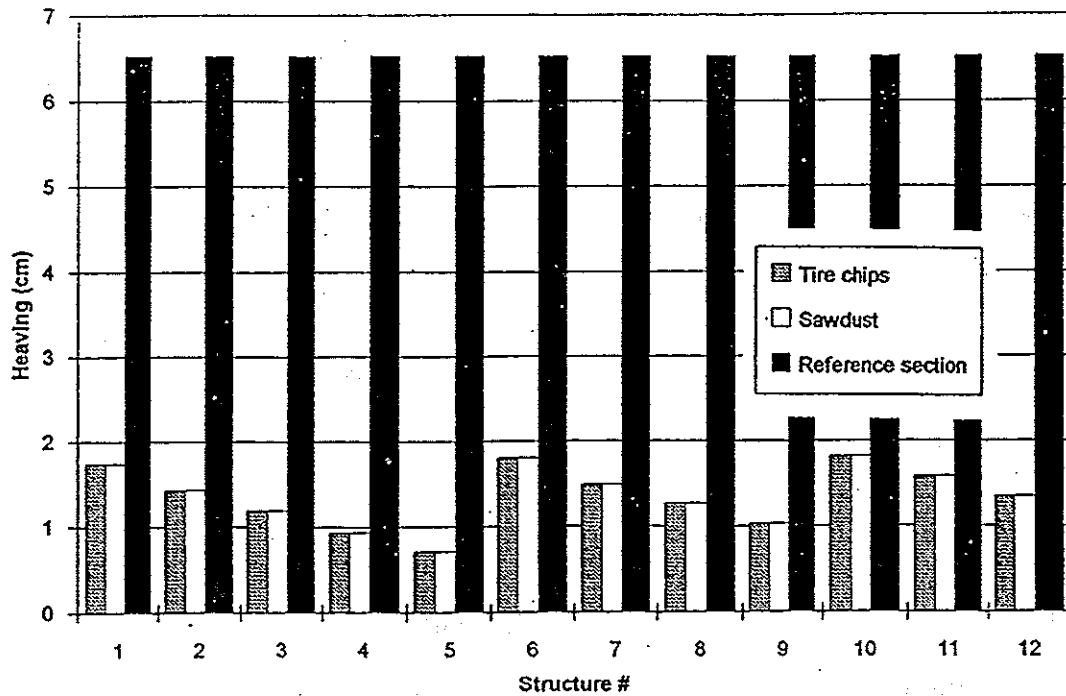


Figure 2.4 Caclulated maximum heave (after Dore, et al., 1995)

2.2.3 Benson, et al. (1996) Thermal Conductivity Measurement

Benson, et al. (1996) reported the thermal conductivity of tire chips as 0.020 W/m·°C (0.012 Btu/hr-ft·°F). The laboratory test was part of a project using tire chips as insulation for the slope of a landfill liner. Five types of material were studied using a laboratory thermal probe technique. Maximum tire chip size was 100 mm (4 in.) and samples were tested dry in a polystyrene bucket. The densities were not reported. This value is less than one-tenth those reported by Shao, et al. (1995) and Dore, et al. (1995), who used more reliable techniques.

2.3 PERMEABILITY OF TIRE CHIPS

The permeability (or hydraulic conductivity) of tire chips and tire chip/soil mixtures has been measured with constant head permeameters ranging in diameter from 203 mm to 305 mm (Bressette, 1984; Hall, 1990; Humphrey, et al., 1992, 1993; Humphrey and Sandford, 1993; Edil and Bosscher, 1992, 1994; Ahmed, 1993; Ahmed and Lovell, 1993). Some permeameters had provisions to apply a vertical stress to the sample to simulate the compression that would occur under the weight of overlying soil cover.

The permeability of tire chips determined in several investigations is summarized in Table 2.7. Permeabilities from 0.58 to 23.5 cm/s (0.6×10^6 to 24.3×10^6 ft/yr) were reported. Results from Edil and Bosscher (1992, 1994) are not included in Table 2.7 because they noted that the limited flow capacity of their permeameter casts doubt on the reliability of their reported permeabilities.

The permeabilities of tire chip/soil mixtures have been measured by Edil and Bosscher (1992, 1994), and Ahmed (1993). Edil and Bosscher (1992, 1994) used mixtures of tire chips with a 75-mm (3-in.) maximum size and a clean uniform sand. Surcharge pressures up to 138 kPa (2,880 psf) were applied to the samples. Their results are summarized in Figure 2.5. Ahmed (1993) used mixtures of tire chips with either a 13 or 25-mm (0.5 or 1.0-in.) maximum size and two soil types: (1) uniformly graded Ottawa sand; and (2) a fine grained glacial till (Crosby Till). No surcharge pressure was applied to the samples. The results are summarized in Table 2.8. For both studies, the permeability increased as the percent tire chips in the mix increased.

Table 2.7. Summary of reported permeabilities of tire chips

Particle size (mm)	Void ratio	Dry density (Mg/m ³)	Permeability (cm/sec)	Reference
25 to 64		0.469	5.3 to 23.5	Bressette (1984)
25 to 64		0.608	2.9 to 10.9	
5 to 51		0.470	4.9 to 59.3	
5 to 51		0.610	3.8 to 22.0	
38	----	----	1.4 to 2.6	Hall (1990)
19	----	----	0.8 to 2.6	
10 to 51	0.925	0.644	7.7	Humphrey, et al. (1992, 1993)
10 to 51	0.488	0.833	2.1	
20 to 76	1.114	0.601	15.4	
20 to 76	0.583	0.803	4.8	
10 to 38	0.833	0.622	6.9	
10 to 38	0.414	0.808	1.5	
10 to 38		0.653	0.58	

1 cm/s = 1.035x10⁶ ft/yr

Table 2.8. Permeabilities of mixtures of tire chips and soil (after Ahmed, 1993)

Tire chip maximum size (mm)	Soil type	% tire chips based on total weight	Dry density (Mg/m ³)	Permeability (cm/s)
----	Ottawa sand	0	1.89	1.6 x 10 ⁻⁴
25	Ottawa sand	15.5	1.68	1.8 x 10 ⁻³
25	Ottawa sand	30.1	1.53	3.5 x 10 ⁻³
25	Ottawa sand	37.7	1.41	8.7 x 10 ⁻³
----	Crosby till	0	1.91	8.9 x 10 ⁻⁷
25	Crosby till	14.8	1.70	1.8 x 10 ⁻⁵
25	Crosby till	30.1	1.39	2.1 x 10 ⁻³
25	Crosby till	40	1.20	8.8 x 10 ⁻³
13	Crosby till	40	1.19	9.7 x 10 ⁻³

1 cm/s = 1.035x10⁶ ft/yr

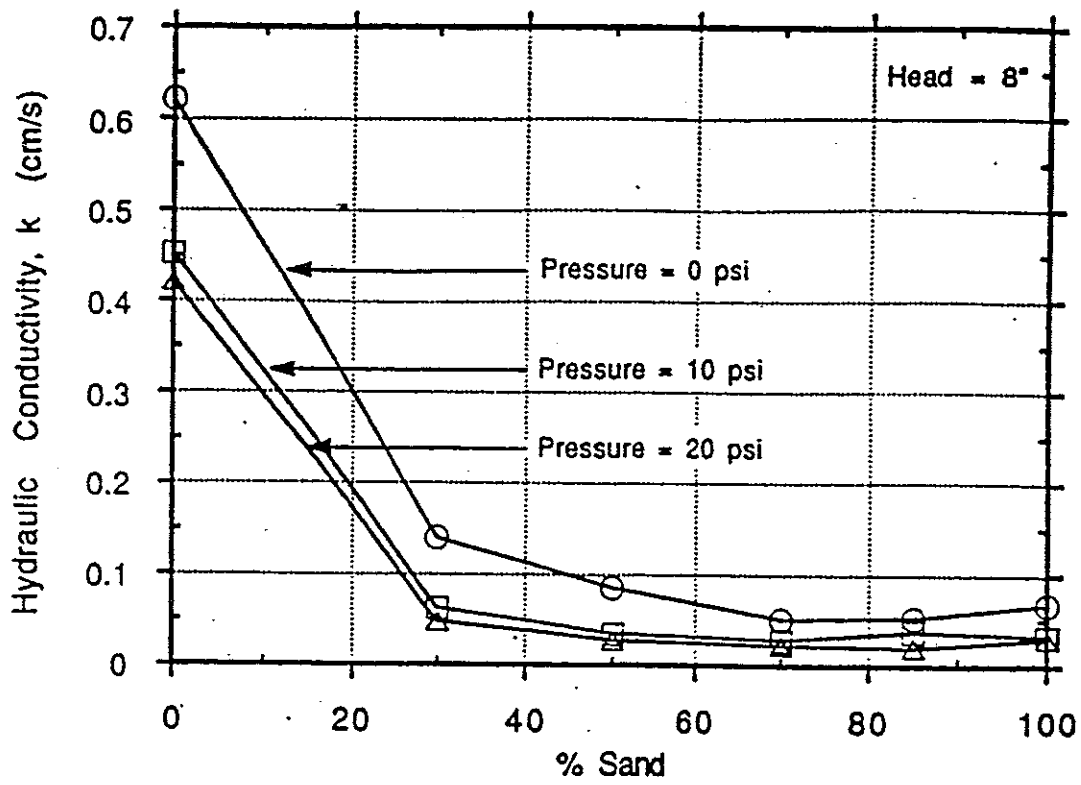


Figure 2.5 Hydraulic conductivities of mixtures of tire chips and clean sand (after Edil and Bosscher, 1992) ($1 \text{ cm/s} = 1.035 \times 10^6 \text{ ft/yr}$)

2.4 CASE HISTORIES

Three case histories using tire chips for subgrade insulation or drainage were available in the literature. The following are summaries of these projects.

2.4.1 Richmond Maine

Late in the summer of 1992 a field trial using tire chips as subgrade insulation was constructed on Dingley Road in Richmond, Maine (Humphrey and Eaton, 1995). The primary goals of this project were to find the thickness of tire chips needed to provide effective insulation and the minimum thickness of overlying soil cover to provide a stable riding surface.

The test site was a dead-end, gravel-surfaced road that was traveled by mainly cars, light trucks, and school buses. One day a month, however, 10 to 40 fully loaded double- and triple-axle dump trucks hauled sewage sludge to farms at the end of the road. Although there was no standing water or wet areas near the test site in the summer and fall, poor drainage and flat topography created areas of standing water during the spring melt. Prior to installation of the tire chip insulation layer, the road became severely rutted at this time of year.

The existing road was surfaced with more than 457 mm (18 in.) of clean sandy gravel and gravelly sand. The native soils ranged from gray silty clay to gray-brown silty gravelly sand and were highly frost susceptible. Refusal occurred below these soils in either glacial till with boulders or bedrock. The water table in the summer and fall was 1 to 3 m (3.3 to 9.8 ft) below the ground surface.

The test site was 290 m (950 ft) long and broken up into five tire chip test sections, two transition sections, and one control section as shown in Figure 2.6. In addition, two existing road sections were monitored. Tire chip thicknesses were 152 and 305 mm (6 and 12 in.) and granular soil thicknesses were 305, 457, and 610 mm (12, 18, and 24 in.). The configurations of the test sections are given in Table 2.9 and a typical cross-section is shown in Figure 2.7. Sections A and B were identical, except that tire chips in Section A were completely enclosed in geotextile (Amoco 2000-2).

The tire chips were uniformly graded with a maximum size of 51 mm (2 in.) and nearly all chips were retained on the No. 4 (4.75-mm or 0.187-in.) U.S.-standard sieve. Tire chips were a mixture of steel- and glass-belted tires from Pine State Recycling of Nobleboro, Maine. The gravel fill was a well-graded mixture of sand and gravel, with less than 5 percent passing the No. 200 (0.075 mm; 0.00295 in.) U.S.-standard sieve and a maximum particle size of 152 mm (6 in.). The surface course had a maximum particle size of 25 mm (1 in.) and about 7 percent passing the No. 200 sieve. Common borrow was utilized from the excavation of the existing roadway. It was a gravelly sand with about 3 percent passing the No. 200 sieve.

Construction began with excavation of the existing road to the starting grade. Some of the soil was stockpiled for use as common borrow, while the rest was disposed of off-site. A small bulldozer was used to grade a 4 percent slope toward the ditch. The exposed grade was compacted with four passes with a vibratory smooth drum roller with a static weight of 9 metric tons (10 U.S. short tons). Tire chips were placed directly on the prepared subgrade, spread with a small bulldozer, and compacted with six passes of

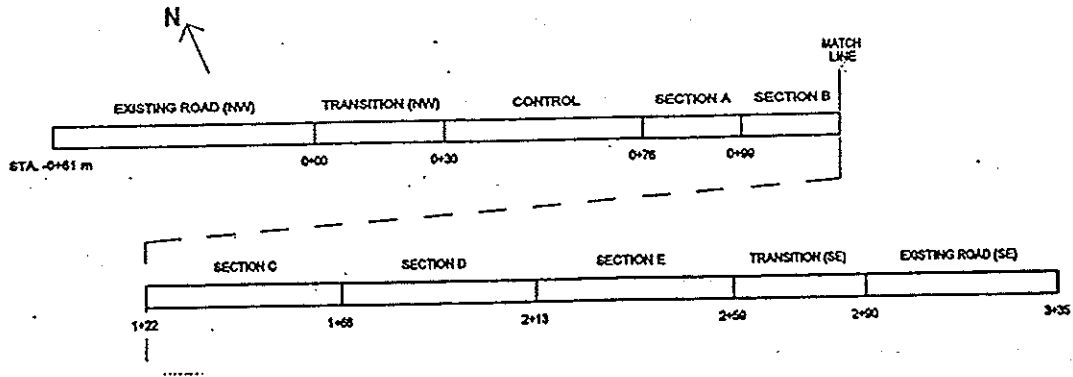


Figure 2.6 Plan view of test site (after Humphrey and Eaton, 1995)

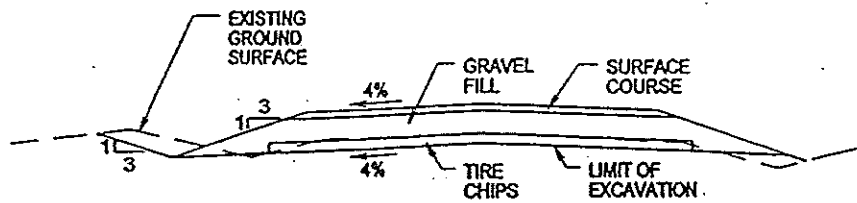


Figure 2.7 Typical cross section (after Humphrey and Eaton, 1995)

Table 2.9 Summary of test section configuration (after Humphrey and Eaton, 1995)

Section	Depth of excavation (mm)	Thickness of layer (mm)			
		Tire chips	Common borrow	Gravel fill	Surface course
Control	----	----	----	203	102
A	152	152	----	203	102
B	152	152	----	203	102
C	152	152	----	356	102
D	305	305	----	356	102
E	457	305	305	203	102

25.4 mm = 1 in.

the smooth drum vibratory roller. Gravel fill was placed over this and also compacted with six passes of the smooth drum vibratory roller. The 102-mm (4-in.) surface course was then placed and compacted with four passes of the roller. The surface was treated with flake calcium chloride to control dust.

The monitoring instrumentation consisted of thermocouples, resistivity gauges, groundwater monitoring wells, and frost-free benchmarks. Thermocouples measured the temperatures in the soil, resistivity gauges detected the depth of the freezing front, and the benchmarks were used as stable reference points for a heave survey. Instrumentation locations are shown in Figure 2.8. A cross-section showing thermocouple and resistivity gauges is shown in Figure 2.9.

Freezing indices for the 1992 to 1993 and 1993 to 1994 seasons were 626°C-days (1128°F-days) and 707°C-days (1273°F-days), respectively. The reported average for the area was 470°C-days (850°F-days) (Bigelow, 1969; Gilman, 1964). Maximum frost penetration for both winters is shown in Figure 2.10. Tire chips reduced the depth of frost penetration by between 22 and 28 percent in Sections A, B, D, and E compared with the control section. Section C had the greatest depth of frost penetration, indicating that insulation effectiveness decreases as soil cover increases. Comparisons of frost penetration depth with time for the 1993 to 1994 season is shown in Figure 2.11. The control and existing road sections showed rapid penetration of frost in the first week of the freezing season to about 750 mm (30 in.), followed by a relatively constant rate of frost penetration for the rest of the freezing season. Tire chip Sections D and E show

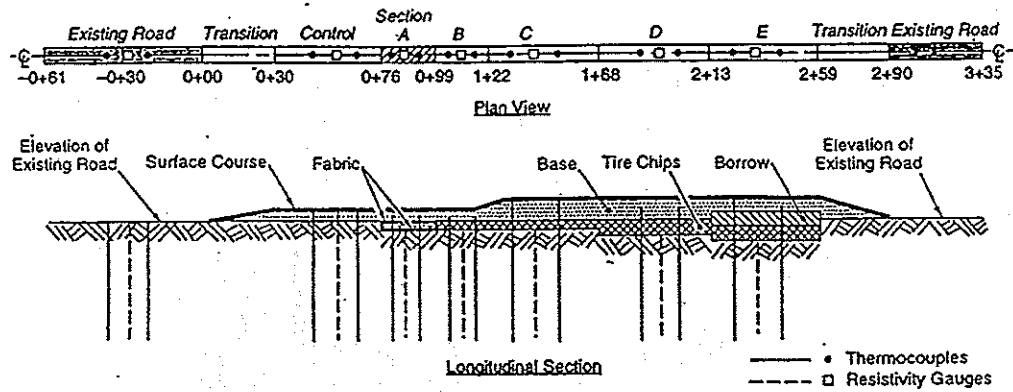


Figure 2.8 Location of instrumentation (after Humphrey and Eaton, 1995)

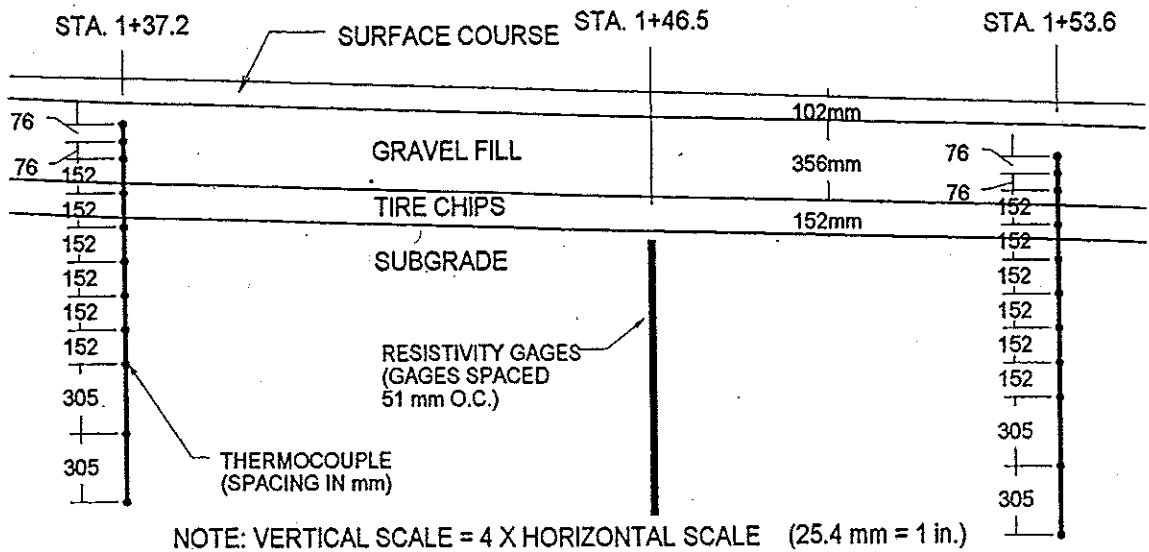


Figure 2.9 Cross section showing thermocouple and resistivity gages (after Humphrey and Eaton, 1995)

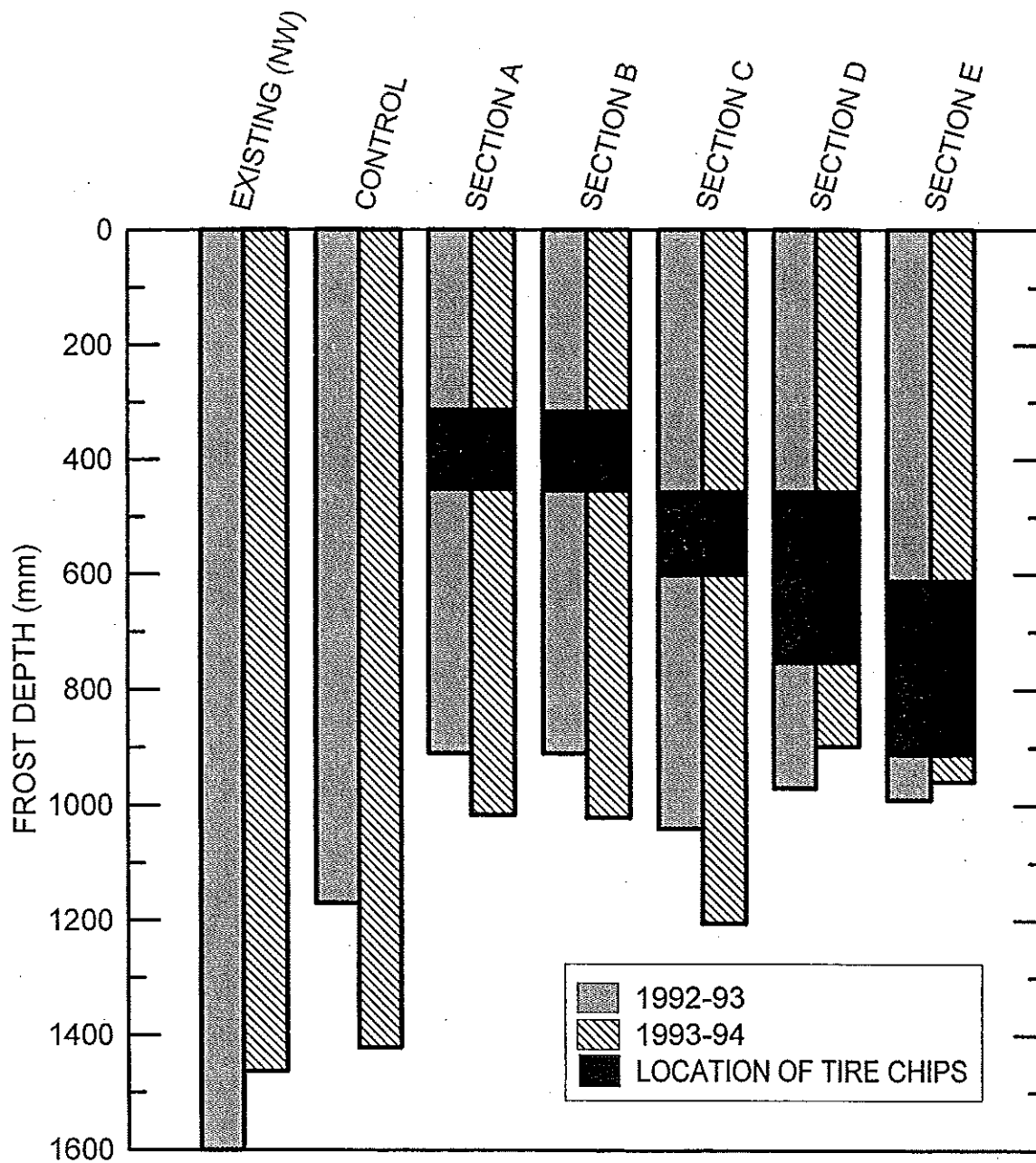


Figure 2.10 Maximum depth of frost penetration (after Humphrey and Eaton, 1995)

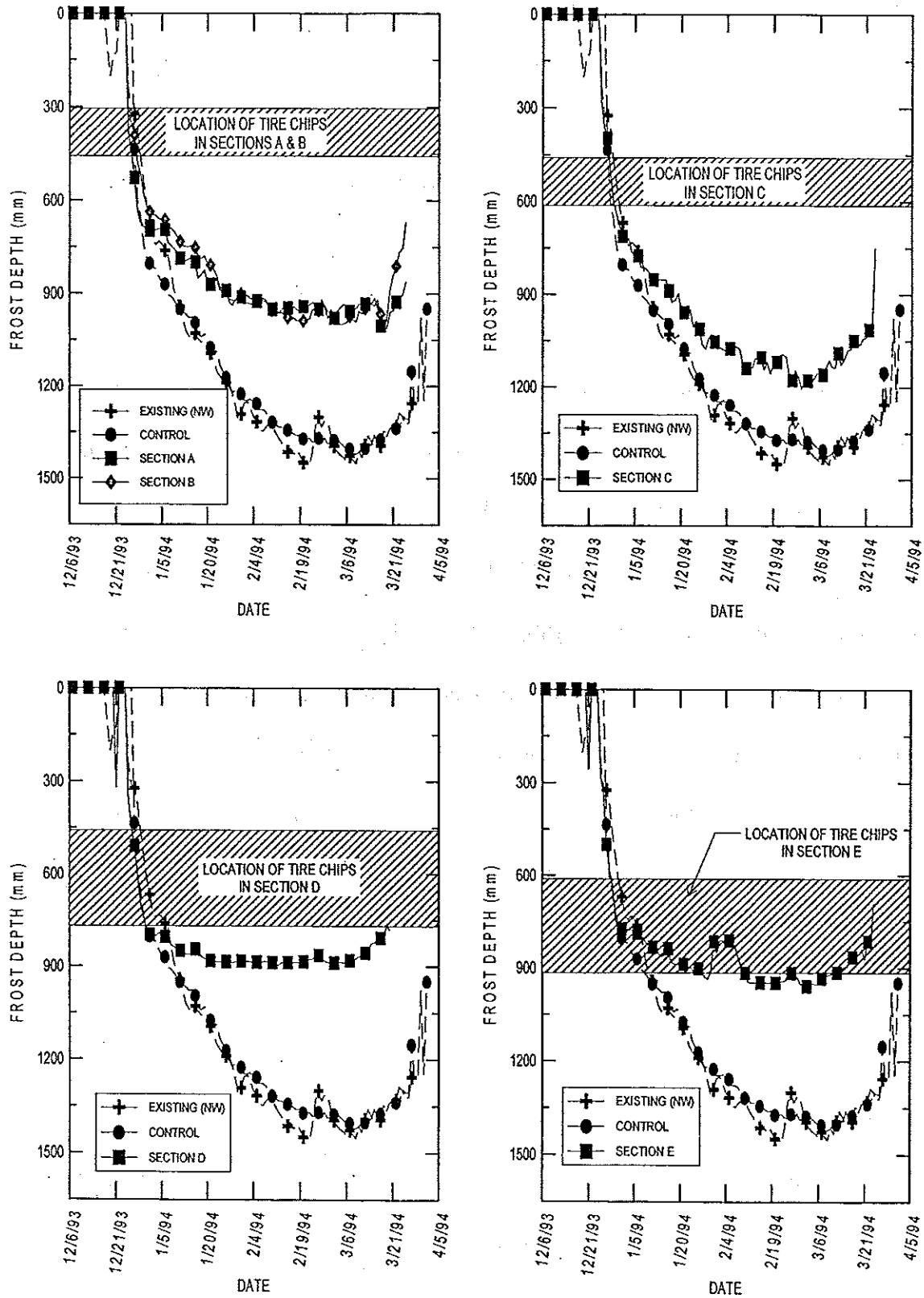


Figure 2.11 Depth of frost penetration versus date (after Humphrey and Eaton, 1995)

different thermal behavior. The initial frost penetration was very similar to the control and existing road, but once the freezing front approached the base of the tire chip layer it essentially stopped and remained at this depth for the remainder of the freezing season. The freezing front in Sections A, B, and C was also less than that of the Control and existing road, however, the frost penetrated below the 152-mm (6-in.) thick tire chip layer.

Figure 2.12 shows temperature profiles on February 16, 1994, which was at the end of a 45-day cold period. The temperatures below the tire chip sections were much warmer than in the control or existing road. The temperature from the top to the bottom of the tire chip sections increased about 3°C to 4°C (5°F to 7°F) for sections with 152 mm (6 in.) of tire chips and 8°C (14°F) for sections with 305 mm (12 in.) of tire chips. The region above tire chips was also typically colder than the same depth in the control and existing road. This shows that the higher thermal resistivity of tire chips reduced heat flow through the tire chip layer. This resulted in higher temperatures below the tire chips and lower temperatures above them.

Frost heave for both winters is shown in Figure 2.13. There was an obvious reduction in heave in the tire chip sections.

2.4.2 Saint-Joachim Quebec Test Sections

Freezing indices in the province of Quebec, Canada range from 900°C-days (1620°F-days) to more than 2000°C-days (3600°F-days), and frost penetration varies from 1 to 3 m (3 to 10 ft) below pavement. This extreme climate necessitates the use of

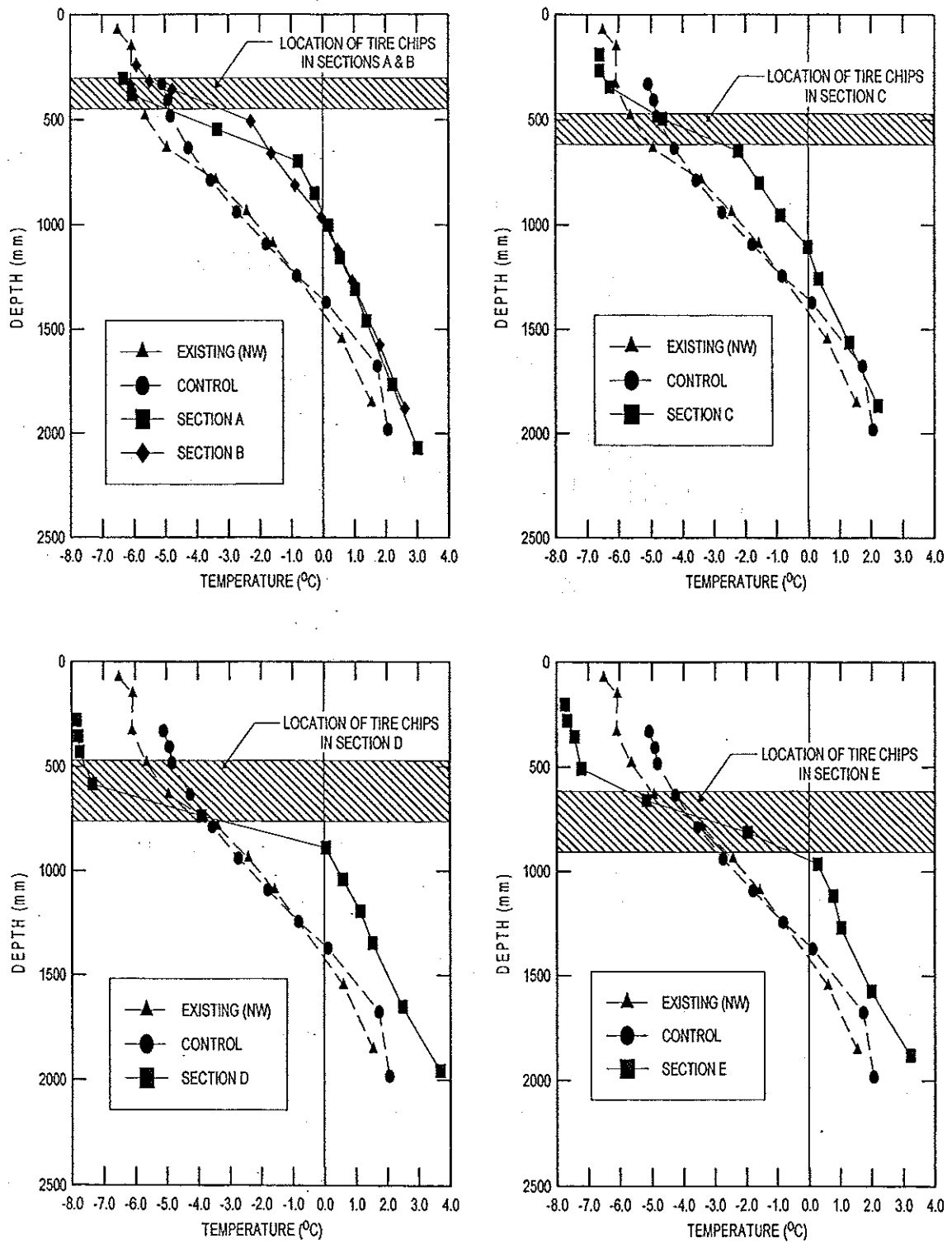


Figure 2.12 Temperature profile on February 16, 1994 (after Humphrey and Eaton, 1995)

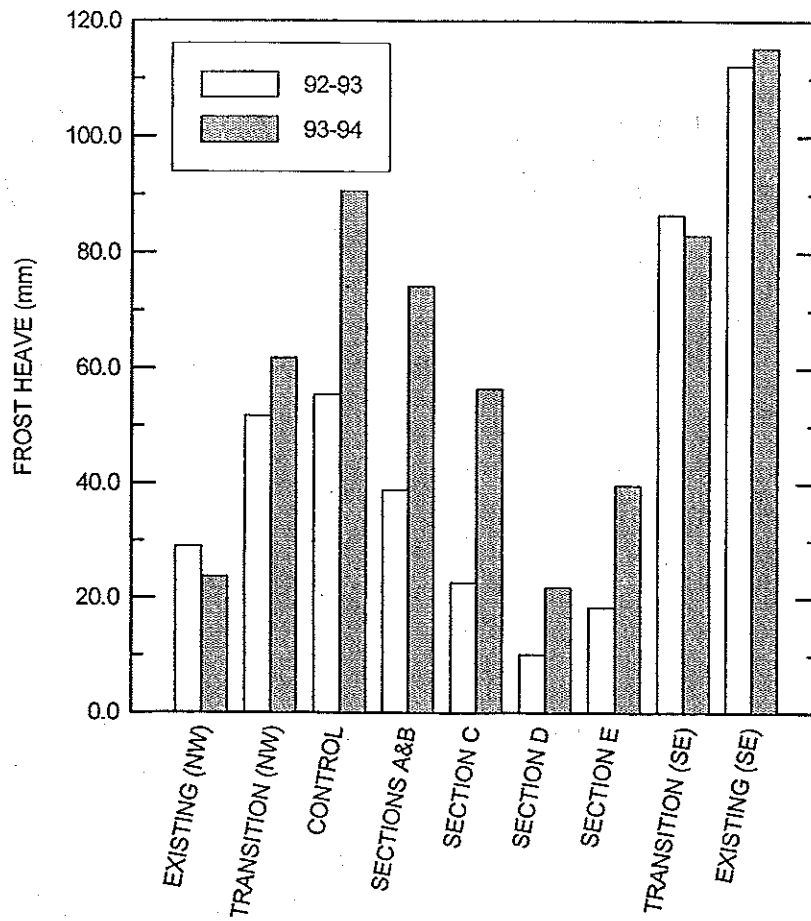


Figure 2.13 Frost heave (after Humphrey and Eaton, 1995)

either a sufficient thickness of non-frost susceptible granular material or insulation. Since large quantities of granular fill may not be readily available or may be expensive, alternative options were investigated. A full scale field trial using extruded polystyrene, sawdust, stacked tires, and tire chips was conducted in the municipality of Saint-Joachim.

Saint-Joachim is located about 40 km (25 mi) northeast of Quebec City, where the mean freezing index is 1334°C-days (2401°F-days) (compiled from 1951-1980 by Environment Canada at the Saint-Fereol Station). Test sections were located in a discontinued section of a working sand pit. The total length of the test sections were 42

m (138 ft) excluding access ramps to the test sections. Profile and plan sections are shown in Figures 2.14 and 2.15, respectively. The test site was divided into seven 6 m long by 6 m wide (20 ft by 20 ft) sections. Cross-sections are shown in Figure 2.16. Tire chips were used in Sections 1 and 2 with thicknesses of 300 mm (12 in.) and 150 mm (6 in.), respectively. Both sections had 700 mm (28 in.) of gravel cover. The gradation of the natural soil, sand, and gravel are shown in Figure 2.17. The completed sections were 1.35 m (4.4 ft) above the natural ground surface. Subsurface exploration indicated that gravely sand extended to a depth of 5 to 10 m (16.4 to 32.8 ft) and that groundwater was at approximately the same depth.

Field trial results were reported through January 26, 1994. Figure 2.18 shows frost penetration vs. time, and Figure 2.19 shows total frost penetration through January 26, 1994. On this date, frost penetration was not reduced significantly by the tire chips. Section 2 had almost the same depth of frost penetration (1.4 percent reduction) as the control, however, Section 1 performed better (10.4 percent reduction). This is still less than the 22% to 28% reduction in frost penetration recorded in Richmond, Maine. This may be due in part to the lack of information on frost penetration for dates later than January 26, 1994. It is likely that there would have been a greater reduction in frost depth later in the winter, as was the case in Richmond.

2.4.3 Georgia Vermont Road Base

A 100-m (330-ft) gravel-surfaced test section using tire chips as a base course was constructed in the town of Georgia, Vermont in 1990 (Frascoia and Cauley, 1995). The road, Town Highway No. 4 (TH4), typically experienced severe rutting during the spring

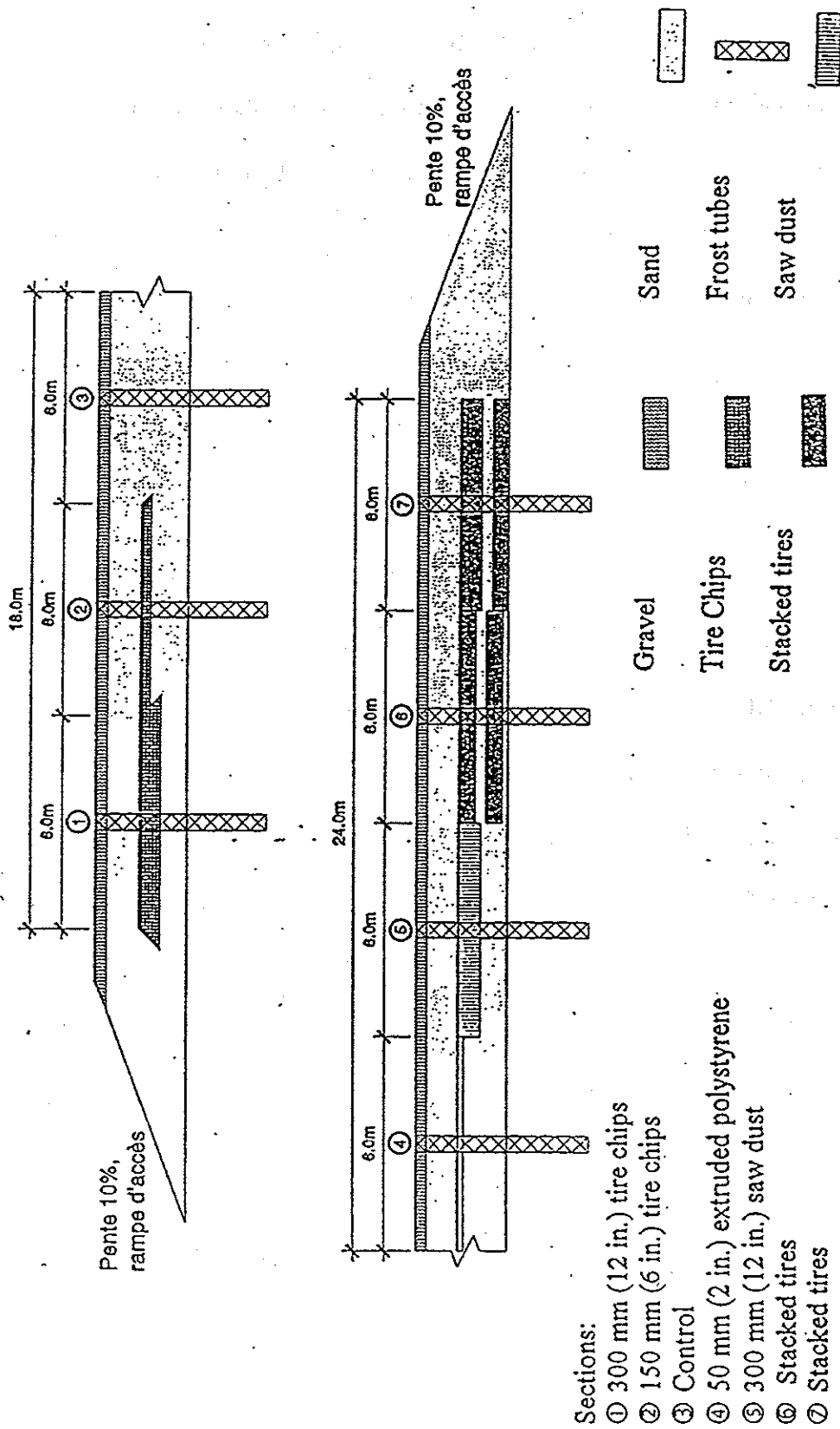


Figure 2.14 Profile of Saint-Joachim, Quebec test sections (after Rioux, 1994)

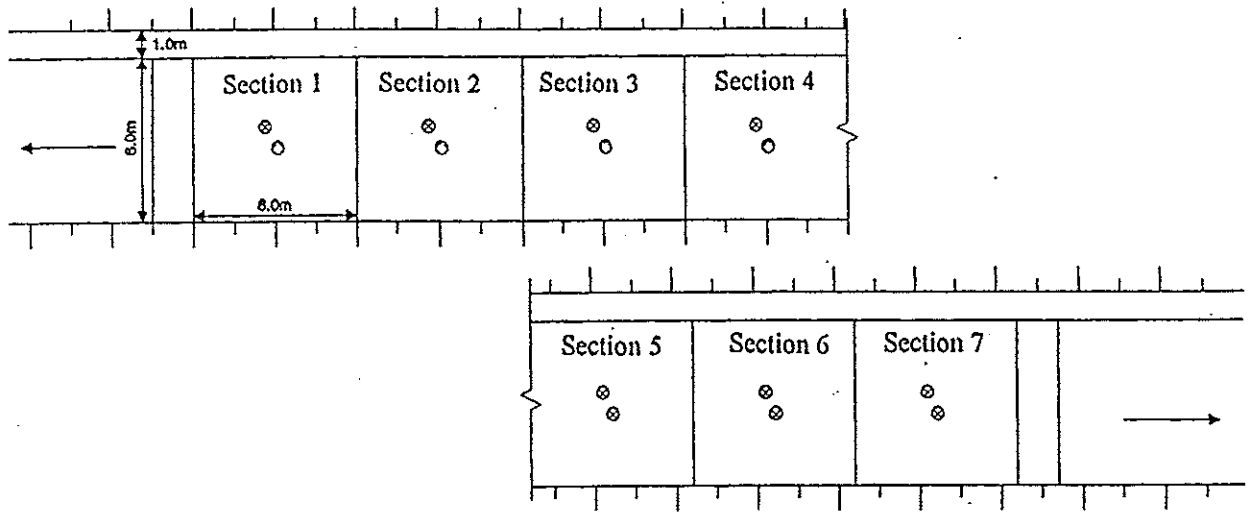


Figure 2.15 Plan of Saint-Joachim, Quebec test sections (after Rioux, 1994)

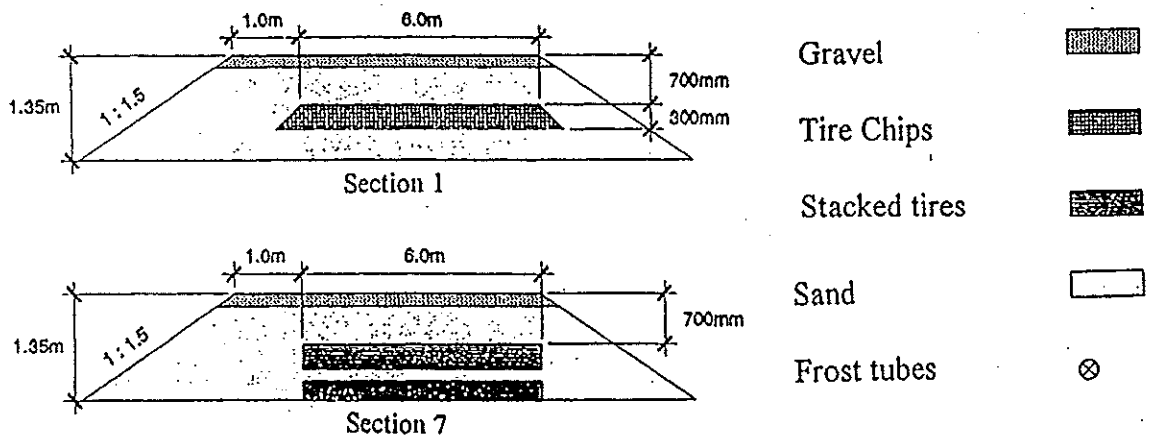


Figure 2.16 Cross sections of Saint-Joachim, Quebec test sections (after Rioux, 1994)

	natural soil	sand	gravel
% Passing			
56 mm	100	100	100
40 mm	97	100	100
28 mm	95	99	100
14 mm	88	98	75
5 mm	77	90	51
1.25 mm	63	71	33
315 μ m	27	19	12
60 μ m	6.3	4.1	3.8
Classification	SP-SM	SP	

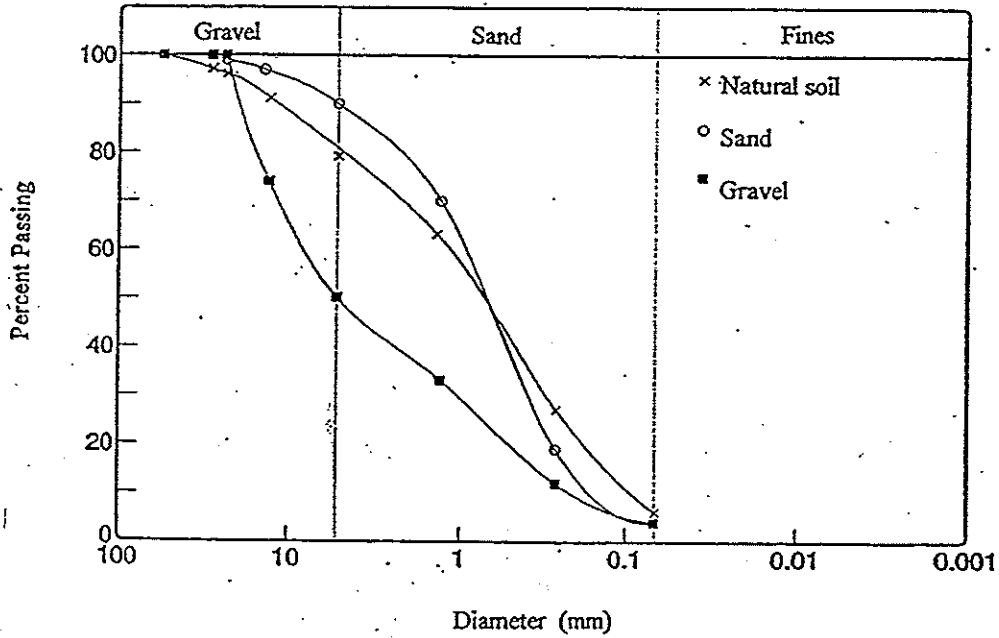


Figure 2.17 Gradation of natural soil, sand, and gravel in Saint-Joachim, Quebec test sections (after Rioux, 1994)

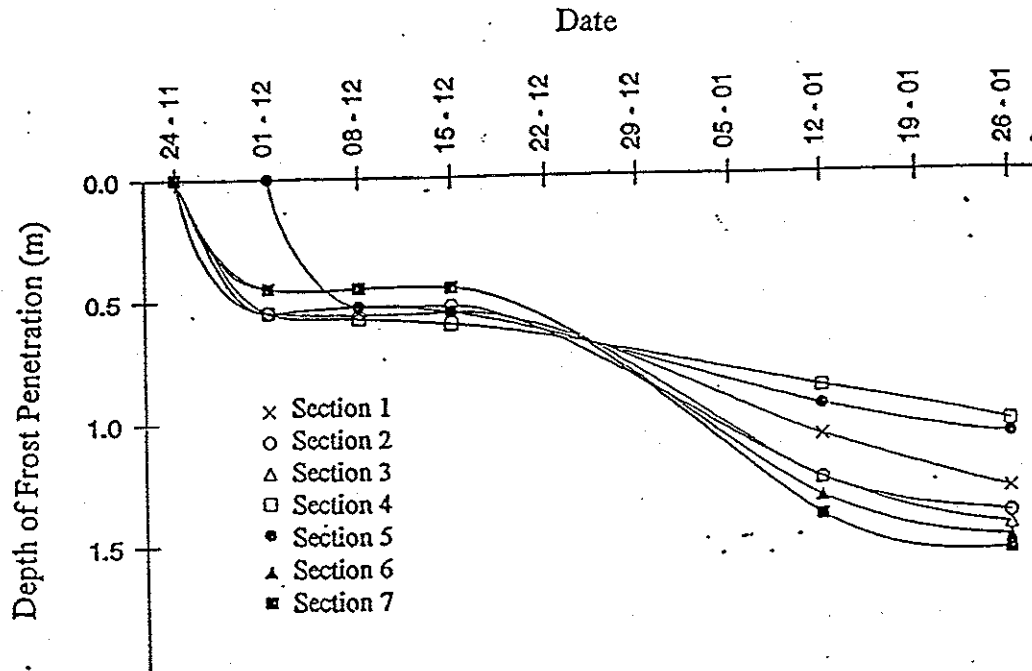


Figure 2.18 Frost penetration vs. time in Saint-Joachim, Quebec test sections (after Rioux, 1994)

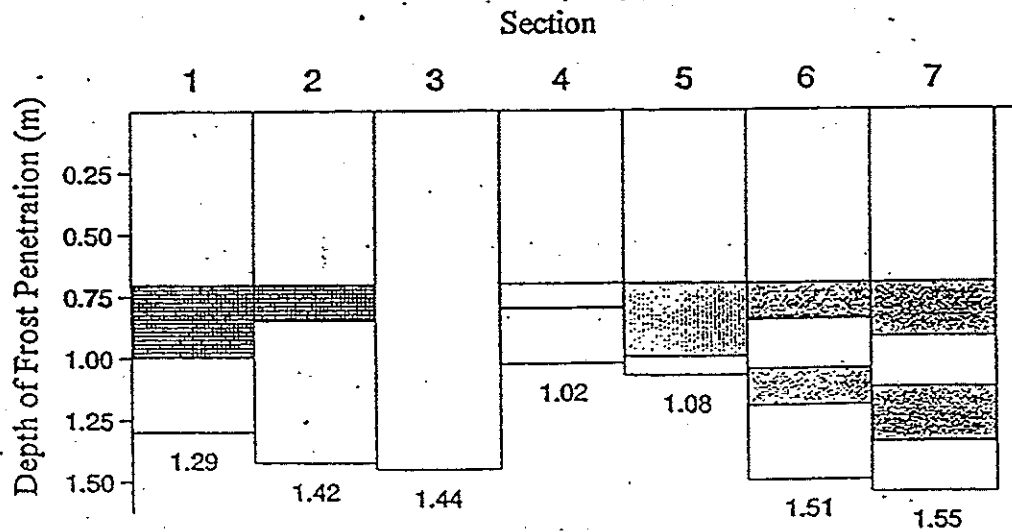


Figure 2.19 Total frost depth through January 26, 1994 for the Saint-Joachim test sections (after Rioux, 1994)

melt. The purpose of the tire chip layer was to provide drainage and to prevent contamination of the gravel base with fines from the subgrade.

Approximately 230 to 305 mm (9 to 12 in.) of tire chips were placed on a silty sand subgrade, which contained 24% to 43% fines. Most of the original gravel (approximately 610 mm or 24 in) and several centimeters of new gravel were placed over the tire chips to complete the road structure (see Figure 2.20). In August 1990, some fine longitudinal and transverse cracks were noted on the surface, however, there was no noticeable rutting in the wheel paths.

The road was inspected in the spring of 1991. The untreated roadway portions were in poor condition, visibly wet with numerous ruts, cracks, and boils, but the tire chip sections were visibly dry and free of rutting. Frascoia and Cauley (1995) concluded that the tire chip layer improved the otherwise poor quality gravel by cutting off the capillary rise of water and by draining water infiltration from the surface away from the gravel. Specific data on the thermal conductivity of the tire chips was not collected. FWD tests were also performed on the test section (see Table 2.10). They concluded that the deflection of the road surface under heavy loads would eliminate the possibility placing bituminous pavement over the sections without the addition of more gravel cover.

2.5 PAVEMENT PERFORMANCE

2.5.1 Quebec Mechanical Properties Model

Part of the investigation by Dore et al. (1995) included modeling of mechanical properties of the same insulating materials and 12 pavement structures as described in

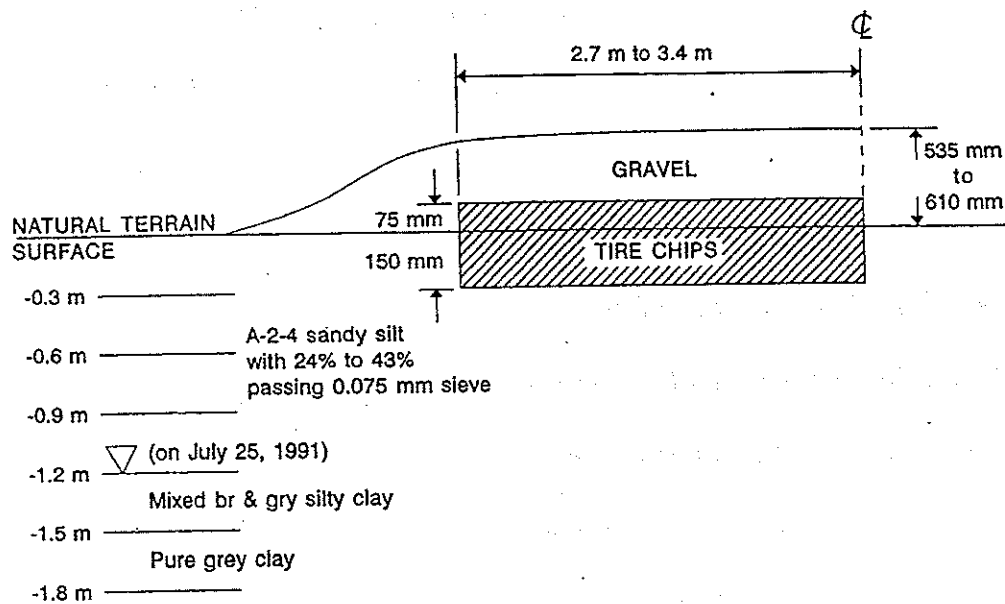


Figure 2.20 Typical section of TH4, Georgia, Vermont: initial construction (after Frascoia and Cauley, 1995)

Table 2.10 Deflections from FWD tests and structural numbers on TH 4, Georgia, Vermont (after Frascoia and Cauley, 1995)

Test Site	Deflection (mm)	Structural No.
1	0.73	2.80
2	0.87	2.52
3	2.60	1.61
4	3.27	1.49

Section 2.2.2. The computer program ELSYM 5 was used to estimate pavement surface deflections and horizontal strain at the base of the asphalt layer. The elastic modulus used for tire chips, sawdust, gravel base, and clayey sand subbase were 1.1 MPa (160 psi), 70 MPa (10,150 psi), 200 MPa (29,000 psi), and 83 MPa (12,040 psi), respectively. The wheel load used in ELSYM5 was not specified. Figure 2.21 shows that deflections in tire chip sections were calculated to be the highest, ranging from 0.73 to 0.99 mm. Figure 2.22 shows that horizontal strains were also calculated to be highest in tire chip sections, from 194×10^{-6} to 213×10^{-6} compared to approximately 180×10^{-6} to 185×10^{-6} for the reference section. The ratio of the strain calculated in the section with 450 mm (17.7 in.) of tire chips and 350 mm (13.8 in.) of cover divided by the strain of the reference section was 1.18. The figures noted these as "tire chips," however, they were referred to in the paper as crumb rubber. Crumb rubber may have different structural properties than the tire chips used in the University of Maine trial. The calculated deflections may therefore be different from those measured in the University of Maine field trial.

2.5.2 North Yarmouth and TWP31-MD Field Trials

Two field studies were performed by Nickels (1995) to determine the performance of tire chips as lightweight and conventional embankment fill beneath paved roads. The first project was located on the southern approach fill for the Route 231 bridge over the Maine Central Railroad in North Yarmouth, Maine. The field trial consisted of four 30.5-m (100-ft) sections each with a 610-mm (24-in.) thick tire chip layer and one 30.5-m (100-ft) long control section. Overlying soil cover ranged from 762 to 1372 mm (30 to 54 in.) and pavement thickness was 127 mm (5 in.). Two types of tire chips, 76-mm

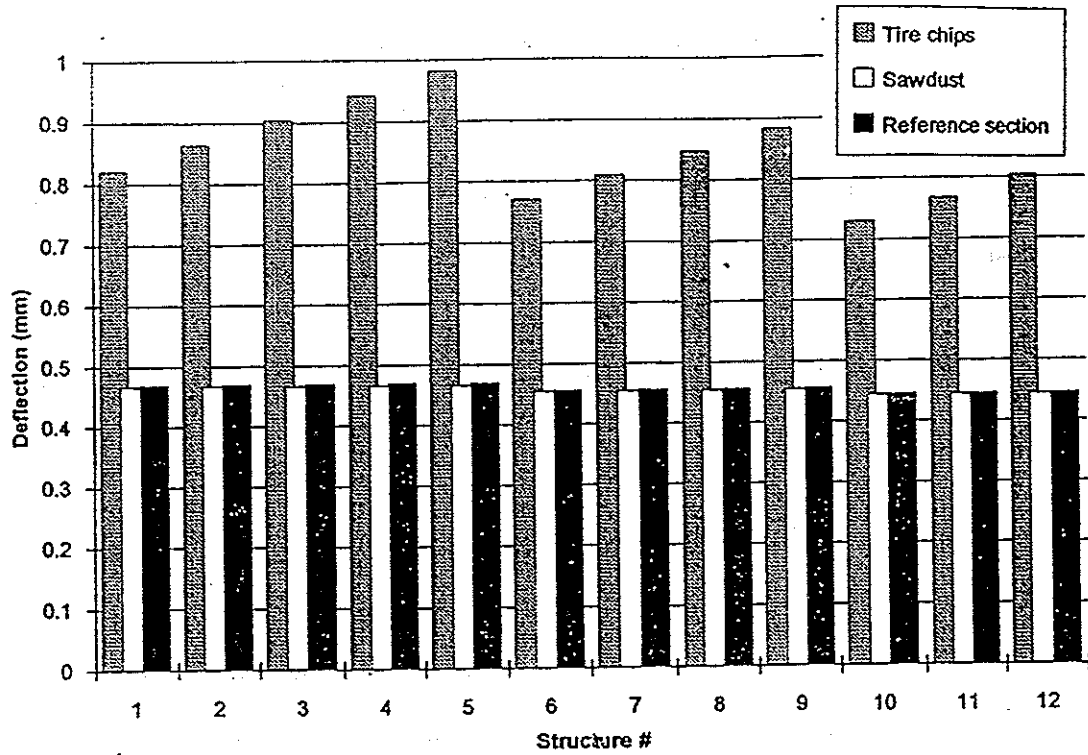


Figure 2.21 Calculated deflection at surface of pavement (after Dore, et al., 1995)

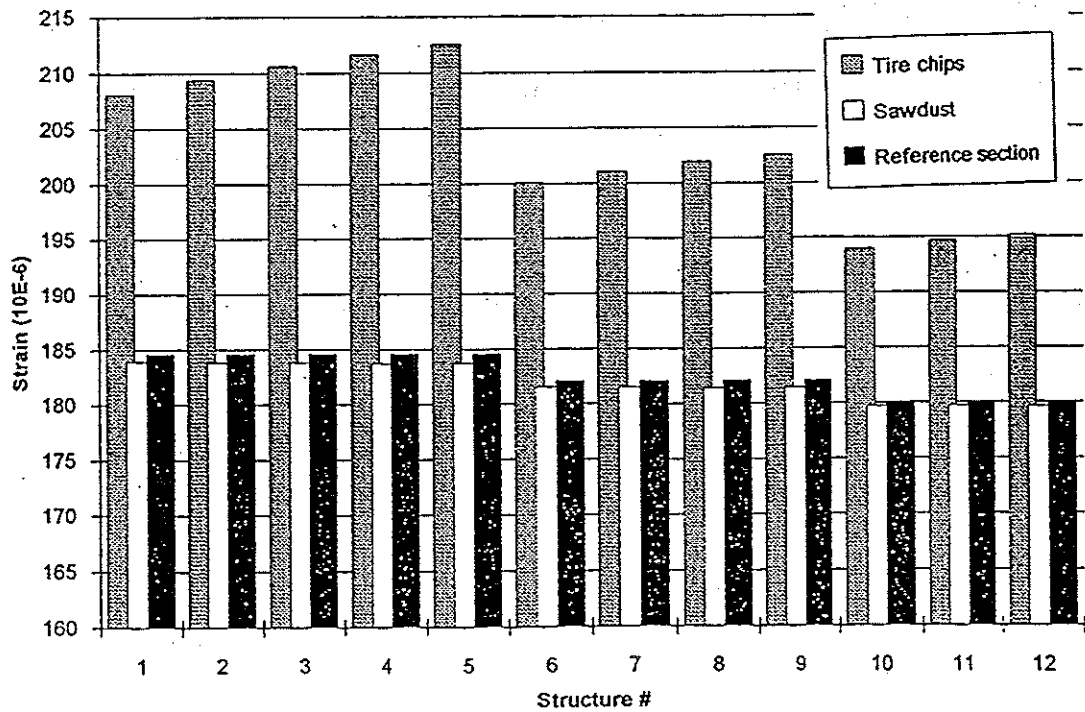


Figure 2.22 Calculated horizontal strain at base of layer (after Dore, et al., 1995)

(3-in.) minus (Type A) and 305-mm (12-in.) minus (Type B), were surrounded in non-woven geotextile (Amoco 4551) to provide separation. A longitudinal layout is shown in Figure 2.23 and a typical cross-section is shown in Figure 2.24. Table 2.11 summarizes the test section configurations.

The second trial, in Township 31-MD (TWP31-MD), Maine, was located on a section of Route 9 approximately 48 km (30 mi) west of Calais, Maine. The field trial consisted of four 30.5-m (100-ft) long test sections each containing a 610-mm (24-in.) thick layer of tire chips and one 30.5-m (100-ft) long control section. There were two 3.7-m (12-ft) wide westbound lanes: one was a travel lane and the other was a truck lane. There was one eastbound 3.7-m (12-ft) wide travel lane and a 3.0-m (10-ft) wide breakdown lane. The soil cover over the tire chips ranged in thickness from 1245 to 2464 mm (49 to 97 in.). Bituminous pavement thickness was 229 mm (9 in.) in the travel and truck lanes. The breakdown lanes were covered with 51 mm (2 in.) of pavement underlain with recycled milled asphalt that served as an aggregate base. Similar to North

Table 2.11 Test section configuration for North Yarmouth test sections (after Nickels, 1995)

Section	Tire chip type	Thickness of layer (mm)			
		Tire chips	Borrow cover	Subbase course	Pavement
1	B	610	130	635	127
2	A	610	430	635	127
3	A	610	740	635	127
4	A	610	130	635	127
Control	----	----	----	635	127

Note: 1 inch = 25.4 mm

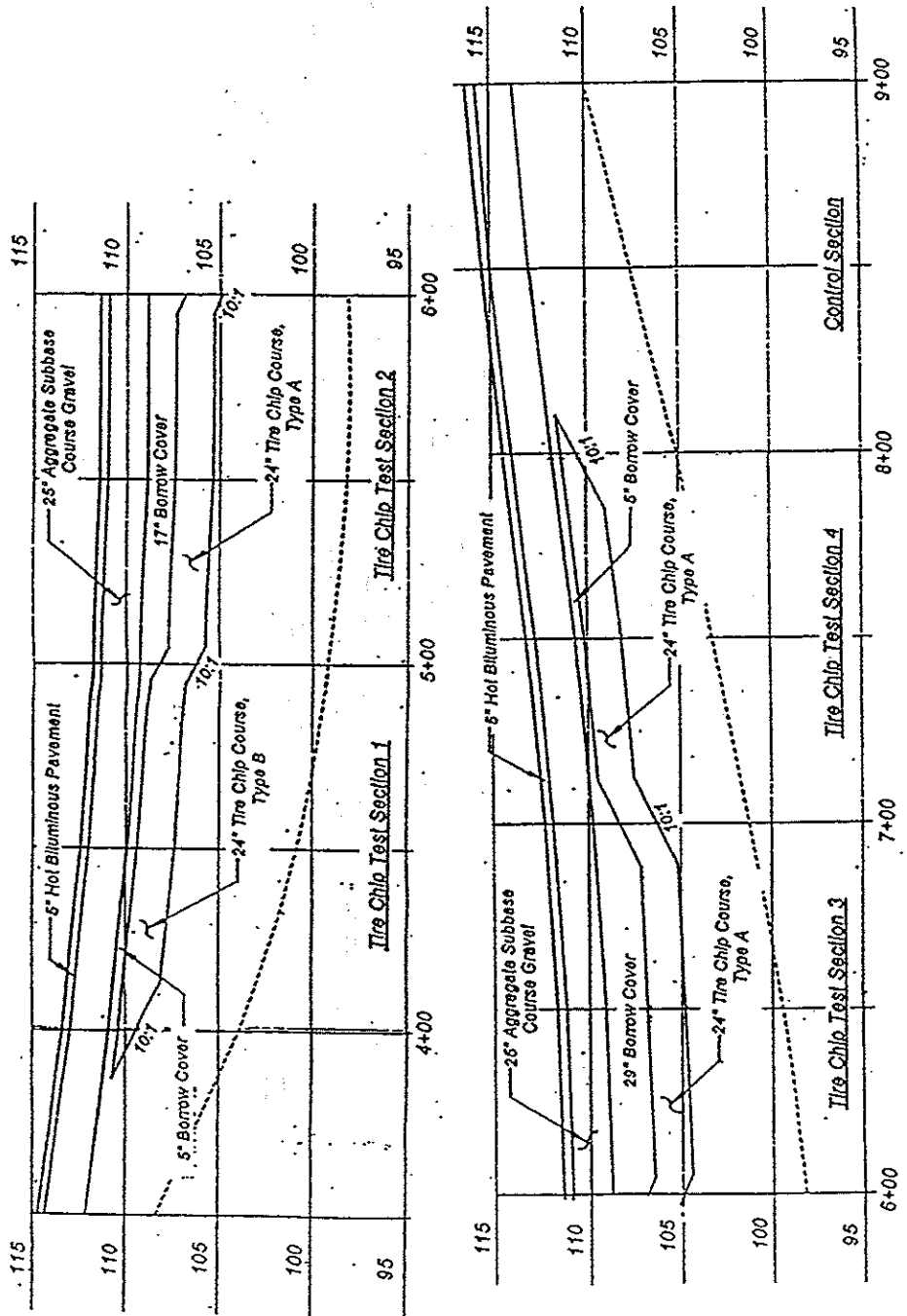


Figure 2.23 North Yarmouth longitudinal layout (after Nickels, 1995)

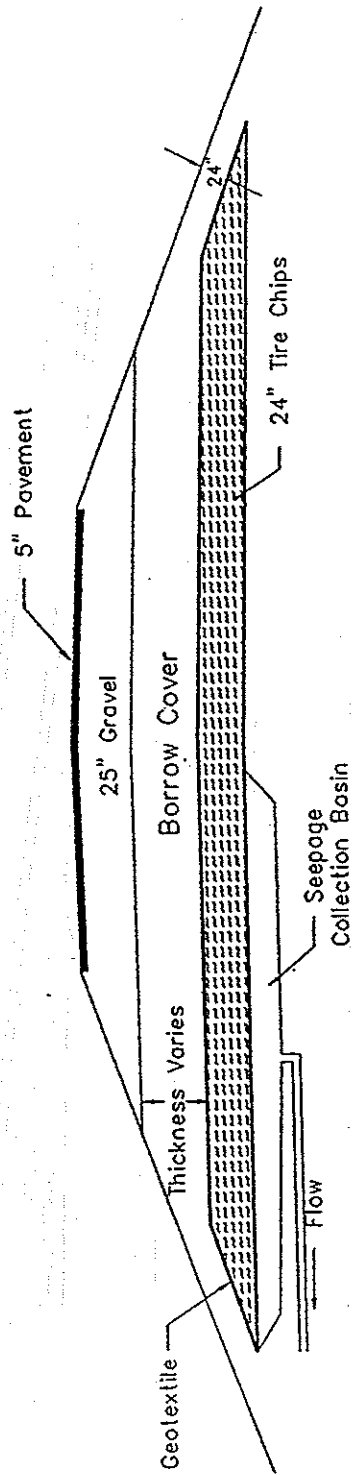


Figure 2.24 North Yarmouth typical cross-section (after Nickels, 1995)

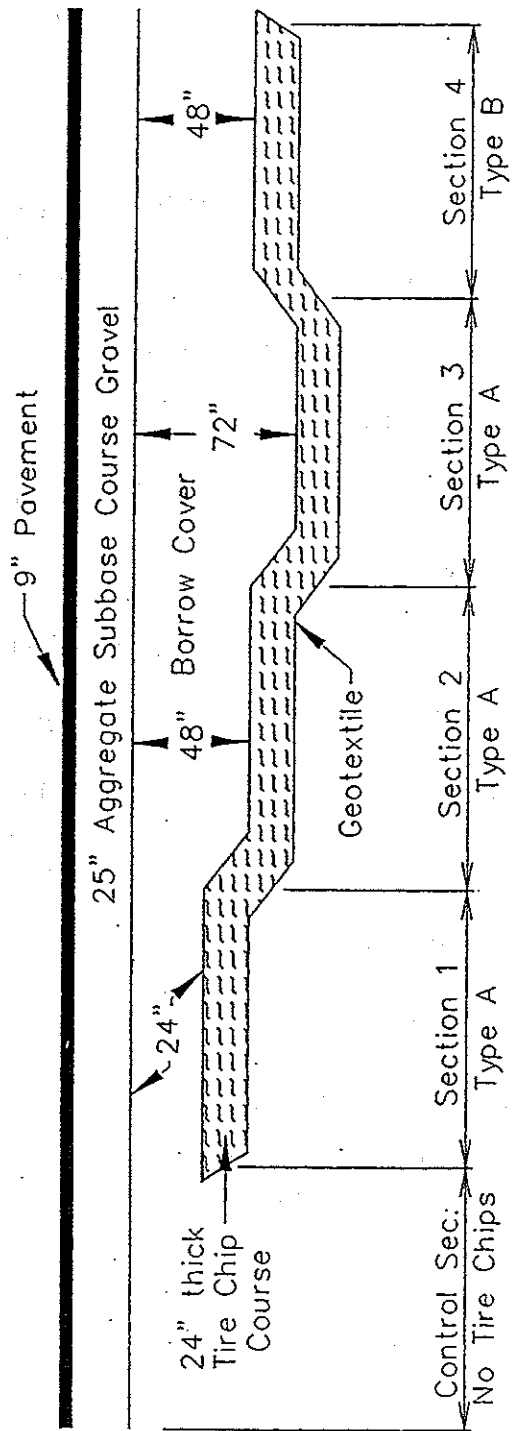
Yarmouth, tire chip sections were surrounded by a non-woven geotextile (Mirafi 180N), and tire chip Types A and B were used. A longitudinal section and typical cross-section is shown in Figures 2.25 and 2.26, respectively. Table 2.12 summarizes the test section configurations.

Benkelman Beam tests were performed at both sites. A summary of the maximum deflection basins for each section at each site are shown in Figures 2.27 and 2.28. Tables 2.13 and 2.14 summarize pavement deflections directly under the wheel load for each section. Deflection basins for the North Yarmouth trial show that Type B (Section 1) tire chips with 762 mm (30 in.) of cover showed the greatest deflections. Sections 2, 3, and 4 contained Type A tire chips with 1067 mm (42 in.), 1372 mm (54 in.), and 762 mm (30 in.) of soil cover, respectively, and exhibited the expected trend of decreasing deflections with increasing soil cover. The deflection basins of tire chips are similar and extend to 3.0 to 4.6 m (10 to 15 ft) from the point of loading. Nickels hypothesized that this broad, flat shape spread over a larger distance than in the control would still yield similar tensile strains compared to the control. The deflection basin in the control section extended no more than 0.9 m (3 ft) from the center of the loaded area.

Table 2.12 Test section configuration for TWP31-MD test sections (after Nickels, 1995)

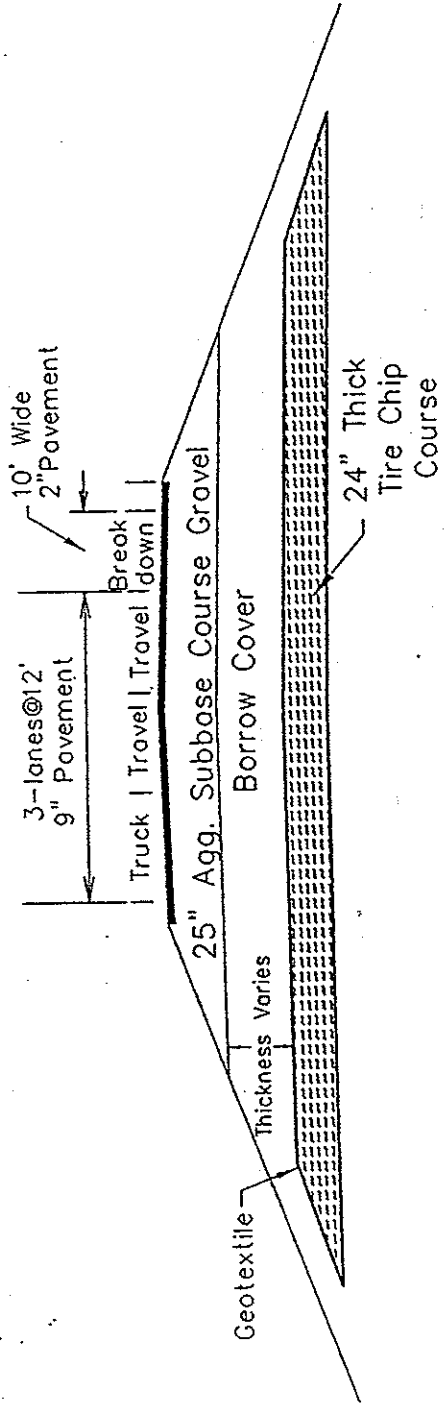
Section	Tire chip type	Thickness of layer (mm)			
		Tire chips	Borrow cover	Subbase course	Pavement (travel lanes)
1	A	610	610	635	229
2	A	610	1219	635	229
3	A	610	1829	635	229
4	B	610	1219	635	229
Control	----	----	----	635	229

Note: 1 inch = 25.4 mm



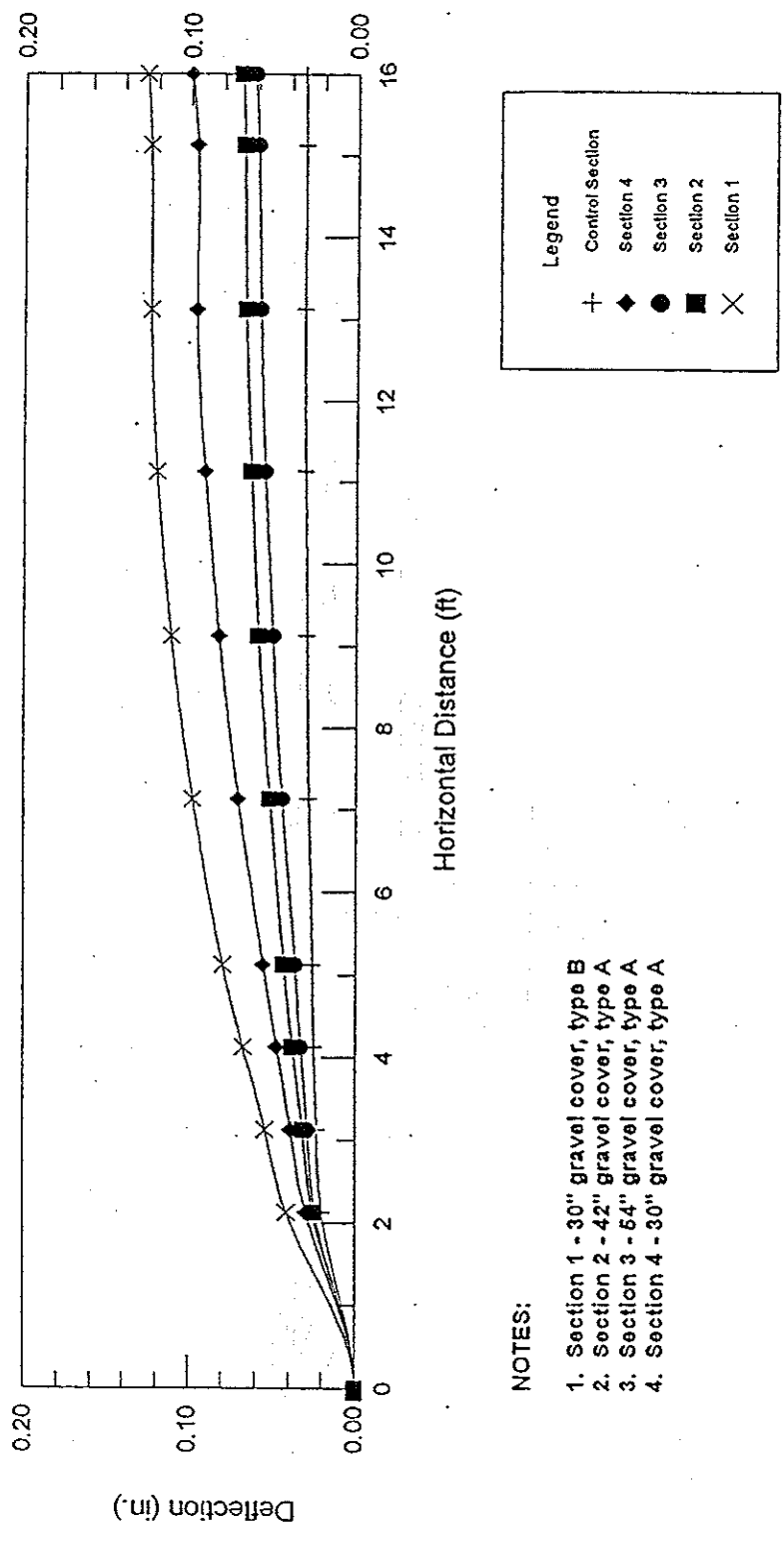
5 Sections of 100' each

Figure 2.25 TWP31-MD longitudinal layout (after Nickels, 1995)



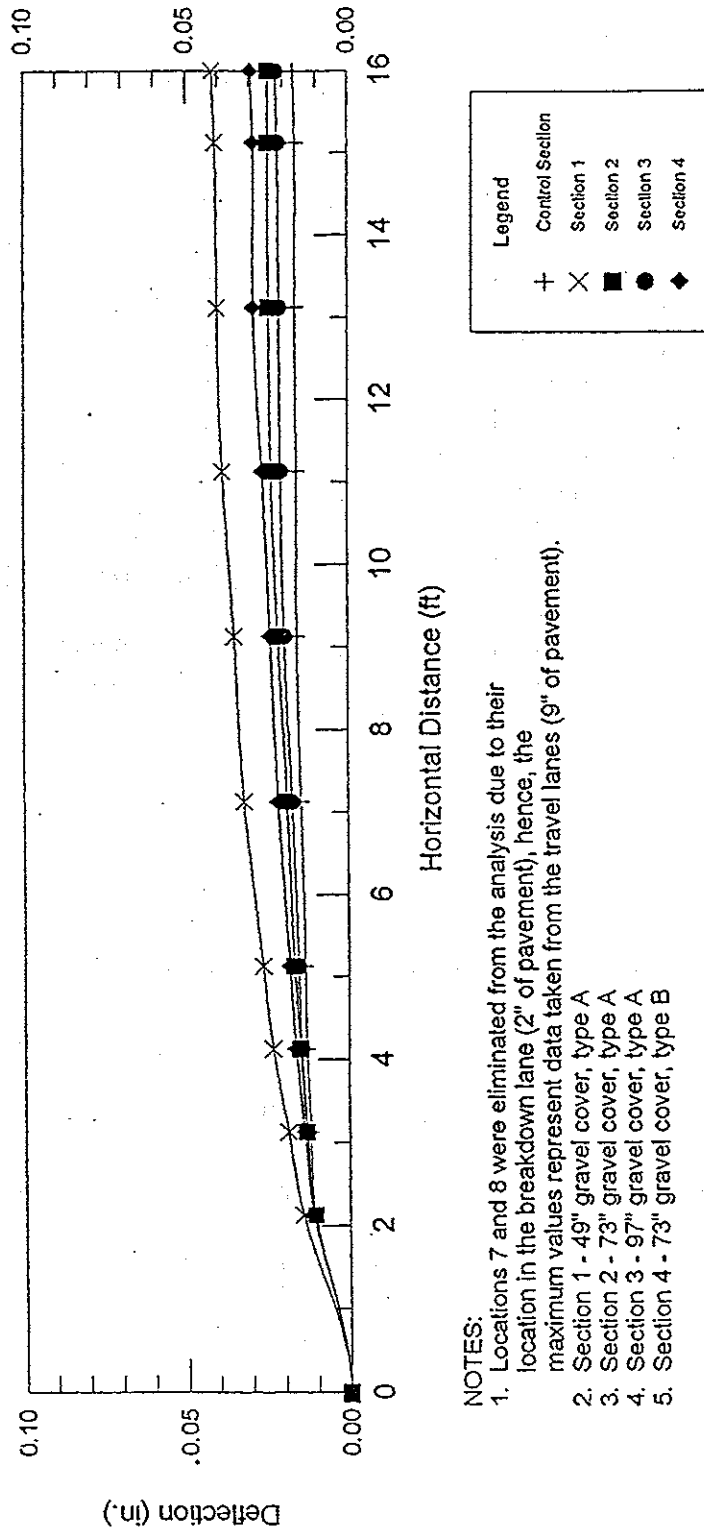
Note: The thickness of recycled asphalt below the breakdown lane is unknown, hence, it is not included in this sketch.

Figure 2.26 TWP31-MD typical cross section (after Nickels, 1995)



- NOTES:
1. Section 1 - 30" gravel cover, type B
 2. Section 2 - 42" gravel cover, type A
 3. Section 3 - 54" gravel cover, type A
 4. Section 4 - 30" gravel cover, type A

Figure 2.27 Maximum deflection basins from each section in North Yarmouth (after Nickels, 1995)



NOTES:

1. Locations 7 and 8 were eliminated from the analysis due to their location in the breakdown lane (2" of pavement), hence, the maximum values represent data taken from the travel lanes (9" of pavement).
2. Section 1 - 49" gravel cover, type A
3. Section 2 - 73" gravel cover, type A
4. Section 3 - 97" gravel cover, type A
5. Section 4 - 73" gravel cover, type B

Figure 2.28 Maximum deflection basins from each section in TWP31-MD (after Nickels, 1995)

Table 2.13 Pavement deflections directly under wheel load in North Yarmouth (after Nickels, 1995)

Section 1 30" Cover Type B Chip		Section 2 42" Cover Type A Chip		Section 3 54" Cover Type A Chip		Section 4 30" Cover Type A Chip		Control Section No Tire Chips	
Local	Max. Defl. (in.)	Local	Max. Defl. (in.)	Local	Max. Defl. (in.)	Local	Max. Defl. (in.)	Local	Max. Defl. (in.)
1	0.127	1	0.067	1	0.062	1	0.069	1	0.032
2	0.116	2	0.061	2	0.049	2	0.080	2	0.026
3	0.117	3	0.064	3	0.049	3	0.093	3	0.022
4	0.115	4	0.059	4	0.058	4	0.090	4	0.018
5	0.098	5	0.070	5	0.038	5	0.057	5	0.023
6	0.094	6	0.049	6	0.040	6	0.084	6	0.021
7	0.121	7	0.067	7	0.046	7	0.091	7	0.028
8	0.093	8	0.060	8	0.036	8	0.100	8	0.023
Min.	0.093	Min.	0.049	Min.	0.038	Min.	0.057	Min.	0.018
Max.	0.127	Max.	0.070	Max.	0.062	Max.	0.100	Max.	0.032
Avg.	0.110	Avg.	0.062	Avg.	0.047	Avg.	0.083	Avg.	0.024
*C.V.	11.9	*C.V.	10.6	*C.V.	19.8	*C.V.	16.9	*C.V.	18.3

*C.V. is the Coefficient of Variation which is the standard deviation divided by the average times 100.

Note: 1 in. = 25.4 mm

The TWP31-MD trial results showed the same trend of decreasing deflection with increasing soil cover. The effect of the higher compressibility associated with Type B tire chips is very small with 1854 mm (73 in.) of soil cover and 229 mm (9 in.) of asphalt pavement (Section 4). Sections 2 through 4 and the control had nearly identical deflections up to 0.65 m (2.125 ft) from the center of the wheel load. Section 1 experienced more deflection to this point, and all tire chip sections experienced more deflection beyond this point.

Table 2.14 Pavement deflections directly under wheel load in TWP31-MD (after Nickels, 1995)

Control Section No Tire Chips		Section 1 49" Cover Type A Chip		Section 2 73" Cover Type A Chip		Section 3 97" Cover Type A Chip		Section 4 73" Cover Type B Chip	
Local	Max. Defl. (in.)	Local	Max. Defl. (in.)	Local	Max. Defl. (in.)	Local	Max. Defl. (in.)	Local	Max. Defl. (in.)
1	0.009	1	0.033	1	0.021	1	0.022	1	0.026
2	0.010	2	0.034	2	0.021	2	0.022	2	0.024
3	0.017	3	0.033	3	0.022	3	0.018	3	0.024
4	0.014	4	0.034	4	0.024	4	0.016	4	0.030
5	0.006	5	0.034	5	0.024	5	0.020	5	0.024
6	0.013	6	0.042	6	0.022	6	0.018	6	0.020
*7	0.033	*7	0.069	*7	0.026	*7	0.038	*7	0.038
*8	0.022	*8	0.051	*8	0.036	*8	0.030	*8	0.035
Min.	0.006	Min.	0.033	Min.	0.021	Min.	0.016	Min.	0.020
Max.	0.017	Max.	0.042	Max.	0.024	Max.	0.022	Max.	0.030
Avg.	0.012	Avg.	0.035	Avg.	0.022	Avg.	0.019	Avg.	0.025
†C.V.	32.8	C.V.	9.9	C.V.	6.2	C.V.	12.7	C.V.	13.1

*Maximum deflection values are based on data from travel lane Locations 1 through 6 where the pavement thickness is 229 mm (9 in.), hence, breakdown lane Locations 7 and 8 which have 51 mm (2 in.) of pavement are not included in the analysis.

†C.V. is the Coefficient of Variation which is the standard deviation divided by the average times 100. Note: 1 in. = 25.4 mm

The deflection data for both field trials was normalized by dividing the average deflection beneath the wheel load in each section by the respective deflection in the Control. Normalized pavement deflection is plotted versus soil cover thickness in Figure 2.29. Normalized deflection decreases as soil cover thickness increases.

Tensile strains at the base of the pavement were calculated from the measured shape of the deflection basin using a finite element program named Algor (1989). Maximum tensile strains for both North Yarmouth and TWP31-MD are shown in Table 2.15.

Normalized strains were calculated by dividing the tensile strain beneath the wheel load at the base of the asphalt layer by the respective tensile strain in the Control. Normalized strains are plotted versus soil cover thickness in Figure 2.30. This shows a trend of decreasing tensile strain with increasing cover thickness. It was noted that for Section 4 in North Yarmouth the normalized strain was 1.399 whereas the normalized deflection was 3.125. Thus, tire chips had a greater effect on deflection than on tensile strain. Nickels (1995) concluded that a 0.6 m (2-ft.) layer of Type A tire chips would have only a small effect on pavement life for soil covers as little as 762 mm (30 in.) and a negligible effect for soil covers in excess of about 1778 mm (70 in.).

Table 2.15 Maximum tensile strains for North Yarmouth and TWP31-MD (after Nickels, 1995)

NORTH YARMOUTH 5 in. Pavement			
Section	Soil cover (in.)	Tire Chip Type	Max. Strain (x10 ⁻² %)
1	30	B	5.660
2	42	A	3.346
3	54	A	3.501
4	30	A	3.741
Control	----	----	2.674
TWP31-MD 9 in. Pavement			
Section	Soil cover (in.)	Tire Chip Type	Max Strain (x10 ⁻² %)
1	49	A	2.998
2	73	A	2.157
3	97	A	2.401
4	73	B	2.250
Control	----	----	2.292

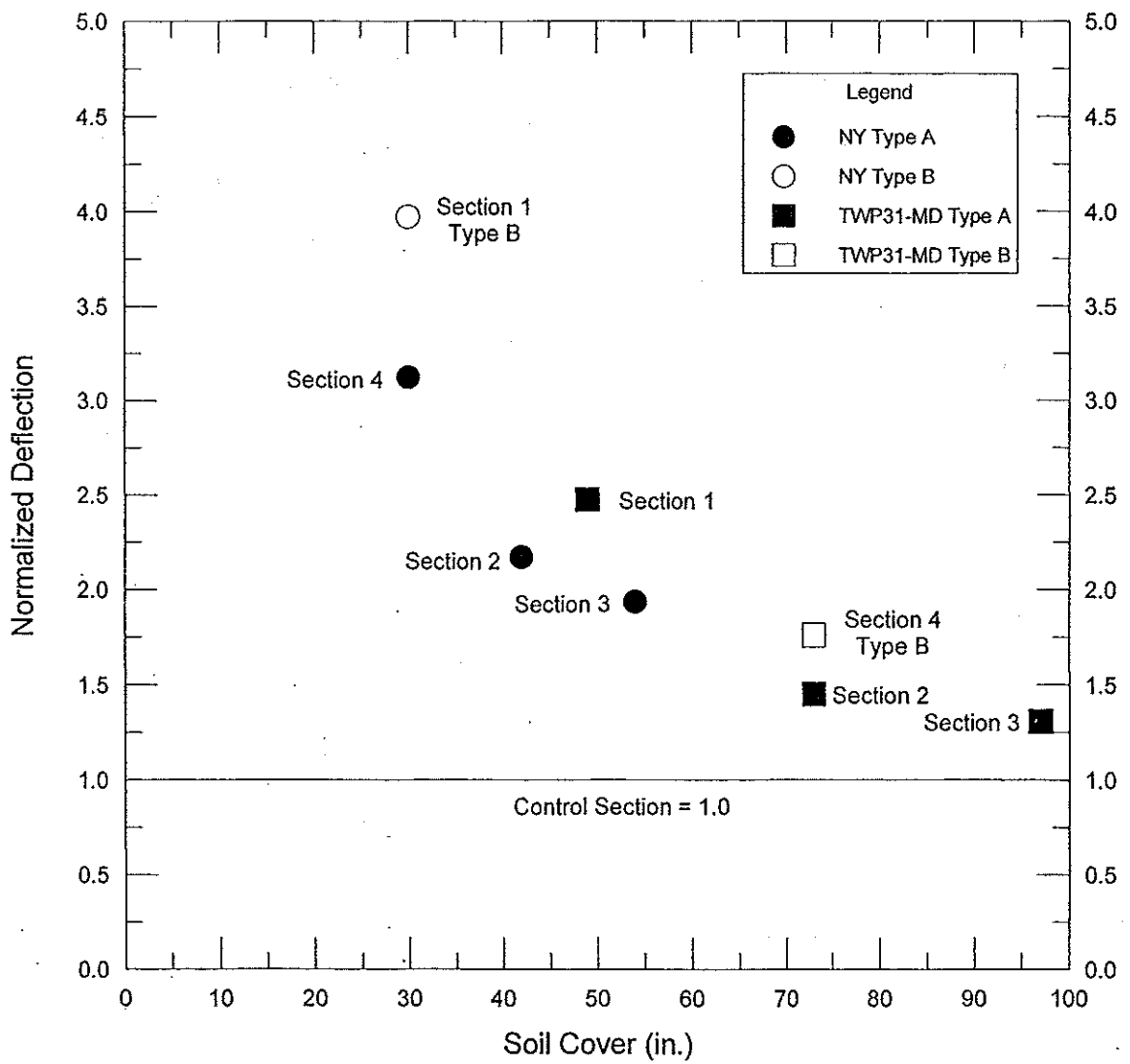


Figure 2.29 Normalized pavement deflection data for North Yarmouth and TWP31-MD (after Nickels, 1995)

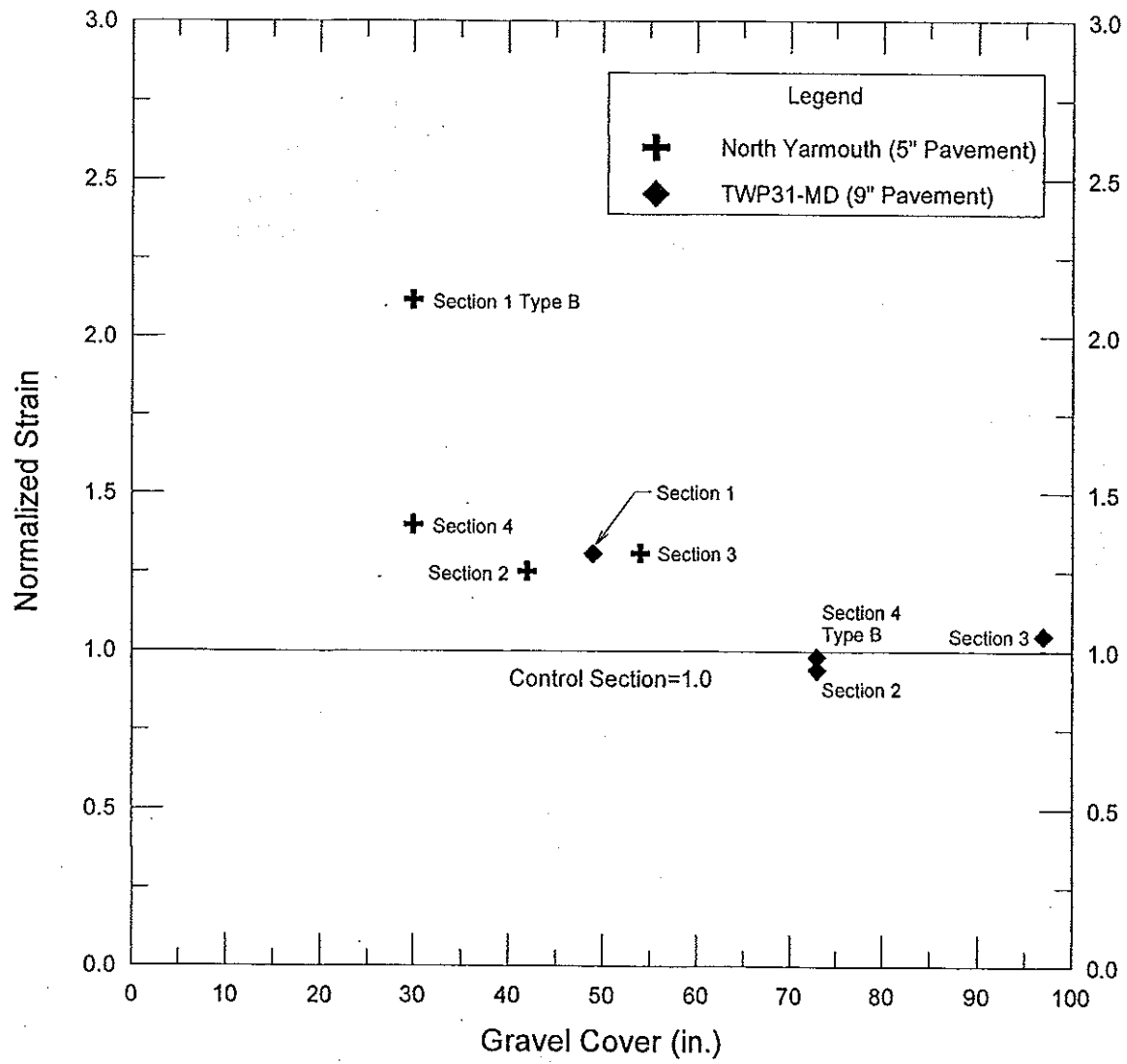


Figure 2.30 Normalized maximum asphalt tensile strains for North Yarmouth and TWP31-MD (after Nickels, 1995)

2.6 SUMMARY

Thermal properties, permeability, and case histories relating to the thermal and mechanical properties of tire chips were reviewed. Laboratory thermal conductivities of tire chips ranged from 0.097 W/m·°C (0.056 Btu/hr·ft·°F) for unwetted, thawed rubber buffings (80% passing the #10 (2.0-mm, 0.08-in.) sieve) at a water content of less than 1% (Shao, et al., 1995) to 0.38 W/m·°C (0.22 Btu/hr·ft·°F) for a 50% tire chip (20 to 40 mm, 0.8 to 1.6 in.)/50% ground tire (1 to 4 mm, 0.04 to 0.16 in.) mixture (Dore, et al., 1995). The values from Benson, et al. (1996) are not included in this comparison due to the much lower value of K compared to the other values found by more reliable methods.

In a study performed by Dore, et al. (1995), computer modeled pavement surface deflections ranged from 0.73 to 0.99 mm (0.029 to 0.039 in.) for tire chip thicknesses ranging from 250 to 450 mm (9.8 to 17.7 in.), and base cover thicknesses ranging from 350 to 450 mm (13.8 to 17.7 in.). Horizontal strain at the base of the pavement was calculated from the computer model to be from 194×10^{-6} in a section with 450 mm (17.7 in.) of cover and 250 mm (9.8 in.) of tire chips, to 213×10^{-6} in a section with 350 mm (13.8 in.) of cover and 450 mm (17.7 in.) of tire chips. Frost penetration and frost heave were estimated from a numerical bi-dimensional model developed at Laval University. Tire chips theoretically reduced frost penetration from 36 to 44 percent and frost heave from 72 to 90 percent.

The permeability of tire chips have been reported to range from 0.58 to 23.5 cm/s (0.60×10^6 to 24.3×10^6 ft/yr). Permeability of tire chip/soil mixtures was found to decrease as the percent soil in the mix increased.

Three case histories in the literature dealt mainly with thermal and drainage properties of tire chips. The frost penetration in the Richmond project was reduced by 22 to 28 percent. Heave was also substantially reduced. The Saint-Joachim, Quebec project saw a reduction in frost penetration depth up to about 10.4 percent, however, data was only available up until January 26, 1994. Tire chips were used on a town highway in Georgia, Vermont. Here visual inspection indicated that while untreated roadway sections were in poor condition, tire chip sections were visibly dry and free of rutting. No attempt was made to measure the thermal conductivity of these tire chips. The improvement in performance was attributed to the free draining nature of tire chips.

The final case histories were located in North Yarmouth, Maine and TWP31-MD, Maine. The effect of tire chips on pavement performance was investigated. Nickels (1995) found that while the deflection basin was much larger for tire chips, the strains at the base of the pavement could be acceptable with enough soil cover. Nickels (1995) concluded that a 0.6 m (2-ft) layer of Type A tire chips would have only a small effect on the durability of 127 mm (5 in.) of bituminous pavement for soil covers as little as 762 mm (30 in.).

3. MATERIAL CHARACTERIZATION FOR LABORATORY TESTS

3.1 MATERIAL SOURCES

Three types of materials were tested in laboratory thermal conductivity and permeability tests: tire chips, gravel, and tire chip/gravel mixtures. Five types of tire chips were obtained from four suppliers. The suppliers were: F&B Enterprises in New Bedford, Massachusetts; Palmer Shredding in North Ferrisburg, Vermont; Pine State Recycling in Nobleboro, Maine; and Sawyer Environmental Recovery in Hampden, Maine. The tire chips were:

- F&B Enterprises, 38-mm (1.5-in.) maximum size with glass belts (no steel belts)
- F&B Enterprises, 51-mm (2-in.) maximum size with partial removal of steel belts
- Palmer Shredding, 76-mm (3-in.) maximum size with steel belts
- Pine State Recycling, 76-mm (3-in.) maximum size with steel belts
- Sawyer Environmental Recovery, 51-mm (2-in.) maximum size with partial removal of steel belts

Photographs of the tire chips are given in Figures 3.1 through 3.5. The Pine State and Palmer chips (Figures 3.3 and 3.4, respectively) are the largest (76-mm (3-in.) maximum size) and contained large pieces, even bundles, of steel belts. Some of the pieces from Palmer Shredding were mostly steel belts with a small amount of rubber coating. Figures 3.2 and 3.5 show the 51-mm (2-in.) samples from F&B Enterprises, steel belted, and Sawyer Environmental Recovery. Although they both have the same maximum nominal size, the chips from Sawyer are slightly larger and less

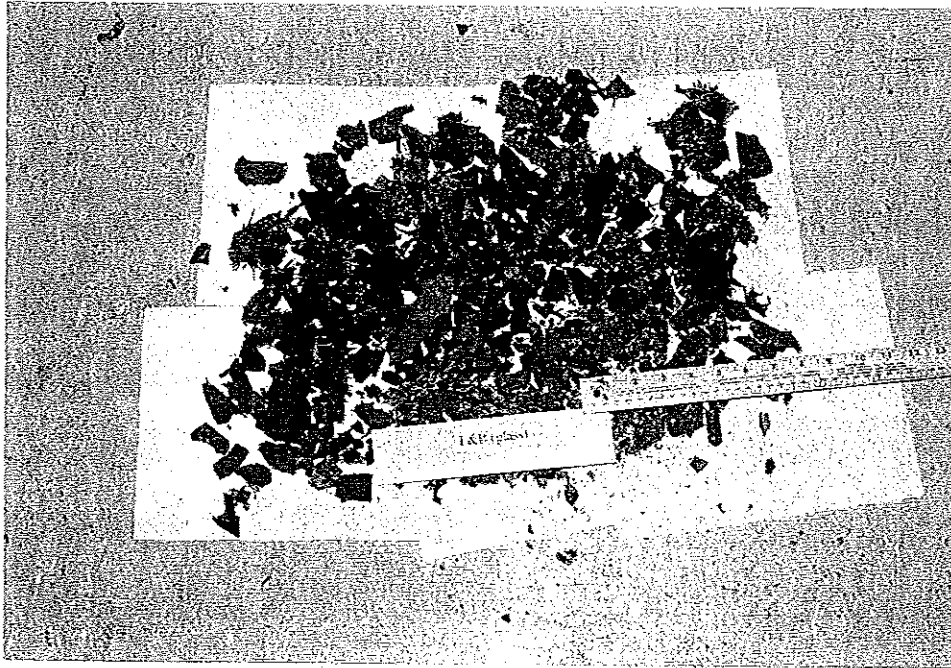


Figure 3.1 Photograph of F&B glass belted tire chips

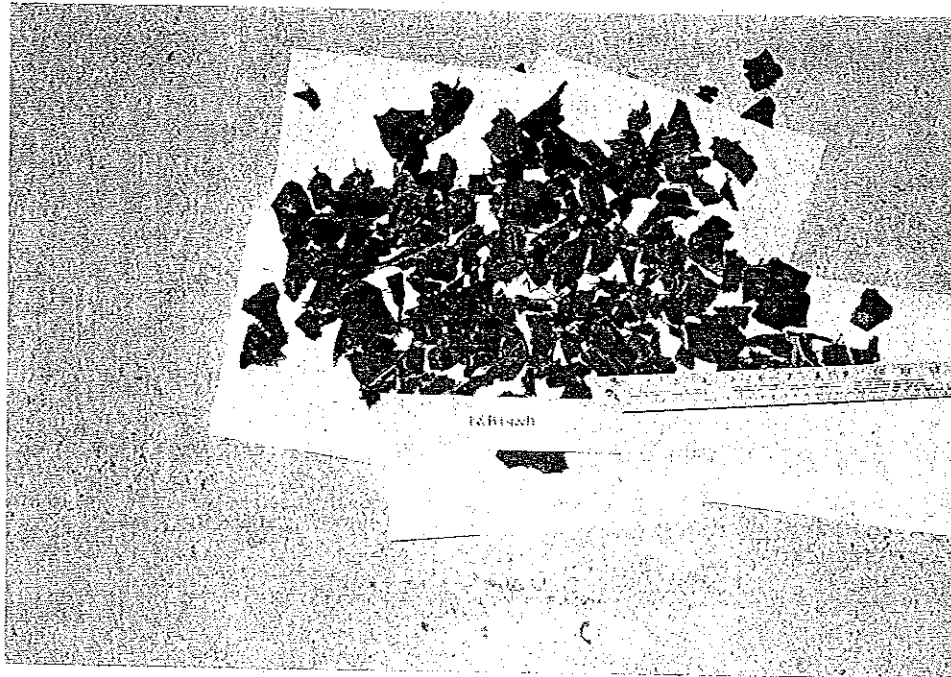


Figure 3.2 Photograph of F&B steel belted tire chips

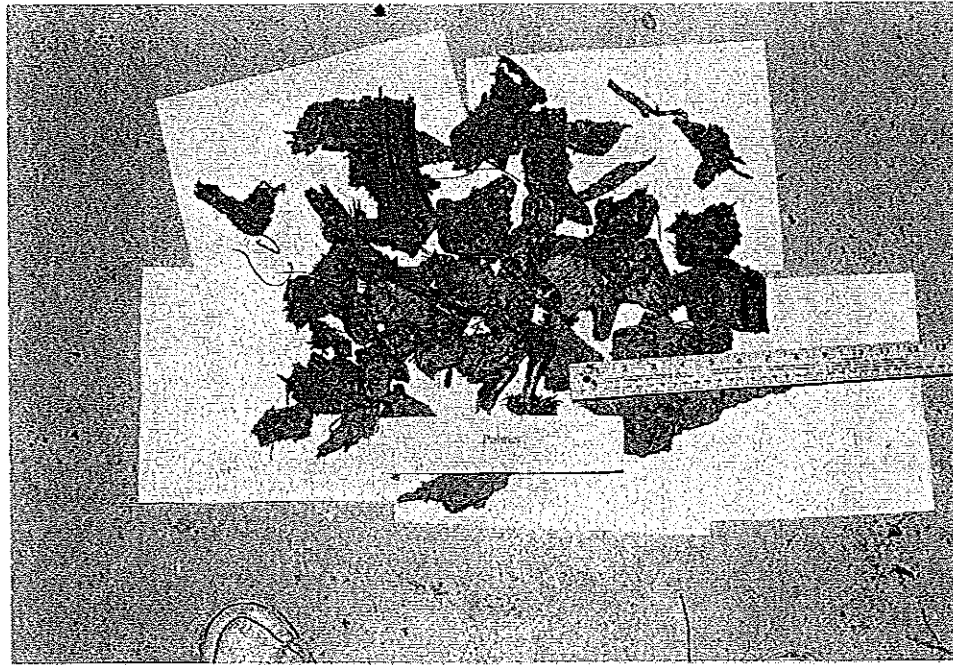


Figure 3.3 Photograph of Palmer tire chips

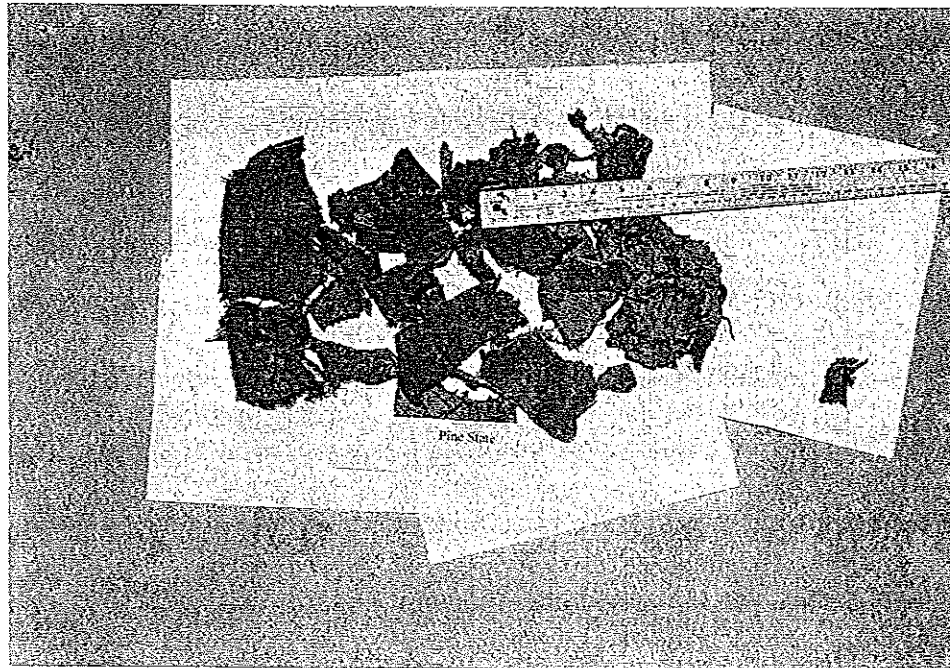


Figure 3.4 Photograph of Pine State tire chips

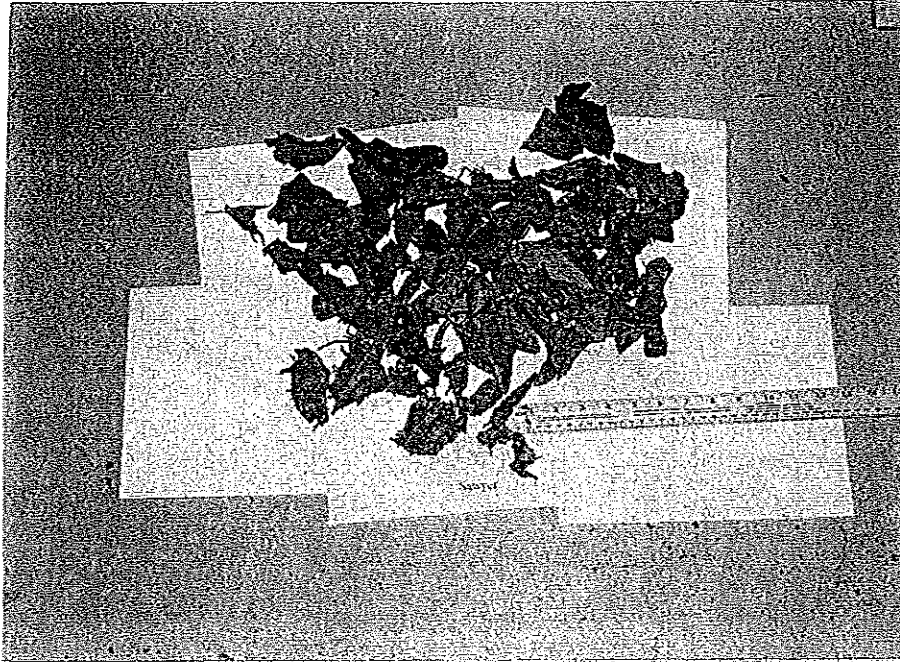


Figure 3.5 Photograph of Sawyer tire chips

equidimensional than the F&B steel-belted chips. Both of these samples have fewer steel belts than the 76-mm (3-in.) maximum size Palmer and Pine State chips. F&B glass-belted chips are the smallest chips.

The "38-mm (1.5-in.) maximum size with glass belts" as supplied by F&B Enterprises had a maximum size of about 75 mm (3 in.). They were reduced to 38-mm (1.5-in.) maximum size by Sawyer Environmental Recovery. The five types of tire chips included in this study encompass the range of tire chip sizes and proportion of steel belts likely to be considered for use in thermal insulation and drainage projects. Gravel was obtained from Owen J. Folsom Construction in Old Town, Maine. The gravel had a maximum size of 51 mm (2 in.) and meet Maine Department of Transportation

Requirements for Type D subbase aggregate. A photograph of the gravel is shown in Figure 3.6

Six tire chip/soil mixtures were tested in the laboratory. The proportions of tire chips and gravel were based on their solid volume and were expressed in terms of a percentage of the total volume of the sample. Compared to "percent based on weight", this was more representative of the quantity of tire chips and gravel in a sample because of the large difference in the specific gravity of tire chips and gravel (about 1.2 vs. 2.7).

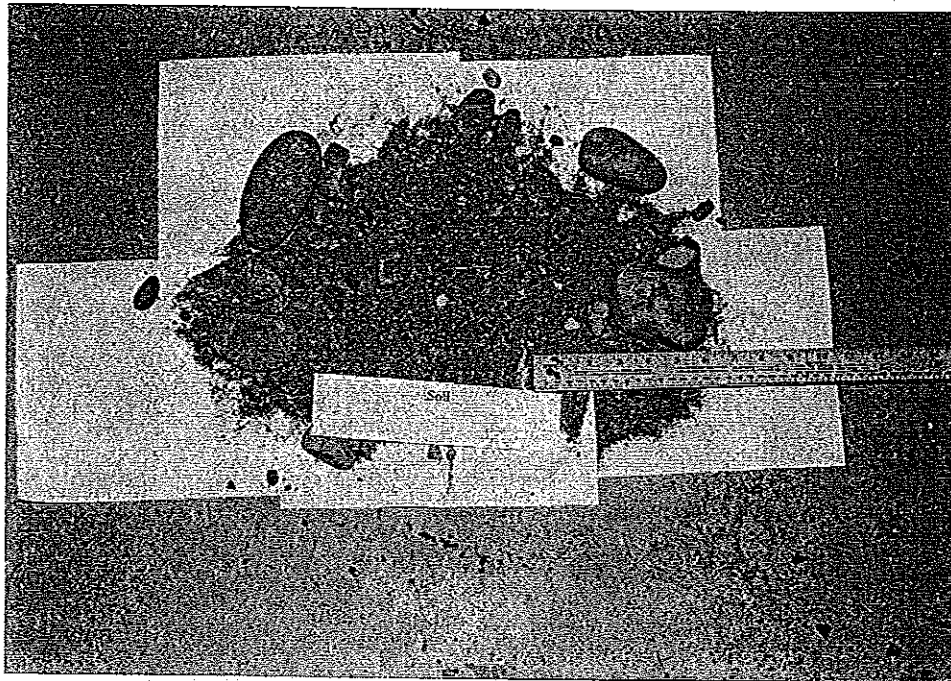


Figure 3.6 Photograph of gravel

The mixtures tested were:

- 33% 51 mm (2-in.) F&B steel belted chips / 67% gravel
- 67% 51 mm (2-in.) F&B steel belted chips / 33% gravel
- 33% 38 mm (1.5-in.) F&B glass belted chips / 67% gravel
- 67% 38 mm (1.5-in.) F&B glass belted chips / 33% gravel
- 33% 76 mm (3-in.) Palmer chips / 67% gravel
- 67% 76 mm (3-in.) Palmer chips / 33% gravel

Photographs of the tire chips/soil mixtures are given in Figures 3.7 through 3.12.

The gradation and specific gravity of the materials used for the laboratory thermal conductivity and permeability tests are given in the following sections. Additional gradation tests specific to the field trial are given in Chapter 9.

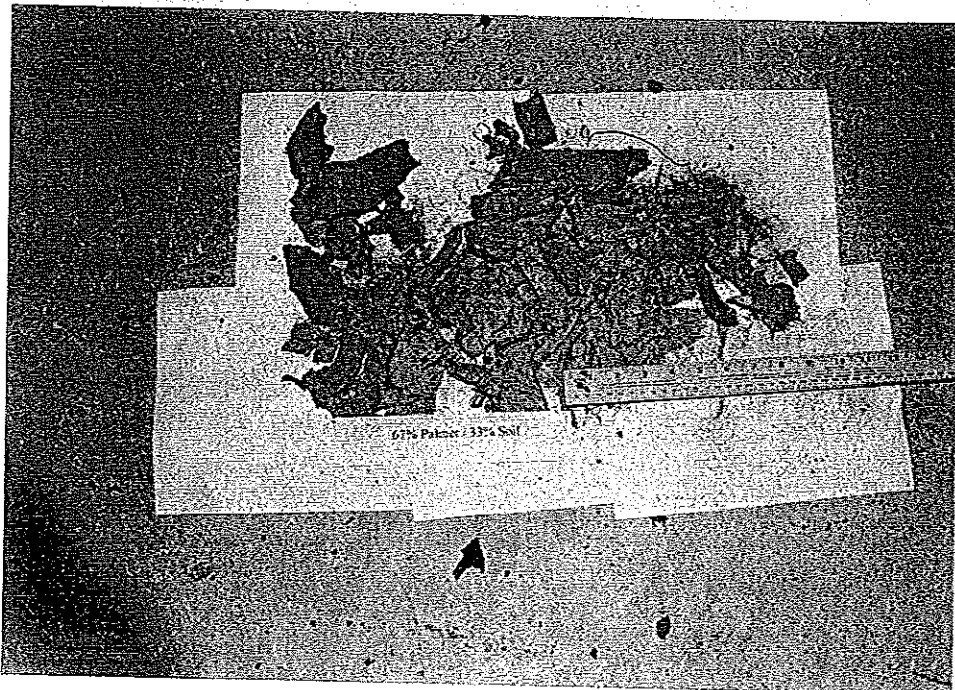


Figure 3.7 Photograph of 67% Palmer/33% gravel

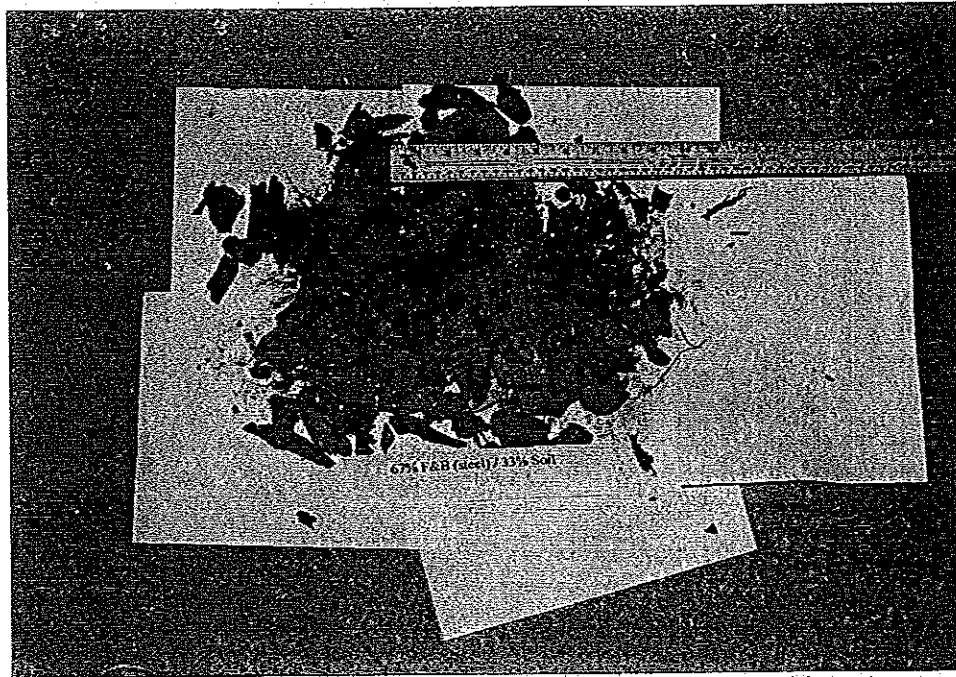


Figure 3.8 Photograph of 67% F&B steel belted/33% gravel

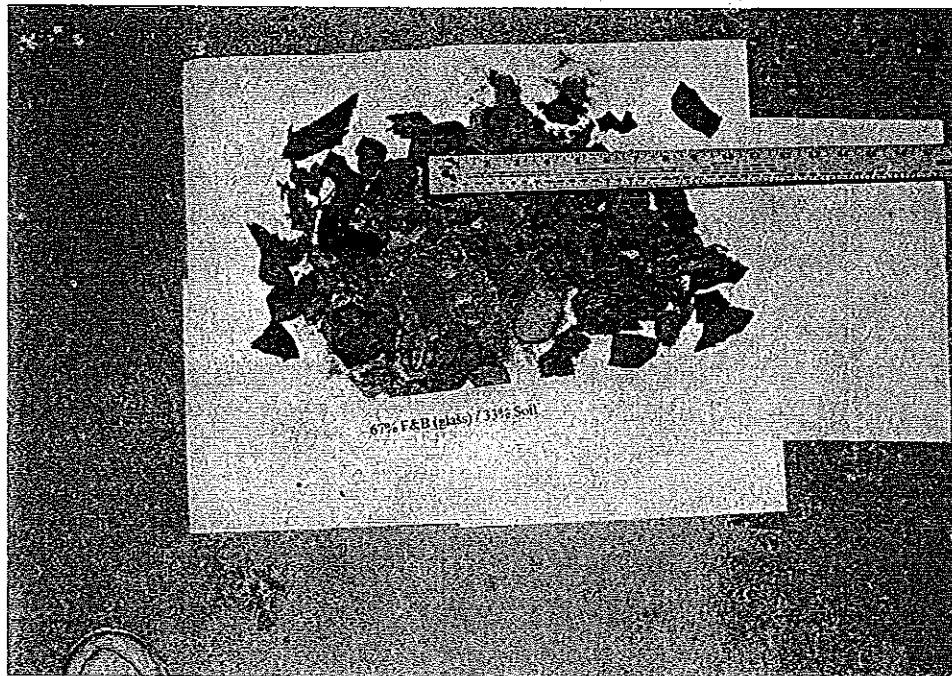


Figure 3.9 Photograph of 67% F&B glass belted/33% gravel

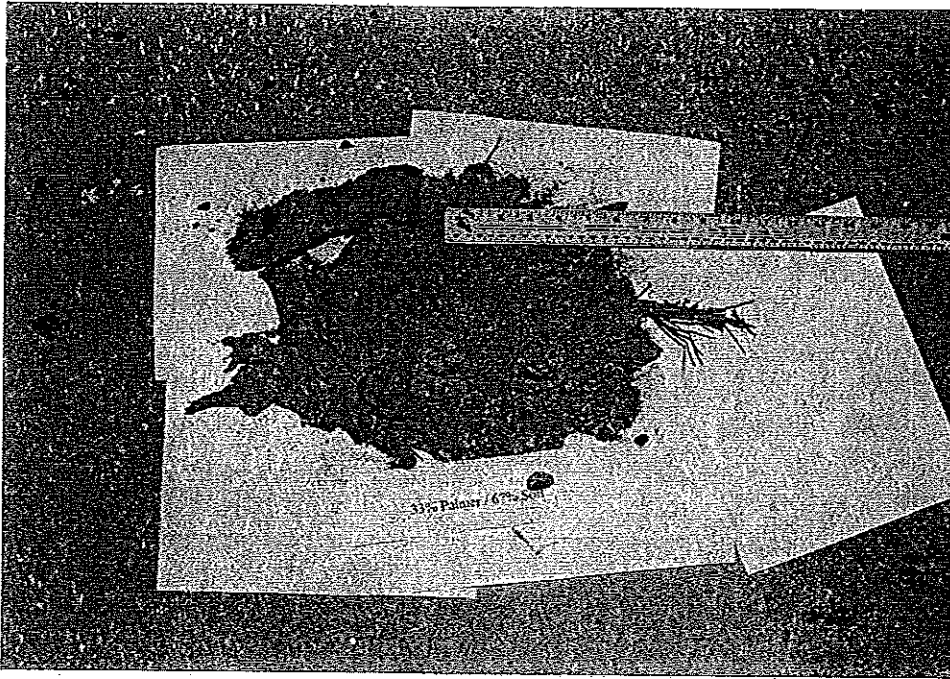


Figure 3.10 Photograph of 33% Palmer/67% gravel

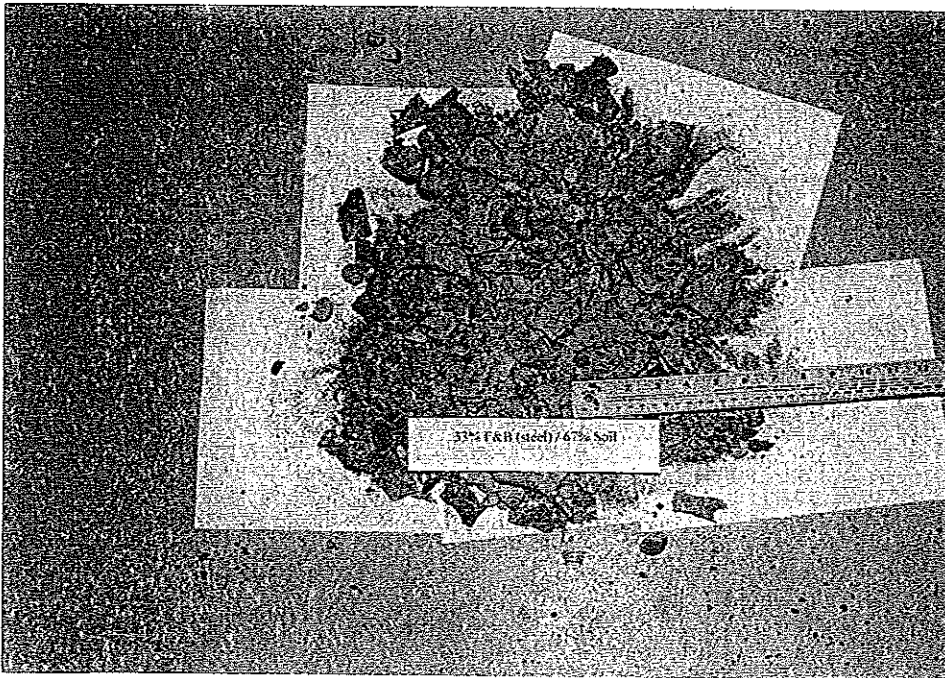


Figure 3.11 Photograph of 33% F&B steel belted/67% gravel

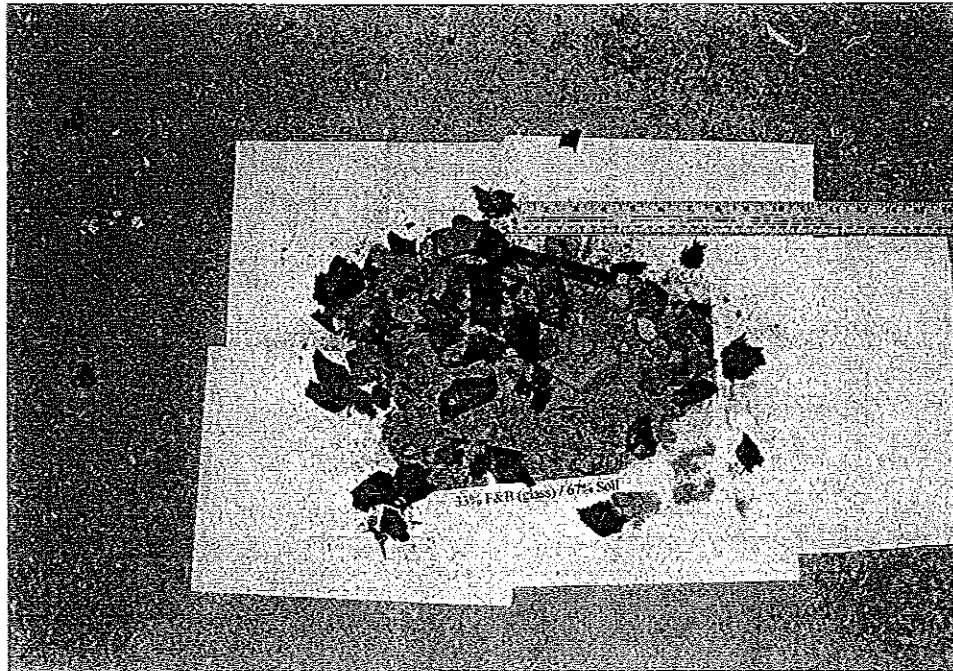


Figure 3.12 Photograph of 33% F&B glass-belted/67% gravel

3.2 GRADATIONS

The gradations were found using AASHTO designation T 27-87, "Sieve analysis of fine and coarse aggregates" (AASHTO, 1986). The following sieve sizes were used for tire chip samples: 76.2-mm (3-in.); 50.8-mm (2-in.); 38.1-mm (1-1/2-in.); 25.4-mm (1-in.); 19.05-mm (3/4-in.); and #4 (4.75-mm; 0.19-in.). For gravel samples, the following sieve sizes were used: 50.8-mm (2-in.); 25.4-mm (1-in.); 12.7-mm (1/2-in.); 6.4-mm (1/4-in.); #4 (4.75-mm; 0.19-in.); #10 (2.00-mm; 0.08-in.); #20 (0.85-mm; 0.03-in.); #40 (0.0425-mm; 0.02-in.); #100 (0.015-mm; 0.006-in.); and #200 (0.075-mm; 0.003-in.).

The gradation results for tire chips are shown in Figure 3.13 and the results for gravel are shown in Figure 3.14. The F&B and Sawyer samples are finer and more uniform than the Pine State and Palmer samples. Nearly 100% of the F&B and Sawyer

samples pass the 50.8 mm (2-in.) sieve, and 70% to 80% of the samples fall between the 38.1-mm (1-1/2-in.) and 19.05-mm (3/4-in.) sieve. The Palmer samples are the coarsest with a maximum size of 76 mm (3 in.) and only 10% passing the 25.4-mm (1-in.) sieve.

3.3 SPECIFIC GRAVITY

The specific gravity of tire chips were determined using AASHTO designation T85-85, "Specific gravity and absorption of coarse aggregate" (AASHTO, 1986), with the exception that the samples were air dried rather than oven dried prior to testing. The

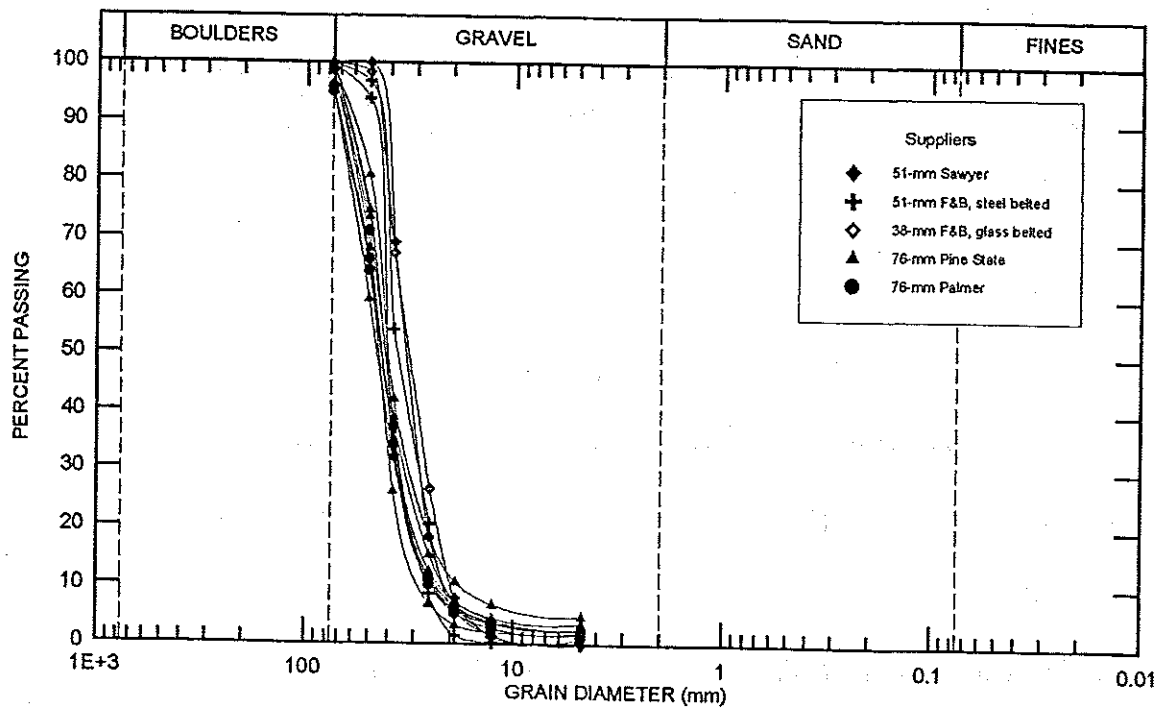


Figure 3.13 Gradation of tire chip samples

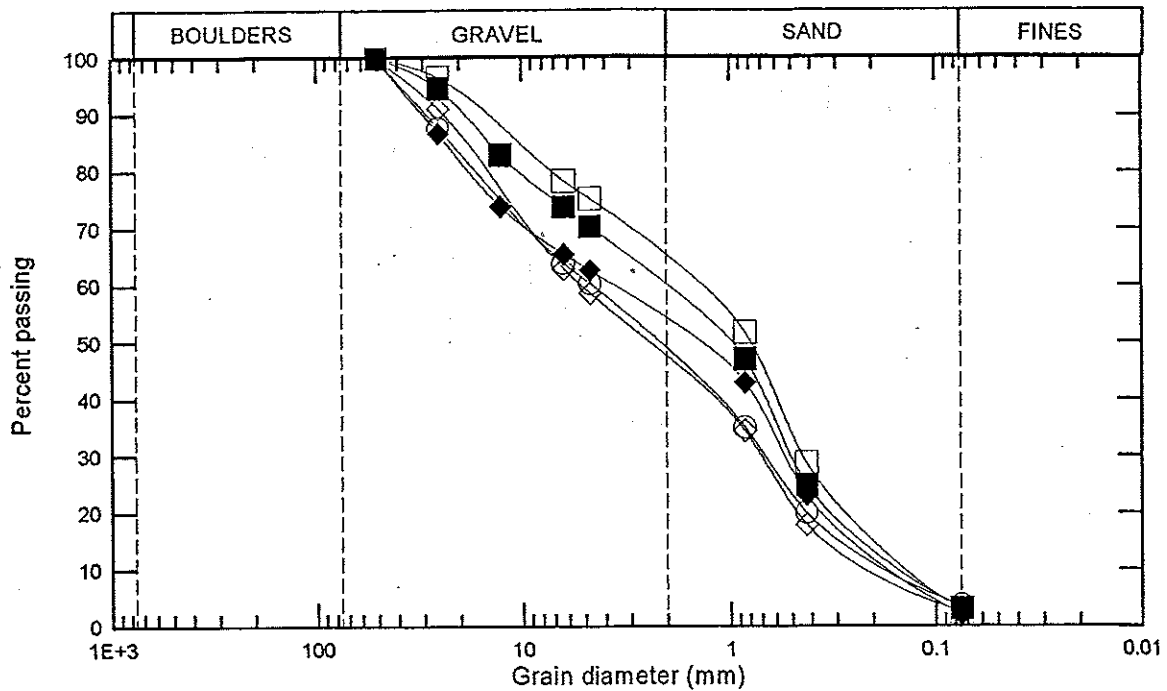


Figure 3.14 Gradation of gravel samples

results were reported as the apparent specific gravity which was the specific gravity of the solid making up the material. Some of the specific gravities were taken from the previous study by Humphrey, et al. (1992). The apparent specific gravities are presented in Table 3.1. Each value was the average of two tests. The specific gravity of gravel was also determined using AASHTO T85-85. The resulting specific gravity was 2.67. The specific gravity of tire chip/gravel mixtures were determined from the specific gravity of the tire chips ($G_{s,chip}$) and gravel ($G_{s,gravel}$), and the percentage of gravel volume relative to the total volume of the mixture (α) using the equation given below:

$$G_{s,mixture} = \alpha \cdot G_{s,gravel} + (1 - \alpha) \cdot G_{s,chip} \quad (3.1)$$

The specific gravities calculated with the above equation are given in Table 3.2.

Table 3.1 Summary of apparent specific gravity of tire chips

Supplier	Specific Gravity
F&B Enterprises (glass belted)	1.14*
F&B Enterprises (steel belted)	1.16
Pine State Recycling	1.24*
Palmer Shredding	1.27*
Sawyer Environmental Recovery	1.23*

*after Humphrey, et al. (1992)

Table 3.2 Specific gravity of tire chip/gravel mixtures

Mixture	Specific Gravity
33% 76 mm (3-in.) Palmer chips / 67% gravel	2.21
67% 76 mm (3-in.) Palmer chips / 33% gravel	1.73
33% 51 mm (2-in.) F&B steel belted chips / 67% gravel	2.17
67% 51 mm (2-in.) F&B steel belted chips / 33% gravel	1.66
33% 38 mm (1.5-in.) F&B glass belted chips / 67% gravel	2.15
67% 38 mm (1.5-in.) F&B glass belted chips / 33% gravel	1.64

4. TESTING METHODOLOGY

4.1 INTRODUCTION

The large size and high compressibility of tire chips made it necessary to design and build a customized test apparatus to measure their thermal conductivity. The design was based on ASTM C177-85 "Standard Test Method for Steady-State Heat Flux¹ Measurements and Thermal Transmission Properties by Means of the Guarded-Hot-Plate Apparatus" and C1044-90 "Standard Practice for Using the Guarded-Hot-Plate Apparatus in the One-Sided Mode to Measure Steady-State Heat Flux and Thermal Transmission Properties". The apparatus constructed for this project could accommodate a 305-mm (1-ft) thick sample with plan dimensions of 914 mm by 914 mm (3 ft × 3 ft). A vertical stress up to 17.9 kPa (375 psf) could be applied to simulate compression of the sample under the weight of overlying soil and pavement.

Thermal conductivity (K) is the time rate of steady state heat flow through a unit area of a homogeneous material induced by a unit temperature gradient in a direction perpendicular to that unit area (ASTM C168-90). It is computed as follows:

$$K = q \cdot \frac{\Delta L}{\Delta T} \quad (4.1)$$

where: q = heat flux

$\frac{\Delta L}{\Delta T}$ = temperature gradient in the direction of heat flow

¹ heat flux is the heat flow rate through a surface of unit area perpendicular to the direction of heat flow. It is also called heat flow rate density.

The thermal conductivity measured in this study is the apparent thermal conductivity whose value will vary with emittance² of bounding surfaces, specimen thickness, and air flow. These variations are caused by the following nonconductive modes of heat transfer: radiation and free convection. These modes will occur under field conditions. Thus, the apparent thermal conductivity as measured in this study is the value that should be used as the K in a field design.

4.2 TESTING METHOD

There are two kinds of standard test methods stated in ASTM for steady-state heat flux measurements: absolute (or primary) and comparative (or secondary). Both methods create a steady state heat flux through the specimen as shown in Figure 4.1.

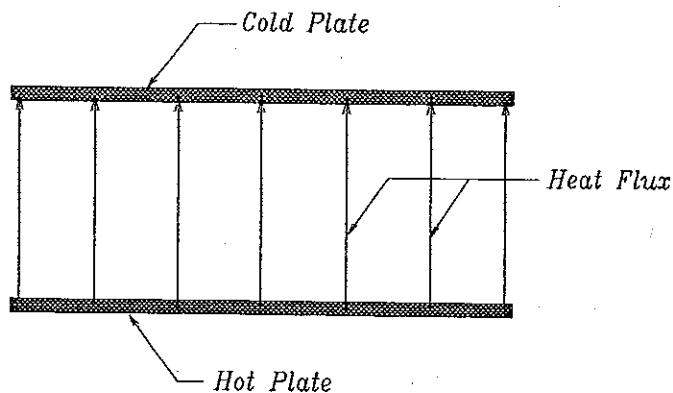


Figure 4.1 Principal of operation of test apparatus

The difference between these two methods is how the heat flux is measured. In the absolute method, the heat flux is determined from the heat flow rate and area through which the heat flow is passing. The heat flow, which is the input energy rate, is measured

² emittance is the ratio of radiant flux emitted by a specimen to that emitted by a black body at the same temperature and under the same conditions.

directly by a watt meter or by measuring the voltage and current. The thermal conductivity is computed by the following equation:

$$K = \frac{Q}{A} \cdot \frac{\Delta L}{\Delta T} \quad (4.2)$$

where: Q = heat flow rate

A = area through which Q passes

$\frac{\Delta L}{\Delta T}$ = temperature gradient in the direction of heat flow

In the comparative method, the heat flux is measured by heat transducers. The thermal conductivity of a specimen is computed by the following equation:

$$K = S \cdot E \cdot \frac{\Delta L}{\Delta T} \quad (4.3)$$

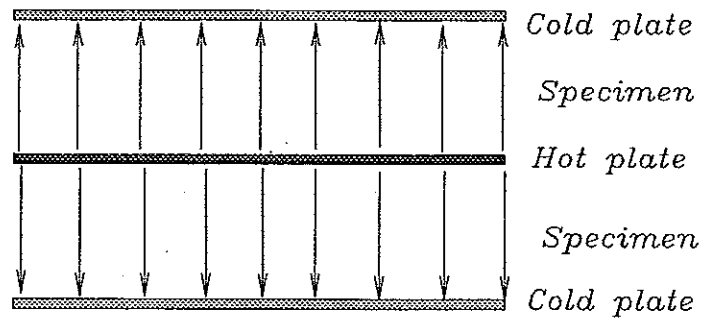
where: S = sensitivity of heat flow transducer

E = heat flow transducer output

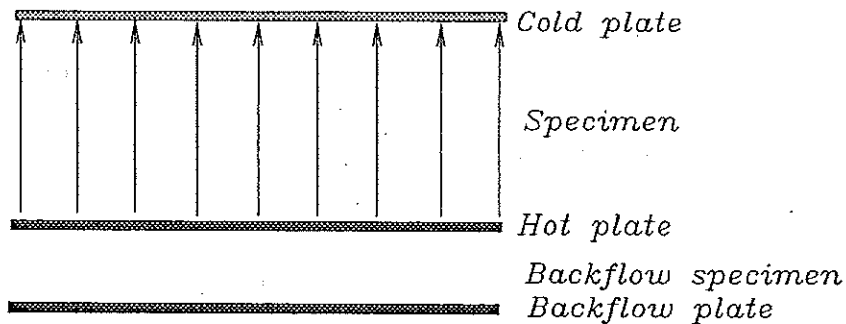
$\frac{\Delta L}{\Delta T}$ = temperature gradient in the direction of heat flow

In this method, a standard specimen with known thermal conductivity should be tested at the beginning of a test to determine the sensitivity of the heat flow transducer.

The absolute and comparative methods can be used with one-sided and double-sided mode apparatus. The difference between these two apparatus are shown in Figure 4.2. In the double-sided mode, the specimen is composed of two identical pieces: one located above and one located below the hot plate. The measured thermal conductivity is the average of these two pieces. In the one-sided mode, only one piece of specimen is used, and a backflow specimen and a heated backflow plate are used to force all the heat introduced at the hot plate to flow up through the test specimen. Details of the one-sided mode apparatus are discussed in the next paragraph.



(a) Double-Sided Mode



(b) One-Sided Mode

Figure 4.2 Comparison of one-sided mode and double-sided mode apparatus

The apparatus designed and built for this project is an one-sided mode apparatus using absolute steady-state heat flux measurement. The idealized principle of the method is straight forward. Figure 4.2(b) illustrates the core components of the idealized system: isothermal cold plate, isothermal hot plate and backflow plate. Sandwiched between these three units are the sample, whose thermal conductivity will be measured, and a backflow specimen. The material used for the backflow specimen is selected to have a similar thermal conductivity to the sample. The temperature of the backflow plate is adjusted to be identical to that of the hot plate. Consequently all the heat generated from the hot plate

will flow to the cold plate. The energy input to the hot plate is measured to obtain the heat flow rate for use in Equation 4.2

The differences between the idealized principle and the experimental realities lead to distortions of the isothermal surfaces and lines of constant heat flux density within the test volume. The deviations are caused by specimen inhomogeneities and edge unbalance, which is temperature differences between the outer edge of the assembly and the surrounding environment. Consequently, the power supplied to the hot plate is not exactly equal to that which flows through the test volume. The measured power can be either too small or too large depending on the direction of the edge unbalances (ASTM C177). Minimizing the edge unbalance increases the accuracy of the results. The following discussion shows how this was accomplished for this study.

4.3 APPARATUS

The apparatus is called a one-sided mode insulated-hot-plate apparatus. The apparatus is composed of three parts: sample container, energy source, and data acquisition system. The detailed configuration of each part is described below.

4.3.1 Sample container

A cross section and a plan through the sample container are shown in Figures 4.3 and 4.4. Photographs of the apparatus are shown in Figures 4.5 through 4.7. The sample container was a wooden box made by four pieces of 18-mm (3/4-in.) thick plywood and reinforced by 2x4's at each corner. The sides of the container are insulated with 305 mm

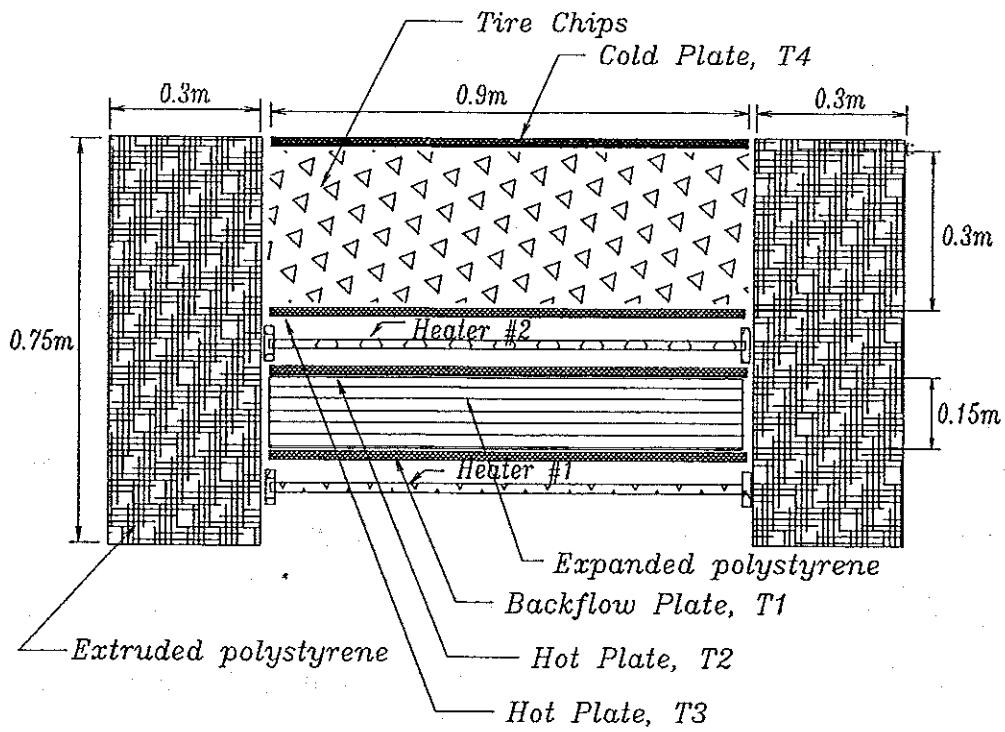


Figure 4.3 Cross-section of the one-sided mode insulated-hot plate apparatus

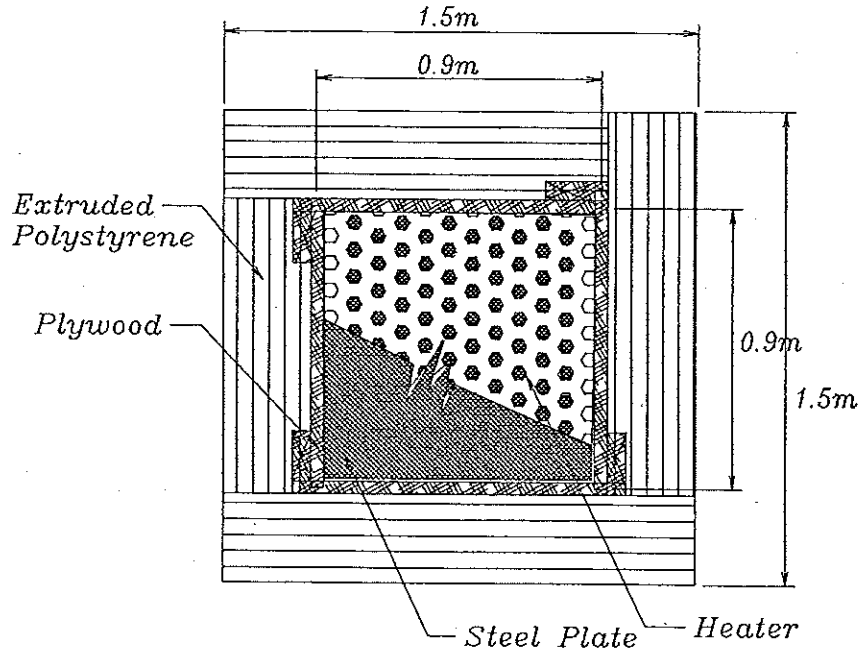


Figure 4.4 Plan view of the apparatus

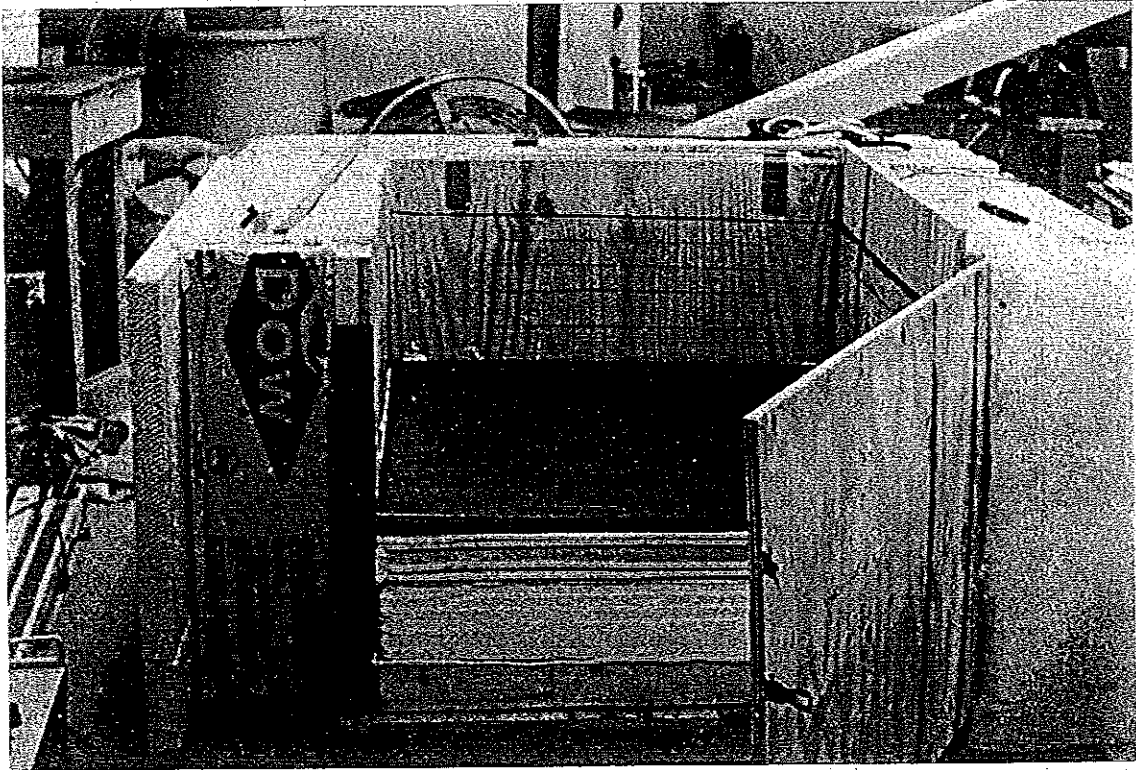


Figure 4.5 Picture showing side view of the apparatus

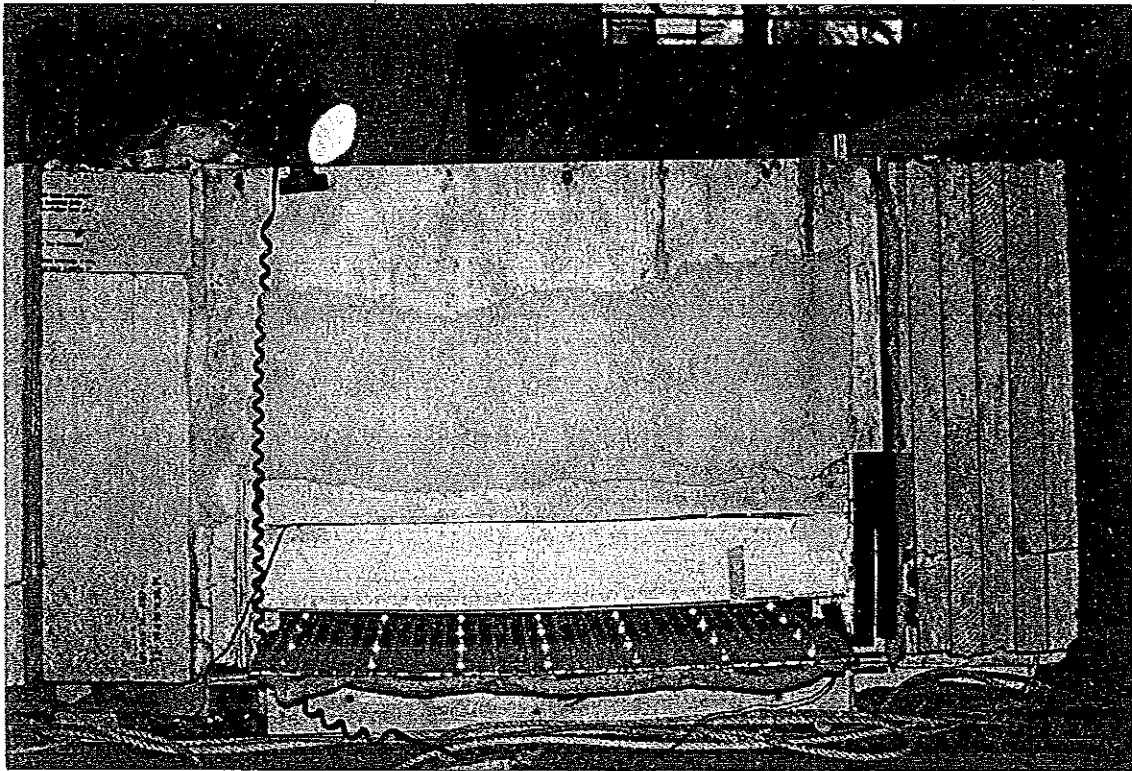


Figure 4.6 Picture showing the light bulbs of Heater #1

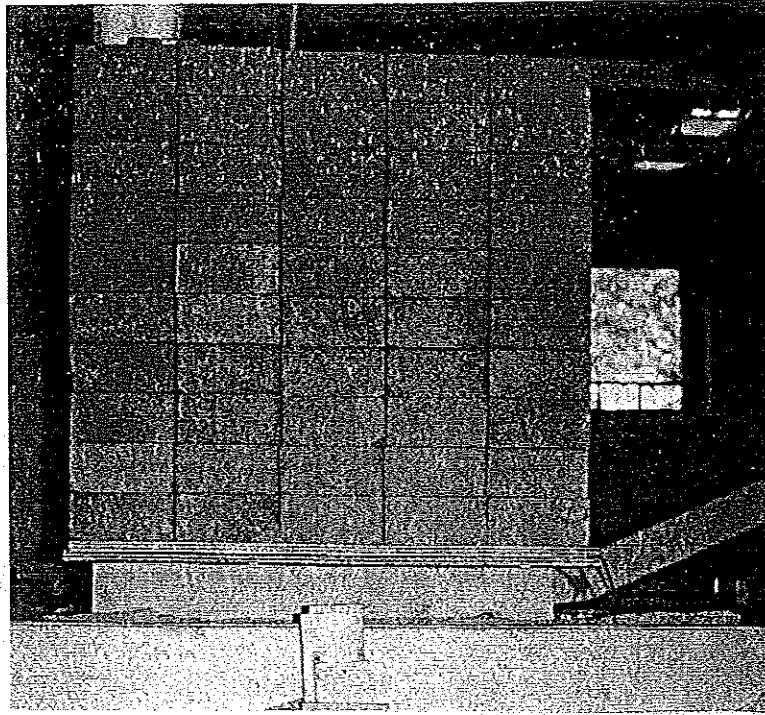


Figure 4.7 Picture of the apparatus under full surcharge

(1 ft) of extruded polystyrene insulation with a mean thermal conductivity of $0.029 \text{ W/m}\cdot\text{C}^\circ$ ($0.017 \text{ Btu/hr}\cdot\text{ft}\cdot\text{F}^\circ$) at 42°C (75°F). Within the wooden box are four steel plates, the test specimen, the backflow specimen, and two heaters. The plan dimensions of the steel sheets and heaters are the same as the interior plan dimensions of the sample container which are 914 mm by 914 mm (3 ft by 3 ft). The steel plates are labeled from bottom to top as backflow plate T1, hot plate T2, hot plate T3, and cold plate T4. Sandwiched between the hot plate T3 and the cold plate T4 is the test specimen. The backflow specimen is between the backflow plate T1 and hot plate T2. The thickness of the test specimen, which is also the distance between cold plate T4 and hot plate T3, is about 305 mm (1 ft). One heater (labeled as Heater #1) is placed beneath the backflow plate T1 and another heater (Heater #2) is placed between the hot plates T2 and T3.

The functions of the cold (T4) and hot (T3) plates are to create isothermal surfaces in contact with both sides of the test specimen. The hot plate T3 acts as a heat source while the cold plate T4 acts as a heat sink. In addition, the hot plate T3 supports the bottom of the sample and the cold plate T4 distributes the applied surcharge load to the sample. Steel was chosen for the hot plates because it has a high thermal conductivity and relatively thin sheets are stiff enough to carry the applied load with little deformation. In this design, the upper two plates (T3 and T4) are 6-mm (1/4-in.) thick steel sheets and the lower two plates (T1 and T2) are 3-mm (1/8-in) thick steel sheets. The arrangement and the function of these plates are discussed below.

The hot plate T3 acts as a heat source which adds a measured amount of energy into the system. The condition of heat flow only through the sample is created by use of the backflow plate and backflow specimen. Theoretically, if the temperatures of the hot plate T2 and the backflow plate T1 are the same, then the heat exchange between these two plates (Q_b) will be zero. Consequently all the energy input at the center heater (Heater #2) will flow only through the test specimen to reach the cold plate. In practice, the condition of $Q_b=0$ cannot be precisely achieved. However, the energy exchange Q_b is minimized by adjusting the energy input to the lower heater (Heater #1) to maintain the temperature of the backflow plate T1 as close as possible to the temperature of the hot plate T2. To minimize the energy exchange between the hot plate and the backflow plate (Q_b), the backflow specimen should have a low heat capacity³ to minimize the time needed to achieve steady-state test conditions and have a thermal conductivity similar to that of

³ heat capacity is the amount of heat to change the temperature of a unit mass of material by one degree C.

the test sample. Rigid insulation board meets these criterion. Also, the backflow specimen should be thick enough to reduce Q_b to a very small value if the temperature of the hot plate and the backflow plate are not identical. However, the thicker the backflow specimen, the larger the edge heat loss. Thus, there will be an optimal thickness of the backflow specimen that will result in a minimum uncertainty in Q_b (Peavy and Rennex, 1986). According to ASTM C177, to maintain the edge losses to below about 0.5%, the recommended maximum thickness of a specimen is one-third the plan dimension of the sample. In this test, 152 mm (6 in.) of expanded polystyrene with a thermal conductivity of $0.144 \text{ W/m}\cdot\text{C}^\circ$ ($0.083 \text{ Btu/hr}\cdot\text{ft}\cdot\text{F}^\circ$) is used as the backflow specimen.

A test error is introduced because of heat loss at the perimeter of the test sample. This is termed edge loss or edge unbalance. In general, the temperature of the room in which the test is conducted is different from the temperature of the specimen, so some energy exchange between the specimen and the environment occurs. To minimize the uncertainty in energy input to the sample caused by this edge loss, ASTM standards recommend a guarded-hot-plate. A guarded-hot-plate is shown in Figure 4.8. The function of the guard portion of the isothermal hot plate is to provide the additional power necessary to minimize edge unbalance of the central portion of the specimen. However, a guarded hot plate apparatus that could accommodate tire chips would be very large, which was neither economical nor practical. As an alternative, extruded polystyrene foam was used to insulate the edge thereby reducing edge loss. Later in this chapter, it will be shown that the lateral heat loss can be reduced to an acceptable level by using 304 mm (1 ft) of extruded polystyrene insulation.

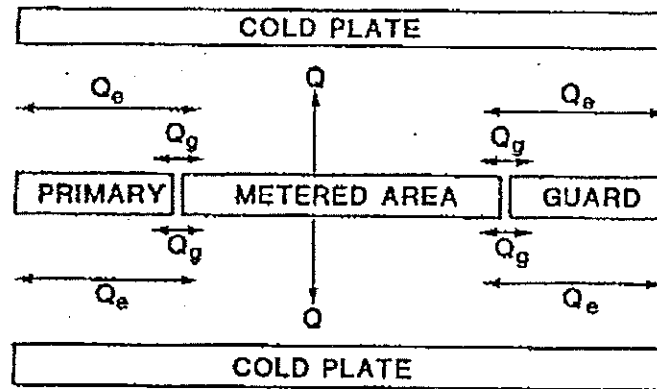


Figure 4.8 Illustration of guarded hot plate apparatus (after ASTM C177, 1992)

4.3.2 Energy source

ASTM C518 requires that the temperature difference across the specimen be not less than 10°C (18°F). For the expected thermal conductivity of tire chips and tire chip/gravel mixtures, only a small amount of energy was needed to cause a large temperature difference across the test specimen. In this particular case, the size of the test specimen is 914 mm by 914 mm (3 ft by 3 ft) in plan with a thickness of 305 mm (1 ft). Based on the field trial conducted in Richmond, Maine the expected thermal conductivity of tire chips was 0.17 to $0.52 \text{ W/m}\cdot^{\circ}\text{C}$ (0.1 to $0.3 \text{ Btu/hr}\cdot\text{ft}\cdot^{\circ}\text{F}$). Thus, only about 8.5 W (29 Btu/hr) is needed to create a 10°C (18°F) temperature difference across the 305-mm (1-ft) thick specimen. This small amount of energy has to be distributed uniformly across the 914 mm by 914 mm (3 ft by 3 ft) area.

To meet the criteria given above, two special heaters were built. A set of Christmas light bulbs was used as a heat source in each heater. The heater was a 914 mm by 914 mm (3 ft by 3 ft) peg board framed by 19-mm ($3/4$ -in.) thick pine. The Christmas light bulbs were uniformly distributed in the holes in the peg board as shown in Figures 4.9 and

4.10. The electric resistance of the series of light bulbs was 24Ω . The input energy is adjusted by controlling the input voltage.

The input energy is determined from a voltage meter and a current meter. AC power measurements are more prone to error than DC measurements, so DC power was used. Two KEPCO model ATE150-0.3M variable DC power supplies were purchased for this purpose. The maximum output of these power supplies are 150 V and 0.3 A with a resolution of 0.1 V. The required input voltage ranged from 60 V to 100 V for tire chips, gravel, and tire chip/gravel mixtures. The input voltage and current are measured by two digital multimeters. The voltage reading is accurate to 0.1 V and the current reading is accurate to 0.1 mA. The arrangement of the equipment is shown in Figures 4.11 and 4.12.

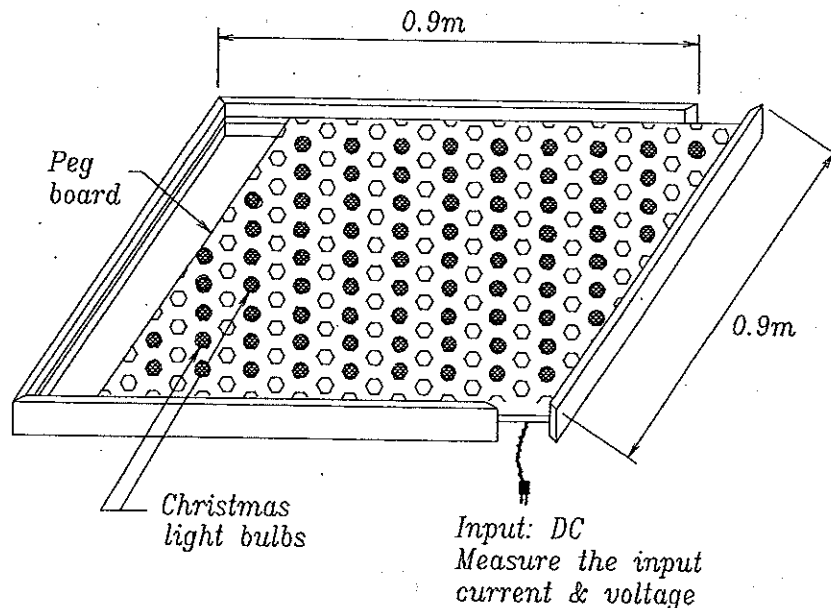


Figure 4.9 Diagram of a heater

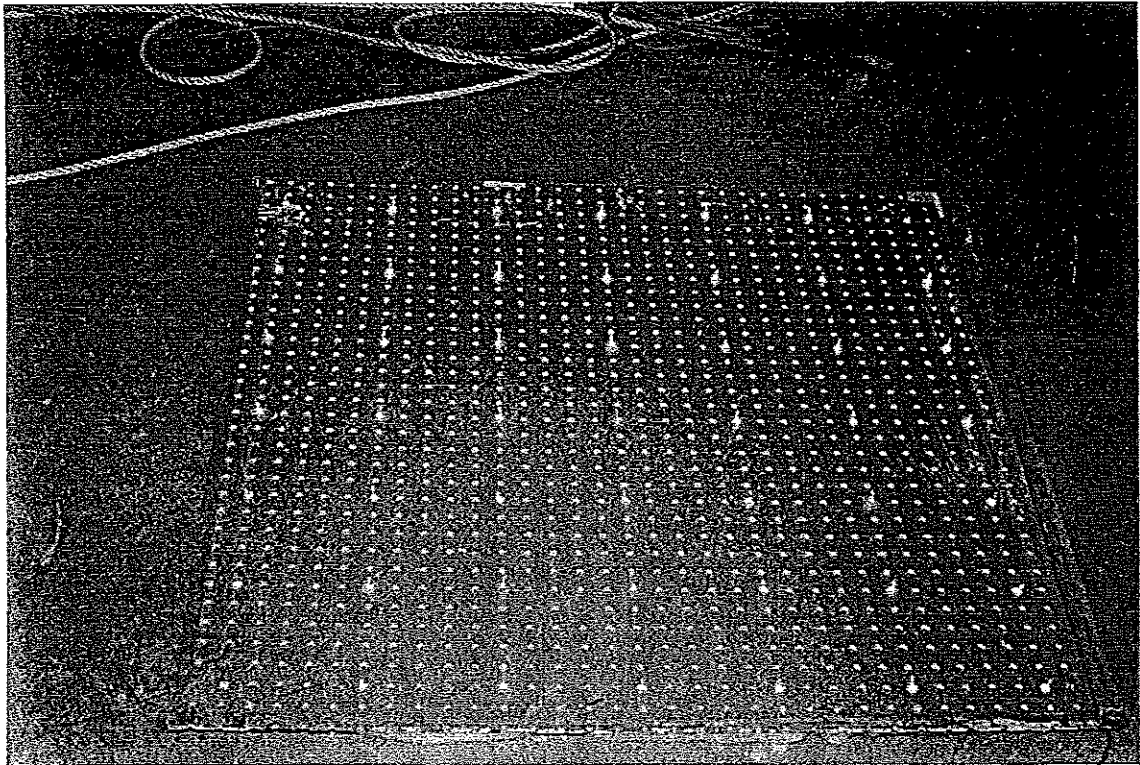


Figure 4.10 Picture of a heater

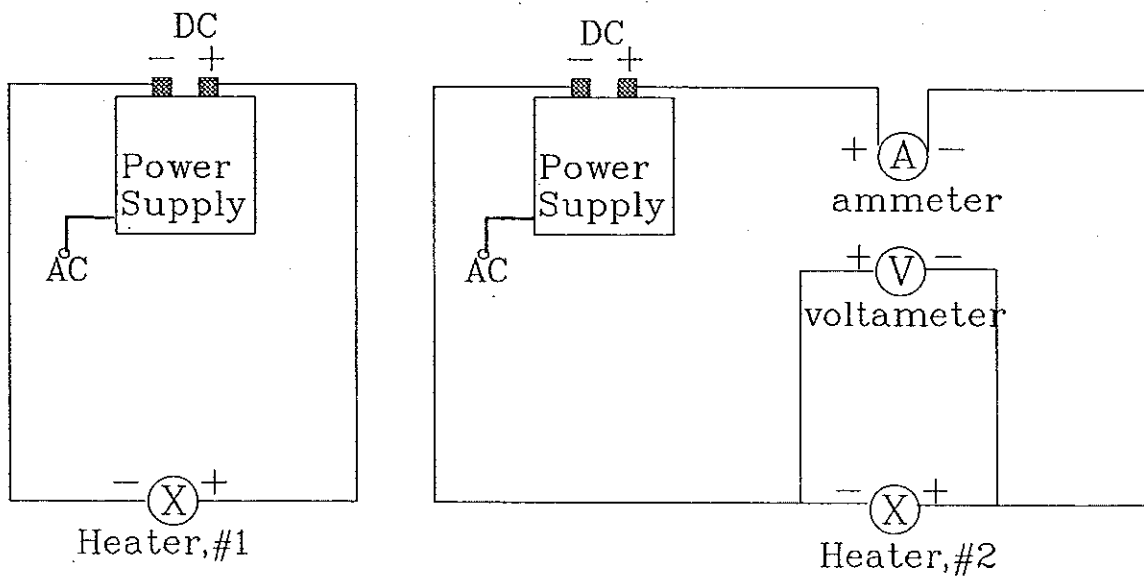


Figure 4.11 Energy source and measurement

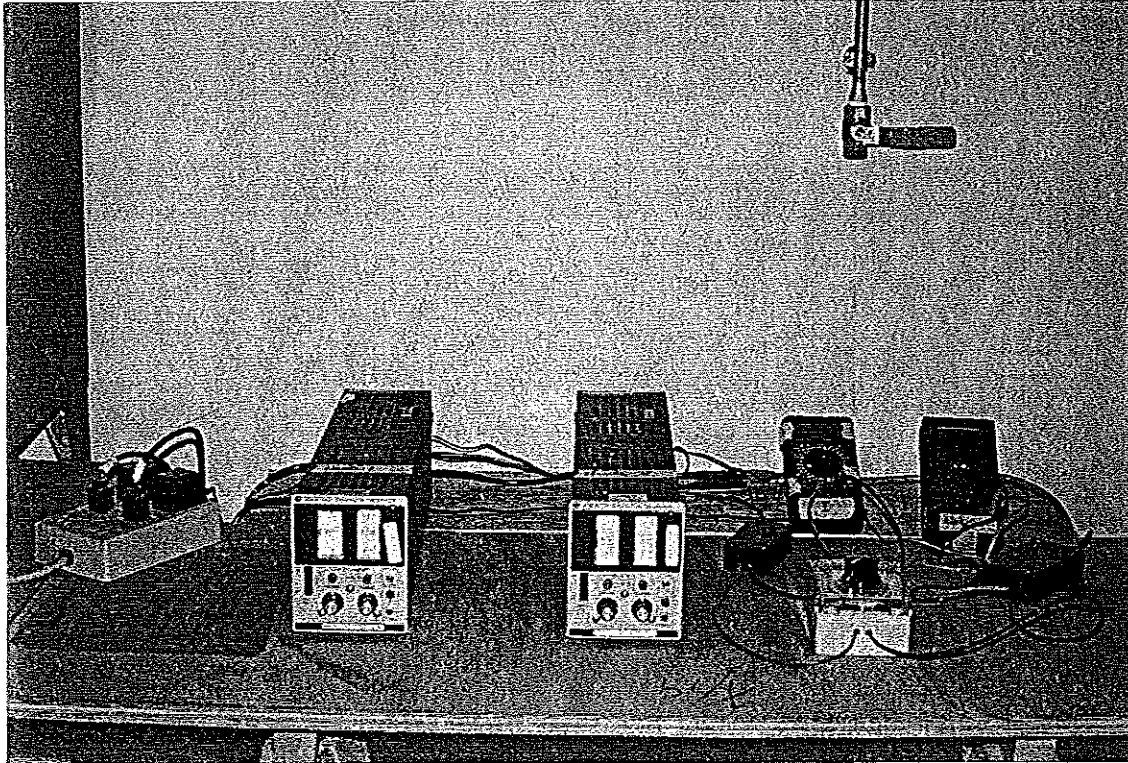


Figure 4.12 Picture of the power supplies and multimeters used in the test

4.3.3 Data acquisition system

The temperatures were measured by the data acquisition system. The system was made up of an analog to digital converter card, a terminal panel, temperature sensors, and data acquisition software.

Thermocouples⁴ were used as the temperature sensors. Teflon insulated twisted/shielded Type T thermocouples (*Copper-Constantan*) were selected (Omega Engineering, Inc. model No. as FF-T-24-TWSH) which have a working temperature range from -200 to 350°C (-328 to 662°F). Twenty-four gage wire was selected because this

⁴ A thermocouple is "a temperature-measuring device formed by joining the ends of two strips of dissimilar metals in a closed loop, with the two junctions at different temperatures." The "voltage that arises in this circuit is proportional to the temperature difference between the junctions", thus, "the temperature at one junction can be determined if the other junction [cold junction] is maintained at a known temperature" and the resulting voltage difference is measured. (Columbia University Press, 1995)

provided a good balance between higher stability⁵ compared to smaller wire and smaller heat leakage compared to larger wire. Shielded wire results in less noise from outside electrical sources. The voltage difference produced by the thermocouples and subsequent conversion into temperature was done by computer. The thermocouples wires were connected to a Strawberry Tree model T21 terminal block and Strawberry Tree model ACPC-16-16-T42 Analog to Digital board which was installed in a 286 computer.

The temperature of the isothermal steel plates are required to determine the thermal conductivity. Four thermocouples were installed in the hot plate T3 which was beneath the test specimen and three in the cold plate T4 which was above the test specimen. The average of these four or three thermocouple readings are used to represent the temperature of the hot and cold plates, respectively. As a result, the temperature of both sides of the test specimen was determined.

Only the temperature difference between the top and bottom of the backflow specimen was needed. To accomplish this, twenty-five thermocouple pairs were connected in series (called a thermopile). The purpose of this kind of connection is to amplify the total voltage difference between T1 and T2. They were joined in such a way that the total output of this connection is zero when the temperature of these plates T1 and T2 is identical.

The temperature measured by a thermocouple is determined from the voltage output of the thermocouple based on an empirical relationship between voltage and temperature.

⁵ high stability results in a decreased tendency for the temperature to drift with time due to higher thermal inertia

This relationship is nonlinear but it can be approximated by a polynomial equation, which is called a thermocouple characteristic curve. The practical way to obtain this relationship is to divide the thermocouple characteristic curve into a certain number of temperature ranges or sections, and each section is approximated by a lower order polynomial such as a third-order polynomial.

The procedure for installing the thermocouples in the steel plate was as follows. A 6 mm (1/4 in.) diameter hole was drilled in the steel plate and the tip of the thermocouple was inserted in the hole, resting against the side of the hole. Silicon caulking was then used to fill the hole and fix the thermocouple to the plate. Care was used to make sure that the thermocouple tip and the steel plate were in good contact. Otherwise the thermocouple would measure the temperature of the silicon caulking.

4.4 INTERPRETATION OF RESULTS

The primary data required to calculate thermal conductivity include electrical power, surface temperatures, sample plan area, and sample thickness. Except thickness and plan area, the data are either calculated from other more fundamental measurements or are converted by an electrical device. The manner in which these variables can be obtained and their accuracy or uncertainty are discussed below.

4.4.1 Calculation of thermal conductivity

Thermal conductivity K (W/m \cdot °C or Btu/hr-ft \cdot °F) is computed using:

$$K = q \cdot \frac{\Delta L}{\Delta T} = \frac{3.413 \cdot I \cdot U}{A} \cdot \frac{\Delta L}{T_3 - T_4} \quad (\text{Btu/hr-ft}\cdot\text{°F}) \quad (4.4)$$

$$(1 \text{ Btu/hr-ft}\cdot\text{°F} = 1.728 \text{ W/m}\cdot\text{°C})$$

where: q = heat flow rate per unit cross-section area (Btu/hr-ft²)

$\Delta L/\Delta T$ = temperature gradient (ft/°F)

ΔL = the thickness of test specimen (ft)

T_3 = temperature of hot plate (°F)

T_4 = temperature of cold plate (°F)

I = current input from heater (A)

U = voltage input from heater (V)

A = plan area (ft²)

In this test, the plan area A is a constant which is 0.84 m² (9 ft²); I and U are the input to the middle heater (Heater #2). They are measured by multimeters. The constant 3.412 is the conversion between Btu/hr and Watt (1 A·V = 1 Watt).

4.4.2 Precision and bias

There are some possible sources of error in the measured values of thermal conductivity, including heat radiation, heat convection, and resolution of the energy and temperature measuring systems. Detailed analyses are given below.

1) *Error in input energy caused by heat radiation*

The heat loss caused by the heat radiation cannot be reduced to zero in this design. However, the temperature level in this test is so low that the heat loss caused by radiation can be ignored (McQuiston and Parker, 1977).

2) *Heat loss caused by convection between gaps*

There are some small gaps located between the wooden box and the surrounding insulation, and at the connections between pieces of the sample container. Most of the

gaps were filled with an aerosol based expanding foam insulation. However, there were still some small gaps that could not be filled with this insulation. As a result, there will be some heat convection between these gaps that will cause some uncertainty in the input heat flux. This kind of heat convection can be classified as convection between two parallel surfaces. According to the heat transfer mechanics, free convection between two flat plates depends on the gap width and the inclination angle of the plates. The convection decreases rapidly as the gap width decreases. When the gap is smaller than 10 mm (0.4 in.), the convection will be very small and can be ignored (Kreith and Dreider, 1978). The gaps in the apparatus used in this test were typically about 2 mm (0.1 in.). Thus, the heat convection between the gaps can be ignored.

3) *Edge heat loss*

The uncertainty introduced by edge heat loss is the main concern in this design. According to ASTM C1044, a guarded-hot-plate should be used to minimize this uncertainty. However, this was not possible for this large scale design. Instead, 305 mm (1 ft) of insulation was used to minimize edge heat loss. Because there is heat conduction through the surrounding insulation materials, there is still heat loss at the edge. An analysis was done to determine how sensitive the test was to this source of error. The K value was corrected based on the estimated edge loss.

The edge heat losses include the heat loss at the edges of the sample, middle heater (Heater #2), and part of the back flow specimen. The error analyses used for the sample edge loss were based on the heat conduction equation (Equation 4.1). However, the heat flow at the edges of the sample is two-dimensional or three-dimensional, which means that

the temperature gradient within the surrounding insulation is different at each point. None the less, to make the analysis tractable, it was assumed that the temperature changed linearly through the insulation⁶. Thus, the temperature difference across the insulation leading to this heat loss were estimated as the temperature difference between the mean temperature of the inner side of the insulation adjacent to the edge of the sample and room temperature. The heat flow area was the four sides of the test specimen. The edge heat loss is computed as follows:

$$\begin{aligned}
 Q_{\text{edge1}} &= K_{\text{insulation}} \cdot \frac{\Delta \bar{T}_{\text{edge1}}}{\Delta L_{\text{insulation}}} \cdot A_{\text{side1}} \\
 &= K_{\text{insulation}} \cdot \frac{\left(\frac{T_3 + T_4}{2} - T_R\right)}{\Delta L_{\text{insulation}}} \cdot 4 \cdot (\Delta L_{\text{sample}} \cdot 0.9\text{m})
 \end{aligned}
 \tag{4.5}$$

where: $K_{\text{insulation}}$ = thermal conductivity of extruded polystyrene

$$= 0.029 \text{ W/m}\cdot\text{°C} \text{ (0.017 Btu/hr}\cdot\text{ft}\cdot\text{°F)}$$

T_3 = temperature of hot plate

T_4 = temperature of cold plate

T_R = room temperature = 24.4°C (76°F)

$\Delta L_{\text{insulation}}$ = thickness of insulation, which is 0.3 m (1-ft)

A_{side1} = side area of a test sample = 0.9 m (3-ft) × thickness of test sample

ΔL_{sample} = thickness of test sample

The estimated heat losses at the edges of Heater #2 and part of the backflow specimen were also based on the heat conduction equation (Equation 4.1). The two backflow plates T1 and T2 were maintained at the same temperature, thus, the inner side

⁶ the effect of assuming one-dimensional heat flow was checked with a two-dimensional finite element program; assuming one-dimensional heat flow would result in a 1.5% error in the computed K for the sample, thus the assumption is reasonable.

temperature of the extruded polystyrene at the edge of the middle heater (Heater #2) and the edge of the backflow specimen can be assumed to be the same as the temperature of the hot plate (T3). However, because there is no guard heater around the backflow plates T1 and T2, the middle edge temperature of the backflow specimen will be a little lower than the temperature of the hot plate (T3). The magnitude of this temperature can be estimated by Equation 4.6, which is based on heat transfer in layered materials. The heat loss at the edge of the heater (Q_{edge2}) and half of the edge of the backflow specimen (Q_{edge3}) are computed as follows:

Temperature at the middle edge of backflow specimen:

$$T_m = \frac{240 \cdot T_2 + 12 \cdot T_R}{252} \quad (4.6)$$

where: T_2 = temperature of backflow plate $T_2 = T_3$

$$\begin{aligned} Q_{\text{edge2}} &= K_{\text{insulation}} \cdot \frac{\Delta \bar{T}_{\text{edge2}}}{\Delta L_{\text{insulation}}} \cdot A_{\text{side2}} \\ &= K_{\text{insulation}} \cdot \frac{(T_{\text{heater}} - T_R)}{\Delta L_{\text{insulation}}} \cdot 4 \cdot (\Delta L_{\text{heater}} \cdot 0.9\text{m}) \end{aligned} \quad (4.7)$$

where: T_{heater} = temperature of the edge of Heater #2 = T_3

ΔL_{heater} = thickness of heater = 0.08 m (3 in.)

$$\begin{aligned}
Q_{\text{edge3}} &= K_{\text{insulation}} \cdot \frac{\Delta \bar{T}_{\text{edge3}}}{\Delta L_{\text{insulation}}} \cdot A_{\text{side3}} \\
&= K_{\text{insulation}} \cdot \frac{\left(\frac{T_2 + T_m}{2} - T_R\right)}{\Delta L_{\text{insulation}}} \cdot 4 \cdot (\Delta L_{\text{back}} \cdot 0.9\text{m})
\end{aligned} \tag{4.8}$$

where: T_2 = temperature of backflow plate $T_2 = T_3$

ΔL_{back} = half thickness of backflow specimen = 0.08 m (3 in.)

Typical values of sample thickness, T_3 , and T_4 are 0.3 m (1-ft), 25°C (77°F) and 35°C (95°F), respectively. Thus, the estimated edge heat loss is about 1.1 Watt (3.7 Btu/hr). Compared to the total input energy, which typically is 8.5 Watt (29 Btu/hr), this heat loss is about 13%. However, the direction and magnitude of this heat flow are known, so the heat loss at the edge can be used in the computation of the thermal conductivity to correct this error. In that case, the uncertainty in the thermal conductivity will only come from the uncertainty in parameters used to calculate the heat loss. There was about 1.1°C (2°F) uncertainty in the temperature. This results in about 0.1 W (0.4 Btu/hr) uncertainty in the input energy calculation, which is about 1.4% of the total input.

4) Bottom heat loss

Bottom heat loss is caused by heat exchanged between the lower hot plate T_2 and the backflow plate T_1 . The bottom heat exchange Q_{bottom} can be estimated by:

$$Q_{\text{bottom}} = A \cdot K_{\text{backflow}} \cdot \frac{\Delta T_{\text{backflow}}}{\Delta L_{\text{backflow}}} \tag{4.9}$$

where: A = plan area of test specimen

K_{backflow} = thermal conductivity of backflow specimen (0.144 W/m·°C;
0.083 Btu/hr-ft·°F)

$\Delta T_{\text{backflow}}$ = temperature difference between the hot plate T1 and T2;

$\Delta L_{\text{backflow}}$ = backflow specimen thickness, which is 152 mm (6 in.).

The maximum difference between T1 and T2 that was allowed during the tests was 0.02°C (0.04°F). For this worst case condition, $Q_{\text{bottom}} = 0.2 \text{ W}$ (0.7 Btu/hr) which is about 2.3% of the total input energy.

5) *Free heat convection within test sample*

This type of convection is different from the convection between gaps. The heat convection within the voids of the test sample is classified as the convection in porous material. The magnitude of the convection in a porous material depends on several factors including temperature gradient, sample thickness, sizes of the voids, direction of the heat flow, and temperature level (Gebhart, 1961). It is generally impossible to separate the heat conduction from the convection in a porous material. In practice, the K value is treated as the combination of heat conduction, radiation, and free convection which is called apparent thermal conductivity. This approach was adopted for this study, and as noted previously, it is apparent thermal conductivity that is needed for field design with tire chips.

6) *Power measurement error*

Power measurement errors include the errors from the multimeters and power supply. The multimeters used in determining the input power have 100 mV resolution with $\pm 0.5\%$ accuracy for 200 V range DC voltage measurement and 100 μA resolution

with $\pm 1.0\%$ accuracy for 200 mA range DC current measurement. The uncertainty in the input energy introduced by them is less than 0.1%. The voltage output fluctuation of the power supplies were less than 0.5% during the tests. Thus, the power measurement error introduces less than 0.5% error in K

7) Temperature measurement errors

This is one of the major sources of uncertainty in the calculated thermal conductivity. It can be further subdivided into calibration error, instrumentation measurement error, and sensor positioning error. The calibration error is a systematic error as long as the same calibration is used. In this test, the thermocouples were calibrated at three points: temperature of boiling distilled water (100°C ; 212°F), temperature of ice-distilled water mixture (0°C ; 32°F), and room temperature. The readings were converted to temperature using the conversion factors supplied by the manufacturer. The resulting temperatures were plotted versus the actual temperature. This resulted in a straight line with a slope of 0.99, which is very close to 1.00. The slope and offset of this line were used to correct the measured results, thus removing this source of error. However, there remains a systematic error in the correction factor itself.

Similar to the power measurement error, the temperature instrumentation measurement error contains both systematic and random errors. Each component will be estimated from equipment manufacturer's specifications. In addition, short-term fluctuation contributes uncertainty to the measured temperature. This uncertainty was minimized by collecting data over an extended time, and using the average of those readings to represent the temperature of the isothermal surface. The period of time was 4

hours with a reading interval of about one second. In addition, the maximum and minimum readings during this period were also recorded.

The last potential source of error in temperature measurement is caused by the positioning of the sensor or the disturbance caused by the sensor itself. In the case of mounting a sensor on a plate surface, the thermal contact resistance between the plate and specimen will be a source of error. The technique for estimating this error is to mount sensors both within the plate and within the specimen surface (ASTM C177). This technique, however, could not be used because of the limited number of channels on the data acquisition system.

The possible magnitude of the uncertainty in temperature difference (ΔT) can be calculated as follow:

$$\delta\Delta T = \delta(T_3 - T_4) \quad (4.10)$$

where: T_3 = measured temperature of hot plate T_3

T_4 = measured temperature of cold plate T_4

This uncertainty depends primarily on the accuracy of the acquisition system and the number of data points collected. The resolution and accuracy of the ACPC-16 for type T thermocouples is 0.01 to 0.02°C (0.02 to 0.04°F) while the accuracy is $\pm 0.7^\circ\text{C}$ (1.3°F) within temperature range of -25 to 200°C (Strawberry Tree, 1993). The temperatures used in the calculation are the average of about 35,000 readings. An error analysis shows that this will result in about 0.2°C (0.4°F) uncertainty in the average value. For a typical

temperature difference of 10°C (18°F), this may result in 2% uncertainty in the final result of computed thermal conductivity.

8) *Specimen thickness errors*

The specimen thickness error is determined by the ability to measure the plate spacing. In this test, the thickness of the test specimen used in the calculation of thermal conductivity is the average of the spacing between the hot plate T3 and cold plate T4. The error is labeled as $\delta\Delta L$. The causes of this error are the accuracy of the tape measure and random error introduced by the person who performs the measurements. The accuracy of the tape measure was 1.6 mm (1/16-in.).

9) *Uncertainty in metered area*

This area is a fixed region. The uncertainty is so small that it can be assumed to be zero.

4.4.3 Summary of error analysis

The errors analyzed in this section include both systematic and random errors. A systematic error is any component of error that remains fixed during the test. It does not include any components of errors that are known both in magnitude and sign as a correction can be applied to account for these errors. A random error is that component of error that varies both in sign and magnitude during a test (ASTM C177). The total effect of random and systematic errors is taken to be the square root of the sum of squares of individual sources of error. Based on the above analysis, the total uncertainty in input energy can be determined as follows.

Uncertainty in heat flow, δQ

This component includes the uncertainties in edge heat loss, bottom heat loss, and the instrumental accuracy.

$$Q_t = I \cdot U - Q_{\text{edge}} - Q_{\text{bottom}} \approx I \cdot U - (Q_{\text{edge1}} + Q_{\text{edge2}} + Q_{\text{edge3}}) \quad (4.11)$$

$$\frac{\delta Q_t}{Q_t} = \sqrt{\left(\frac{\delta Q_{\text{edge}}}{Q_{\text{edge}}}\right)^2 + \left(\frac{\delta Q_{\text{accuracy}}}{Q_t}\right)^2} \quad (4.12)$$

Total uncertainty in thermal conductivity, δk

The total uncertainty in thermal conductivity includes the uncertainty in heat flow, temperature difference, sample thickness, and sample plan area.

$$\frac{\delta k}{k} = \sqrt{\left(\frac{\delta Q_t}{Q_t}\right)^2 + \left(\frac{\delta \Delta T}{\Delta T}\right)^2 + \left(\frac{\delta \Delta L}{\Delta L}\right)^2 + \left(\frac{\delta A}{A}\right)^2} \quad (4.13)$$

Results from the error analysis and the above equation were used to calculate the final uncertainty. For a typical test with total input energy of 8.5 W (29 Btu/hr), T4 of 25°C (77°F), T3 of 35°C (95°F), sample thickness of 0.3 m (1 ft), and 0.02°C (0.04°F) difference between lower two plates (T1 and T2), the total uncertainty in K computed by the above equations will be about 3.4%.

5. TEST PROCEDURES

5.1 INTRODUCTION

This chapter describes preparation of the data acquisition system, calibration of the thermocouples, and test specimen preparation. As stated in Section 4.3.3, the hardware includes an A/D converter board, a terminal panel, and thermocouples. The software provided with the A/D converter was modified to meet the requirements of this study.

5.2 DATA ACQUISITION SYSTEM

5.2.1 Hardware

The A/D board used in this study was a Strawberry Tree model ACPC-16-16-T42, which has 16 differential analog input channels, 16 bit resolution, accurate cold junction compensation, and linearization for thermocouples. The terminal panel was a Strawberry Tree model T21. It has a large aluminum isothermal plate with screw terminals for connection of the thermocouples. The function of the isothermal plate is to attenuate the temperature differences at the cold junction connection. The A/D board was installed in a Zenith Data System model Z-200 PC Series computer.

Additional details on the A/D board and T21 terminal panel are given in the following Strawberry Tree manuals: "Instruction Manual Analog Connection PC" and "Data Acquisition Systems User Manual" (Strawberry Tree Computers, 1987, 1993).

5.2.2 Thermocouples

The thermocouples used in this study were made from Omega Engineering model FF-T-24-TWSH thermocouple wire. They are Teflon insulated, twisted/shielded, 24 gage, type T thermocouple wires. The thermocouple wire consists of an outer covering of Teflon insulation with three 24 gage wires twisted inside: a red Teflon insulated wire, a blue Teflon insulated wire and a bare wire. The blue wire is copper (C_U or positive), and the red wire is copper-nickel alloy (C_N or negative), and the bare wire is ground. The wires were formed into thermocouples by welding together ends of a twisted pair of blue (C_U) and red (C_N) wire.

5.2.3 Attachment of thermocouples

The thermocouple wires are attached to the screw terminals located inside the T21 terminal panel. There are a total of eight analog input channels, each with a "+", "-", and "COM" terminal screws. The "-" terminal is connected to "COM" using a shorting bar to provide a ground reference for the thermocouple. In this test, Channels 1 through 4 measure the temperature of hot plate T_3 , Channels 6 through 8 measure the temperature of the cold plate T_4 , and Channel 5 measures the temperature difference between the two backflow plates T_{1-2} .

5.3 THERMOCOUPLE CALIBRATION

For each channel, thermocouple readings were taken for three temperatures: ice-distilled water mixture (0°C), boiling distilled water (100°C), and room temperature (as read with a thermometer). The thermocouple readings were plotted versus temperature

and the best fit straight line through the three data points was obtained. The slope and y-intercept of this line are the scale and offset factors for this channel. The test procedure is discussed in detail in the following.

1) Collect 0°C reading

- Mix about 1 liter of ice and distilled water in a small extruded polystyrene box.
- Use a thermometer to check the temperature of this mixture. After the thermometer shows that the temperature of the mixture is stable at 0°C, put the ends of the thermocouples into the icy water. Make sure the tips of the thermocouples are immersed in the water and that no ice touches the tips. Cover the box.
- Turn on the data acquisition program. Collect data for a half hour with a 1 second interval between readings.
- For each channel, save the average of these readings taken during the half hour interval as the 0°C reading.

2) Collect 100°C reading

- Boil about 1 liter of distilled water in a glass beaker. Keep the water boiling.
- Put the ends of thermocouples into the boiling water. Make sure the tips of the thermocouples are immersed in the water without touching the glass wall.
- Check the temperature of the boiling water. Wait until the thermometer shows that the temperature is steady at 100°C (212°F).
- Start the data acquisition program. Collect data for a half hour with a 1 second interval between readings.
- For each channel, save the average of these readings taken during the half hour interval as the 100°C reading.

3) Collect room temperature reading

- Mount the thermocouple to the steel plate using silicon glue.

- Set the room temperature thermostat to about 21°C (70°F).
- Expose the steel plate with the attached thermocouples to the air for one day.
- Start the data acquisition program. Collect data for a half hour with a 1 second interval between readings.
- For each channel, save the average of these readings taken during the half hour interval as the room temperature reading.
- Take readings with a thermometer accurate to 0.1°C, at the beginning, middle, and end of the half hour. Use the average of these three readings as the room temperature.

4) Plot the thermocouple reading vs. temperature

- For each channel plot the three average readings corresponding to 0°C, measured room temperature, and 100°C.
- Obtain the best fit straight line through the points.

Record the slope and y-intercept of each line as the slope and offset factors for each channel.

5.4 TEST PROCEDURE

5.4.1 Sample preparation

For air dried samples, the tire chips or tire chip/gravel mixture were first air dried at room temperature. For moist samples, sufficient water was added to bring the samples to the desired water content. The test specimen was compacted using 60% of standard Proctor energy. Specimens were compacted in five layers each approximately 60 mm (2.5 in.) thick. Each layer was compacted with 891 blows using a 4.5-kg (10-lb) rammer with a 457-mm (18-in.) drop. The finished samples were about 305 mm (1 ft) thick. For moist

samples, the compacted sample was completely enclosed in 6-mil plastic to prevent moisture loss during the test.

For samples that are a mixture of tire chips and gravel, the specific gravity of the tire chips and soil was used to convert the desired volumes of tire chips and gravel to the corresponding weight. An example is given below:

Example: For 33% F&B glass belted tire chips/ 67% gravel mixture, compute the weight of tire chips and gravel needed in the test.

Specific gravity of tire chips and gravel:

$$G_{s\text{-chip}} = 1.14$$

$$G_{s\text{-gravel}} = 2.67$$

Volume of tire chips and gravel needed:

$$V_t = 0.9\text{m} \cdot 0.9\text{m} \cdot 0.3\text{m} = 0.255\text{m}^3 (9\text{ft}^3)$$

$$V_{s\text{-chip}} = 0.33 \cdot V_t = 0.09\text{m}^3 (3\text{ft}^3)$$

$$V_{s\text{-gravel}} = 0.67 \cdot V_t = 0.17\text{m}^3 (6\text{ft}^3)$$

Weight of tire chips and gravel needed in one test:

$$W_s = V_s \cdot G_s \cdot \gamma_w$$

$$W_{s\text{-chips}} = 0.09 \text{ m}^3 \cdot 1.14 \cdot 1000\text{kg/m}^3 = 96.6 \text{ kg (213 lbs)}$$

$$W_{s\text{-gravel}} = 0.17 \text{ m}^3 \cdot 2.67 \cdot 1000\text{kg/m}^3 = 453 \text{ kg (999 lbs)}$$

Weigh the computed amount of tire chips and gravel for this proportion and mix them together thoroughly. Compact the mixture using 60% of standard Proctor energy.

After finishing compaction, the steel plate T4 was placed on top of the sample. The sample thickness was determined by measuring the distance from the top edge of the

wooden box to the steel plate T4 at four corners, then subtracting this value from the distance from the top edge of the wooden box to the top of steel plate T3. The average thicknesses at the four corners was used as the sample thickness. The final sample density was computed from the total sample weight and the total sample volume, which is the sample thickness times the steel plate area.

5.4.2 Surcharge

Three levels of surcharge were used: no surcharge, half surcharge (9 kPa; 187 psf), and full surcharge (18 kPa; 375 psf). The full surcharge corresponds to the stress caused by a 914-mm (3-ft) thick overlying gravel cover.

Solid concrete blocks were used as surcharge weights. Each concrete block weighs about 13.6 kg (30 lbs). To allow air to circulate over the top of the steel plate, the concrete blocks were placed on a wooden frame, leaving a gap of about 300 mm (12 in.) between the bottom of the frame and steel plate T4 for air circulation.

5.4.3 Testing procedure

Each test took about three weeks. First, it took four to five days to heat up the whole system under no surcharge. Second, data was collected for three days. Then, the apparent thermal conductivity was computed from the collected data. If relatively constant results over time were obtained, as evidenced by the most sensitive controlling factor, T_{1-2} , being stable, the half surcharge was added to the sample and the same procedure was repeated. After the half surcharge was done, the procedure was repeated for the full surcharge.

6. THERMAL CONDUCTIVITY TEST RESULTS

6.1 INTRODUCTION

This chapter presents thermal conductivity test results for tire chips, gravel, and tire chip/gravel mixtures. A full example of the data analysis procedure is also included. The influence of density, void ratio, tire chip size, steel belt content, water content, and percent gravel in tire chip/gravel mixtures on the apparent thermal conductivity are discussed in detail.

6.2 DATA ANALYSIS

The data analysis procedure can be broken down into the following steps. The subsequent paragraphs explain each step in detail.

- 1) An Excel spreadsheet was used to calculate the K value for each data collection period, then K was corrected for lateral heat loss.
- 2) Plots were made of K and T_{1-2} versus time, and T_{3-4} versus time.
- 3) A plot was made of K and K-corrected (for lateral heat loss) versus T_{1-2} . The best fit line through the data was determined. The zero intercept of the line, which represents the condition of no heat flow through the backflow sample, was taken to be the final K for this test.

An example spreadsheet for Palmer tire chips under half surcharge is given in Figure 6.1. The spreadsheet can be explained as follows: T_{1-2} is the reading of Channel 5 and is the voltage corresponding to the temperature difference between the two backflow plates. The "Ave." value is the average of the readings taken at a 1 second interval over a four hour period. The "Max." and "Min." are the maximum and minimum readings

U=59.0V I=141.6 mA Q=28.493 Btu/hr dL=0.792 ft

Date	Time	T1-2 (V)		T3 (deg. F)		T4 (deg. F)		T3-4(deg F)						
		Ave.	Max.	Min.	Ch.1.	Ch.2.	Ch.3.	Ch.4.	Ave.	Ch.6.	Ch.7.	Ch.8.	Ave.	
5-Mar	9:56	4.05E-06	5.94E-06	2.64E-06	90.84	91.06	90.98	91.38	91.07	72.71	72.66	72.79	72.72	18.35
	13:56	6.62E-06	1.11E-05	2.79E-06	90.91	91.13	91.07	91.42	91.13	72.82	72.73	72.86	72.80	18.33
	17:56	8.28E-06	1.51E-05	2.79E-06	90.91	91.13	91.07	91.42	91.13	72.82	72.73	72.86	72.80	18.33
	21:56	1.26E-05	1.71E-05	9.31E-06	90.85	91.06	90.99	91.35	91.06	73.09	73.03	73.15	73.09	17.97
6-Mar	1:56	1.32E-05	1.77E-05	9.30E-06	90.85	91.06	90.99	91.35	91.06	73.09	73.03	73.15	73.09	17.97
	5:56	1.43E-05	1.79E-05	1.16E-05	90.84	91.06	90.99	91.37	91.07	73.11	73.03	73.15	73.10	17.97
	9:56	1.42E-05	1.81E-05	1.16E-05	90.84	91.06	90.99	91.37	91.07	73.11	73.03	73.15	73.10	17.97
	13:56	1.45E-05	2.04E-05	8.40E-06	90.86	91.08	91.02	91.37	91.08	73.09	73.02	73.12	73.08	18.01
	17:56	1.52E-05	2.04E-05	8.40E-06	90.86	91.08	91.02	91.37	91.08	73.09	73.02	73.12	73.08	18.01
	21:56	1.68E-05	2.04E-05	1.40E-05	90.86	91.09	91.03	91.38	91.09	73.33	73.26	73.37	73.32	17.77
7-Mar	1:56	1.64E-05	2.06E-05	1.21E-05	90.86	91.09	91.03	91.38	91.09	73.33	73.26	73.37	73.32	17.77
	5:56	1.35E-05	1.87E-05	9.27E-06	90.92	91.14	91.11	91.41	91.15	73.19	73.13	73.17	73.16	17.98
	9:56	1.23E-05	1.87E-05	7.06E-06	90.92	91.14	91.11	91.41	91.15	73.19	73.13	73.17	73.16	17.98
	13:56	1.05E-05	1.46E-05	6.88E-06	90.90	91.13	91.05	91.42	91.13	72.99	72.92	73.03	72.98	18.15
	17:56	1.12E-05	1.64E-05	6.88E-06	90.90	91.13	91.05	91.42	91.13	72.99	72.92	73.03	72.98	18.15
	21:56	1.29E-05	1.69E-05	9.74E-06	90.86	91.08	91.03	91.40	91.09	73.15	73.08	73.18	73.14	17.96
8-Mar	1:56	1.31E-05	1.71E-05	9.74E-06	90.86	91.08	91.03	91.40	91.09	73.15	73.08	73.18	73.14	17.96
	5:56	1.38E-05	1.81E-05	1.08E-05	90.90	91.13	91.07	91.41	91.13	73.23	73.18	73.27	73.23	17.90
	9:56	1.39E-05	1.82E-05	1.08E-05	90.90	91.13	91.07	91.41	91.13	73.23	73.18	73.27	73.23	17.90
	13:56	1.45E-05	1.94E-05	1.12E-05	90.83	91.04	90.98	91.37	91.06	73.17	73.18	73.29	73.21	17.84
	17:56	1.53E-05	2.10E-05	1.12E-05	90.83	91.04	90.98	91.37	91.06	73.17	73.18	73.29	73.21	17.84
	21:56	1.73E-05	2.18E-05	1.44E-05	90.88	91.10	91.03	91.42	91.11	73.31	73.30	73.43	73.35	17.76
9-Mar	1:56	1.74E-05	2.19E-05	1.44E-05	90.88	91.10	91.03	91.42	91.11	73.31	73.30	73.43	73.35	17.76
	5:56	1.67E-05	2.13E-05	1.32E-05	90.91	91.13	91.07	91.43	91.14	73.27	73.30	73.41	73.33	17.81
	9:56	1.59E-05	2.13E-05	1.10E-05	90.91	91.13	91.07	91.43	91.14	73.27	73.30	73.41	73.33	17.81
	13:56	1.47E-05	1.83E-05	1.20E-05	90.94	91.14	91.09	91.46	91.16	73.34	73.30	73.43	73.36	17.80
	17:56	1.50E-05	1.83E-05	1.20E-05	90.94	91.14	91.09	91.46	91.16	73.34	73.30	73.43	73.36	17.80

Palmer tire chips; half surcharge

Figure 6.1 Spreadsheet Example: Palmer tire chips under half surcharge

Date	Time	dT/dL (deg. F/ft)	dT_side1 (deg. F)	dQ_side1 (Btu/hr)	Tm (deg F)	dQ_side2 (Btu/hr)	dQ_side3 (Btu/hr)	K-corrected (Btu/hr.ft.°F)
5-Mar	9:56	23.16	9.17	1.45	90.19	0.75	0.71	0.123
	13:56	23.14	9.16	1.45	90.26	0.76	0.71	0.123
	17:56	23.14	9.16	1.45	90.26	0.76	0.71	0.123
	21:56	22.69	8.99	1.42	90.21	0.75	0.71	0.125
6-Mar	1:56	22.69	8.99	1.42	90.21	0.75	0.71	0.125
	5:56	22.69	8.98	1.42	90.21	0.75	0.71	0.125
	9:56	22.69	8.98	1.42	90.21	0.75	0.71	0.125
	13:56	22.73	9.00	1.43	90.23	0.75	0.71	0.125
	17:56	22.73	9.00	1.43	90.23	0.75	0.71	0.125
	21:56	22.44	8.89	1.41	90.24	0.75	0.71	0.127
7-Mar	1:56	22.44	8.89	1.41	90.24	0.75	0.71	0.127
	5:56	22.70	8.99	1.42	90.29	0.76	0.71	0.125
	9:56	22.70	8.99	1.42	90.29	0.76	0.71	0.125
	13:56	22.91	9.07	1.44	90.26	0.76	0.71	0.124
	17:56	22.91	9.07	1.44	90.26	0.76	0.71	0.124
	21:56	22.67	8.98	1.42	90.24	0.75	0.71	0.125
8-Mar	1:56	22.67	8.98	1.42	90.24	0.75	0.71	0.125
	5:56	22.60	8.95	1.42	90.28	0.76	0.71	0.126
	9:56	22.60	8.95	1.42	90.28	0.76	0.71	0.126
	13:56	22.53	8.92	1.41	90.21	0.75	0.71	0.126
	17:56	22.53	8.92	1.41	90.21	0.75	0.71	0.126
	21:56	22.43	8.88	1.41	90.26	0.76	0.71	0.127
9-Mar	1:56	22.43	8.88	1.41	90.26	0.76	0.71	0.127
	5:56	22.49	8.90	1.41	90.29	0.76	0.71	0.127
	9:56	22.49	8.90	1.41	90.29	0.76	0.71	0.127
	13:56	22.48	8.90	1.41	90.31	0.76	0.72	0.127
	17:56	22.48	8.90	1.41	90.31	0.76	0.72	0.127

Figure 6.1 Spreadsheet Example: Palmer tire chips under half surcharge (continued)

during this four hour period. $T_3 - T_4$ is the difference between T_3 average (temperature at the bottom of sample) and T_4 average (temperature at the top of sample), which is the temperature difference across the sample. T_3 average is the average reading of Channels 1 through 4, and T_4 is the average of Channels 6 through 8. The " dT/dL " is the temperature gradient across the sample. T_m is the estimated temperature at the middle edge of the backflow specimen computed by Equation 4.7. The " dQ_{side1} ", " dQ_{side2} ", and " dQ_{side3} ", are the edge heat loss computed by Equations 4.6, 4.8, and 4.9 respectively. The K modified for the lateral heat loss (K -corrected) is calculated as:

$$K - \text{corrected} = \frac{(Q - Q_{\text{edge}})}{A} \cdot \frac{\Delta L}{T_3 - T_4} \quad (6.1)$$

where: Q = total input energy from middle heater (Heater #2)

Q_{edge} = total edge heat loss = $Q_{\text{edge1}} + Q_{\text{edge2}} + Q_{\text{edge3}}$

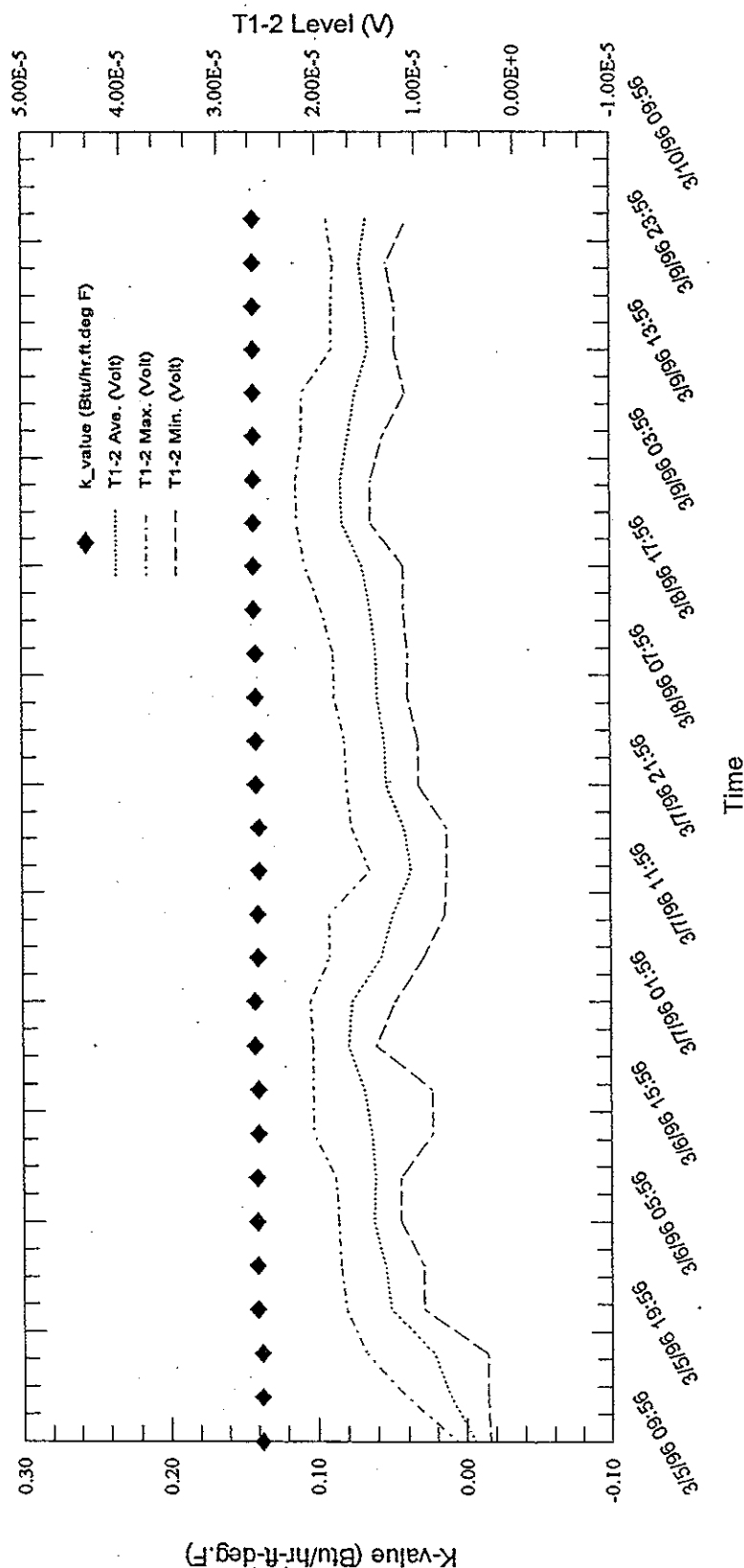
A = plan area of specimen

ΔL = sample thickness

$T_3 - T_4$ = average temperature difference between hot and cold plates

Step 2 is used to assess the quality of the test data. Example plots are shown in Figures 6.2 and 6.3. If K remains relatively constant versus time and T_{1-2} average varies within a range of no more than $\pm 2.5E-5$ V, the test was deemed to have reached steady state conditions. The "Max." and "Min." T_{1-2} readings on Figure 6.2 show the magnitude of the reading fluctuation during a 4-hour period. T_{3-4} is the temperature difference between the hot and cold plates (Figure 6.3). The difference was generally less than $\pm 0.4^\circ\text{C}$ ($\pm 0.7^\circ\text{F}$).

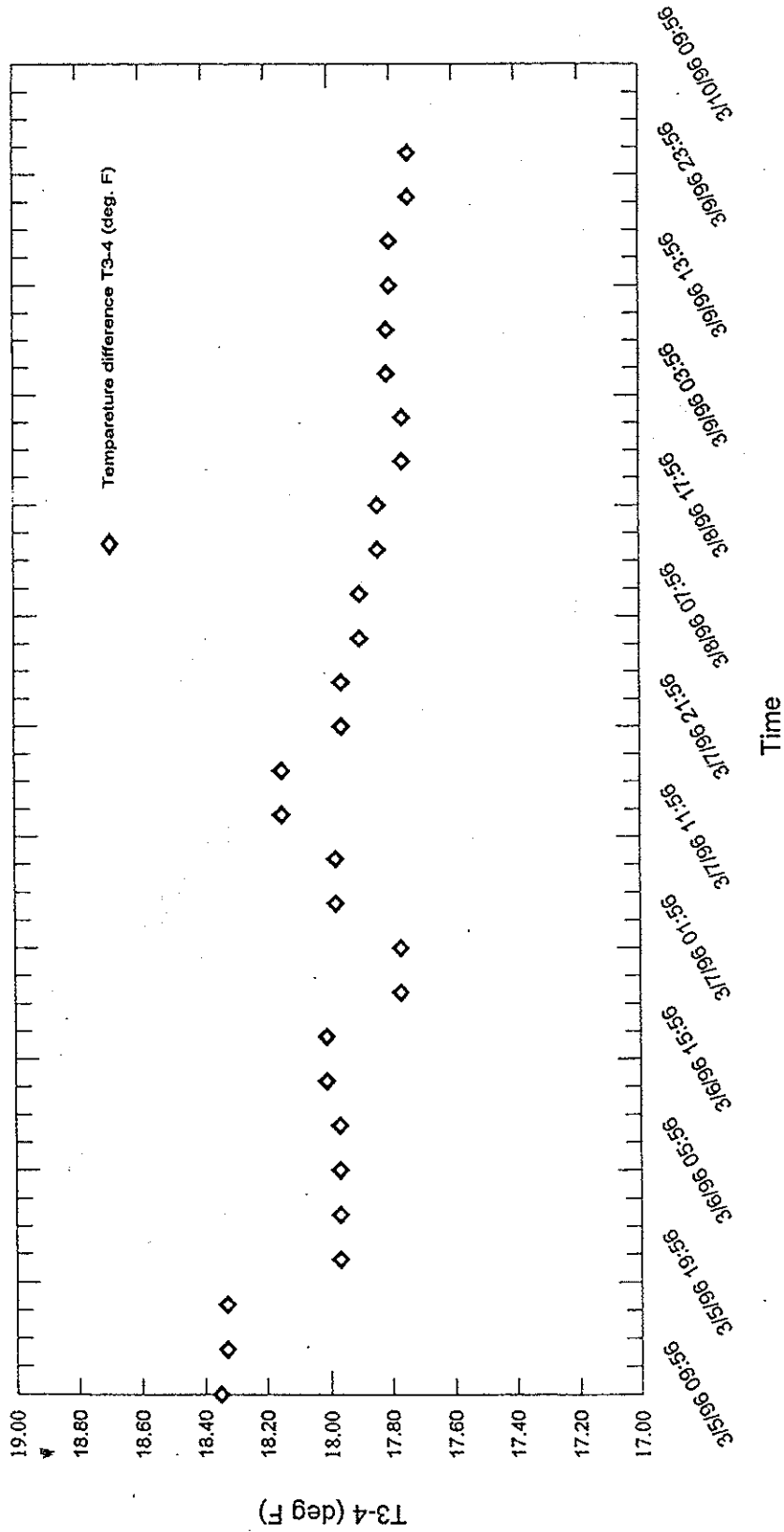
Thermal Conductivity of Tire Chips
K-value vs. time



Note: Palmer tire chip half surcharge for four days.
(Temperature gradient is about 15 deg.F/ft)
file: K-t_h1a.grf

Figure 6.2 K-value versus time

Thermal Conductivity of Tire Chips
T3-4 vs. time



Note: Palmer tire chip half surge for four days.
(Temperature gradient is about 15 deg.F/ft)
file: k-t_h1a.grf

Figure 6.3 T3-4 versus time

The final step is to determine the K at zero T_{1-2} by plotting K versus T_{1-2} as shown in Figure 6.4. This reduces the error caused by a small heat exchange between the lower two hot plates and the influence of small fluctuations in the input energy on K. It is recalled that $T_{1-2} = 0$ is the idea condition of no heat exchange between the lower two plates. In addition, this technique was a way to select a K value that would be consistent from test to test.

The dry density of the samples under each surcharge were computed directly from the measured weight of the sample and total sample volume. The total sample volume was calculated from the sample thickness and the plate area. The plate area was 0.84 m² (9 ft²). The void ratio of each sample was calculated from the dry density (ρ_{dry}) and specific gravity (G_s) of the sample using

$$e = \frac{G_s \cdot \rho_w}{\rho_{dry}} - 1 \quad (6.2)$$

where ρ_w is the density of water, which is 1 Mg/m³ (62.4 pcf). The water content of moist samples were determined at the beginning of a test. As a check, the water content of selected moist samples was also determined at the end of a test.

6.3 RESULTS

The thermal conductivity for air dried samples under each surcharge condition along with the corresponding density and void ratio are summarized in Table 6.1. The results for moist samples are presented in Table 6.2. The following sections discuss the results for gravel, tire chips, and tire chip/gravel mixtures.

T1-2 vs. K-value
 Palmer, half surcharge
 Mar. 10, 1996

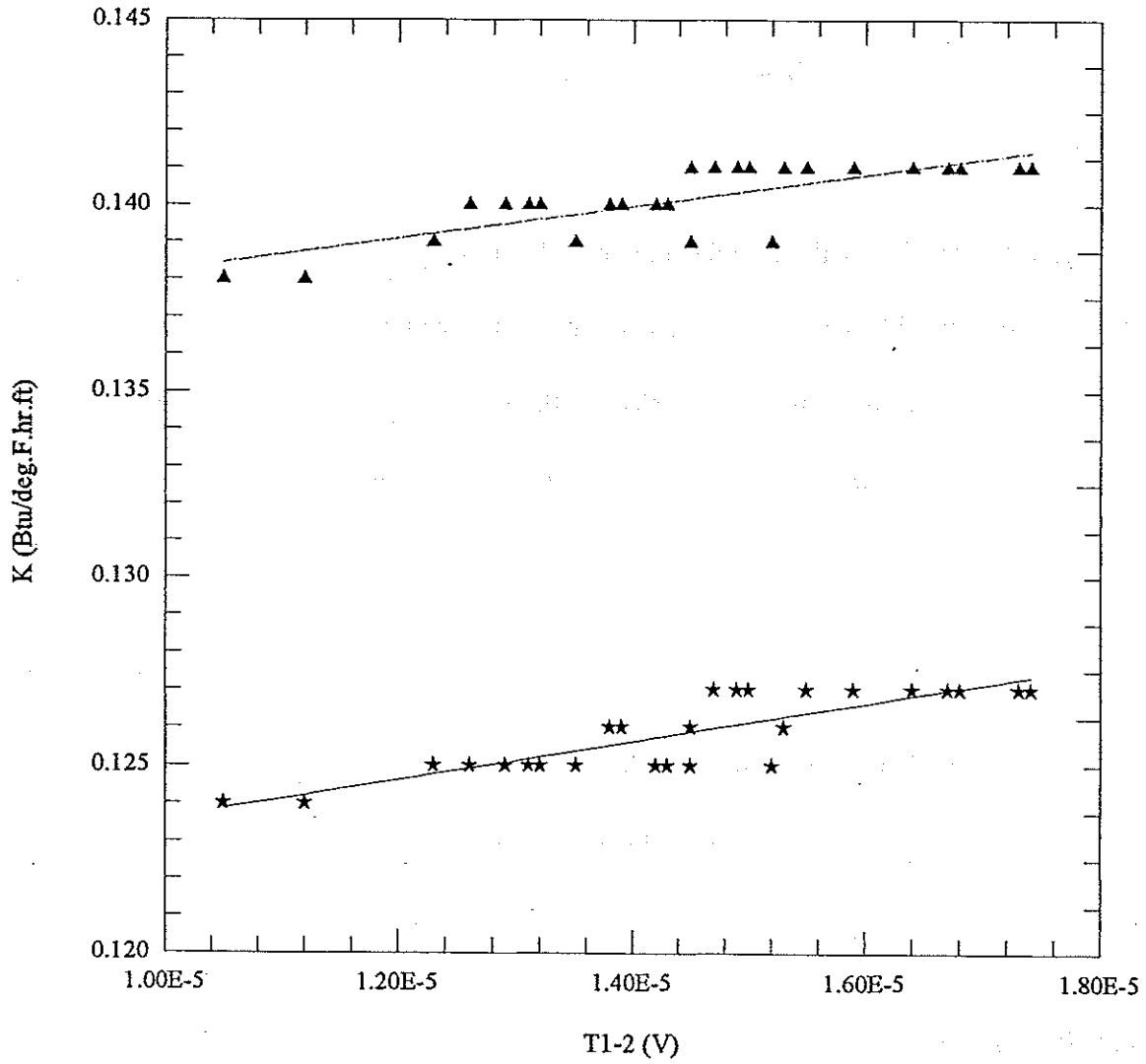
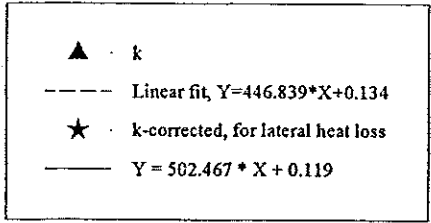


Figure 6.4 T₁₋₂ versus K-value

Table 6.1 Summary of test results for air dried samples

Sample	Density		Void Ratio	Apparent thermal conductivity		Surcharge
	(pcf)	(Mg/m ³)		(Btu/hr-ft. ² -°F)	(W/m. ² -°C)	
gravel	117.6	1.88	0.41	0.295	0.510	none
	121.6	1.95	0.36	0.326	0.563	half
	123.0	1.97	0.34	0.345	0.596	full
F&B-g	38.5	0.62	0.85	0.120	0.207	none
	43.3	0.69	0.64	0.113	0.195	half
	45.4	0.73	0.56	0.114	0.197	full
F&B-s	39.1	0.63	0.85	0.145	0.251	none
	42.8	0.69	0.69	0.130	0.225	half
	45.3	0.73	0.60	0.134	0.232	full
Palmer	39.7	0.64	0.998	0.159	0.275	none
	45.1	0.72	0.76	0.119	0.206	half
	48.5	0.78	0.63	0.125	0.216	full
Pine State	39.2	0.63	0.97	0.158	0.273	none
	45.4	0.73	0.7	0.139	0.240	half
	49.6	0.79	0.56	0.114	0.197	full
Sawyer	36.0	0.58	1.13	0.184	0.318	none
	41.0	0.66	0.87	0.148	0.256	half
	43.7	0.70	0.76	0.156	0.270	full
33% F&B-g /67% gravel	101.5	1.63	0.32	0.282	0.487	none
	106.8	1.71	0.26	0.273	0.472	half
	108.3	1.73	0.24	0.212	0.366	full
67% F&B-g /33% gravel	64.9	1.04	0.58	0.209	0.361	none
	70.5	1.13	0.45	0.189	0.327	half
	73.4	1.18	0.39	0.173	0.299	full
33% F&B-s /67% gravel	106.8	1.71	0.27	0.328	0.567	none
	109.8	1.76	0.23	0.328	0.567	half
	111.2	1.78	0.22	0.327	0.565	full
67% F&B-s /33% gravel	71.7	1.15	0.44	0.292	0.505	none
	75.7	1.21	0.37	0.193	0.334	half
	77.0	1.23	0.35	0.196	0.339	full
33% Palmer /67% gravel	101.7	1.63	0.36	0.335	0.579	none
	108.1	1.73	0.27	0.229	0.396	half
	111.2	1.78	0.24	0.257	0.444	full
67% Palmer /33% gravel	65.0	1.04	0.67	0.239	0.413	none
	74.0	1.19	0.47	0.206	0.356	half
	77.9	1.25	0.39	0.216	0.373	full

Table 6.2 Summary of test results for moist samples

Sample (initial and final water content)	Dry Density		Void Ratio	Apparent thermal conductivity		Surcharge
	$\frac{\text{lb}}{\text{ft}^3}$	$\frac{\text{Mg}}{\text{m}^3}$		$\frac{\text{Btu}}{\text{hr} \cdot \text{ft} \cdot ^\circ\text{F}}$	$\frac{\text{W}}{\text{m} \cdot ^\circ\text{C}}$	
Gravel w (initial) = 8.9% w (final) = 8.3%	127.9	2.05	0.30	0.700	1.21	none
	N.R.	N.R.	N.R.	0.942	1.63	half
	130.8	2.10	0.274	0.939	1.62	full
F&B glass belted w (initial) = 3.5% w (final) = N.R.	38.5	0.62	1.24	0.142	0.245	none
	42.8	0.69	1.00	0.150	0.259	half
	45.8	0.73	0.88	0.145	0.251	full
Palmer w (initial) = 4.3% w (final) = 5.0%	40.2	0.64	0.94	0.161	0.278	none
	44.8	0.72	0.74	0.145	0.251	half
	47.6	0.76	0.64	0.134	0.232	full
33% Palmer/67% gravel w (initial) = 7.5% w (final) = N.R.	102.2	1.64	0.35	0.607	1.048	none
	108.2	1.73	0.27	0.464	0.801	half
	110.7	1.77	0.25	0.485	0.838	full
67% Palmer/33% gravel w (initial) = 6.5% w (final) = 5.5%	72.6	1.16	0.49	0.242	0.419	none
	79.4	1.27	0.36	0.249	0.431	half
	82.3	1.32	0.31	0.226	0.391	full

N.R. = not recorded

6.3.1 Gravel

The results for air dried gravel are listed in Table 6.1 and the relationship between the density and apparent thermal conductivity is plotted in Figure 6.5. The test results show that the apparent thermal conductivity of air dried gravel increases from 0.510 to 0.596 W/m·°C (0.295 to 0.345 Btu/hr·ft·°F) as the density increases from 1.88 to 1.97 Mg/m³ (117.6 to 123 pcf). Thus, the apparent thermal conductivity of gravel increases as the density increases. This is caused by a decrease of the volume of air voids as the density increases. Air has a very low thermal conductivity (0.026 W/m·C or

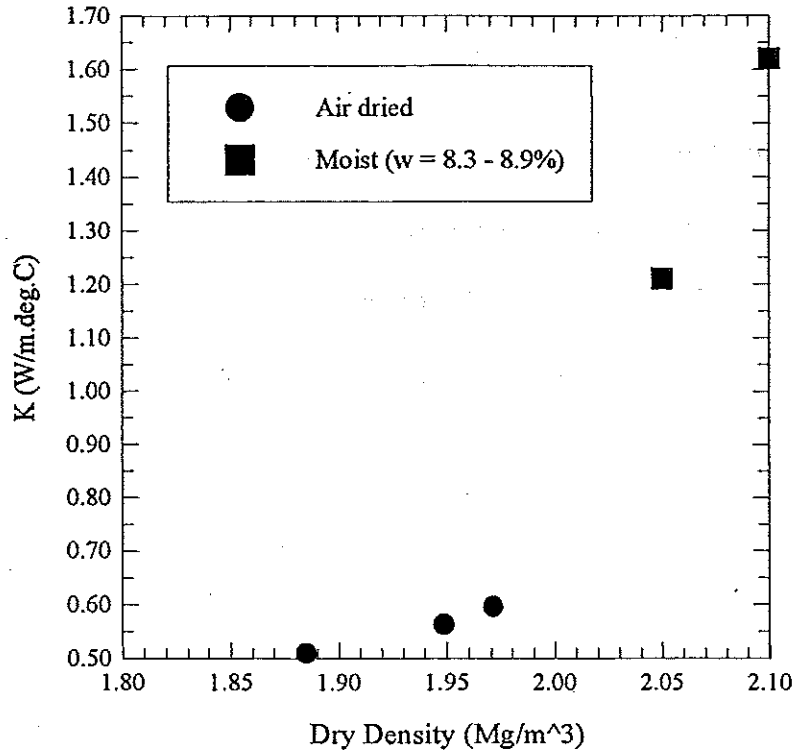


Figure 6.5 Gravel: apparent thermal conductivity versus density

0.015 Btu/hr-ft-°F) (Andersland and Ladanyi, 1994), compared to the thermal conductivity of quartz (8.4 W/m-°C or 4.86 Btu/hr-ft-°F), a mineral that is the main content of many gravel particles. Thus, the less air in the sample relative to gravel particles, the higher the thermal conductivity of the composite air/gravel mixture.

The results for moist gravel are listed in Table 6.2 and are plotted versus density in Figure 6.5. The initial and final water contents of the sample were 8.9% and 8.2%, respectively. The density of this sample was higher than for the air dried sample, most likely due to the water content being near the soil's optimum. The thermal conductivity of the moist sample was much greater than for the air dried sample. This is due to both the higher density and water content of the moist sample (Kersten, 1949; Andersland and Ladanyi, 1994).

The thermal conductivities from this study are plotted on a graph of results from Andersland and Ladanyi (1994) as shown in Figure 6.6. Their data only extends down to a water content of about 1%, however, extrapolation of their data is consistent with the air dried K measured in this study. The moist result is somewhat low for the measured water content and density. For a density of 2.0 Mg/m^3 and water content of 8.5%, Andersland and Landyi (1994) predict a thermal conductivity of about $2.5 \text{ W/m}\cdot^\circ\text{C}$ ($1.4 \text{ Btu/hr}\cdot\text{ft}\cdot^\circ\text{F}$) compared to a measured value of $1.62 \text{ W/m}\cdot^\circ\text{C}$ ($0.939 \text{ Btu/hr}\cdot\text{ft}\cdot^\circ\text{F}$) at the full surcharge.

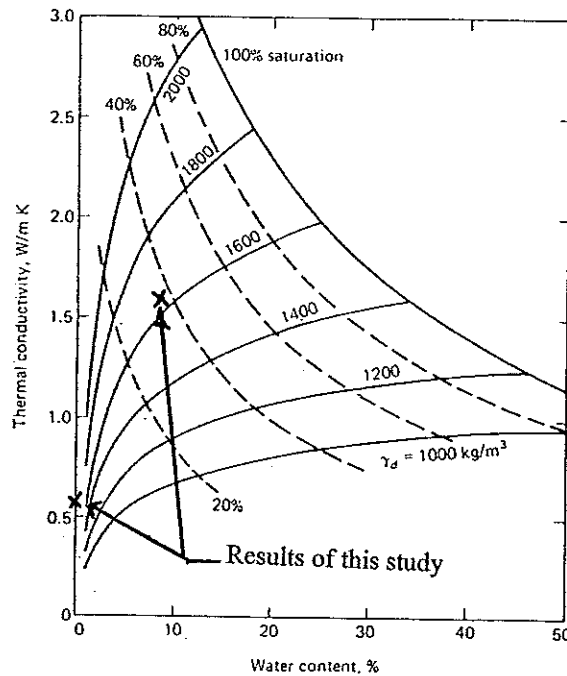


Figure 6.6 Average apparent thermal conductivity for sand and gravel: unfrozen (after Andersland and Ladanyi, 1994)

6.3.2 Tire chips

This section will focus on the effect of density on the apparent thermal conductivity of tire chips. The influence of tire chip size and glass or steel content on the apparent

thermal conductivity will also be discussed. The results for air dried tire chips are listed in Table 6.1. Results for moist samples are listed in Table 6.2.

6.3.2.1 Influence of density

The relationship between apparent thermal conductivity and density for each type of tire chip is shown in Figures 6.7 through 6.11. In addition, results for moist samples of F&B-glass belted and Palmer are shown in Figures 6.7 and 6.9. These figures show results corresponding to the three surcharge conditions. For all samples except the moist F&B-glass belted, it is seen that the K decreases as the density increases from the first to the second data point. This is opposite of behavior observed for gravel. A possible explanation is that the smaller voids at the higher density caused a reduction in heat transfer by convection. This reduction could have been greater than the increase in heat transfer due to conduction that would result from reduced air content. This could explain the net reduction in thermal conductivity. However, as the density increased from the second to the third data point, there was no clear trend in the change in thermal conductivity as both increasing and decreasing values were observed. It could be that densities in this range correspond to a zone where reduction in heat transfer by convection is less important compared to increased heat transfer by conduction. In any case, the change in thermal conductivity from the second to the third data points is relatively small and the pattern of change in thermal conductivity with density may be caused by scatter of the data.

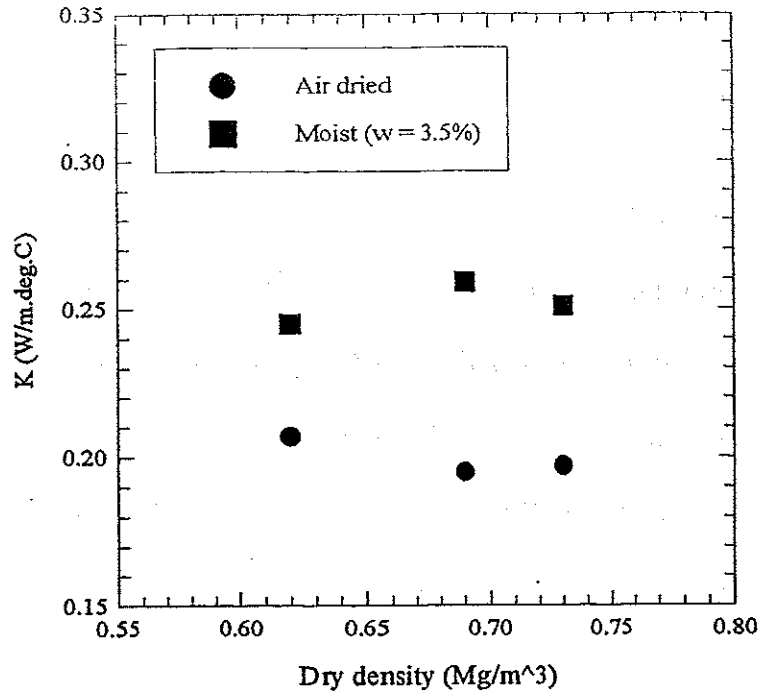


Figure 6.7 F&B glass belted tire chips: apparent thermal conductivity versus density

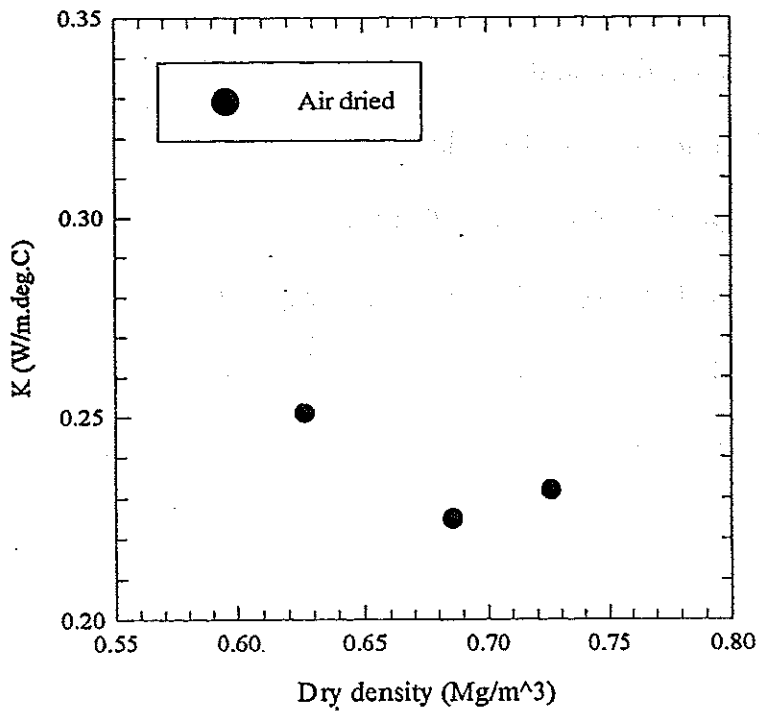


Figure 6.8 F&B steel belted tire chips: apparent thermal conductivity versus density

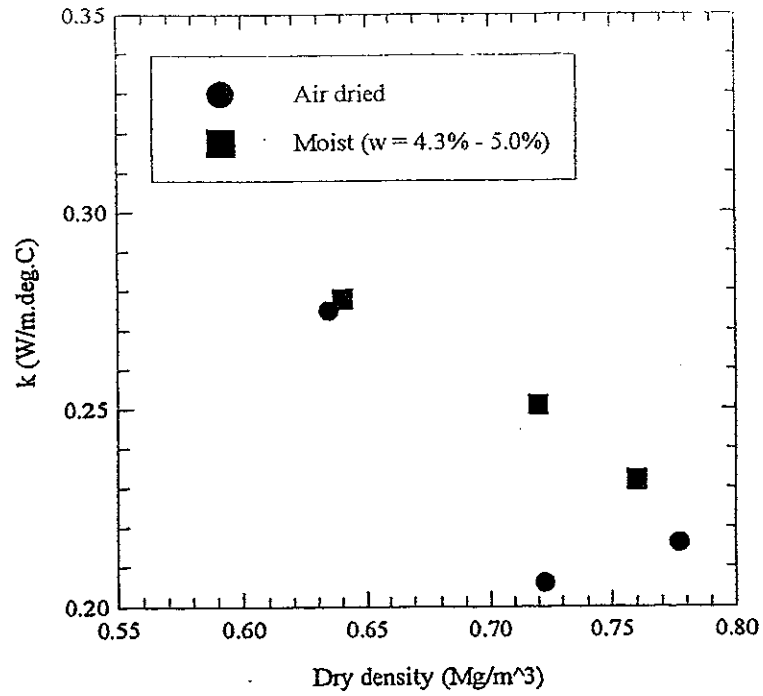


Figure 6.9 Palmer tire chips: apparent thermal conductivity versus density

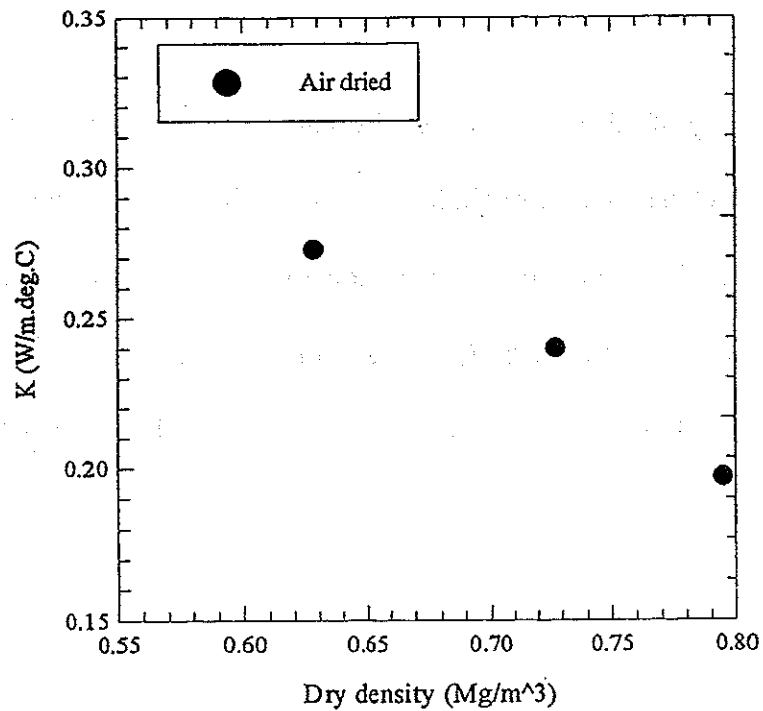


Figure 6.10 Pine State tire chips: apparent thermal conductivity versus density

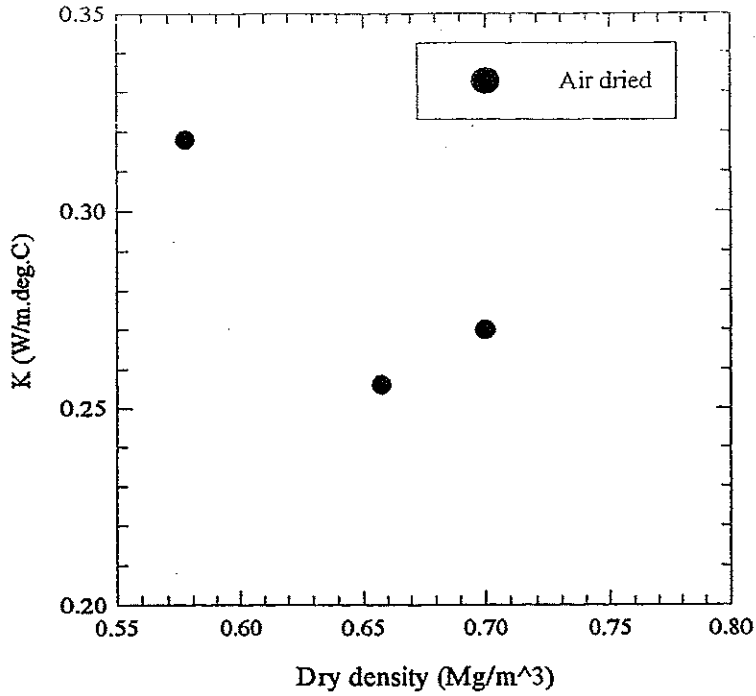


Figure 6.11 Sawyer tire chips: apparent thermal conductivity versus density

A summary of all the results for tire chip tests is shown in Figure 6.12. The data points falling between two straight lines are for both air dried and moist steel belted chips. This plot shows that apparent thermal conductivity of tire chips varies from 0.318 to 0.195 W/m·°C (0.184 to 0.113 Btu/hr·ft·°F) over a density range of 0.58 to 0.79 Mg/m³ (36 to 50 pcf). There is an overall trend that the apparent thermal conductivity of tire chips decreases as the density increases.

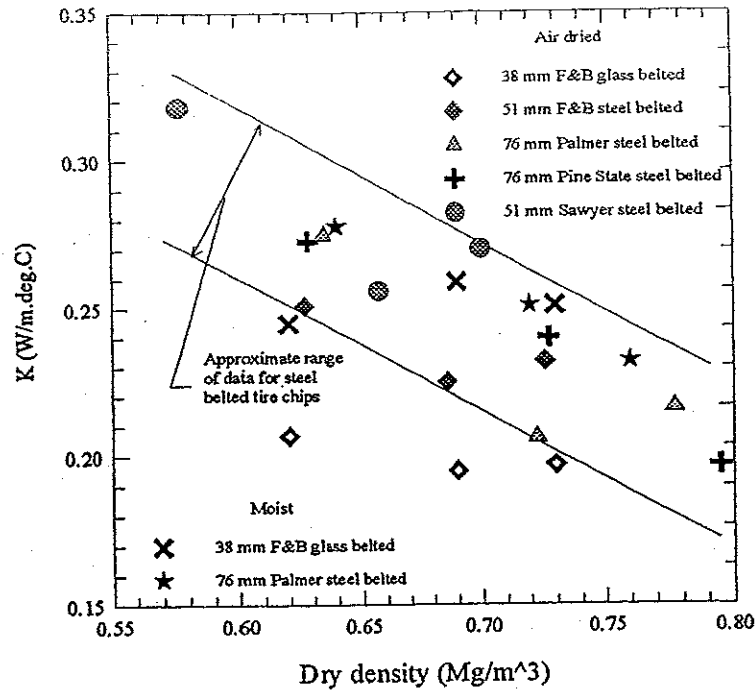


Figure 6.12 Apparent thermal conductivity versus density for tire chips

6.3.2.2 Influence of water content

The thermal conductivity of air dried and moist tire chips are compared in Figures 6.7 and 6.9. Increasing the water content of F&B glass belted tire chips from zero to 3.5% increased the thermal conductivity by about 0.04 W/m \cdot °C (0.02 Btu/hr-ft \cdot °F). For Palmer chips, increasing the water content to between 4.3% and 5.0% increased the thermal conductivity by between 0.01 and 0.05 W/m \cdot °C (0.006 and 0.03 Btu/hr-ft \cdot °F). Examining Figure 6.12 shows that the results for moist Palmer chips fall in the overall band for steel belted chips. Thus, for steel belted chips, the effect of moisture appears to be smaller than other factors which affect thermal conductivity and the overall scatter of the data. On the other hand, moisture increased the thermal conductivity of F&B glass belted chips to the approximate range for steel belted chips.

6.3.2.3 Influence of tire chip sizes

There is no obvious influence of chip size on the apparent thermal conductivity. For example, at a density of 0.63 Mg/m^3 (39 pcf) the K of 51 mm (2-in.) F&B steel belted chips is smaller than K of 76 mm (3-in.) Pine State and Palmer chips, while at a density of 0.72 Mg/m^3 (45 pcf) the F&B steel belted thermal conductivity falls between the values of Pine State and Palmer chips. Thus, for the small range of particle sizes investigated in this study, the maximum size of tire chips is not a controlling factor for apparent thermal conductivity. However, it would be expected that tire chips with a significantly larger size than examined in this study would have larger voids resulting in greater heat transfer by convection. If this is true, thermal conductivity would be expected to increase with significant increases particle size.

6.3.2.4 Influence of glass or steel belt content

Air dried glass belted tire chips have a lower apparent thermal conductivity than steel belted tire chips. From Figure 6.12 it can be seen that, for a given density, air dried glass belted F&B tire chips have a lower apparent thermal conductivity compared to the other tire chips which contain steel belts. Comparing the air dried F&B glass belted and air dried F&B steel belted chips, which have similar gradations (see Figure 3.13), the apparent thermal conductivity of air dried glass belted chips is lower than air dried steel belted chips by about $0.03 \text{ W/m}\cdot\text{C}$ ($0.02 \text{ Btu/hr}\cdot\text{ft}\cdot\text{F}$) at the same density. The lower apparent thermal conductivity of glass belted tire chips is most likely due to the lower thermal conductivity of glass compared to steel belts.

However, moisture negates the insulating advantage of air dried glass belted chips. As shown in Figure 6.12, the results for moist F&B glass belted chips fall largely within the range for all steel belted chips. Thus, for moist field conditions there appears to be no advantage to using glass belted chips rather than steel belted chips. Nonetheless, it would be reasonable to place some restrictions on the amount of steel belt allowed in the tire chips because of the higher thermal conductivity of steel. A maximum of 1% free steel by weight has been allowed on several projects where tire chips were used for insulation, lightweight fill, and retaining wall backfill (Humphrey and Eaton, 1995; Humphrey, et al., 1997). Free steel is defined as steel with no attached rubber.

Figure 6.12 also shows that, for glass belted tire chips, the effect of density on K is much smaller than for steel belted tire chips. The reason for this could not be determined.

6.3.2.5 Comparison with results from other laboratory studies

The results of this study are slightly higher than the results from the University of Alaska Fairbanks (Shao, et al., 1995) and similar to those from Quebec, Canada (Dore, et al., 1995). The laboratory study of the thermal conductivity of tire chips done at the University of Alaska Fairbanks shows that the thermal conductivities of tire chips ranging from 0.097 to 0.171 W/m^{°C} (0.056 to 0.099 Btu/hr-ft^{°F}) for two different moisture contents under thawed and frozen conditions with two different compacted densities. The thermal conductivity of dry tire chips was reported as 0.38 W/m^{°C} (0.22 Btu/hr-ft^{°F}) by Dore, et al. (1995). For comparison, the results from this NETC study ranged from 0.195 to 0.318 W/m^{°C} (0.113 to 0.184 Btu/hr-ft^{°F}). A third study reported the thermal conductivity of tire chips as 0.020 W/m^{°C} (0.012 Btu/hr-ft^{°F})

(Benson, et al., 1996). This was measured with a laboratory thermal probe. This value is suspect as it is an order of magnitude less than that measured by Shao, et al. (1995), Dore, et al. (1995), and this NETC study that used more reliable test methods.

One conclusion drawn by Shao, et al. (1995) was that higher densities result in higher thermal conductivities of tire chips. This result is different from that of this study (Figure 6.12). This is possibly caused by the different degree of the free heat convection within the samples. The sample size of the tests conducted in Alaska, Fairbanks was very small (168 mm (6-5/8 in.) in diameter and 45 mm (1.77 in.) in height). Moreover, the tire chips used by Shoa, et al. (1995) were much smaller, resulting in small voids within the sample. Smaller voids would reduce heat transfer by convection. Thus, the apparent thermal conductivity of tire chips will be dominated by the thermal conductivity of rubber and air. In that case, as the density increases, the air content decreases. Because the thermal conductivity of air is much lower than that of rubber, the apparent thermal conductivity of tire chips decreases.

6.3.3 Tire chip/gravel mixtures

The apparent thermal conductivity of tire chip/gravel mixtures depends on the thermal properties of both tire chips and gravel. The test results for air dried tire chip/gravel mixtures are listed in Table 6.1. Results for moist samples are given in Table 6.2. The influence of density, moisture, and percent gravel in the mixtures is discussed in the following sections.

6.3.3.1 Influence of density

The relationship between the apparent thermal conductivity and density for tire chip/gravel mixtures is similar to that of tire chips alone. The apparent thermal conductivity versus density for each mixture is shown in Figures 6.13 through 6.18. In general, the thermal conductivity decreases as density increases. Possible explanations for this were discussed in Section 6.2.2.1.

6.3.3.2 Influence of percent gravel in the mixture

The apparent thermal conductivity of tire chip/gravel mixtures depends on the thermal conductivity of tire chips, gravel and the percent gravel in the mixture. For a given surcharge, the thermal conductivity of air dried tire chip/gravel mixtures increases as the percent gravel increases as shown in Figures 6.19 through 6.21. This is due to the lower thermal conductivity of rubber compared to gravel. Since the density increases as the percent gravel increases, there is also a relationship between density and thermal conductivity as shown in Figure 6.22. Likewise, there is a general trend of decreasing thermal conductivity with increasing void ratio as shown in Figure 6.23. It is seen that the void ratio tends to be higher as the tire chip content increases. Thus, the better insulating properties of tire chips may be due not only to the lower thermal conductivity of rubber, but also the greater amount of air contained in the voids.

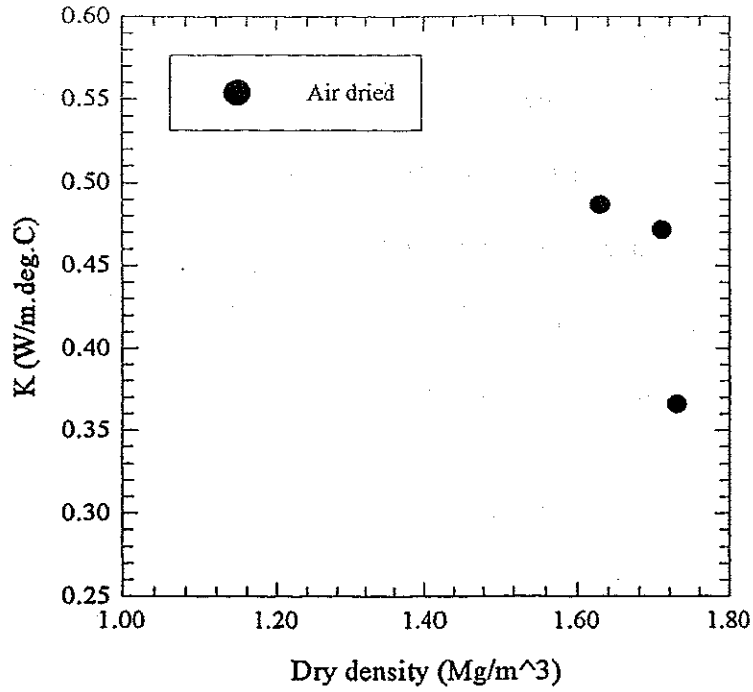


Figure 6.13 33% F&B glass belted/67% gravel mixture: apparent thermal conductivity versus density

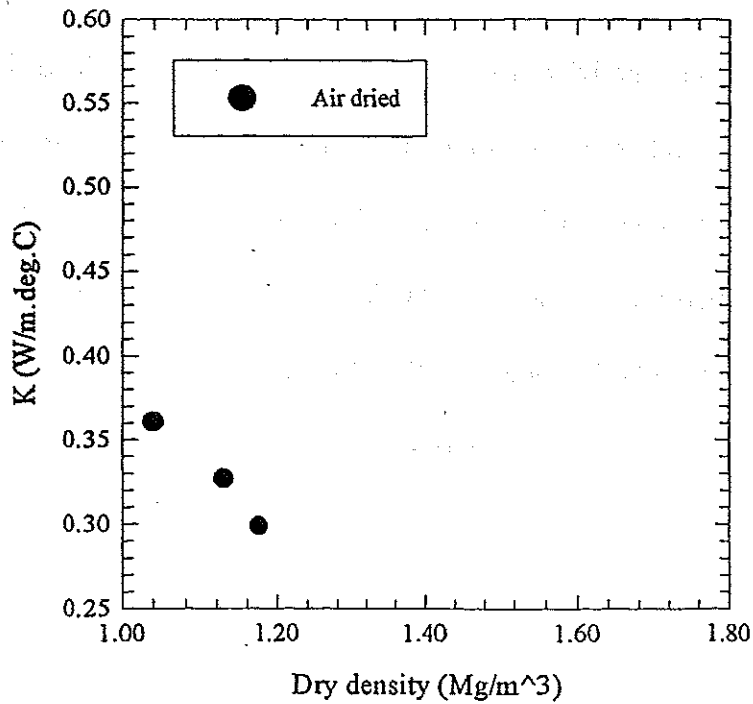


Figure 6.14 67% F&B glass belted/33% gravel mixture: apparent thermal conductivity versus density

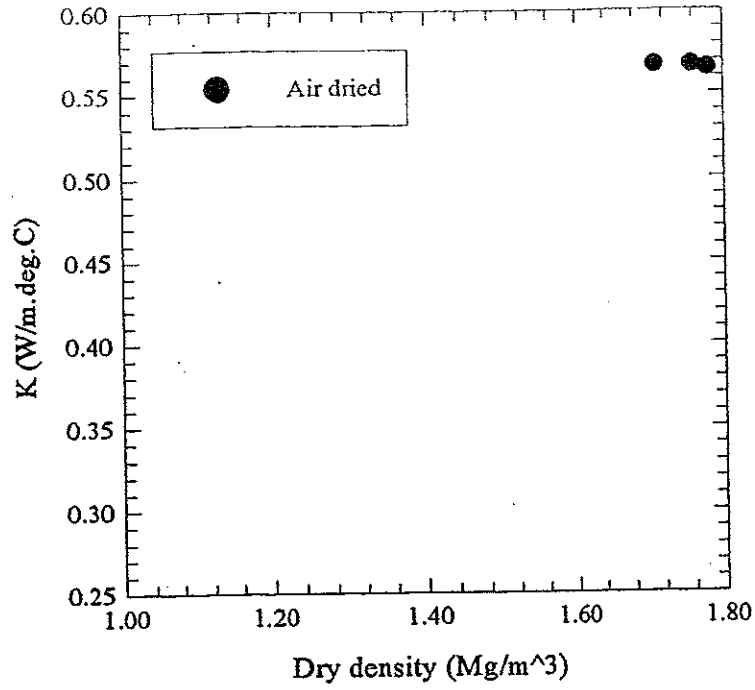


Figure 6.15 33% F&B steel belted/67% gravel mixture: apparent thermal conductivity versus density

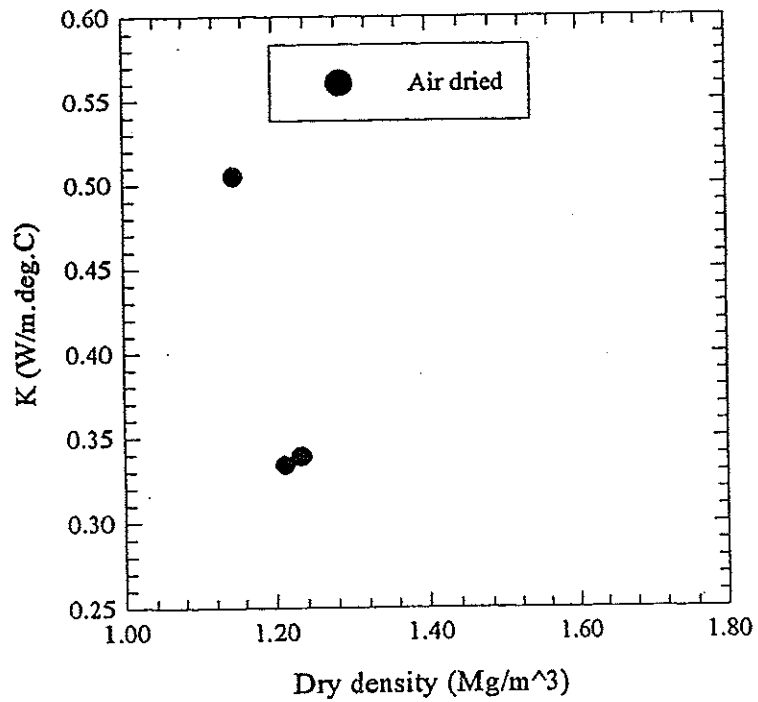


Figure 6.16 67% F&B steel belted/33% gravel mixture: apparent thermal conductivity versus density

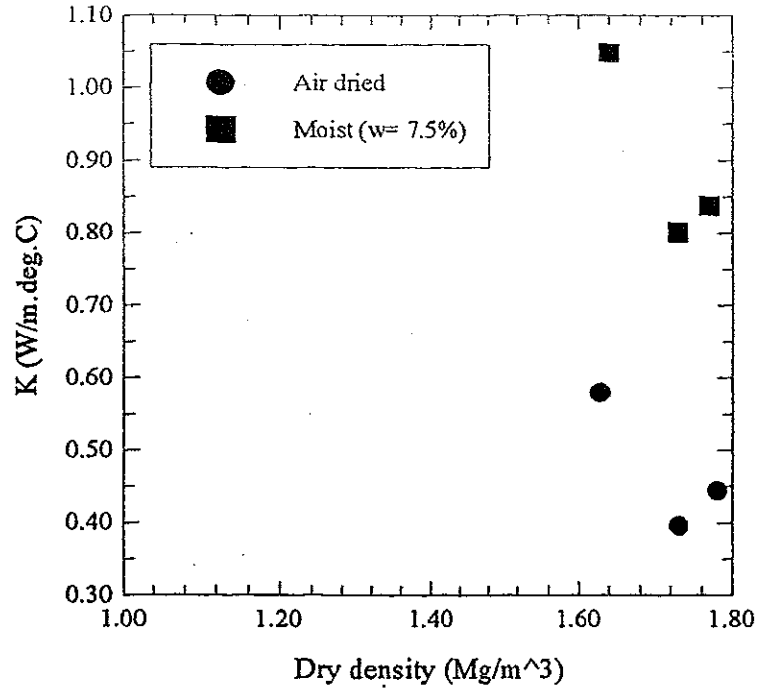


Figure 6.17 33% Palmer/67% gravel mixture: apparent thermal conductivity versus density

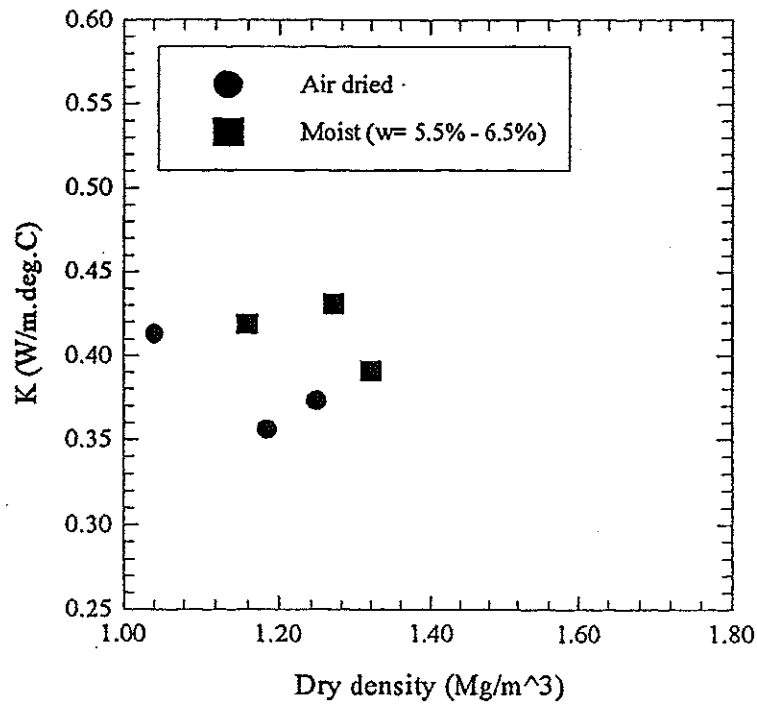


Figure 6.18 67% Palmer/33% gravel mixture: apparent thermal conductivity versus density

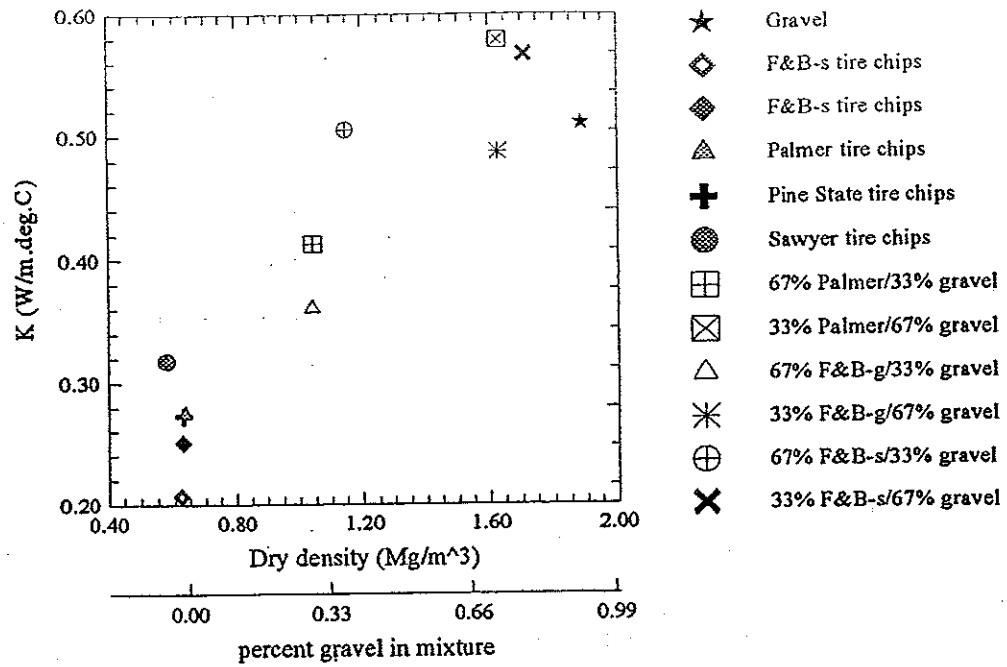


Figure 6.19 Comparison: apparent thermal conductivity versus density for air samples (no surcharge)

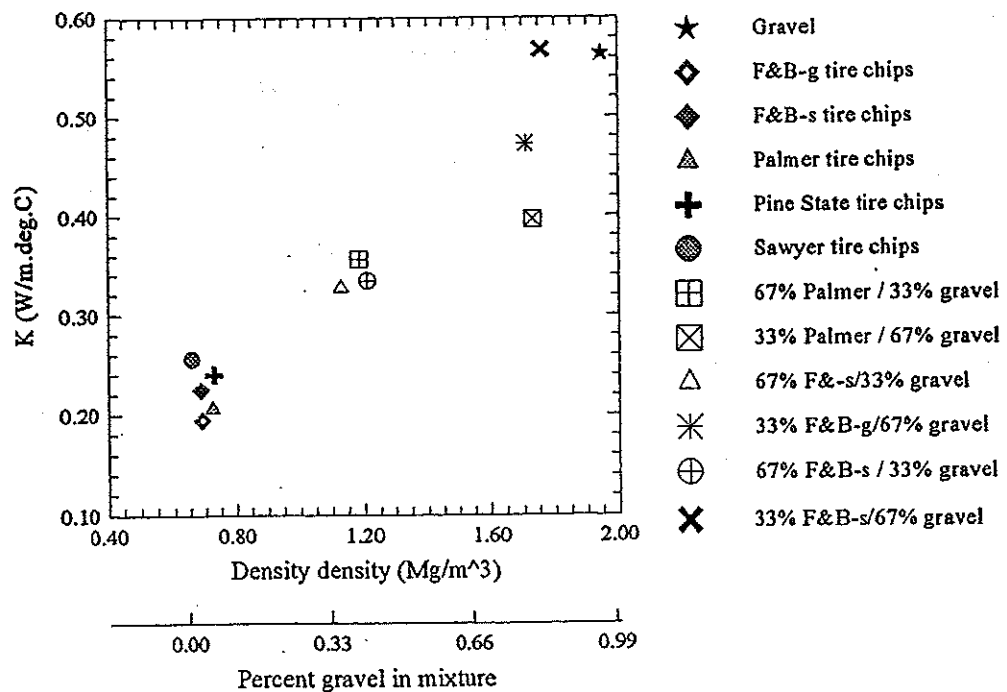


Figure 6.20 Comparison: apparent thermal conductivity versus density for air dried samples (9 kPa surcharge)

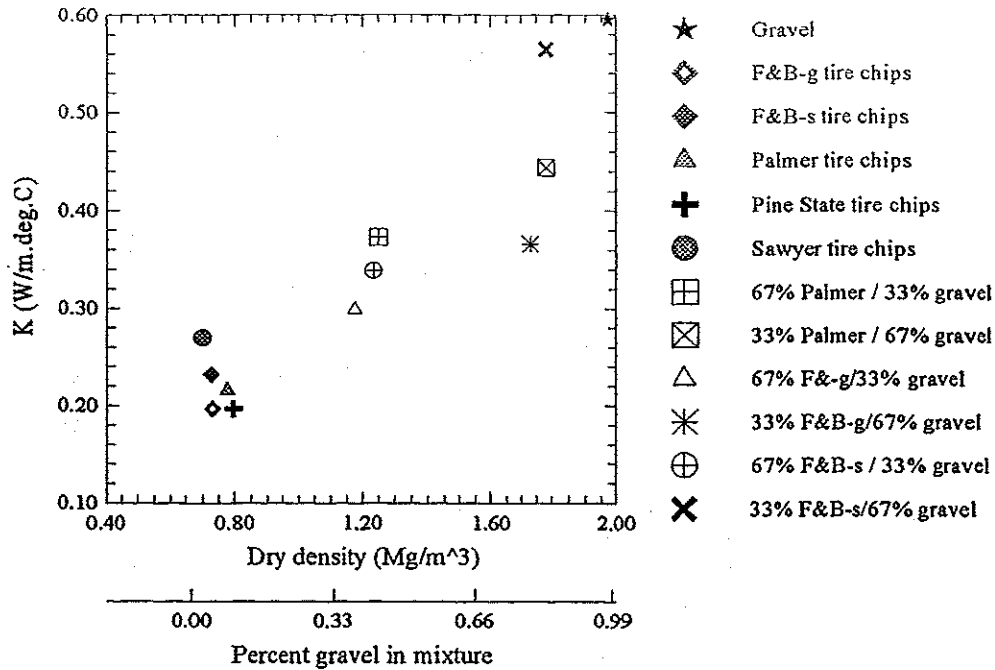


Figure 6.21 Comparison: apparent thermal conductivity versus density for air dried samples (18 kPa surcharge)

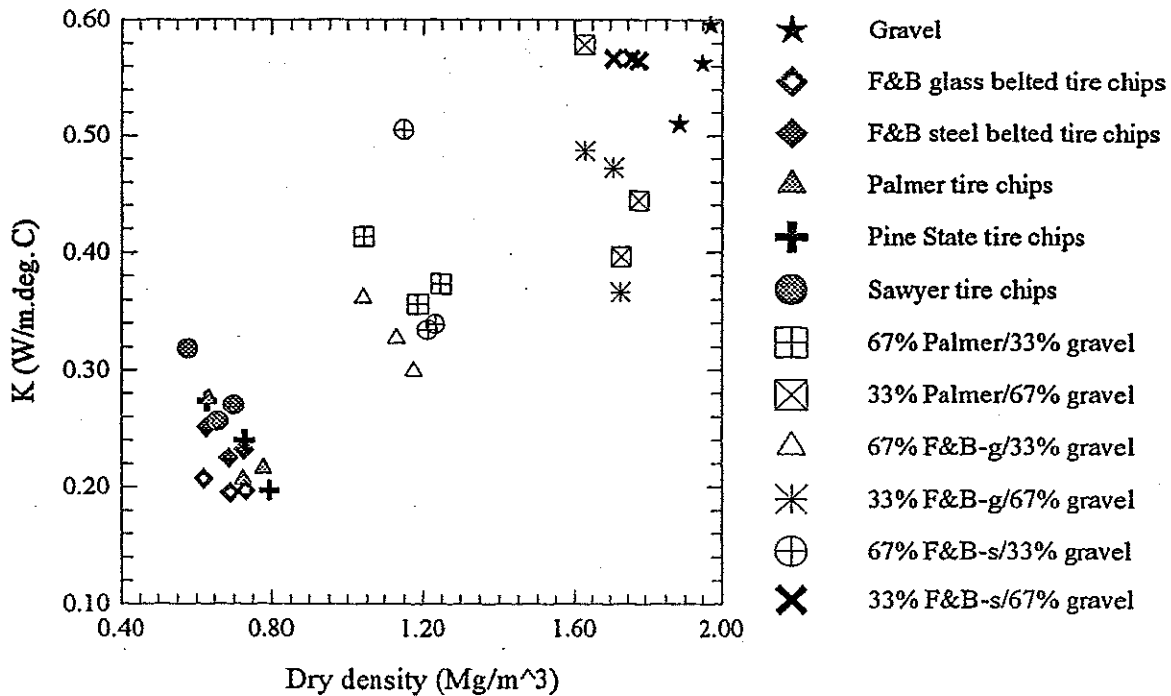


Figure 6.22 Comparison: apparent thermal conductivity versus density for air dried samples

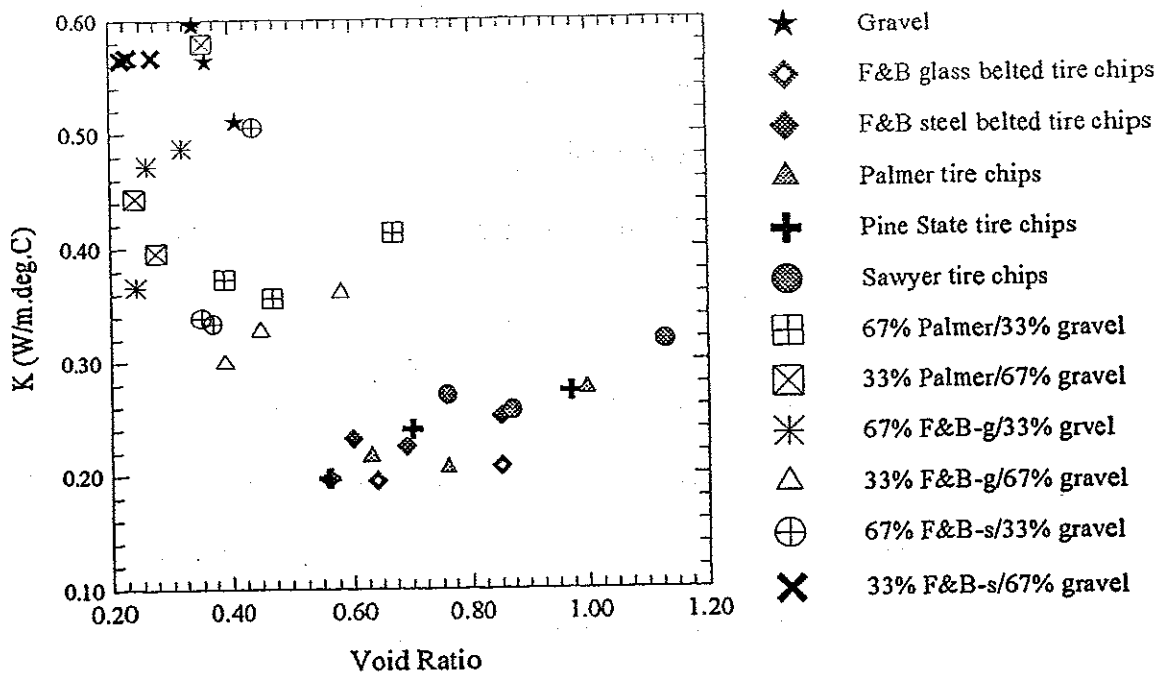


Figure 6.23 Comparison: apparent thermal conductivity versus void ratio for air dried samples

6.3.3.3 Influence of water content

The effect of water content on the thermal conductivity of tire chip gravel mixtures can be seen in Figures 6.17 and 6.18. For the mixture with 33% Palmer/67% gravel, increasing the water content from air dried to 7.5% increased the thermal conductivity by about 0.4 W/m²·°C (0.2 Btu/hr·ft²·°F). In contrast, the thermal conductivity of the mixture with 67% Palmer/33% gravel increased by about 0.05 W/m²·°C (0.03 Btu/hr·ft²·°F) when the water content was increased to between 5.5% and 6.5%. Thus, water content has a large effect on thermal conductivity for mixtures that are composed primarily of gravel, while the effect is small for mixtures composed primarily of tire chips.

6.4 INFLUENCE OF TEMPERATURE GRADIENT

Temperature gradient will affect the magnitude of free heat convection and consequently the resulting apparent thermal conductivity. This was investigated for Pine State tire chips at full surcharge under three temperature gradients. The results are shown in Table 6.3.

Three temperature gradients were investigated: 22.3, 42.8 and 68.5°C/m (12.2, 23.5 and 37.6 °F/ft). The apparent thermal conductivity versus temperature gradient is plotted in Figure 6.24. This figure shows that the K increases by about 40% as the temperature gradient increases by about 46°C/m (25°F/ft). This is probably caused by increased free heat convection as the temperature gradient increases.

All the other samples were tested under a temperature gradient of about 27°C/m (15°F/ft). Thus, the field thermal conductivity of tire chips would be expected to be lower than the laboratory measured value if the temperature gradient in the field is lower than 27 °C/m (15°F/ft).

Table 6.3 Temperature gradient influence - Pine State tire chips under full surcharge

Temperature Gradient		Apparent Thermal Conductivity	
(°F/ft)	(°C/m)	(Btu/hr-ft-°F)	(W/m-°C)
12.22	22.3	0.093	0.161
23.5	42.8	0.114	0.197
37.6	68.5	0.131	0.226

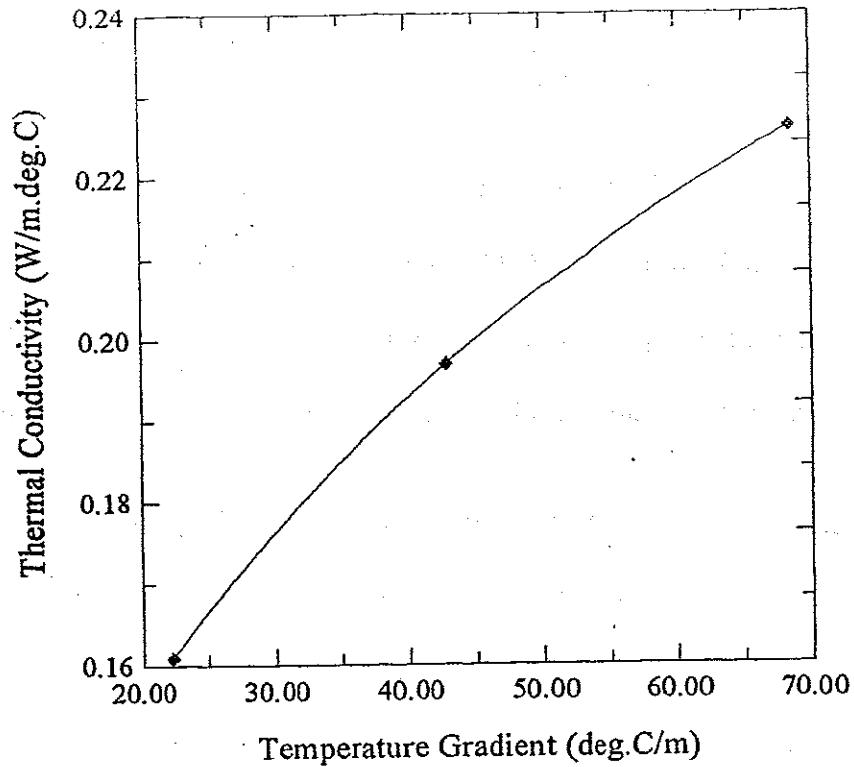


Figure 6.24 Apparent thermal conductivity versus temperature gradient

6.5 SUMMARY

Air dried samples of five types of tire chips, six tire chip/gravel mixtures and one gravel were tested. In addition, moist samples of two types of tire chips, two tire chip/gravel mixtures, and one gravel were tested. The test results show the following:

- (1) Gravel has the highest apparent thermal conductivity of materials tested in this study. The values varied from 0.510 to 0.596 W/m^{°C} (0.295 to 0.345 Btu/hr^{°F}·ft) for air dried samples and 1.21 to 1.63 W/m^{°C} (0.700 to 0.942 Btu/hr^{°F}·ft) for moist samples. Increasing water content significantly increases the thermal conductivity of gravel.

- (2) The apparent thermal conductivity of gravel increases as the dry density increases which is probably caused by the decreased air within the sample.
- (3) Tire chips have the lowest thermal conductivity of materials tested in this study. The values varied from 0.195 to 0.318 W/m·°C (0.113 to 0.194 Btu/hr·°F·ft) for both air dried and moist samples. The effect of moisture on thermal conductivity of tire chips was small and had a smaller influence than other factors such as density.
- (4) The apparent thermal conductivity of tire chips tends to decrease as the dry density increases. This is probably caused by a trade-off of decreased free heat convection which would reduce thermal conductivity and the decrease of trapped air which would increase thermal conductivity.
- (5) For the range of tire chip sizes tested in this study (maximum size from 38 to 76 mm; 1.5 to 3 in.), tire chip size is not a controlling factor on the apparent thermal conductivity of tire chips.
- (6) Air dried glass belted tire chips have a lower apparent thermal conductivity than steel belted chips, however, the apparent thermal conductivity of moist glass belted chips was about the same as for steel belted chips.
- (7) The apparent thermal conductivity of tire chips increases as the temperature gradient increases. This is probably caused by increased free heat convection as the temperature gradient increases.

7. COMPARISON WITH RICHMOND FIELD TRIAL

7.1 INTRODUCTION

A field trial using tire chips as subgrade insulation for a gravel surfaced road was constructed by Humphrey and Eaton (1993a, 1993b, 1994, 1995) in Richmond, Maine, in 1992. Detailed information on this field trial has been included in Section 2.4.1 of this report. The thermal conductivity of tire chips was estimated from the temperature measurements made as part of the field trial. The calculation procedure is presented below. Then in the following section, the backcalculated thermal conductivity is compared to laboratory values measured as part of this study.

7.2 CALCULATION PROCEDURE

The approach used to backcalculate the thermal conductivity from the subsurface temperature measurements made at the Richmond field trial is two fold. First, it was assumed that by mid-February, 1994, the heat flow had reached steady state conditions. This assumption is justified by examination of the depth of frost penetration versus date for the winter of 1993-1994 as shown in Figure 2.11. It can be seen that the depth of frost penetration had stabilized by mid-February in Sections D and E, indicating that the rate at which heat was being removed from the freezing front was approximately equal to the rate at which heat was being supplied by unfrozen soil at greater depths. In Section A, B, and C, the frost was still penetrating at a slow rate indicating that steady state conditions had not been achieved. Thus, calculations using temperatures from these sections would not be as reliable as those from Sections D and E.

The second part of the approach was to use the backcalculated K in the modified Berggren equation (Aldrich, 1956), a non-steady state solution, to calculate the depth of frost penetration. Thus, solutions were obtained using both steady state and non-steady state conditions.

Assuming steady state conditions, a constant temperature gradient is generated across each layer of uniform material, as shown in Figure 7.1. Comparison with Figure 2.12 shows that on February 16, 1994, similar temperature profiles were present in each test section except for Section A. In this section, the zone with the higher gradient did not coincide with the location of the tire chip layer. Perhaps there is an error with the constructed elevations of the tire chip layer or thermocouples in this section.

For steady state conditions, the heat flux across each layer of soil would be the same, therefore

$$q_1 = q_2 = q_3 \quad (7.1)$$

where q_n is the heat flux across layer n.

The equation for steady state one-dimensional heat flow is

$$q_n = K_n \cdot i_n \quad (7.2)$$

Using Equations 7.1 and 7.2, the following relationship can be found between K_2 and K_3 :

$$K_2 = \frac{i_3}{i_2} \cdot K_3 \quad (7.3)$$

If the temperature gradient in two layers and the thermal conductivity of one layer are known, then the thermal conductivity of the other layer can be estimated. In this

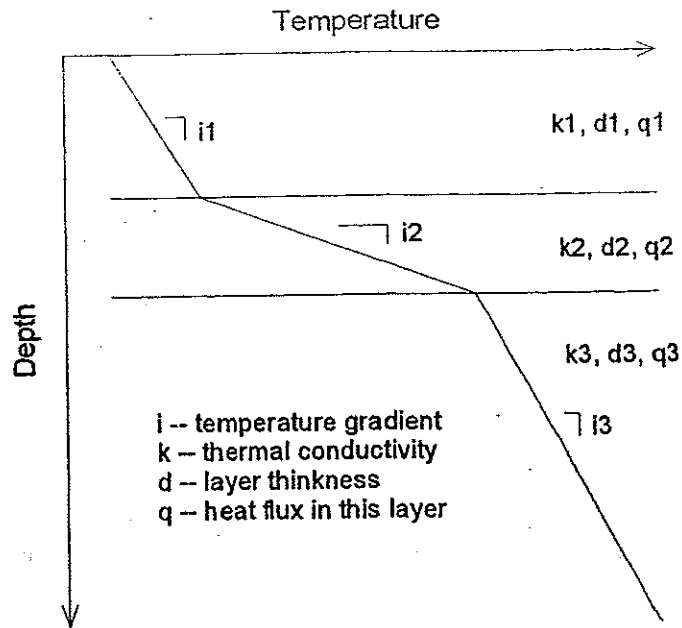


Figure 7.1 Temperature vs. depth

study, the temperature gradient in each layer can be obtained directly from the temperature vs. depth plot (Figure 2.12). For these calculations, layer 2 is taken to be the tire chip layer and layer 3 is taken to be the underlying soil. Thus, if the thermal conductivity of the underlying soil can be estimated, the thermal conductivity of tire chips can be estimated by Equation 7.3. An example calculation is given below.

Example: Section D, February 16, 1994.

305 mm thick tire chip layer with 457 mm of overlying gravel fill; From Figure 2.11 get:

$$i_2 = \frac{\Delta T}{\Delta L} = \frac{(-0.3^\circ C) - (-7.7^\circ C)}{0.305m} = 24.3^\circ C/m$$

$$i_3 = \frac{\Delta T}{\Delta L} = \frac{4^\circ C - (-0.3^\circ C)}{(2.1 - 0.76)m} = 3.21^\circ C/m$$

$$K_2 = \frac{i_3}{i_2} \cdot K_3 = \frac{3.21^\circ C/m}{24.3^\circ C/m} \cdot K_3 = 0.13 \cdot K_3$$

Repeating the above procedure for the other sections, the relationship between the thermal conductivity of the tire chip layer and the thermal conductivity of the underlying layer can be summarized as follows:

Section A	----
Section B	$0.28 \cdot K_3$
Section C	$0.23 \cdot K_3$
Section D	$0.13 \cdot K_3$
Section E	$0.13 \cdot K_3$

The temperature gradient of tire chip layer in Section A could not be reliably determined as noted previously.

The above data shows that thermal conductivity of tire chips is about 13% to 28% of that of the underlying soil. The actual value of $K_{\text{tire-chip}}$ (K_2) depends on the thermal conductivity of the underlying soil (K_3). Based on observations made during construction and measured water levels, the soil beneath the tire chip layer in Sections B and C was unsaturated frozen coarse grained soil, and in Sections D and E it was saturated unfrozen fine grained soil. Referring to Kersten (1949), a K_3 of $2.6 \text{ W/m}\cdot\text{C}$ ($1.5 \text{ Btu/hr}\cdot\text{ft}\cdot\text{F}$) was selected for Sections B and C and $1.6 \text{ W/m}\cdot\text{C}$ ($0.9 \text{ Btu/hr}\cdot\text{ft}\cdot\text{F}$) was selected for Sections D and E. Using these values in the relationships given above, the backcalculated thermal conductivity of tire chips in each section is given in Table 7.1. The backcalculated thermal conductivity of tire chips vary from $0.20 \text{ W/m}\cdot\text{C}$ ($0.12 \text{ Btu/hr}\cdot\text{ft}\cdot\text{F}$) to $0.72 \text{ W/m}\cdot\text{C}$ ($0.42 \text{ Btu/hr}\cdot\text{ft}\cdot\text{F}$).

The modified Berggren method was used to verify the above estimates. This method is a non-steady state solution that considers the volumetric heat of the soils and latent heat of fusion of water as the frost penetrates deeper into the ground. The K values of tire chips in Table 7.1 were used in the modified Berggren equation to calculate the depth of frost penetration. The calculated frost penetration depth was then compared with the measured value. If there is good agreement, this adds credibility to the backcalculated K value. An example calculation is given below (Aldrich, 1956).

Table 7.1 Estimated $K_{\text{tire-chips}}$

Section	Relation	Estimated K_3 (W/m $^{\circ}$ C)	Estimated $K_{\text{tire-chips}}$	
			(W/m $^{\circ}$ C)	(Btu/hr \cdot ft \cdot $^{\circ}$ F)
Section B	$0.28 \cdot k_3$	2.6	0.72	0.42
Section C	$0.23 \cdot k_3$	2.6	0.60	0.35
Section D	$0.13 \cdot k_3$	1.6	0.20	0.12
Section E	$0.13 \cdot k_3$	1.6	0.20	0.12

EXAMPLE

Using data from the winter of 1993-4 and the geometry of Section C

FI (Freezing Index) = 707 $^{\circ}$ C-days (1273 $^{\circ}$ F-days)

Length of freezing season $t = 80$ days

Mean annual temperature $T_0 = 6.1^{\circ}$ C (43 $^{\circ}$ F) (from Linell, 1953, for measured FI)

Soil and tire chip layer thicknesses from Section C

Choose dry density and water content for soil layers based on field data measured during construction and experience with similar soils

Choose dry density of tire chips corresponding to overburden pressure (Humphrey, et al., 1992); choose water content of tire chips based on experience

Choose thermal conductivity of soil layers based on dry density and water content in conjunction with charts presented by Kersten (1949); for this example use a thermal conductivity of tire chips of 0.20 W/m $^{\circ}$ C

Summary of input parameters:

Layer	Thickness x (m)	Dry density ρ_d (Mg/m ³)	Water content w (%)	Thermal conductivity K (W/m·°C)
Surface	0.457	1.92	5	1.8
Tire chips	0.152	0.72	2	0.20
Exist. Grav.	0.35	1.92	5	1.8
Subgrade	3.00	1.76	16	1.7

Calculation procedure:

1. Compute volumetric heat capacity for soil layers in units of Cal/m³ (Jumikis, 1977)

$$\text{unfrozen soil: } c_{vu} = \rho_d [c_{ms} + c_{mw} \cdot w] = \rho_d [0.2 + 1.0 \cdot w] \quad (7.4)$$

$$\text{frozen soil: } c_{vf} = \rho_d [c_{ms} + c_{mi} \cdot w] = \rho_d [0.2 + 0.5 \cdot w] \quad (7.5)$$

where c_{mw} = mass heat capacity of water = 1.0 Cal/kg·°C

c_{mi} = mass heat capacity of ice = 0.5 Cal/kg·°C

c_{ms} = mass heat capacity of soil = 0.2 Cal/kg·°C

w = water content

for calculation use the average of the frozen and unfrozen values:

$$c_v = [c_{vu} + c_{vf}] / 2 \quad (7.6)$$

Thus: surface $c_v = 456 \text{ Cal/m}^3 \cdot ^\circ\text{C}$

existing gravel $c_v = 456 \text{ Cal/m}^3 \cdot ^\circ\text{C}$

subgrade $c_v = 563 \text{ Cal/m}^3 \cdot ^\circ\text{C}$

2. Calculate the volumetric heat capacity of tire chips

The calculation of volumetric heat capacity begins with calculation of the mass heat capacity tire chips from the mass heat capacity of steel and hard rubber.

The calculation is a simple proportion based on the amount of steel in tires as shown below:

$$c_{m\text{-chip}} = \alpha_{\text{steel}} \% \cdot c_{m\text{-steel}} + (1 - \alpha_{\text{steel}}) \% \cdot c_{m\text{-rubber}} \quad (7.7)$$

where: $c_{m\text{-steel}}$ = mass heat capacity of steel = 0.113 Cal/kg·°C

$c_{m\text{-rubber}}$ = mass heat capacity of rubber = 0.280 Cal/kg·°C

α_{steel} = percent steel content by mass = 12%

Thus, $c_{m\text{-chip}}$ is computed as 0.260 Cal/kg·°C (0.260 Btu/lb·°F).

Next, the volumetric heat capacity of tire chips is computed from:

$$c_{v\text{-chip}} = [\rho_{d\text{-chip}}(c_{m\text{-chip}} + c_{mw} \cdot w) + \rho_{d\text{-chip}}(c_{m\text{-chip}} + c_{mi} \cdot w)]/2 \quad (7.8)$$

where: $\rho_{d\text{-chip}}$ = dry density of tire chips in kg/m^3

$c_{m\text{-chip}}$ = mass heat capacity of tire chips in $\text{Cal}/\text{kg}\cdot^\circ\text{C}$ ($\text{Btu}/\text{lb}\cdot^\circ\text{F}$)

For this example $c_{v\text{-chip}}$ is computed to be $198 \text{ Cal}/\text{m}^3\cdot^\circ\text{C}$ ($12.4 \text{ Btu}/\text{ft}^3\cdot^\circ\text{F}$)

3. Compute the latent heat of fusion for each material.

Latent heat of fusion is the amount of heat liberated when water changes from liquid to ice and is given by the following equation:

$$L = \rho_d \cdot w \cdot 80(\text{cal} / \text{kg}) \quad (7.9)$$

Thus: surface	$L = 7680 \text{ Cal}/\text{m}^3$
tire chip	$L = 1152 \text{ Cal}/\text{m}^3$
existing gravel	$L = 7680 \text{ Cal}/\text{m}^3$
subgrade	$L = 22528 \text{ Cal}/\text{m}^3$

4. Calculate the thermal resistance of each layer

$$R_i = \frac{x_i}{K_i} \quad (7.10)$$

5. Compute average volumetric heat capacity and latent heat of fusion

Assume frost penetration depth is: $x_{\text{est}} = 1.15 \text{ m}$ (return to this step later and adjust if needed)

Depth of frost penetration in last layer: $x_4 = x_{\text{est}} - x_1 - x_2 - x_3 = 0.19 \cdot \text{m}$

$$\text{Average } c_v: c_{v\text{-avg}} = \frac{\sum_1^4 c_{ci} \cdot x_i}{\sum_1^4 x_i} = 440 \cdot \text{Cal} / \text{m}^3 \cdot ^\circ\text{C} \quad (7.11)$$

$$\text{Average } L: L_{\text{avg}} = \frac{\sum_1^4 L_i \cdot x_i}{\sum_1^4 x_i} = 9272 \cdot \text{Cal} / \text{m}^3 \quad (7.12)$$

6. Determine correction coefficient λ , which accounts for the initial temperature and volumetric heat capacity of the soil

$$\text{Thermal ratio: } \alpha = \frac{(T_0 - T_f) \cdot t}{FI} = \frac{(T_0 - 0^\circ \text{C}) \cdot t}{FI} = 0.69 \quad (7.13)$$

$$\text{Fusion parameter: } \mu = \frac{c_{v\text{-avg}} \cdot FI}{L_{\text{avg}} \cdot t} = 0.419 \quad (7.14)$$

From Aldrich (1956), get: $\lambda = 0.74$

7. Compute partial freezing index for each layer

$$N_1 = \frac{L_1}{\lambda^2} \cdot x_1 \cdot \frac{R_1}{2} = 33.9 \text{ }^\circ\text{C}\cdot\text{days} \quad (7.15a)$$

$$N_2 = \frac{L_2}{\lambda^2} \cdot x_2 \cdot \left(R_1 + \frac{R_2}{2} \right) = 8.4 \text{ }^\circ\text{C}\cdot\text{days} \quad (7.15b)$$

$$N_3 = \frac{L_3}{\lambda^2} \cdot x_3 \cdot \left(R_1 + R_2 + \frac{R_3}{2} \right) = 227.0 \text{ }^\circ\text{C}\cdot\text{days} \quad (7.15c)$$

8. Compute freezing degree days remaining for last layer

$$N_4 = FI - \sum_1^3 N_i = 437.7 \text{ }^\circ\text{C}\cdot\text{days} \quad (7.16)$$

9. Compute depth of frost penetration into last layer

$$\zeta = -K_4 \cdot \sum_1^3 R_i + \sqrt{K_4^2 \cdot \left(\sum_1^3 R_i \right)^2 + 2 \cdot K_4 \cdot \frac{N_4 \cdot \lambda^2}{L_4}} \quad (7.17)$$

$$\zeta = 0.201 \cdot \text{m} \approx 0.191 \text{ m assumed in step 5, OK}$$

9. Calculated frost penetration depth

$$d = \sum_1^3 x_i + \zeta = 1.16 \cdot \text{m} \quad (7.18)$$

For comparison, the measured frost penetration depth in Section C was 1.21 m. The calculated value is 4% lower than the measured value. This is good agreement, suggesting that the K value of 0.20 is reasonable.

The above calculation procedure was repeated for the control section and the other tire chip sections. The lowest and highest $K_{\text{tire-chip}}$ estimated from the steady state method were used, namely, 0.20 W/m \cdot °C and 0.72 W/m \cdot °C, to represent the possible range of thermal conductivity. Calculated and measured frost penetration depths are compared in Table 7.2.

The results in Table 7.2 show that the estimated frost penetration depth with $K_{\text{tire-chip}} = 0.20$ W/m \cdot °C (0.12 Btu/hr \cdot ft \cdot °F) are close to the measured values. With a $K_{\text{tire-chip}}$ of 0.72 W/m \cdot °C the calculated frost penetration was 25% to 42% greater than the measured values. It is recalled that $K_{\text{tire-chip}} = 0.72$ W/m \cdot °C was obtained from $K_{\text{tire-chip}}/K_{\text{soil}} = 0.28$. This was based on the assumption of steady state conditions in Section B, but this section, as well as in Section C, had not totally attained steady state conditions. Based on this observation and the calculations with the modified Berggren equation, it is felt that $K_{\text{tire-chip}}/K_{\text{soil}} = 0.13$ resulting in a $K_{\text{tire-chip}}$ of about 0.20 W/m \cdot °C

Table 7.2 Frost penetration depth in Richmond, Maine, project

Section	Measured (m)	Calculated (m)			
		$K_{\text{tire-chip}} = 0.20$ W/m \cdot °C	% difference*	$K_{\text{tire-chip}} = 0.72$ W/m \cdot °C	% difference*
Control	1.42	1.42	0%	---	---
A&B	1.06	1.05	-1%	1.33	+25%
C	1.21	1.16	-4%	1.43	+18%
D	0.90	0.97	+8%	1.28	+42%
E	0.96	1.10	+15%	1.36	+42%

* "-" indicates calculated depth less than measured depth; "+" indicates calculated depth greater than measured depth.

(0.12 Btu/hr-ft·°F) is more reliable. In addition, the estimated depth of frost penetration is in very close agreement with the measured value in control section, which indicates the reasonableness of the thermal properties chosen for the non-tire chip layers.

7.3 COMPARISON WITH LABORATORY MEASURED THERMAL CONDUCTIVITY

Tire chips used in the Richmond project were from Pine State Recycling. Laboratory results of the tire chips used in field trial are plotted versus surcharge in Figure 7.2. This figure was used to obtain the laboratory thermal conductivity corresponding to the surcharge present in each test section. The results are summarized in Table 7.3. The laboratory measurements in Figure 7.2 were done under a temperature gradient of about

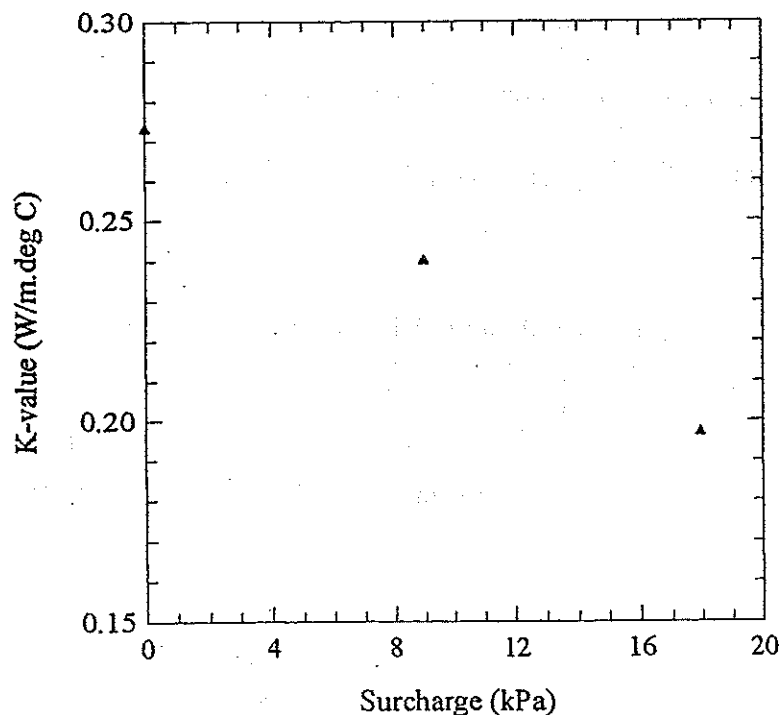


Figure 7.2 Apparent thermal conductivity versus surcharge for air dried Pine State tire chips at a temperature gradient of about 42.8°C/m (23.5°F/ft)

Table 7.3 Summary of field and laboratory condition

Section	Field surcharge (kPa)	Field temperature gradient in tire chip layer (°C/m)	Air dried laboratory K at field surcharge and 42.8°C/m gradient (W/m·°C)	Approximate air dried K corrected to field temperature gradient (W/m·°C)	Percent difference from back-calculated K (0.20 W/m·°C)*
Section A&B	6	13	0.25	0.18	-10%
Section C	9	13	0.24	0.17	-15%
Section D	9	15	0.24	0.18	-10%
Section E	12	17	0.23	0.17	-15%

* "-" indicates that the laboratory K corrected to the field surcharge and temperature gradient is less than the K backcalculated from the field trial.

42.8°C/m (23.5°F/ft), which was twice as high as the temperature gradient measured in the tire chip layer in the Richmond field trial. It is recalled that thermal conductivity decreases as the temperature gradient decreases (see Figure 6.24). The relationship between thermal conductivity and temperature gradient was not available with surcharges corresponding to the field conditions. However, it was assumed that the slope of the plot of thermal conductivity versus gradient measured at a surcharge of 9 kPa (188 psf) would be the same for the field surcharges. This allowed the laboratory measured thermal conductivity to be corrected approximately to the field temperature gradient yielding the values shown in Table 7.3. The difference between the laboratory and back calculated thermal conductivity ranging from 10% to 15%.

This comparison shows that the thermal conductivity of tire chips backcalculated from the Richmond field trial agrees very well with the laboratory measurement. The

small difference between the laboratory measured K and the backcalculated K can possibly be explained by the effect of moisture which slightly increases K as discussed in Section 6.3.2.2 and the different tire chip layer thicknesses in the laboratory and in the field. In addition, the backcalculation of thermal conductivity from the field trial is based on several assumptions. The difference between the assumptions and the actual conditions could also be the cause for the difference.

8. LABORATORY PERMEABILITY TESTS

8.1 INTRODUCTION

The permeabilities of one sample of granular soil, five samples of tire chips, and six samples of tire chip/gravel mixtures were determined. Each sample, except for the granular soil, was compressed to find the relationship between permeability and density. The compression ranged from 0 to 22% for tire chip samples, 0 to 12% for samples containing 67% tire chips/33% gravel, and 0 to 5% for samples containing 33% tire chips/67% gravel. The density and void ratio at each compression were determined. The testing apparatus was constructed for a previous NETC project (Humphrey, et al., 1992). A constant head tank was added to the apparatus to allow measurement of the lower permeabilities of soil and tire chip/gravel mixtures. This modification is discussed in the apparatus section.

8.2 APPARATUS

The testing apparatus was a modification of the apparatus used for a previous NETC project (Humphrey, et al., 1992). The original apparatus was based on a design used by the California Department of Transportation (Bressette, 1984) and is similar to AASHTO T125 *Permeability of Granular Soils (Constant Head)*. The apparatus is a constant head apparatus. The discussion of the apparatus is divided into two parts: the body of the permeameter and the constant head tank. A photograph of the setup is shown in Figure 8.1.

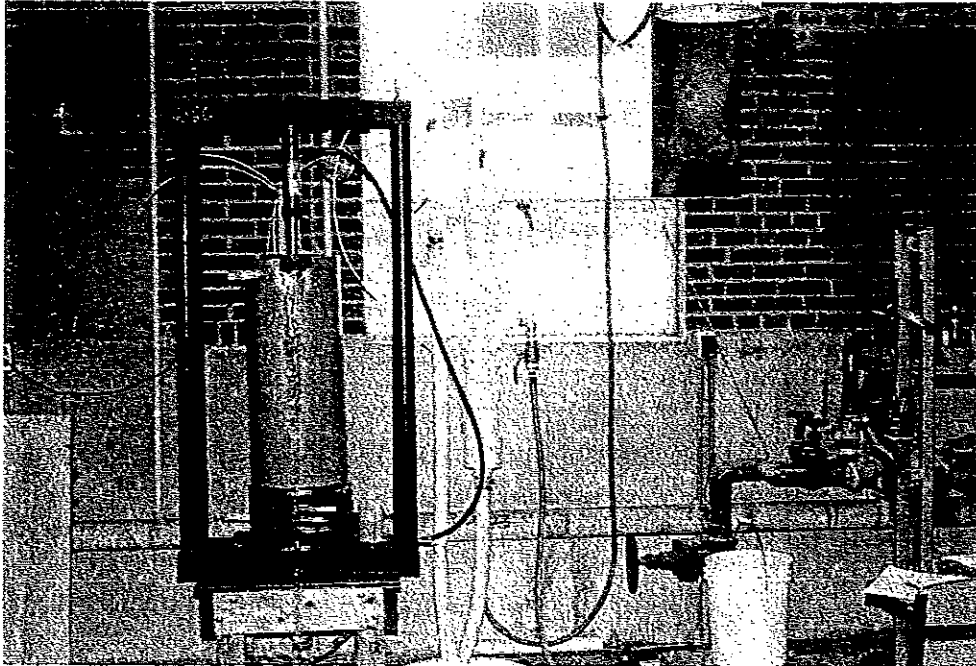


Figure 8.1 Photograph of permeameter and constant head tank

8.2.1 Permeameter body

The permeameter is the original design for a previous NETC project (Humphrey, et al., 1992). The only modification to the permeameter body was the addition of a union fitting connecting the inlet of the permeameter with the outlet of the constant head tank via the flexible hose as shown in Figure 8.2. This made it easier to disconnect the hose when samples were emptied. In the previous design, two garden hoses were hooked into the inlet at the base of the permeameter for water supply. The addition of the constant head tank made this dual inlet unnecessary, since the two garden hoses are now connected to the constant head tank.

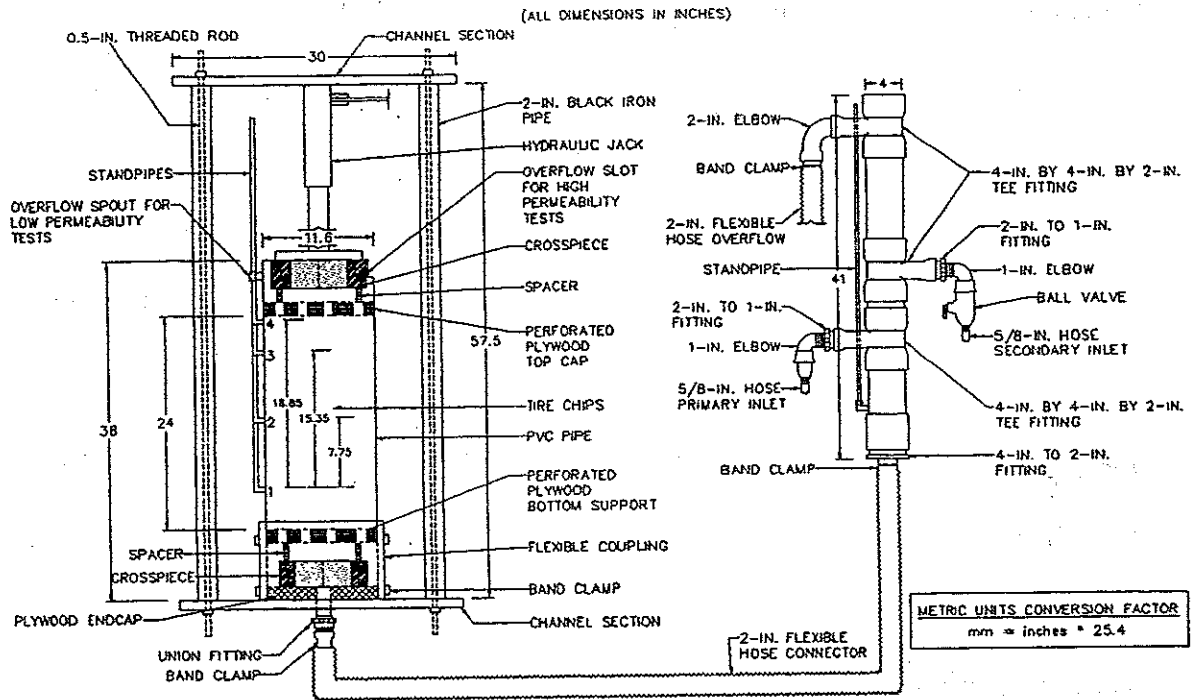


Figure 8.2 Permeameter and constant head tank detail

The permeameter body was a 965-mm (38-in.) long PVC pipe with an inner diameter of 295 mm (11.6 in.), as shown in Figure 8.2. A plywood plug at the bottom of the permeameter was made from two thicknesses of 7.5-mm (3/4-in.) plywood glued together. Silicon caulk was used around the perimeter of the plywood plug and a flexible coupling was tightened onto the outside of the permeameter and plywood plug with band clamps to create a water tight seal. The water inlet was a 38-mm (1.5-in.) hole drilled in the center of the plywood plug over which a pipe flange threaded for 38-mm (1.5-in.) black iron pipe was attached. A 102-mm (4-in.) wide by 51-mm (2-in.) deep slot was cut into the top of the PVC pipe to allow flow of water out of the top of the permeameter when testing high permeability materials as shown in Figures 8.1 and 8.2. For low permeability testing, a 25-mm (1-in.) hole was drilled in the side of the permeameter and a small piece of PVC pipe was attached (shown as "overflow spout" in Figure 8.2) to allow flow of water out of the permeameter into a collection container. The overflow was collected for a measured time interval in a 72-liter (19-gallon) bucket for the high permeability tests and in a small plastic bottle for the low permeability tests. The quantity of flow was determined by weighing the water. To measure the change in head as the water flowed through the apparatus, holes were drilled in the PVC pipe and standpipes were affixed as shown in Figure 8.2.

The sample was supported by a perforated plate constructed of two thicknesses of 7.5-mm (3/4-in.) plywood glued together. The holes in the plate were 25-mm (1-in.) in diameter and resulted in about 40% open surface area. The plate rested on 20.3-mm (0.8-in.) thick spacers made from a stack of 6.4-mm (1/4-in.) washers supported by a crosspiece made from two short lengths of 2 X 4 lumber. A similar perforated plate and

crosspiece was placed on top of the sample. A 9-metric ton (10-ton) hydraulic jack pressing on the top crosspiece was used to compress the samples. A frame made from two channel sections, 12.7-mm (1/2-in.) threaded rods, and 51-mm (2-in.) black iron pipe was used as a reaction for the jack as shown in Figure 8.2.

8.2.2 Constant head tank

A constant head tank was constructed as shown in Figures 8.1 and 8.2 so that a constant input head could be obtained. The tank body consisted of three pieces of 102-mm (4-in.) diameter PVC pipe joined by three tee sections. The entire length of the assembled body is 1041-mm (41-in.) The bottom of the tank was capped by a 102-mm (4-in.) by 51-mm (2-in.) reducing bushing. A 51-mm (2-in.) diameter wire reinforced flexible hose connected the constant head tank outlet to the permeameter inlet.

The 51-mm (2-in.) outlet of the top tee section acted as an overflow to maintain a stable constant head. A 51-mm (2-in.) elbow was attached to the overflow to direct the flow downward. Wire reinforced flexible hose was attached to the elbow, directing the overflow to the floor drains of the laboratory. The middle tee section was connected to the secondary inlet to the constant head tank. This was fed by a 15.9-mm (5/8-in.) garden hose connected to a faucet tap and was used to supply water when testing high permeability materials. A ball valve was placed between the garden hose and the stem of the tee to enable the flow to be adjusted more conveniently. The lowest tee was connected to the primary inlet. This was also fed by a 15.9-mm (5/8-in.) garden hose, but flow was controlled with the spigot on the water faucet. The height of the constant head tank was adjusted by means of a pulley system.

In addition to the standpipes on the permeameter, an additional standpipe was installed on the constant head tank. This was used to measure the head drop between the water levels in the constant head tank and the overflow of the permeameter. This overall measurement was used as a check to compare with the values obtained by the permeameter standpipes for low permeability samples whose flow rate was low enough that head loss in the apparatus itself would be small.

8.3 TESTING METHODOLOGY

Each sample was prepared as follows. The perforated plywood bottom support was placed in the permeameter, and on top of this a fine and coarse screen were placed to prevent soil loss. Each sample was placed in five 122-mm (4.8-in.) thick layers. The proportions of air dried tire chips and air dried gravel for a layer were calculated. The tire chips and soil were weighed on an electronic balance and then mixed in a bucket to create a homogeneous sample. The layers were carefully placed in the permeameter to avoid segregation of the tire chip/soil mixture. Each layer was compacted with 60% of standard Proctor energy. This required 146 blows per layer with a modified Proctor hammer. Although the samples were carefully mixed and placed to prevent segregation, compacting the sample resulted in some segregation. The voids in the tire chips were large enough to allow settlement of the smaller size soil grains. The 67% tire chip/33% gravel samples segregated more than the 33% tire chip/ 67% gravel samples. The total compacted height of a sample was approximately 610 mm (24 in.). Knowing the weight and volume of each sample, the dry density was calculated.

The permeameter and constant head tank were then set up. The faucet(s) were turned on to allow water to fill the constant head tank and start water flowing through the sample and out an overflow on the permeameter. For the tire chip samples, two faucets were required to supply sufficient water. The less permeable mixtures usually required only one faucet to maintain a steady flow to the permeameter. After water was flowing through the sample, the standpipes were monitored until the readings had stabilized. This occurred within 30 to 60 minutes for the tire chip samples, 2 to 8 hours for the tire chip/gravel samples, and up to 24 hours for the gravel sample.

Water was then collected for a measured time interval and weighed on an electronic balance. Water was collected from the overflow slot for the tire chip and 67% tire chip samples and from the overflow spout for 33% tire chip and gravel samples (as shown in Figures 8.1 and 8.2). For tire chip and 67% tire chip samples, water was collected in a 72-liter (19-gallon) bucket and weighed on a 91-kg (200-lb) capacity scale. The scale had accuracy of ± 0.23 kg (0.5 lb) for masses up to 5.7 kg (12.6 lb) and ± 0.45 kg (1.0 lb) for higher masses. For the 33% tire chip and gravel samples water was collected in a small bottle and weighed on a 5,000-gm (11.0-lb) capacity scale with an accuracy of 0.02 gm (4.4×10^{-5} lb). For tests on tire chips, the weight of water collected for a low gradient test was typically between 9.1 and 40.8 kg (20 and 90 lb) per minute. The weight of water collected on the 33% tire chip/67% gravel samples ranged from 3 gm/min (0.0066 lb/min) for 33% F&B steel at a low gradient to about 37 gm/min (0.092 lb/min) for gravel at a high gradient. The weight of water was converted to a volume.

Hydraulic gradients within the sample were measured by noting the difference in water levels between standpipes 1 and 2, 1 and 3, and 1 and 4, and dividing these by their respective distances between standpipes. Using the average of these three gradients and the flow rate, the permeability (k) was found by Darcy's law:

$$k=Q/(iAt) \quad (8.1)$$

where: $i = \Delta h/L =$ hydraulic gradient

$L =$ distance over which the head loss is measured

$\Delta h =$ head loss over length L

$A =$ cross sectional area of permeameter

$t =$ time over which flow is measured

$Q =$ quantity of flow in time t

This method was used to test 12 samples. Each sample was observed three times without compression at a low flow rate. Then the flow rate was raised and three additional observations were made. The reported permeabilities are an average of the permeabilities at high and low gradients. This procedure was then repeated at each compression increment (approximately 51 mm (2 in.) per increment for tire chip samples). A 9-metric ton (10-ton) jack was used to compress the samples. The maximum compression that could be obtained ranged from 0% for the gravel sample to 21.6% for the F&B glass-belted tire chip sample. The density and void ratio at each compression increment was computed.

8.4 RESULTS

The measured permeabilities for each of the 12 samples are listed in Table 8.1. Also listed are the corresponding unit weights, densities, percent mixture by weight, and void ratios for each compression. The samples were tested at four compressions (including 0% compression), with the exception of the F&B steel-belted chips, which were tested at three compressions, and the gravel sample, which was tested only at 0% compression. The reported value of permeability is an average of the high and low flow values for each trial.

Examination of Table 8.1 shows that the permeabilities at all compressions for the tire chip samples range from 1.5 to 26.5 cm/s (1.6×10^6 to 27.4×10^6 ft/yr). These permeabilities are equal to or greater than typical values for clean gravels (Holtz & Kovacs, 1981). Mixtures containing 67% tire chips had permeabilities ranging from 8.0×10^{-2} to 2.9 cm/s (0.08×10^6 to 3.0×10^6 ft/yr). These values are typical of soils ranging from clean sands to clean gravel (Holtz & Kovacs, 1981). Mixtures containing 33% tire chips had permeabilities ranging from 4.1×10^{-4} to 9.7×10^{-3} cm/s (420 to 10,000 ft/yr). These values are typical of glacial tills or very fine sands (Holtz & Kovacs, 1981).

Mixtures with Palmer tire chips had the largest permeabilities. This is especially pronounced in the sample with 67% tire chips. A possible reason is that Palmer tire chips were the largest (76-mm; 3-in.) tire chips tested in this study. Moreover, the Palmer samples often contained pieces that incorporated curved portions of the tire, and greater amounts and larger pieces of steel. Tire chips of with these characteristics may have created larger voids for the water to flow through. In contrast, F&B glass-belted tire

Table 8.1 Summary of permeability results

Mixture % by volume	% chips by weight	Compression %	Unit Weight pcf	Density Mg/m ³	Void Ratio	Permeability cm/s
100% Gravel	0	0.0	126.0	2.02	0.307	0.0022
33% F&B (steel) 67% Gravel	15	0.0	117.9	1.89	0.144	0.00055
		2.1	120.3	1.93	0.120	0.00061
		3.1	121.6	1.95	0.108	0.00051
		3.6	122.3	1.96	0.102	0.00055
33% F&B (glass) 67% Gravel	17	0.0	111.5	1.79	0.209	0.00071
		1.6	113.2	1.81	0.190	0.00062
		3.2	115.1	1.84	0.171	0.00047
		4.7	117.0	1.87	0.152	0.00041
33% Palmer 67% Gravel	19	0.0	94.8	1.52	0.448	0.00097
		3.0	97.7	1.57	0.405	0.00055
		4.3	99.0	1.59	0.386	0.00072
		5.2	99.9	1.60	0.374	0.00055
67% F&B (steel) 33% Gravel	47	0.0	78.8	1.26	0.307	0.15
		4.2	82.2	1.32	0.252	0.18
		8.3	86.0	1.38	0.198	0.12
		10.4	88.0	1.41	0.170	0.12
67% F&B (glass) 33% Gravel	46	0.0	75.5	1.21	0.281	0.23
		5.7	80.1	1.28	0.207	0.21
		9.4	83.3	1.34	0.161	0.14
		11.5	85.3	1.37	0.134	0.08
67% Palmer 33% Gravel	48	0.0	75.3	1.21	0.441	2.9
		2.7	77.4	1.24	0.402	2.7
		6.5	80.6	1.29	0.347	2.3
		12.5	86.1	1.38	0.261	1.5
100% F&B (glass)	100	0.0	42.0	0.67	0.693	7.6
		8.9	46.1	0.74	0.541	6.1
		17.4	50.9	0.81	0.399	2.4
		21.6	53.6	0.86	0.328	1.5
100% Pine State	100	0.0	41.7	0.67	0.857	16.3
		8.3	45.4	0.73	0.703	11.1
		16.7	50.0	0.80	0.548	5.5
		16.8	50.1	0.80	0.546	5.6
100% Sawyer	100	0.0	41.0	0.66	0.873	25.9
		7.0	44.0	0.71	0.743	17.7
		12.6	46.9	0.75	0.637	13.1
		19.6	50.9	0.82	0.506	6.3
100% Palmer	100	0.0	42.7	0.68	0.856	26.3
		8.4	46.6	0.75	0.699	16.5
		16.8	51.4	0.82	0.543	8.6
		20.5	53.7	0.86	0.475	6.5
100% F&B (steel)	100	0.0	40.9	0.66	0.831	26.5
		8.3	44.6	0.72	0.678	15.2
		16.7	49.1	0.79	0.526	8.9

1 cm/s = 1.035x10⁶ ft/yr

chips were the smallest (38-mm; 1.5-in.) tested and were nearly equidimensional. These two properties may have allowed the F&B glass-belted tire chips to blend more easily with the soil and may have resulted in smaller voids and lower permeabilities.

The gravel sample had a measured permeability of 2.2×10^{-3} cm/s (2,300 ft/yr). This is in the range of permeability for clean sands and clean sand and gravel mixtures (Holtz and Kovacs, 1981). This is consistent with the sample's classification of A-1-a according to the AASHTO soil classification system and GW in the Unified Soil Classification System.

Increasing the percentage of gravel significantly reduced permeability as shown in Figure 8.3. This reduction of permeability is close to 5 orders of magnitude from 0% to 100% gravel. The gravel sample has a slightly higher permeability than the 33% tire chip samples. The shape and size of the tire chips are a possible explanation. The tire chips were generally larger and flatter than the soil particles. For the 33% tire chip sample, the flat chips were surrounded by the smaller soil particles, creating a more tortuous path for the water, resulting in lower permeabilities.

Figures 8.4 through 8.6 show that compressing the samples also reduced the permeability, but to a lesser degree than increasing the percentage of gravel. The reduction in permeability due to compression was never greater than 1 order of magnitude for each sample. The plots for 67% and 100% tire chips follow a nearly linear relationship between permeability and compression. For 33% tire chip samples (Figure 8.4), there is only a general trend of decreasing permeability with increasing compression.

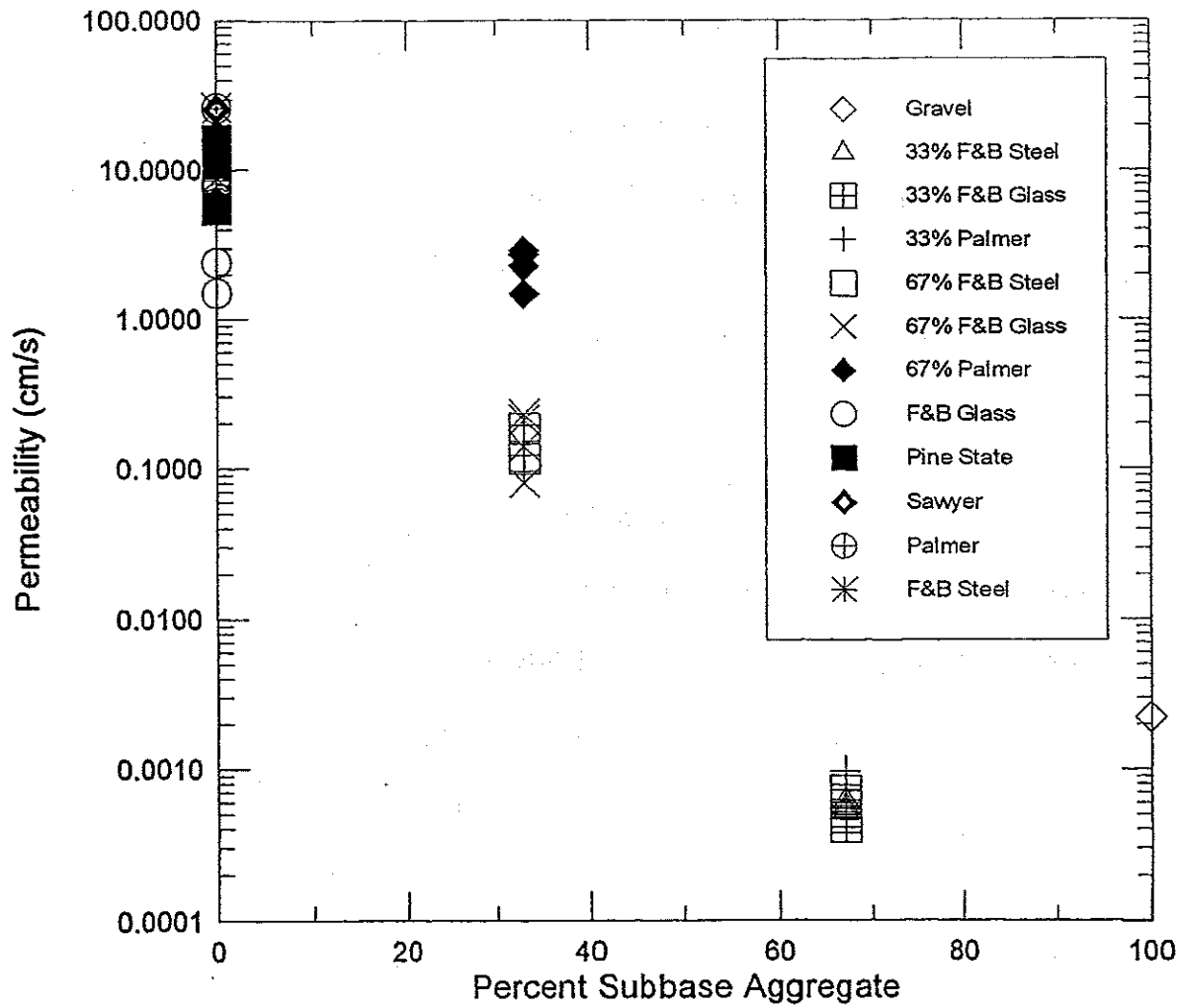


Figure 8.3 Permeability versus percent gravel subbase aggregate

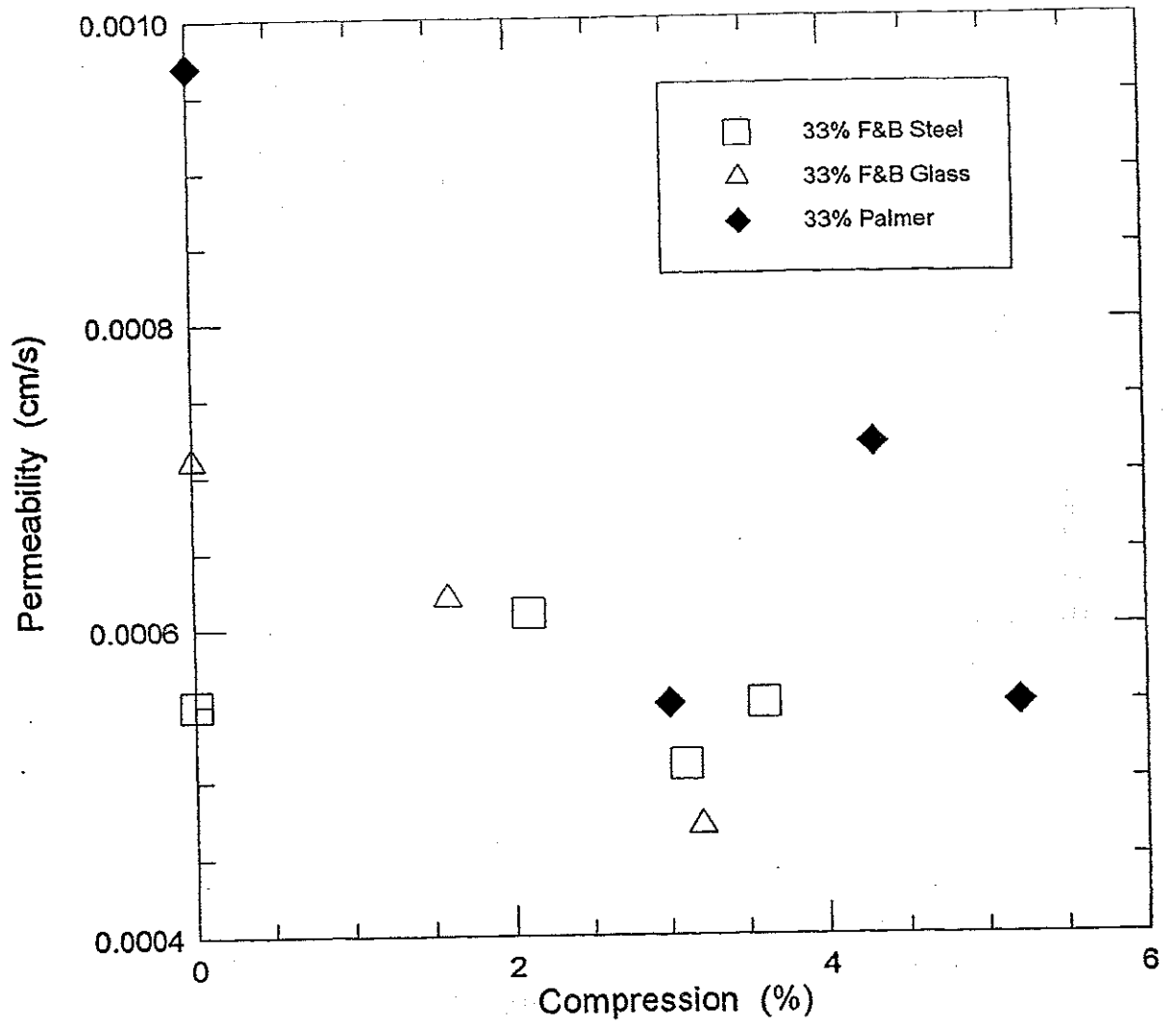


Figure 8.4 Permeability versus percent compression for 33% tire chips

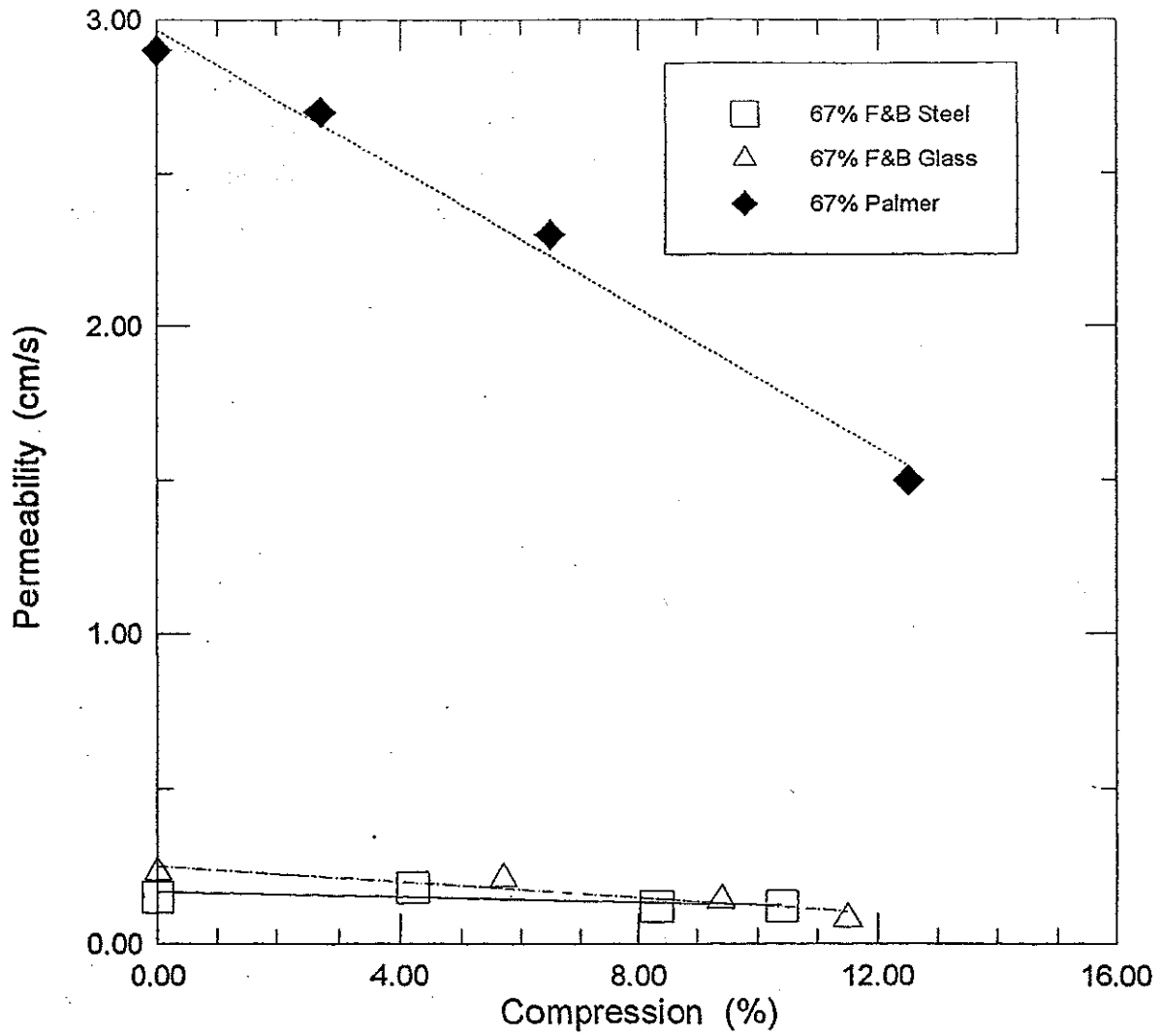


Figure 8.5 Permeability versus percent compression for 67% tire chips

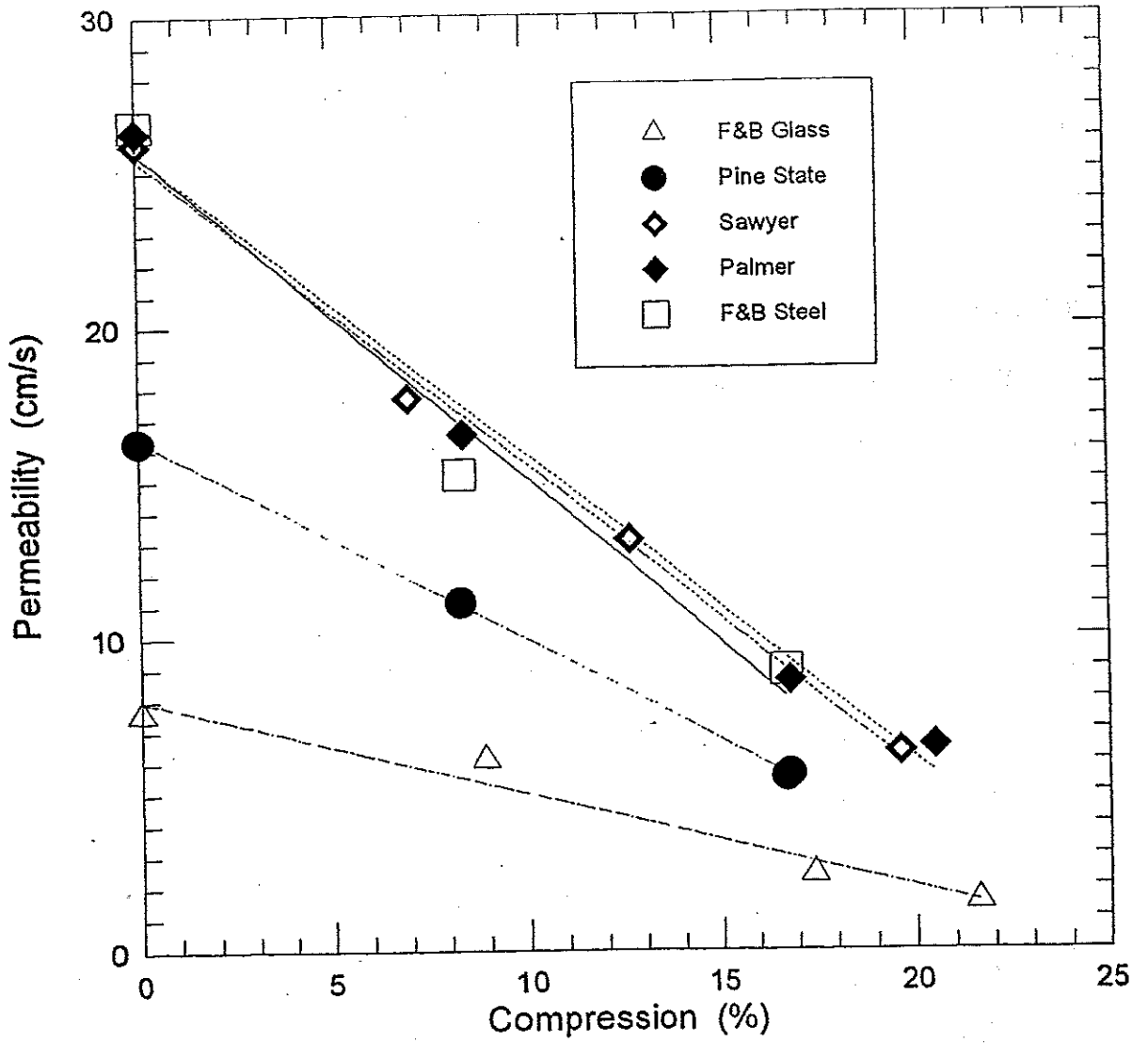


Figure 8.6 Permeability versus percent compression for tire chips

Figures 8.7 through 8.9 show the relationship between permeability and void ratio. The tire chip samples and the 67% tire chip samples have nearly linear relationships. The 33% tire chip samples show only a general trend of decreasing permeability with decreasing void ratio. This is similar to the plots of permeability versus percent compression.

8.5 SUMMARY

Permeabilities of tire chip/soil mixtures were found using a constant head apparatus that was a slightly modified version of an apparatus constructed for a previous NETC project. These modifications helped to maintain a constant head through the sample once equilibrium was reached and made it easier to change samples. Samples were proportioned on a volume basis and then compacted with 146 blows of a modified Proctor hammer in five 122-mm (4.8-in.) thick layers. Although tire chip/gravel mixtures were carefully placed in layers to avoid segregation, compaction resulted in some segregation of tire chips and gravel.

There was a significant trend of decreasing permeability with increasing percentage of gravel. As seen in Figure 8.3, tire chip samples had similar permeabilities, with F&B glass-belted chips having the lowest permeability because they have the smallest maximum size. The permeability of the 33% Palmer mixture is an order of magnitude greater than the two 33% F&B mixtures due to the larger size, curved shape, and greater size and amount of steel belts of the Palmer chips. The 67% tire chip mixtures have lower

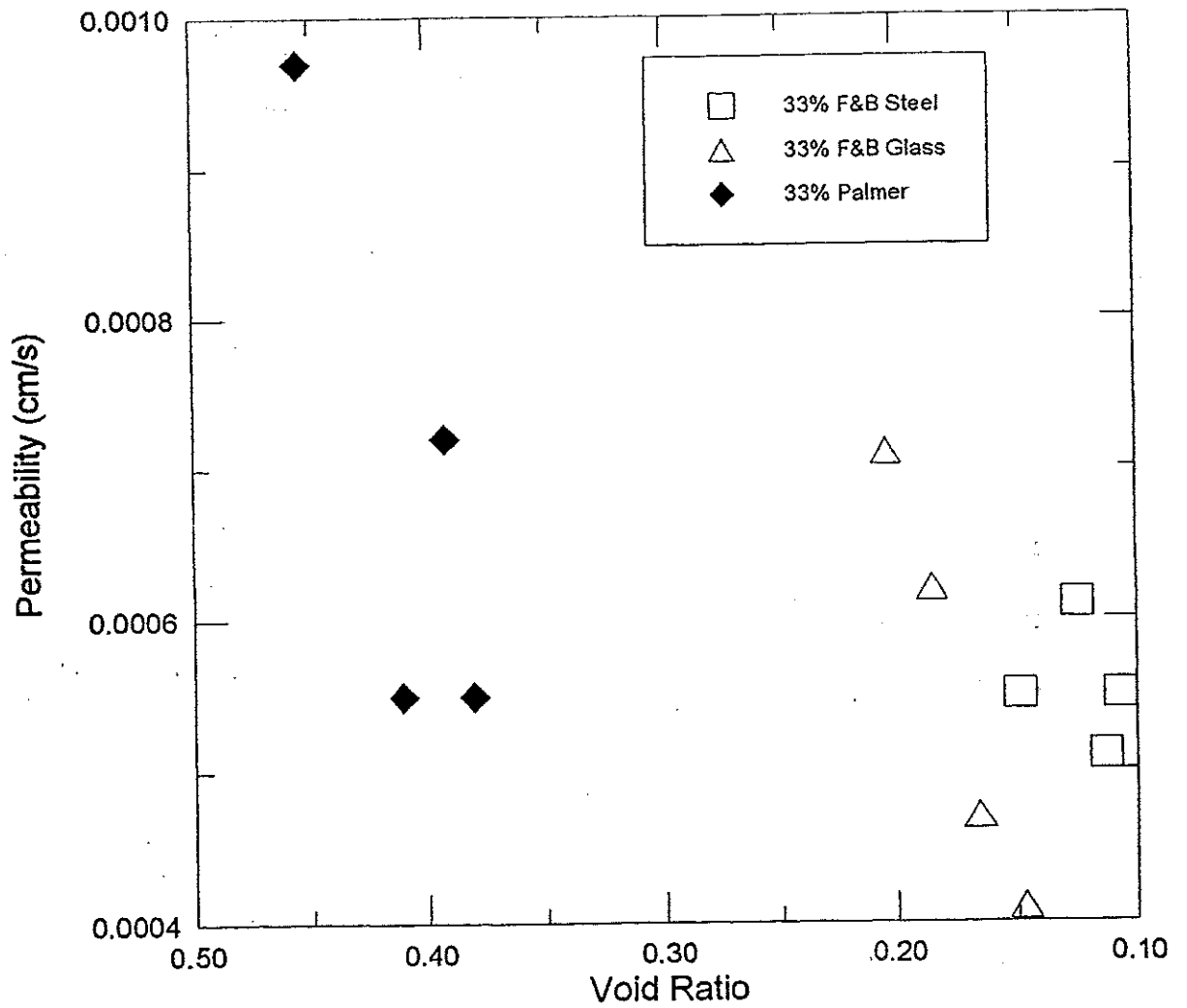


Figure 8.7 Permeability versus void ratio for 33% tire chips

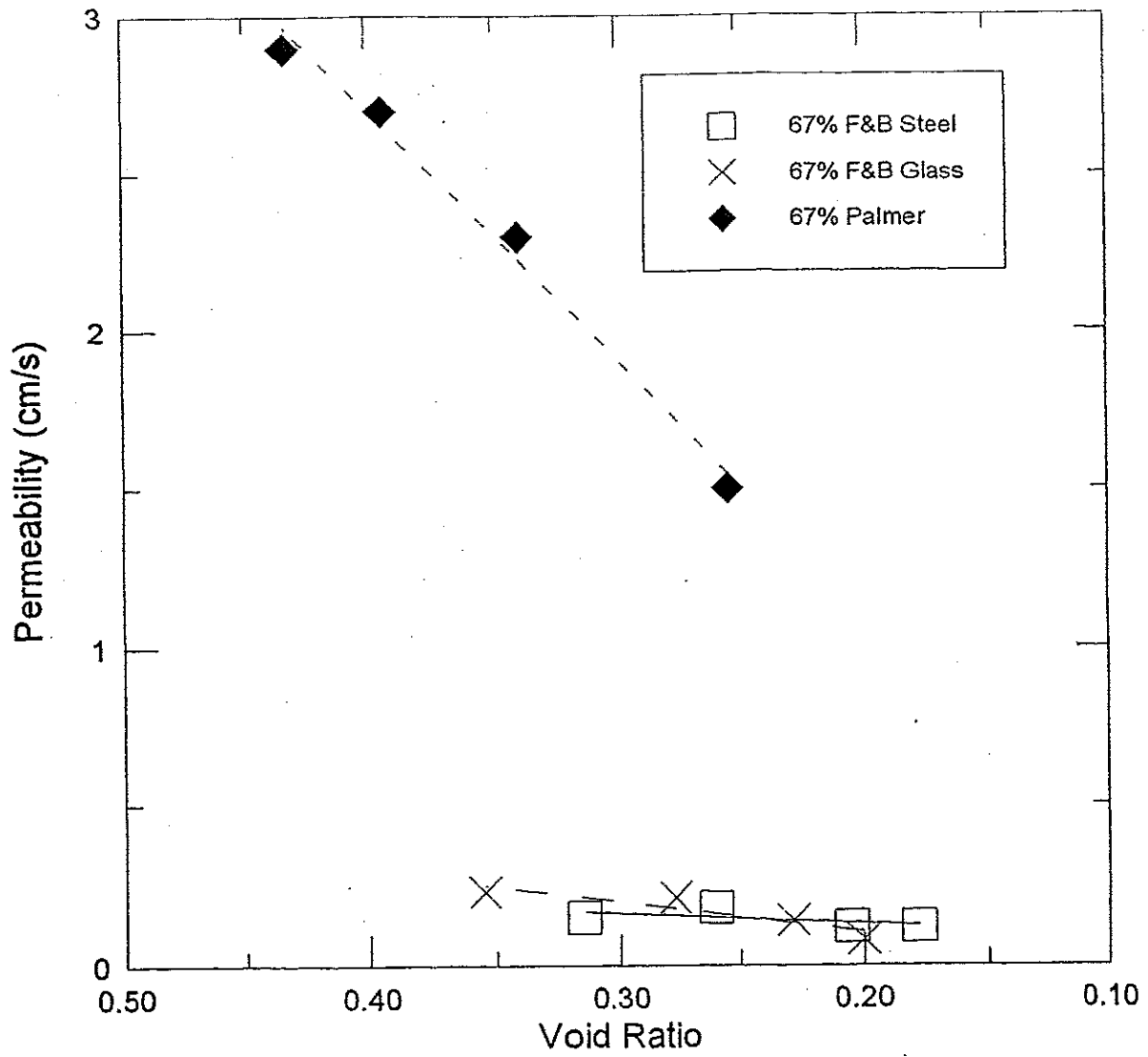


Figure 8.8 Permeability versus void ratio for 67% tire chips

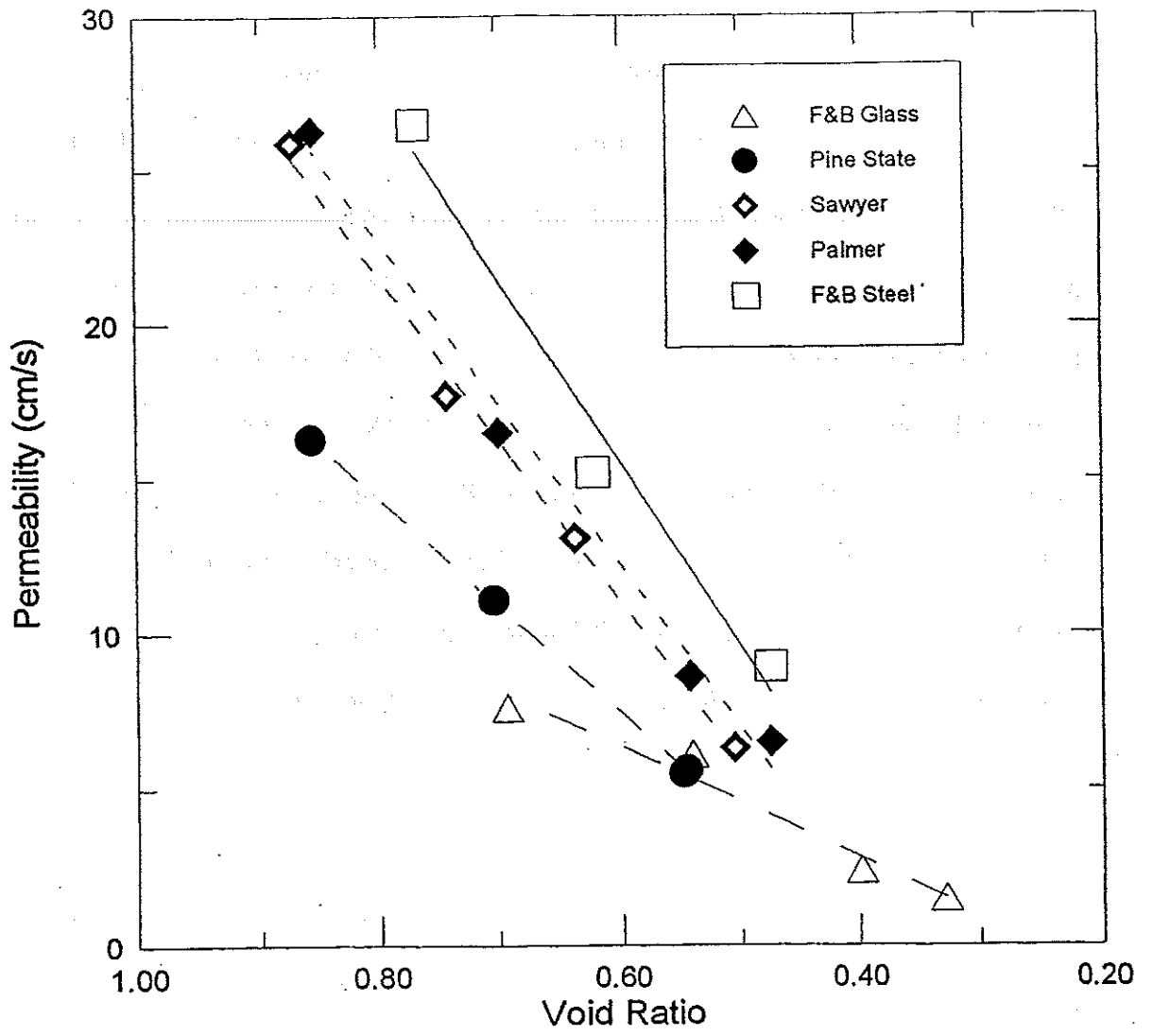


Figure 8.9 Permeability versus void ratio for tire chips

permeabilities than even the gravel sample. A possible explanation for this is the longer and flatter shape of the tire chips which created a more tortuous path.

There was a linear relationship between permeability and compression, as well as between permeability and void ratio for the tire chip and 67% tire chip samples, but these relationships were more of a general trend for the 33% tire chip samples. The lowest permeability of the uncompressed samples was 5.5×10^{-4} cm/s (570 ft/yr) for 33% F&B steel-belted, which is roughly comparable to a glacial till or very fine sands. The highest permeability was 26.5 cm/s (27.4×10^6 ft/yr) for 100% F&B steel-belted, which is equal to or greater than values for a clean gravel. For comparison, the Federal Highway Administration (FHWA) recommends a minimum permeability of 0.35 cm/s (FHWA, 1990). A study conducted for MDOT found that the in-situ permeability of subbase aggregate at six sites ranged from 6×10^{-6} to 1.7×10^{-2} cm/s (Manion, et al., 1995).

9. FIELD TRIAL LAYOUT AND CONSTRUCTION

9.1 INTRODUCTION

A full scale field trial was constructed to investigate the use of tire chip/soil mixtures to reduce frost penetration and improve drainage of paved roads. The trial is located on a dead end road leading to the University of Maine's Whitter Farm in Orono, Maine. The portion of the road that was used for the 73.2-m (240-ft) long trial section is located about 0.6 km (0.4 mi) from the intersection of Whitter Farm Road and College Avenue. The portion of the road used for the test section was gravel surfaced. The new pavement connects to existing pavement covering the last 0.6 km (0.4 mi) of the road leading up to the farm. The total length of the test section, including approaches at each end, is 77.7 m (255 ft).

The road runs from west to east (from College Avenue to Whitter Farm). A wooded area lies to the south of the road and a farm pasture lies to the north. The land is relatively flat with a small hill to the east, on which the Whitter Farm is located. The wooded area to the south is slightly elevated above the road and the field to the north is slightly depressed below the road. The road is mostly used by farm vehicles, people who work or take classes at the farm, and a family who lives next to the farm. Only a small number of vehicles travel on this road, so pavement performance measurements were used to estimate the useful life of the pavement under heavier traffic.

This chapter describes the design, layout, materials, construction, and instrumentation for the full scale field trial.

9.2 DESIGN

There were two major criteria for site selection. The first, and most important, was to find a site that had a sufficient depth of natural frost-susceptible soil. This allowed the researchers to test the effectiveness of tire chips and tire chip/soil mixtures under conditions that would normally cause pavement damage due to frost heave. The second criteria was to find a site on or near the University. The tire chips to be used in this project were used in a previous research project and were being stored on the University grounds. Thus, a site near the University would reduce transportation costs.

Exploratory hand borings were drilled at five possible sites prior to selection of the Farm Road. All of these sites were unacceptable because of insufficient depth to bedrock or non-frost susceptible subgrade soil. At the Farm Road, borings F-1 and F-2 were drilled to depths of 1.0 meters (3.3 ft) and 2.1 meters (6.9 ft), respectively. The plan location of the borings is shown on Figure 9.1 and boring logs are shown in Figure 9.2. Water content and specific gravity tests were performed on samples taken from these borings. During construction, bulk samples were taken in each section after excavation was completed. Samples were also taken when holes for thermocouples were augered at the center of each section. Atterberg limit, gradation, hydrometer, and specific gravity tests were performed on some of these samples. Table 9.1 summarizes the results of these tests. Gradations of the subgrade soil are given in Figure 9.3. Subgrade samples were classified as a CL according to the USCS (Unified Soil Classification System) and A-4(8) or A-6(8) according to the AASHTO classification system.

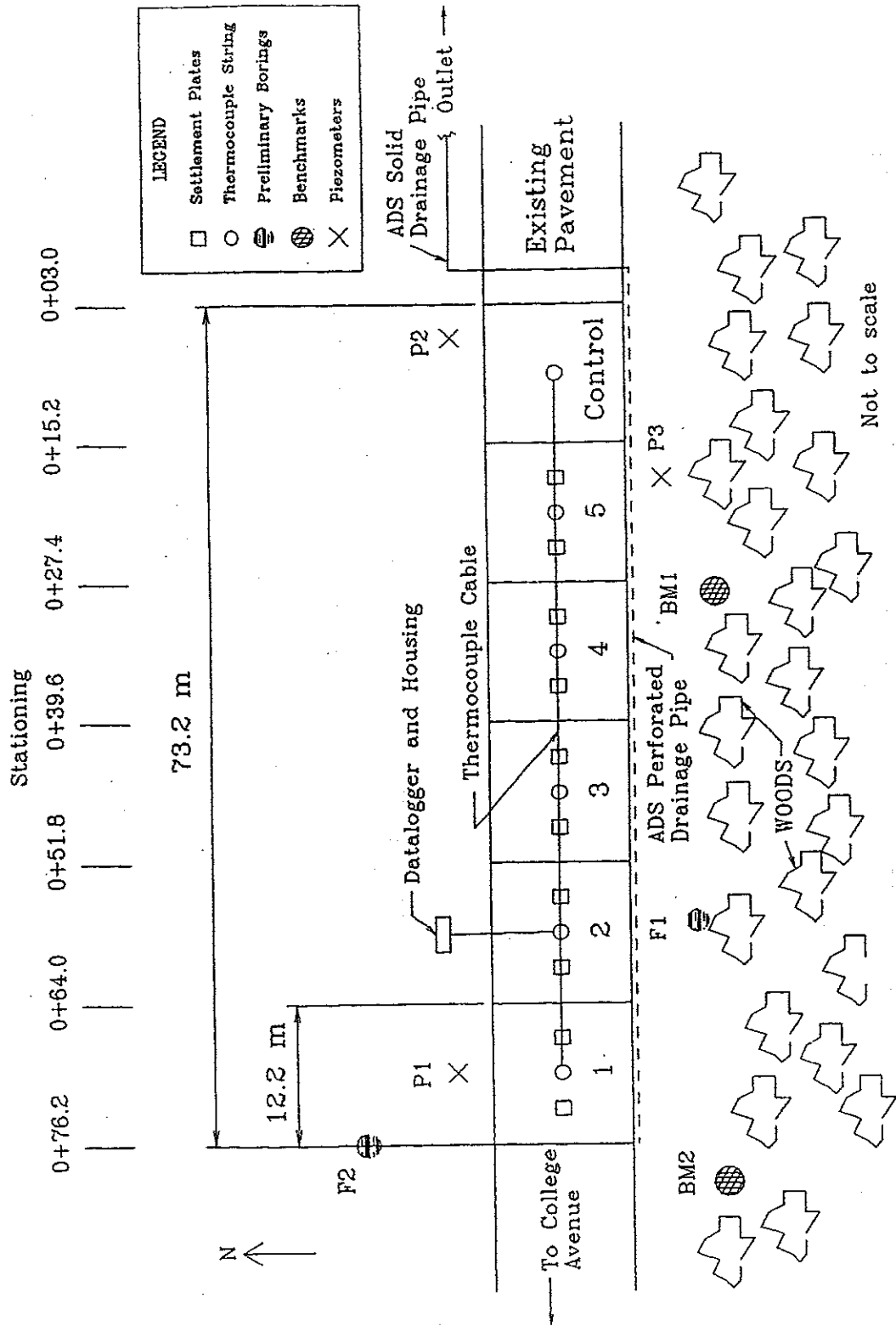
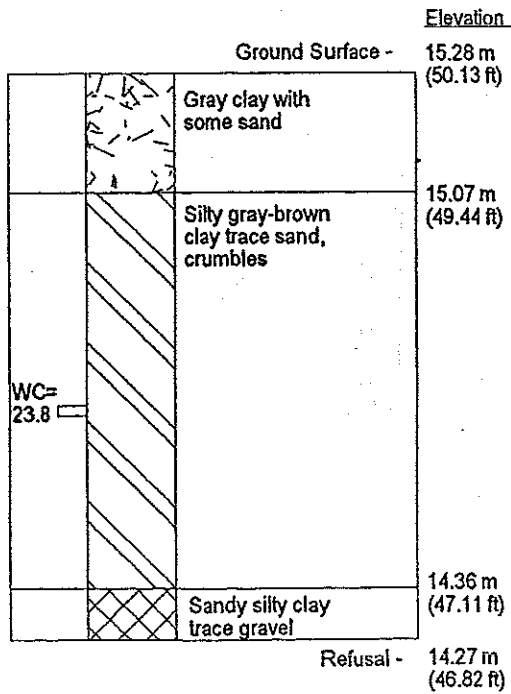


Figure 9.1 Plan view of full scale field trial

WC = water content in percent
 □ = location of sample
 ▽ = observed water table elevation

Elevation referenced to arbitrary site datum.

Boring F1



Boring F2

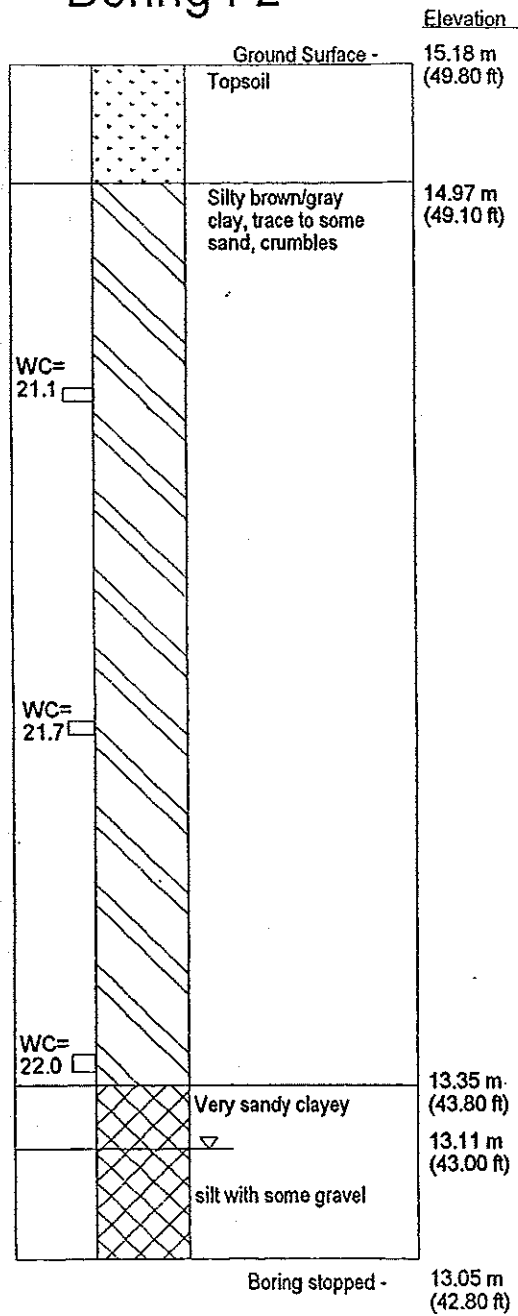


Figure 9.2 Boring logs next to trial road

Table 9.1 Laboratory index properties of cohesive subgrade material

Sample Type	Location	Natural Water Content	Plastic Limit	Liquid Limit	Plasticity Index	Specific Gravity	Depth (m)
Boring	F1	23.8					0.6
	F2	21.1					0.6
	F2	21.7				2.72	1.2
	F2	22.0				2.74	1.8
Bulk Subgrade	Section 1	20.4					
	Section 2	24.1	24	32	8	2.64	
	Section 3	17.3					
	Section 4	18.4	22	33	11	2.65	
	Section 5	18.4					
	Control	17.7	21	27	6		
Auger	Section 1	20.4					0.0-0.9
	Section 1	15.5					0.9-1.5
	Section 2	20.7					0.0-0.9
	Section 2	14.4					0.9-1.5
	Section 3	21.7					0.0-0.9
	Section 3	22.9					0.9-1.5
	Section 4	18.5					0.0-0.9
	Section 4	24.7					0.9-1.5
	Section 5	19.7					0.0-0.9
	Section 5	32.8					0.9-1.5
	Control	20.7					0.0-0.9
	Control	32.1					0.9-1.5

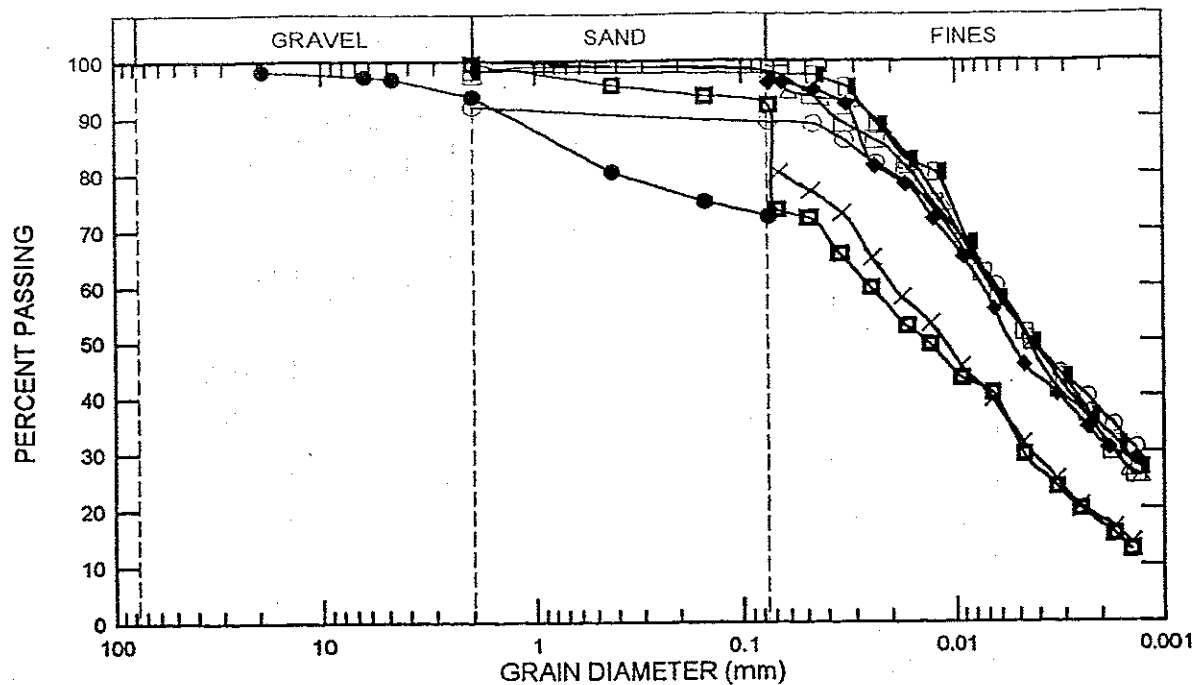


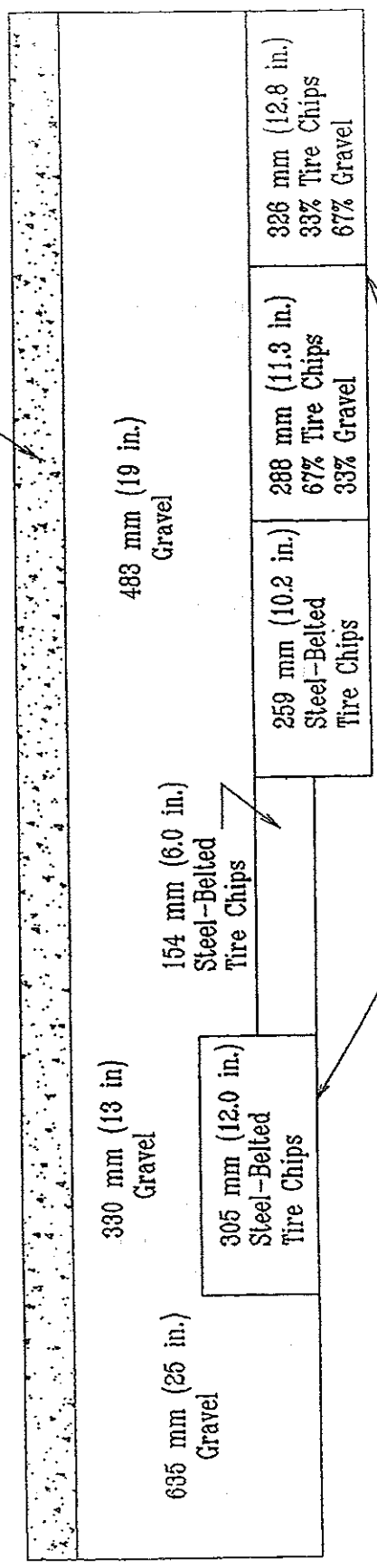
Figure 9.3 Gradation curves of cohesive soil from borings, subgrade samples, and auger holes made for thermocouple installation

9.3 LAYOUT

The field trial consists of six 12.2-m (40-ft) long paved sections. Figure 9.4 shows a longitudinal cross-section. A plan view is shown in Figure 9.1. Five test sections contain from 152 to 305 mm (6 to 12 in.) of tire chips or tire chip/soil mixtures overlain by 330 mm (13 in.) to 483 mm (19 in.) of MDOT Type D subbase aggregate. Tire chip/soil mixture proportions were based on volume of solids rather than weight of solids because of the large difference in specific gravity. Two front end loader bucket loads of chips to one bucket load of gravel was used for the 67% tire chip/33% gravel section. For the 33% tire chip/67% gravel section, two bucket loads of chips to three bucket loads of gravel were used because the tire chips tend to be very loose when loaded into the bucket. This was estimated to yield a percentage of tire chips close to 33%. The

Control 5 4 3 2 1

127 mm (5 in.) Bituminous Pavement



Subgrade

Figure 9.4 Longitudinal cross-section along centerline of road

remaining 12.2 m (40-ft) long section is a control section with 635 mm (25 in.) of MDOT Type D subbase aggregate. Table 9.2 gives a summary of the configuration of each test section including the as built thickness of tire chip/soil mixtures determined as described in Section 9.5.2. Stationing is shown on Figure 9.1. Stationing is given in meters unless otherwise noted. Station 0+00 is at the east end of the test section.

As built cross-sections are shown in Figures 9.5 through 9.10. The width of the pavement is 5.5 m (18 ft), and its thickness is 127 mm (5 in). The tire chips and tire chip/soil mixtures were encased in a non-woven geotextile (Synthetic Industries Type 701) to prevent migration of soil into the tire chip layers. The geotextile protects the integrity of the tire chip layers while allowing drainage to occur through them.

A drainage trench runs parallel to the road on the south side. Trench width varied from 0.66 to 1.07 m (2.2 to 3.5 ft), and it was filled with the same material as the adjacent test section. For example, the trench in Section 2 (Station 0+64 to 0+52), was

Table 9.2 Summary of test section configuration

Section	Depth of excavation (mm)	Thickness of layer (mm)		
		Tire chip/soil mixtures	Gravel fill	Paved surface
1	914	326 (33% t.c.)	483	127
2	914	288 (67% t.c.)	483	127
3	914	259 (100% t.c.)	483	127
4	762	154 (100% t.c.)	483	127
5	762	305 (100% t.c.)	330	127
Control	762	----	635	127

25.4 mm = 1 in.

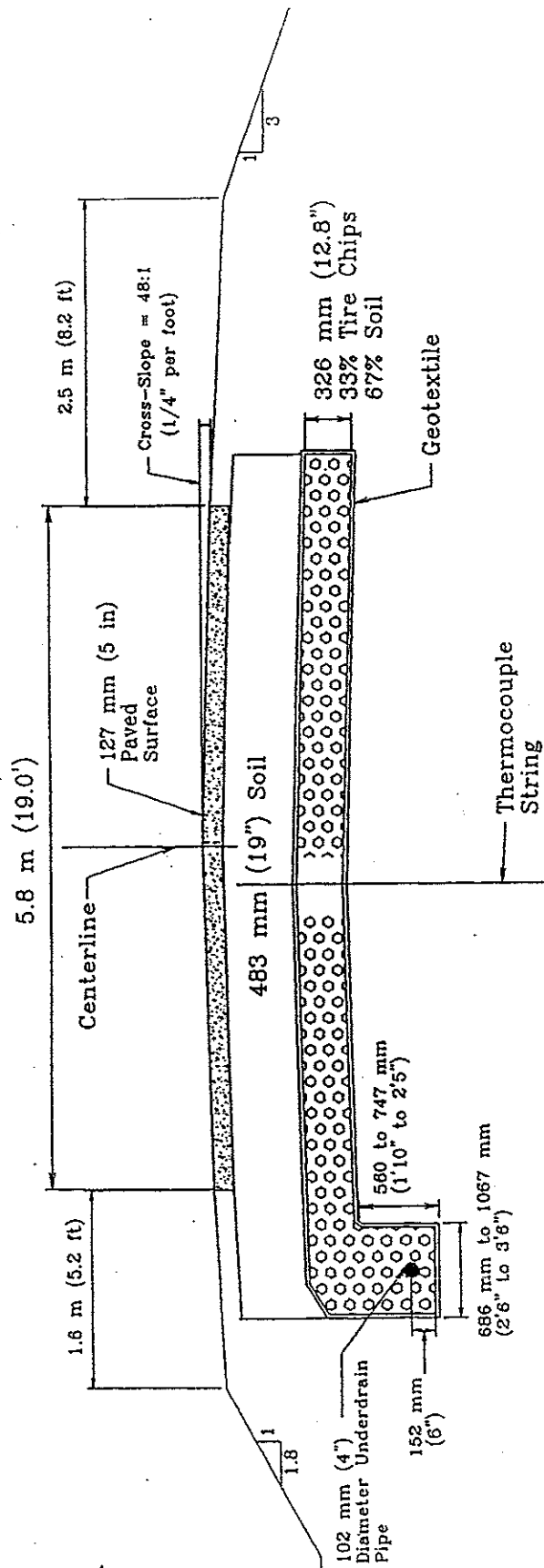


Figure 9.5 Cross section of Section 1

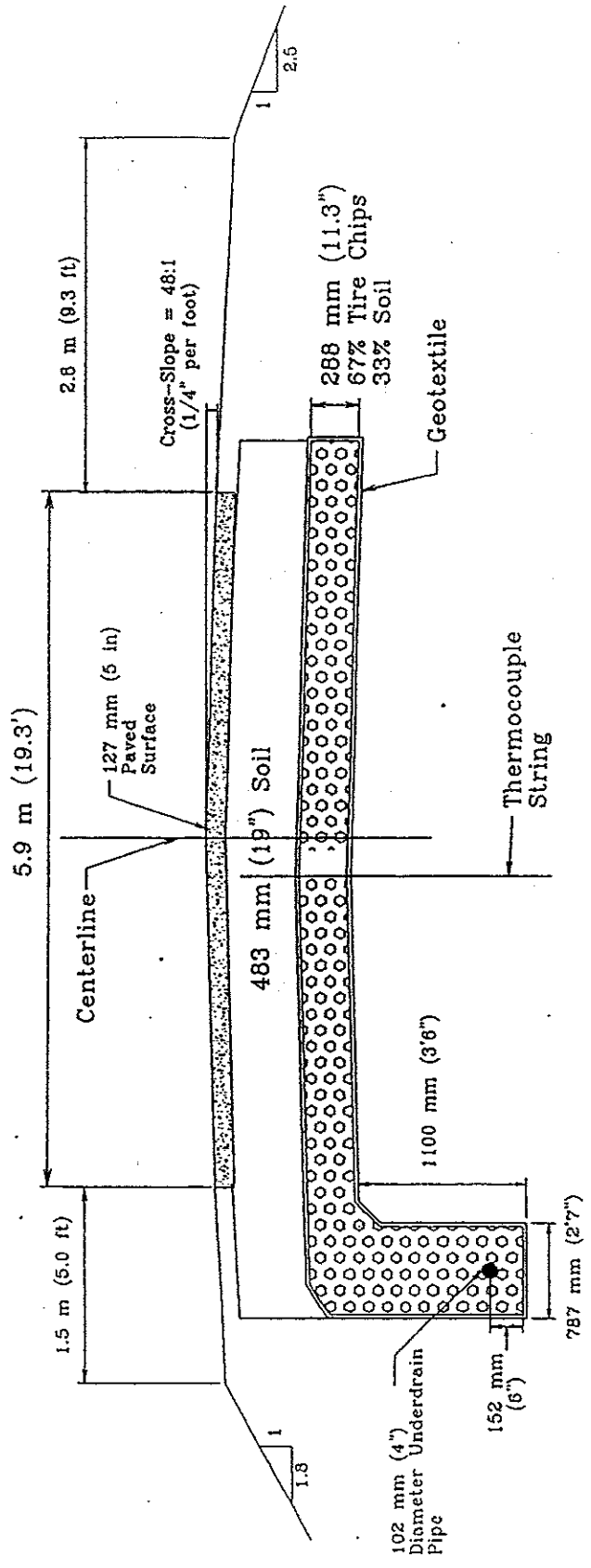


Figure 9.6 Cross section of Section 2

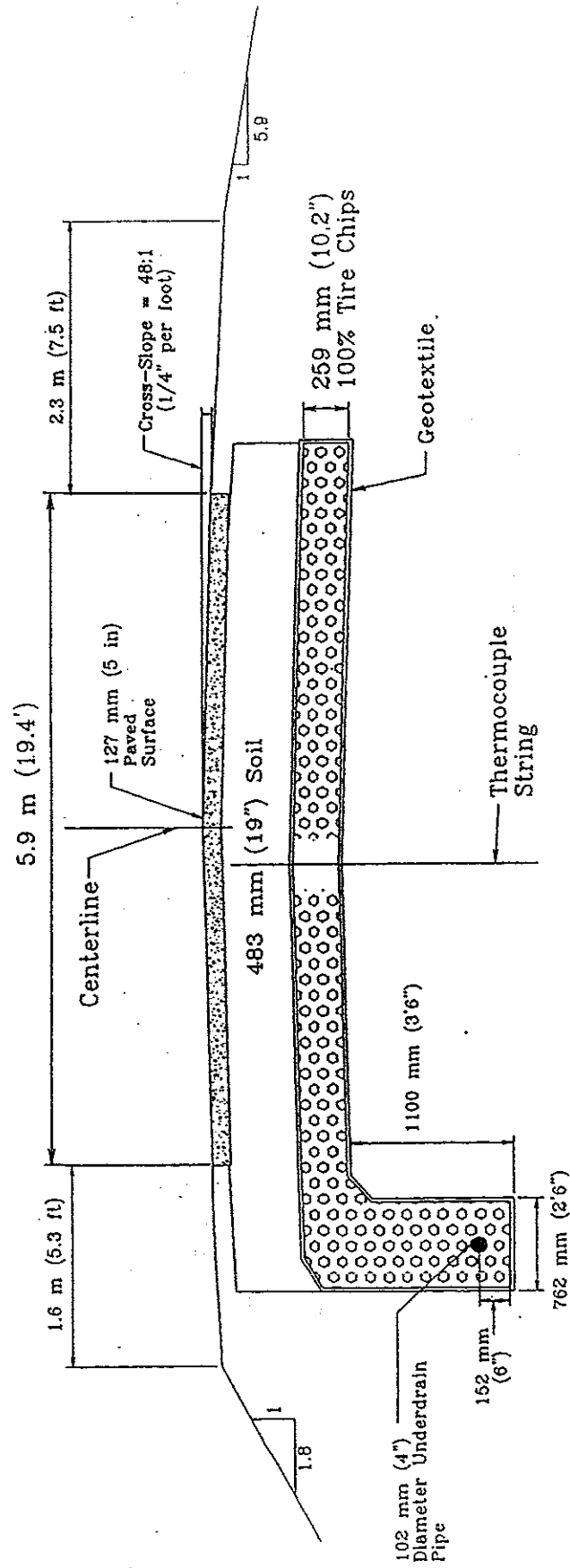


Figure 9.7 Cross section of Section 3

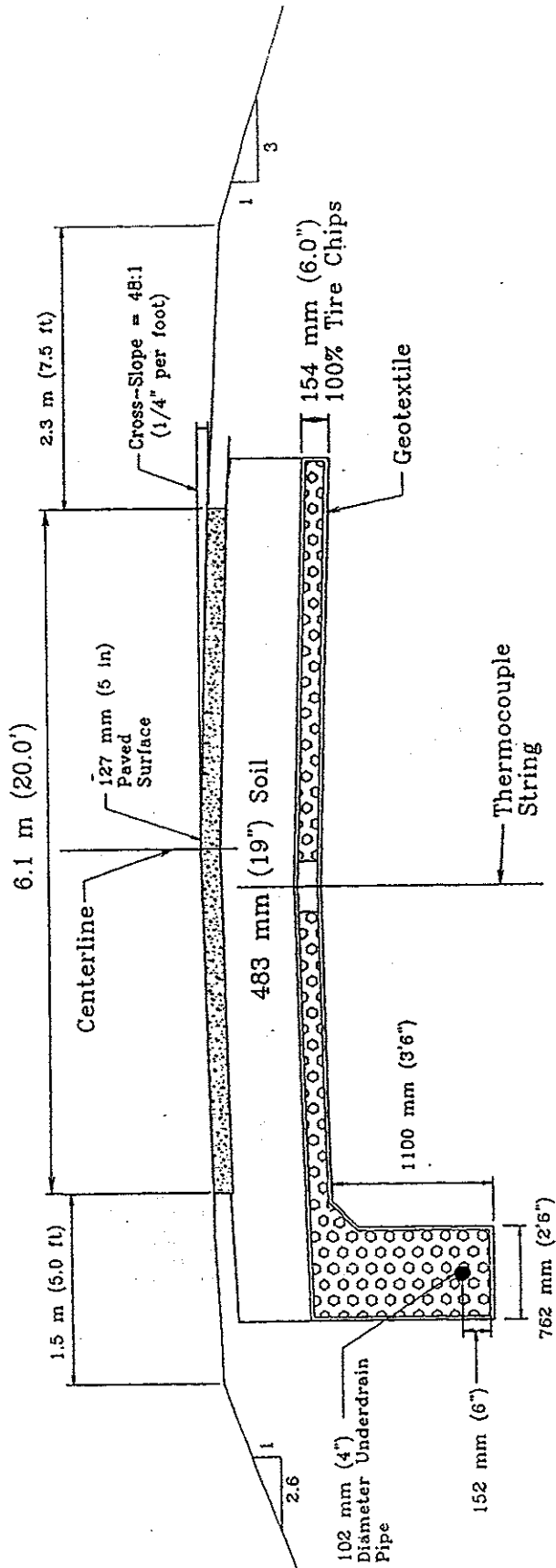


Figure 9.8 Cross section of Section 4

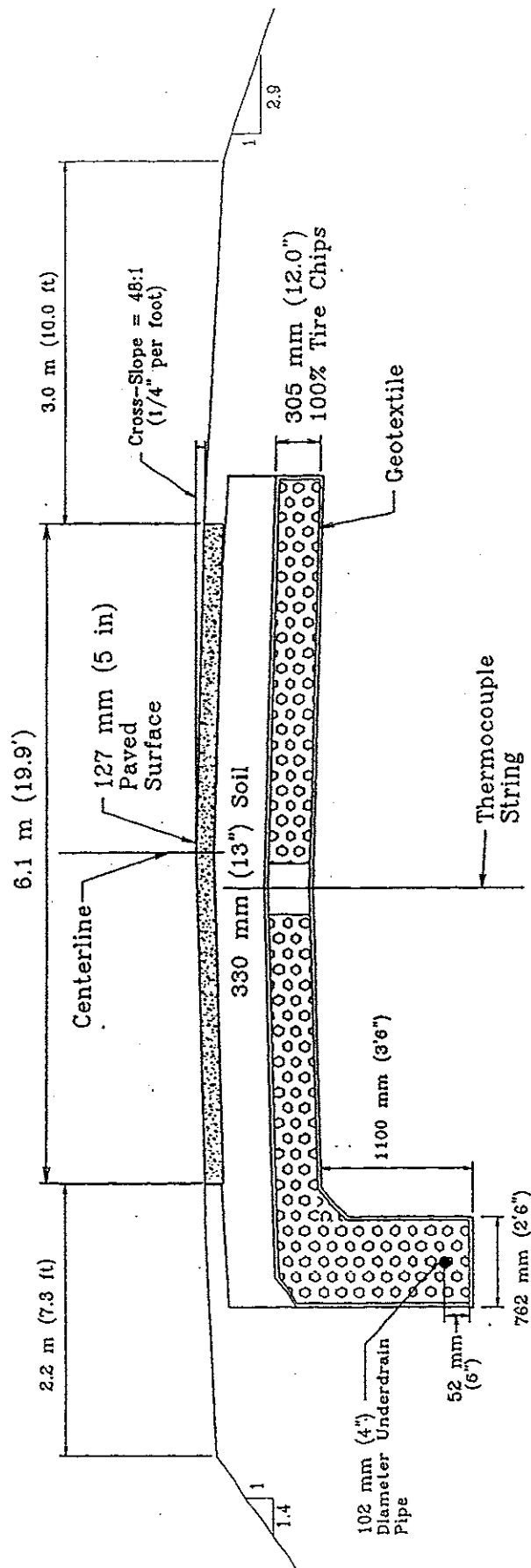


Figure 9.9 Cross section of Section 5

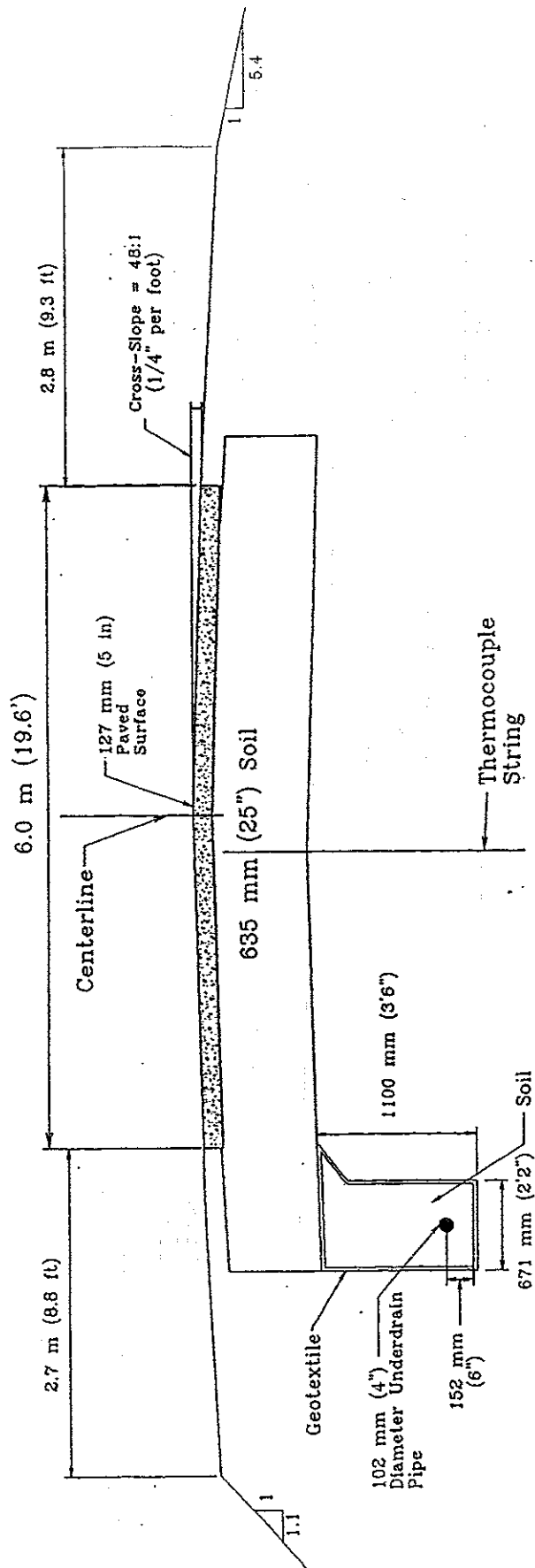


Figure 9.10 Cross section of Control

filled with 67% tire chips/33% gravel. The trench was lined with geotextile in each test section (Station 0+76 to 0+03). A total of 76 m (250 ft) of 102-mm (4-in.) diameter perforated ADS pipe was buried in the trench at a typical depth of 1.07 m (3.5 ft) below the subgrade. The perforated pipe runs from Station 0+76 to Station 0+00. The pipe sloped downward to from high station to low station (west to east). The perforated pipe connects to solid 102-mm (4-in.) diameter ADS pipe at Station 0+00, turns north to cross the road, and then turns east to its drainage point located in a field approximately 67 m (220 ft) prior to the start of the Control Section. Figure 9.1 shows the layout of the ADS pipes in plan view.

9.4 MATERIALS

The tire chips had been used on a previous NETC research project and were stockpiled on campus. They were obtained from Palmer Shredding in North Ferrisburg, Vermont and Pine State Recycling in Nobleboro, Maine. They meet MDOT specifications for Type A tire chips and generally had a 76-mm (3-in.) maximum size. A few pieces that were obviously larger than 76 mm (3 in.) were removed by hand as they were placed. Gradation curves of tire chips sampled from this project are shown in Figure 9.11. Gradation curves of the mixtures with 67 percent tire chips and 33 percent soil and 33 percent tire chips and 67 percent soil are shown in Figure 9.12.

The granular subbase was 102-mm (4-in.) maximum size processed gravel and met Maine DOT Specification 703.06, Type D (152-mm (6-in.) maximum size, 25 to 70% passing the 6.4 mm (1/4-in.), 30% maximum passing the No. 40, and 7% maximum

finer). This material was used for subbase over the tire chips and tire chip/soil mixtures as well as for the subbase course in the Control Section. Gradation curves from field samples are shown in Figure 9.13.

The granular material used for the edge drains and tire chip/soil mixtures was available on campus from a previous NETC research project. This granular material meets MDOT requirements for Type D subbase aggregate. Figure 9.14 shows the results of the gradation analysis done on this material by Tweedie, et al. (1998). No particles were retained on the 76-mm (3-in.) sieve, approximately 18 to 30% passed the No. 40 sieve, and approximately 3% passed the No. 200 sieve.

Bituminous pavement aggregate met MDOT specification 703.09 for Types B and C. Type B was the first course placed, which contains coarser aggregate, with 100% passing the 25-mm (1-in.) sieve, 50 to 85% passing the 13-mm (0.5-in.) sieve, 14 to 39% passing the No. 16 sieve, and 1 to 8% passing the No. 200 sieve. Type C was placed over Type B as the surface course. Specifications require Type C aggregate to have 100 percent passing the 19-mm (0.75-in.) sieve, 80 to 100% passing the 13-mm (0.5-in.) sieve, 17 to 40% passing the No. 16 sieve, and 2 to 7% passing the No. 200 sieve.

9.5 CONSTRUCTION

9.5.1 Excavation

Excavation of the road took place on September 9, 1996. The researchers were responsible for layout and grade control. The grade was initially laid out with a theodolite and grade stakes. The roadbed was excavated to +/- 25 mm (1 in.) using a

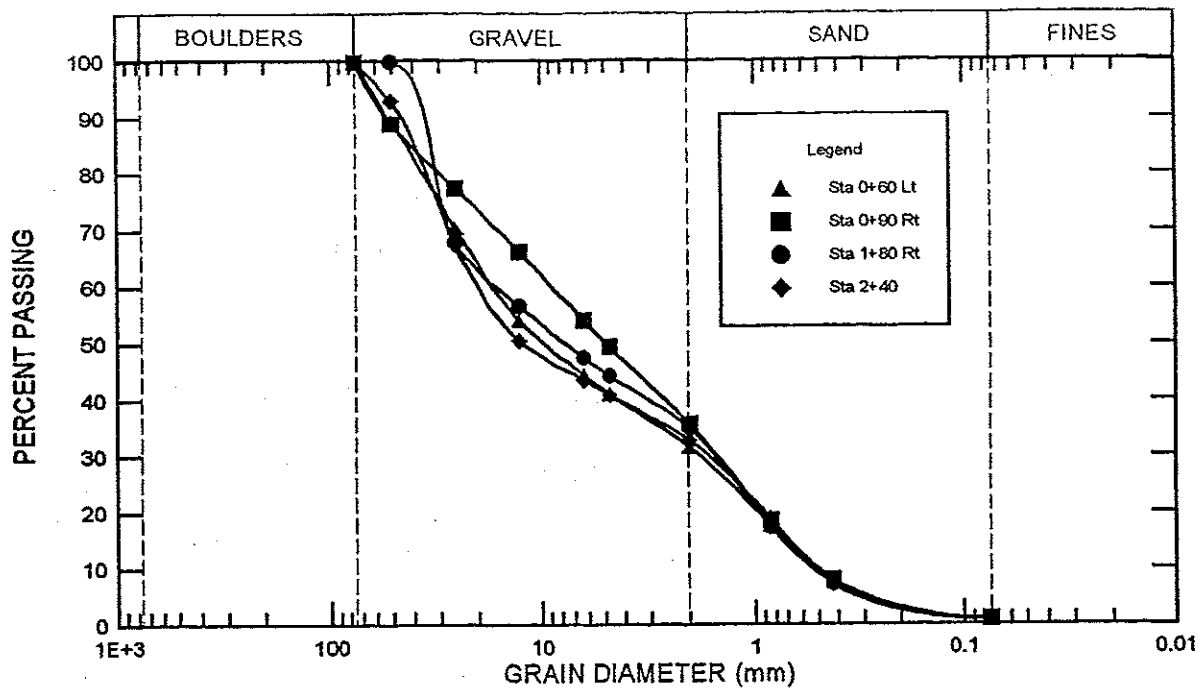


Figure 9.13 Gradation curves of MDOT subbase obtained from outside contractor

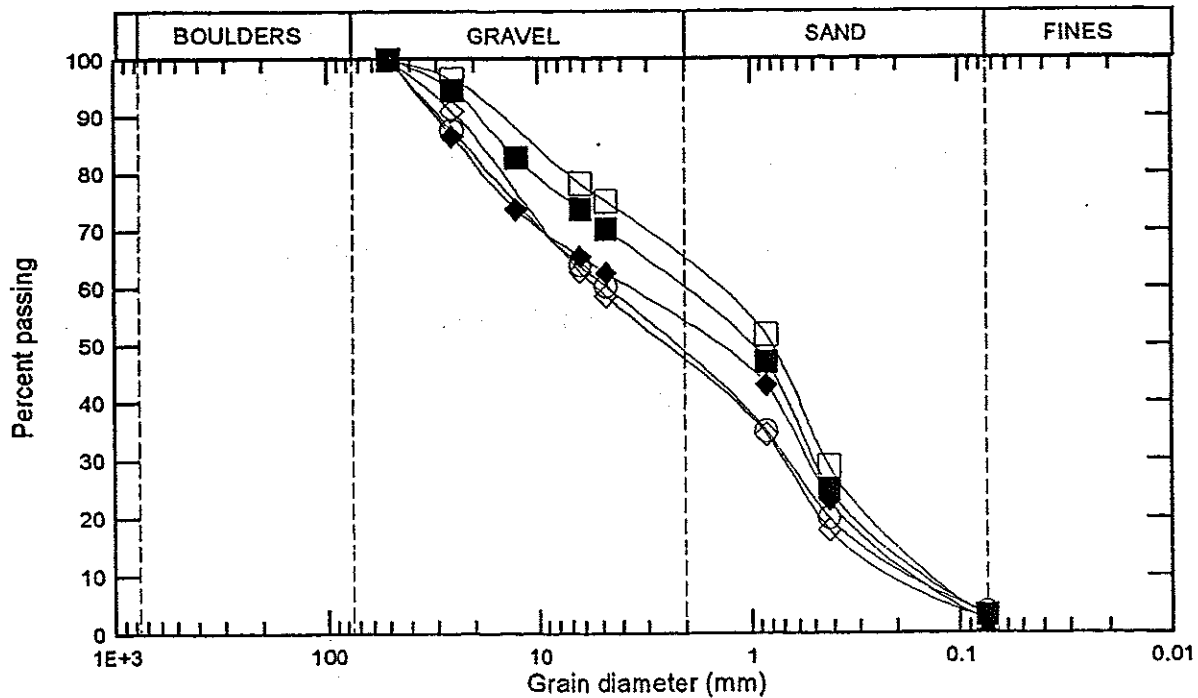


Figure 9.14 Gradation curves of MDOT Type D subbase aggregate available from previous NETC project (after Tweedie, et al., 1998)

tracked excavator with a 1.2-m (48-in.) wide bucket as shown in Figure 9.15. Grade was checked with a hand level.

Sections 1, 2, and 3 were excavated to 0.91 m (36 in.) below the top of pavement and Sections 4, 5, and control were excavated to 0.76 m (30 in.) below the top of pavement. As the left side of the road was being excavated with the tracked excavator, a Case 580 equipped with a 0.6-m (24-in.) wide bucket excavated a trench for the edge drain (see Figure 9.16). The trench was excavated to 1.07 m (3.5 ft) below the subgrade elevation. During construction a very large boulder was encountered in the trench around station 0+64. Neither the Case 580 nor the hydraulic tracked excavator could lift the boulder out of the trench so it was necessary to leave the boulder in place. Station 0+64 could be excavated only 0.56 m (1.85 ft) below subgrade to the top surface of the

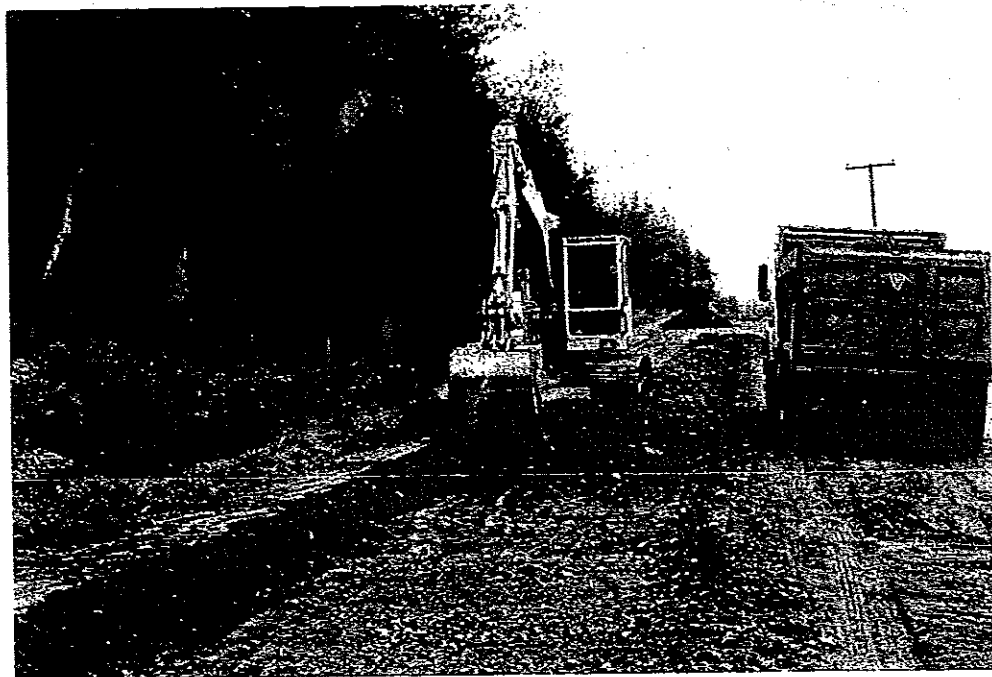


Figure 9.15 Photograph of excavation of roadbed with hydraulic excavator

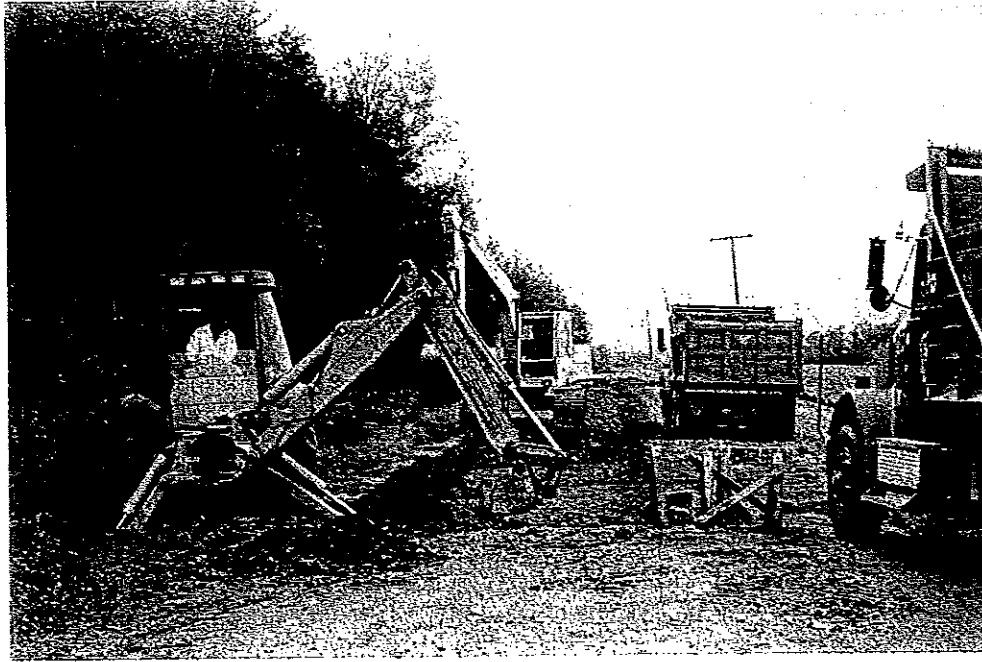


Figure 9.16 Photograph of excavation of trench with Case 580

boulder. From Station 0+67, just beyond the boulder, to the end of the trench at Station 0+76 the trench was gradually raised from 0.75 m (2.45 ft) to 0.60 m (1.97 ft) below subgrade. A total of 306 m³ (400 yds³) of material was excavated from the road and the trench.

Since the entire road was excavated in one day and the exposed subgrade would be impassable to traffic for about one month, it was necessary to build a bypass lane. Some of the granular soil excavated from the road was placed on the right side of the road to form a temporary vehicle bypass lane. In addition, approximately 191 m³ (250 yd³) of the excavated soil was stockpiled west of the test sections to use for shoulders after the road was surfaced. Excess excavation was disposed of at the Whitter Farm.

Subgrade soil samples were taken after excavation. In addition, soil samples were taken from auger holes drilled for thermocouple installation. Specific gravity, grain size analysis, and Atterberg Limits were performed on these samples. These are shown in Table 9.1 and Figure 9.3. The average specific gravity of the samples was 2.65. Natural water content ranged from 14.4 to 32.8%. The average plastic limit was 22 and the average liquid limit was 31. Approximately 73 to 100% passed the #200 sieve. This soil is classified as an F4 soil with low to very high frost susceptibility according to the US Army Corps of Engineers classification system (Chamberlain, 1981).

9.5.2 Placement of Tire Chips and Tire Chip/Soil Mixtures

Tire chips from a previous NETC tire chip research project were utilized for this project. Tire chips were loaded into a 4.6-m³ (6-yd³) dump trailer with a small tractor outfitted with a front end loader bucket. Tire chip/soil mixtures were made by dumping a ratio of two buckets of tire chips to one bucket of soil for the 67% tire chip / 33% soil mixture, and two buckets of tire chips to three buckets of soil for the 33% tire chip / 67% soil mixture. The latter ratio was necessary to obtain the desired 2 to 1 ratio based on percent of solids volume. After mixing in the trailer with shovels and rakes, the mixture was transported to the construction site. Because of time constraints, the last half of the 33% tire chip / 67% gravel section (Section 1) was loaded, transported, and placed with a Case 580 and dump truck from a local contractor. Mixing was done in the same fashion.

It was difficult to maintain a homogeneous mixture of tire chips and soil for Sections 1 and 2. The mixing process in the trailer or dump truck resulted in a relatively uniform mixture, but dumping and spreading the mixtures resulted in segregation. This

was especially evident for the 67% tire chip/33% soil mixture in Section 2. The large void spaces in uncompacted tire chips allowed soil particles to settle. This resulted in a higher concentration of tire chips near the top of the layer. The difficulty of maintaining a uniform mixture limits the practicality of using mixtures with greater than 33% tire chips on typical highway construction projects. To provide the greatest ease of construction, use of mixtures should be avoided and 100% tire chips should be used wherever possible.

9.5.2.1 Filling Trench

Geotextile lined the bottom and sides of the trench. The tire chips or tire chip/soil mixtures were dumped in the trench from the trailer. Two to four people spread the material with rakes and shovels. First, a 152-mm (6-in.) lift of tire chip/soil mixture was placed and compacted, then the perforated 102-mm (4-in.) diameter ADS drainage pipe was placed on top of this. The lift placed over the pipe was 305 mm (12 in.) thick to provide adequate protection to the drainage pipe during compaction. Subsequent lifts were 203 mm (8 in.) thick and were placed and compacted until the trench was filled.

After a lift was in place, it was compacted by "dynamic compaction" with a 354 kg (780 lb) concrete block lifted with the front bucket of a tractor, as shown in Figure 9.17. This method was used because the researchers could not find a walk behind roller that was narrow enough to fit in the trench. Compaction was achieved with ten drops of the concrete block at each location. The trench was wider near the top, permitting the use of a Rammax RW1403 walk-behind compactor, with a width of 838-mm (33-in.) and an operating weight of 1,315 kg (2,900 lb). The walk-behind compactor made a minimum of six passes for each lift. Figure 9.18 shows compaction with the walk-behind



Figure 9.17 Photograph of trench compaction with tractor and concrete block



Figure 9.18 Photograph of trench compaction with walk-behind compactor

compactor. Placement and compaction of material continued to the top of the trench, which matches the adjacent subgrade elevation.

9.5.2.2 Filling Roadbed

The roadbed tire chips and tire chip/soil mixtures were transported to the site by the dump trailer pulled by a pickup truck. As with the material for the trench, the tire chips or tire chip/soil mixtures were dumped and spread by hand using rakes and shovels (see Figure 9.19). Sections 1 through 5 were filled in 305-mm (12-in.) or 152-mm (6-in.) lifts of tire chips or tire chip/soil mixtures and compacted with a Case 1102 smooth drum vibratory roller. The operating weight of the compactor was 10.9 metric tons (12.0 tons) and compaction was achieved with a minimum of six passes. Tire chips are compressible,



Figure 9.19 Photograph of tire chips being spread over geotextile

so the tire chip lifts with 100% tire chips were overbuilt by up to 63 mm (2.5 inches) so the thickness of the layer would be as planned for during design after it was compressed by the weight of the overlying subbase and pavement. The 67% tire chip mixture was overbuilt by 26 mm (1.0 in.) and the 33% tire chip mixture was overbuilt 48 mm (1.9 in.), although the latter was larger than intended. Compression of the tire chips layers was measured with settlement plates whose design is described in Section 9.6.1. Table 9.3 gives initial thicknesses of the tire chip and tire chip/soil mixtures in each section. The final thickness of Sections 2 and 3 after paving (as measured on 7/2/97) were below the design thickness of 305 mm (12 in.), while the Sections 1 and 5 were above their design thicknesses of 305 mm (12 in.) and Section 4 was above its design thickness of 152 mm.

As with the trench, the tire chip/soil mixtures were completely surrounded by non-woven geotextile (Synthetic Industries Type 701) which met MDOT Specification 722.02 for Class A geotextile. Seams were overlapped 457-mm (18 in.). The purpose of the geotextile was to prevent migration of the fines into the voids in the tire chip or tire chip/soil mixtures from either the subgrade or subbase soils.

9.5.3 Placement of Subbase Course

Subbase was hauled to the site by a local contractor using 10.7- and 12.2-m³ (14- and 16-yd³) dump trucks. The material, MDOT Type D subbase aggregate, was dumped and spread with the tractor. The subbase was placed in 305-mm (12-in.) maximum lifts and compacted with six or more passes of the Case 1102 smooth drum vibratory roller, as shown in Figure 9.20. The subbase was placed over the tire chip and tire chip/soil mixtures, except in the control section, which consisted entirely of gravel subbase.

Table 9.3 Thickness of tire chip and tire chip/soil layers from settlement plate data

Plate Location (m)	Section	Thickness of tire chip or tire chip/soil layer (mm)										Average Compression (%)	
		Initial 9/26/96	Fill Complete 10/3/96	10/8/96	Before Paving 11/13/96	After Paving 7/2/97	Average Initial 9/26/96	Average After Paving*** 7/2/97					
0+18		368	360	348	**	321*							
0+24	5	306	286	287	**	**	368	321					12.9
0+30		202	189	176	171	170							
0+37	4	173	149	141	139	138	187	154					17.8
0+43		268	240	233	235	233							
0+49	3	319	303	287	289	284	294	259					11.9
0+55		341	316	303	305	302							
0+61	2	321	295	292	273	275	331	288					12.9
0+67		357	345	337	330	330							
0+73	1	349	329	329	321	322	353	326					7.6

25.4 mm = 1 in.

* This reading was taken on 8/12/97

** These readings were not taken because settlement plates were temporarily buried

*** Average of two settlement plate readings after paving was completed, i.e. the average of 0+18 and 0+24 for Section 5

Compaction of the Control Section was also achieved with a minimum of six passes with the smooth drum vibratory roller. Although the trench in the Control Section was lined with geotextile, the roadbed was not. Several samples of the subbase were taken during placement for later gradation analysis. Placement of the subbase was completed on October 5, 1996. At this point the temporary passing lane was closed and traffic was allowed to drive on the road. Bumps and potholes that developed in the road were leveled with the tractor bucket as necessary to maintain a driveable road surface.

Field density tests were performed on the subbase on November 6, 1996, 32 days after completion of subbase placement. Field density tests were performed by digging to a



Figure 9.20 Photograph of compaction of MDOT Type D subbase with vibratory roller

depth of at least 20 mm (8 in.) in the base course gravel and performing sand-cone tests. Table 9.4 shows the field dry density, water content, and relative compaction for the test sections. A laboratory moisture-density test was performed in accordance with AASHTO T99. The optimum water content was 7.1 percent, and the maximum density was 2.25 Mg/m³ (140 lb/ft³). Relative compaction ranged from 92 to 105 percent.

Table 9.4 Results of field density tests

Section	Dry Density	Water Content	Relative Compaction
	Mg/m ³	%	%
Control	2.09	3.6	92
1	2.32	3.4	103
2	2.27	2.5	101
3	2.37	2.9	105
4	2.24	3.1	100
5	2.17	3.5	96

Tire chips need time to settle under surcharge because they exhibit some time dependent settlement. Tweedie, et al. (1998) reports that for a 4.6 m (15 ft) thick tire chip fill, the majority of time dependent settlement was completed in 50 days. For this reason the researchers decided to allow the tire chips and tire chip/soil mixtures to settle under the weight of the subbase for at least three weeks before the road was paved. This was important because excessive time dependent settlement of the road after paving could damage the test sections. The actual time between completion of subbase placement and paving was 40 days.

9.5.4 Bituminous Pavement

Fine grading to ± 10 mm (3/8 in.) was performed on November 13, 1996 with a University road grader. Grade was checked using a hand level. After final grading, the surface was recompact with the Case 1102 smooth drum vibratory roller.

The road section was paved on November 14, 1996. The temperature was -8° C (17° F) at 7 am, when paving began. By midday the temperature had risen to about 2° C (36° F). The first lift of 89-mm ($3\frac{1}{2}$ -in.) lift of MDOT Type B base course was placed and compacted, and then a 38-mm ($1\frac{1}{2}$ -in.) lift of MDOT Type C surface course was placed and compacted. The length of newly paved road, including 4.6 m (15 ft) before and after the start of the test sections, totaled 77.7 m (255 ft). The new pavement was matched into the existing pavement 3.0 m (10 ft) from the beginning of the control section at Station 0+00.

The paving machine was a Caterpillar AP800. Compaction was performed first by a Hyster C350D steel wheel roller with a 10.0-metric ton (11-ton) operating weight, then by a PS180 CAT pneumatic tire roller with a 10.9-metric ton (12-ton) operating weight, then again by the Hyster C350D roller, and final rolling was done by a Bomag BW120AD mini roller with a 4.5-metric ton (5-ton) operating weight.

Several bituminous samples were taken during paving. Three samples were taken for bulk specific gravity, stability, and flow tests for both the base and the surface course. Table 9.5 lists the results of these tests. The average specific gravity of the base course was 2.28 and the average specific gravity of the surface course was 2.35.

Table 9.5 Results of stability and flow tests

Sample	Specific Gravity	Marshall Stability lb.	Flow 1/100 inch
Base 1	2.26	416	29
Base 2	2.27	1440	35
Base 3	2.30	2030	35
Surface 1	2.36	2420	27
Surface 2	2.36	2590	30
Surface 3	2.32	1100	61

9.6 INSTRUMENTATION & MONITORING

The instrumentation placed during construction were settlement plates, thermocouples, frost-free benchmarks, datalogging equipment, and piezometers. These are described in the following subsections.

9.6.1 Settlement Plates

Settlement plates were installed to measure the actual thickness of the tire chip layers after compression and to find the settlement of the tire chip layers as subbase and pavement were added. Each test section contained two settlement plates spaced 3.0 m (10 ft) on either side of the mid-station of the section. Settlement plates were made from 3.1 mm (1/8-in.) diameter all thread, 203 mm (8-in.) by 254 mm (10-in.) by 3.1 mm (1/8-in.) thick steel plate, and 12.7-mm (1/2-in.) diameter, schedule 40 black iron pipe. Typical dimensions and a picture of a settlement plate are shown in Figures 9.21 and 9.22, respectively. No settlement plates were installed in the control section.

The lower portion of the each settlement plate was all-thread and steel plate, fastened together with two nuts and a lock washer. This part was placed on the subgrade.

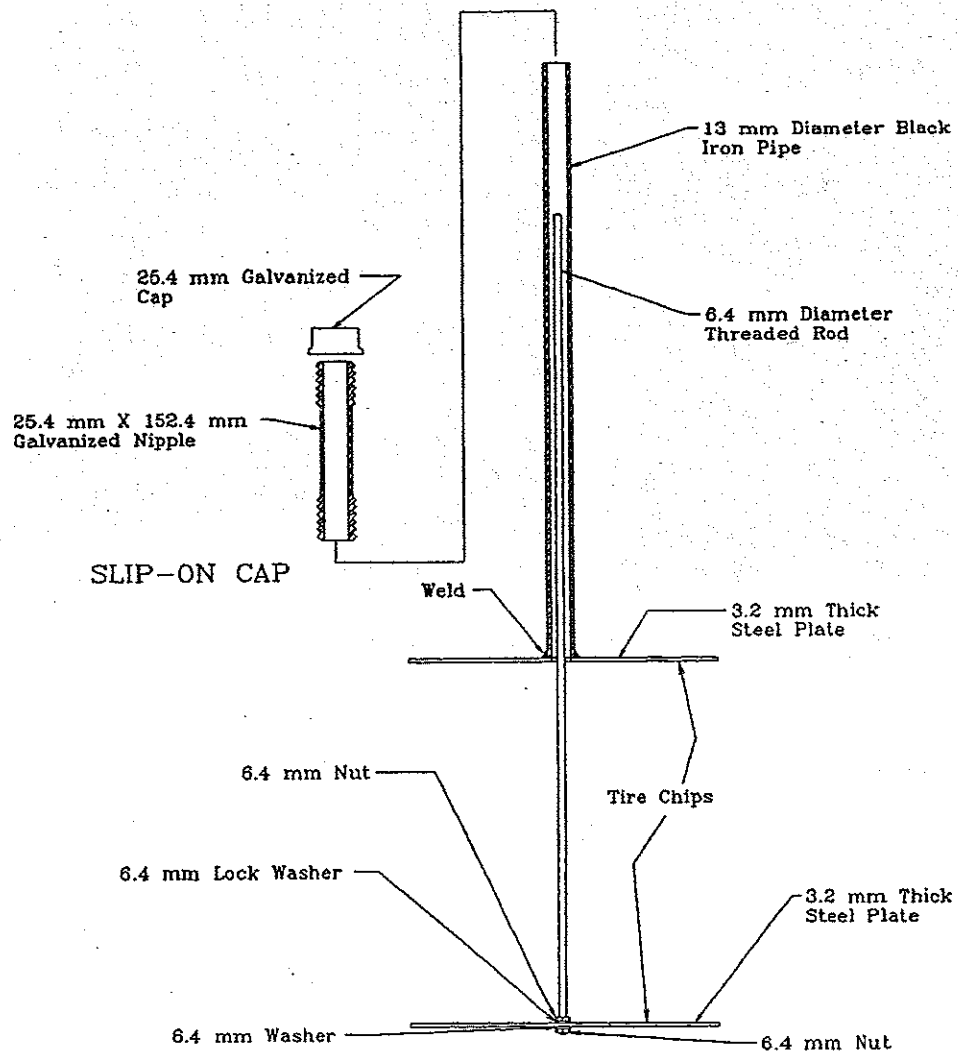


Figure 9.21 Settlement plate detail

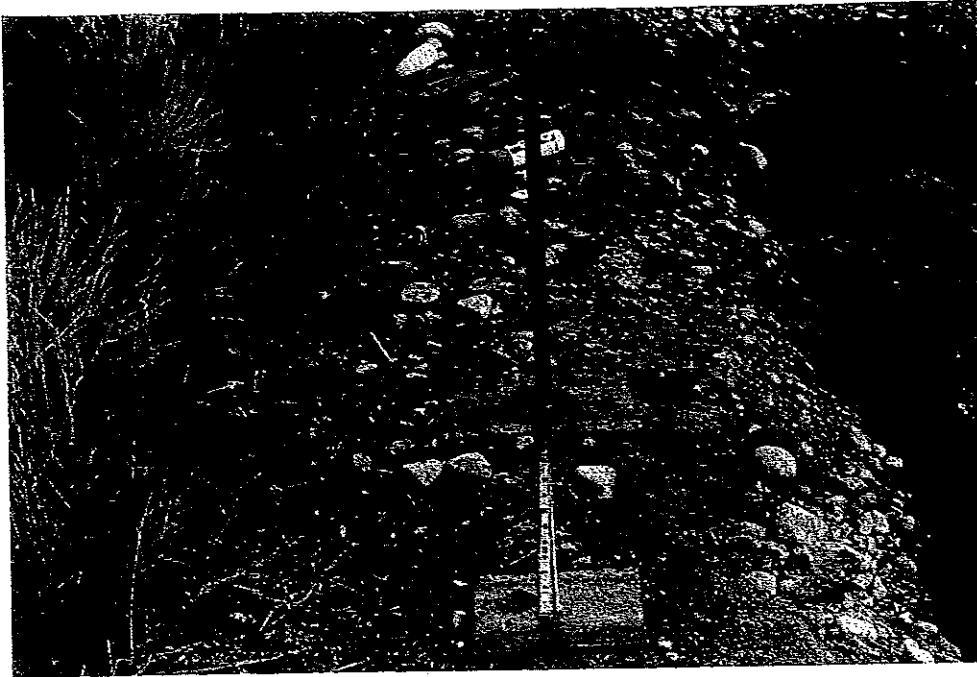


Figure 9.22 Photograph of settlement plate before placement in roadbed

The settlement plates were located on the centerline of the road. Geotextile was then put over the base of the lower plate. Small holes were cut in the geotextile to accommodate the all-thread. Tire chips or tire chip/soil mixtures were then placed, geotextile was placed over the top, and the upper portion of the plate was then placed over the all-thread. The upper portion was constructed of black iron pipe welded to a steel plate.

A summary of the settlement of tire chip and tire chip/soil mixtures for the test sections was shown in Table 9.3. Section 4 appeared to have the greatest percent compression from September, 1996 to July, 1997 at 17.8%. The Station 0+18 reading did not seem valid since the measured thickness was greater in July, 1997 than in October, 1996. Section 1, with 33% tire chips, had the smallest compression at 7.6%.

9.6.2 Thermocouples

Six sets of thermocouples were placed in the road on September 19, 1996. One thermocouple string was installed in the center of each section. Each string contained from twelve to twenty 20-gage copper constantan (Type T) thermocouples. The initial calibration tolerances for the thermocouples was ± 1.1 °C (2 °F) for standard limits. A total of 96 thermocouple pairs were used for this project. The thermocouple pairs were fabricated and mounted on 25-mm (1-in.) diameter wooden dowels by the U.S. Army Corps of Engineers Cold Regions Research and Engineering Laboratory.

Thermocouples were installed in 102-mm (4-in.) diameter holes drilled by a tractor-mounted auger. The string of thermocouples was then placed in the hole and the hole was packed with the soil removed from the hole. Each cable-dowel system had one or two fliers, which are longer-lead thermocouple pairs whose tips are not attached to the dowel. This allows the top of the dowel to be buried so the upper layer of subbase could be placed and compacted with fewer obstructions. After placement of gravel was completed, the researchers dug down to the top of the dowels, pulled up the fliers, and placed them at the appropriate depth. A picture of a partially buried cable-dowel system is shown in Figure 9.23.

Fifty of the subsurface thermocouples were read by a datalogger and 46 subsurface thermocouples were read manually. An additional three thermocouples were used to measure air temperature and were attached to the datalogger. The depths of the thermocouples measured by the datalogger and the locations of the manually read

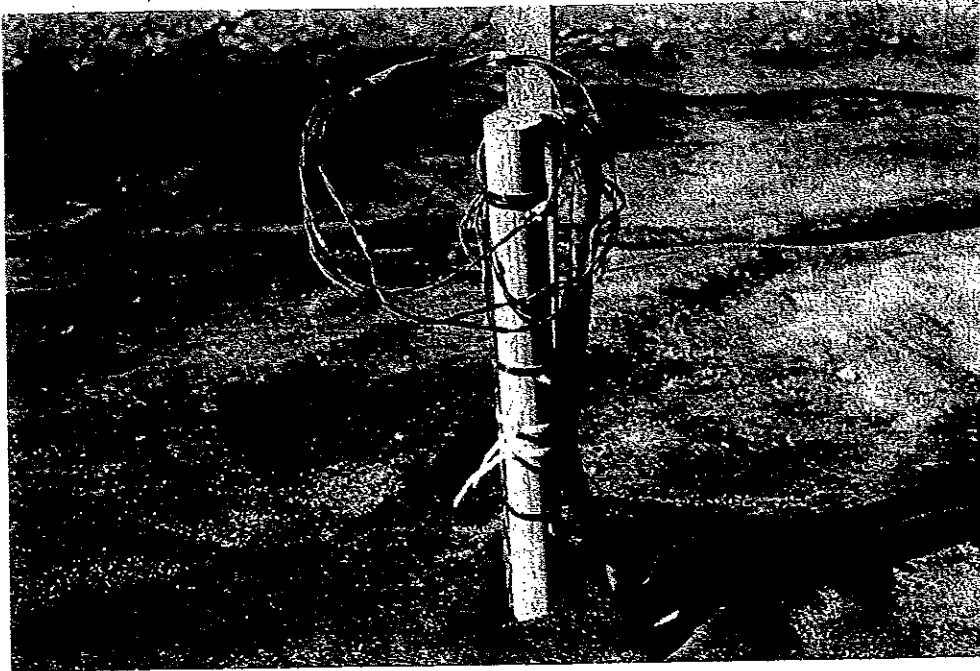


Figure 9.23 Photograph of thermocouple-dowel setup

thermocouples are shown in Figure 9.24. The datalogger is discussed in the next subsection. The path of the thermocouple cables was along the centerline of the road to Station 0+58, after which they were angled approximately 90 degrees to the right, fed through a 102 mm (4-in.) diameter Schedule 40 PVC pipe under the right shoulder of the road, and up into a weather-resistant and insulated box where the datalogger is housed. A shallow trench was dug for the portion of cables in the roadbed which would be driven over during construction. The cables were placed in this shallow trench and covered with some of the subgrade soil that had just been dug out.

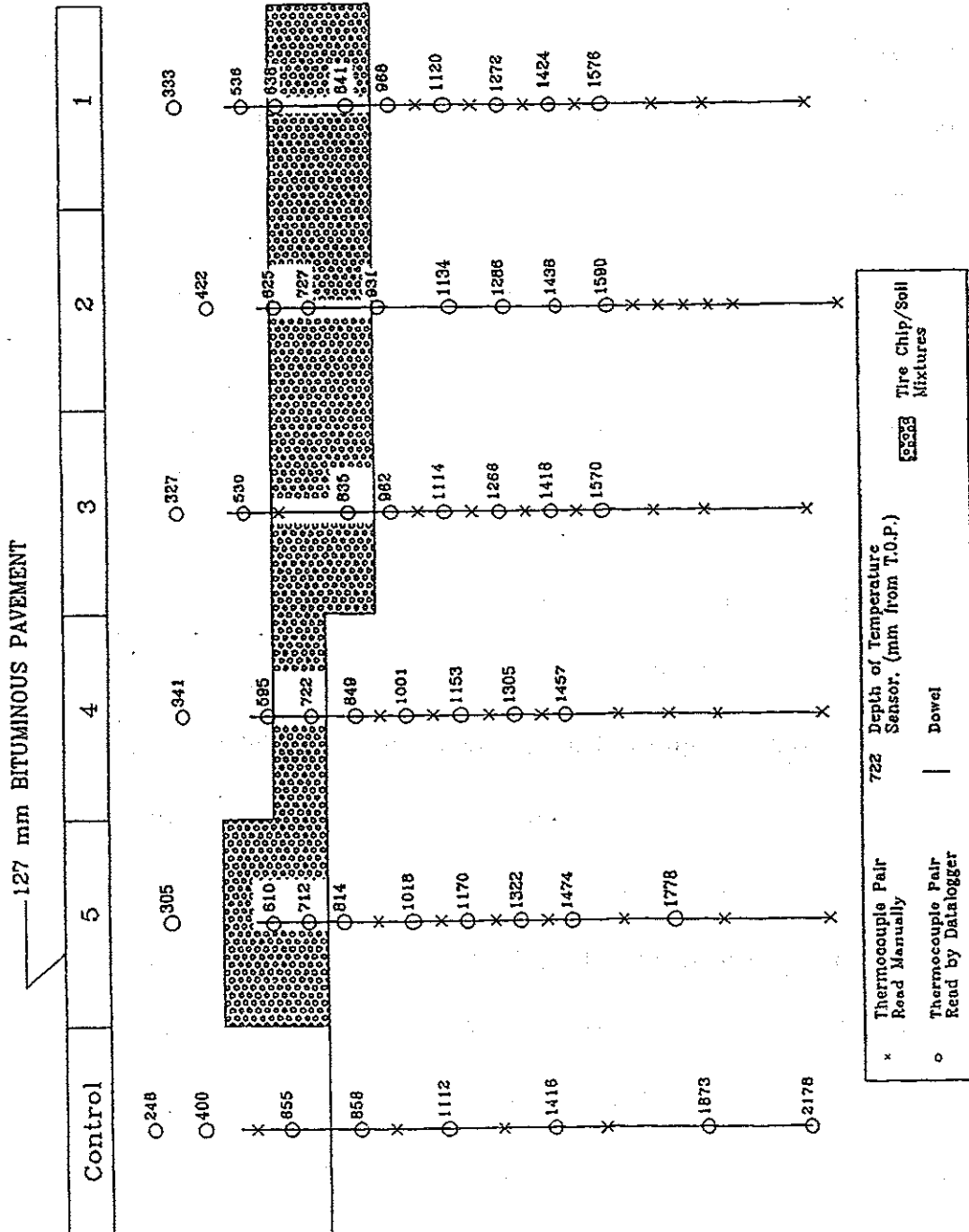


Figure 9.24 Thermocouple pair positions beneath test sections

9.6.3 Datalogger

The datalogger was housed in a small plywood structure at approximately Station 0+58 on the right side of the road. The housing for the instrumentation was made to be watertight and to protect the instrumentation panel from large variations in temperature. Electricity was needed to run the datalogging equipment, so University electricians connected 12 gage UF wire from a nearby telephone pole. Approximately 122 m (400 feet) of wire was used to bring electricity to the datalogger.

There were four main components to the datalogging system, all manufactured by Campbell Scientific, Inc.: CR10X datalogger, wiring panel, power supply, and two AM25T solid state multiplexers. Campbell Scientific, Inc. (1996) reports that the accuracy of the CR10X and the AM25T is ± 0.2 °C in the range from -25 to +50 °C.

Data for fifty subsurface thermocouples was taken electronically. These readings were taken every hour by the datalogger and stored in memory. The stored data was retrieved with a laptop computer which was connected to the datalogger via an optically isolated RS232 interface (Campbell Scientific model SC32A). Temperatures of the other 46 thermocouples were monitored manually with an electronic thermometer (Omega Model 450 ATT) designed to read Type T thermocouples. Thermocouples were read manually approximately every 10 days from December 11, 1996 to February 9, 1997. However, readings were discontinued because they did not match the readings taken by the datalogger. This was due to the inability to keep the electronic thermometer and thermocouple clips at a constant temperature. If the thermometer could have been kept at

a constant temperature, the datalogger and thermometer readings should have been in agreement.

9.6.4 Frost Free Benchmarks

Two frost-free benchmarks were installed by the US Army Corps of Engineers. The two benchmarks are founded 2.4 to 3.0 m (8 to 10 feet) below the surface of the ground. A 229-mm (9-in) diameter hole was drilled with a tractor-mounted power auger to about 1.5 m (4.9 ft). A 13-mm (1/2-in.) diameter piece of rebar was driven into the ground and then a 102-mm (4-in.) diameter piece of PVC pipe was placed over the rebar down to the bottom of the hole. Soil from the hole was placed back in the holes outside the PVC pipes. BM1 was located at Station 0+28, offset 7.6 m left of centerline, and BM2 was located at Station 0+80, offset 8.2 m left of centerline. Benchmarks were installed to serve as stable elevation references for measurements of frost heave during the winter. Pavement elevations were measured in the fall and in the winter near the time of maximum frost heave. Sixteen points were measured in each section. Chapter 10 describes the spacing of the frost heave survey points.

9.6.5 Piezometers

Three open standpipe piezometers were installed at the site to measure groundwater elevation. The groundwater elevation is important because accessible groundwater is necessary for frost heaving. The piezometers consist of 51-mm (2-in.) diameter schedule 40 PVC pipe slotted for the bottom 610 mm (2 ft). Holes were drilled with a 229-mm (9-in.) diameter post hole digger attached to a tractor. The bottom 152 mm (6 in.) of the hole was filled with concrete sand and then the PVC pipe, capped on the end, was placed

in the hole. Sand was added to bring the level of sand to about 152 mm (6 in.) above the top of the slotted portion of the PVC pipe. Approximately 610 mm (2 ft) of coarse grade Wyoming bentonite chips were used as a seal over the sand. The remainder of the hole was filled with natural soil. Figure 9.25 shows a typical cross-section of a piezometer as well as the stations and offsets of the three piezometers. The plan location of the piezometers is shown in Figure 9.1. Readings were taken in November, April, May, and July. The groundwater elevations from these readings are summarized in Table 9.6. For reference, the top of pavement elevations at the center of Sections 1, 3, and 5 are 16.24 m (53.27 ft), 15.91 m (52.20 ft), and 15.59 m (51.16 ft), respectively.

9.7 SUMMARY

A field trial was constructed in the fall of 1996 at the University of Maine using tire chips and tire chip/soil mixtures to insulate the subgrade and provide drainage for the road. The test site is located on a University road to the Whitter Farm, approximately 1.6 km (1 mile) from the center of the University of Maine campus. A subsurface investigation revealed that the subgrade was frost susceptible silty clay.

Table 9.6 Groundwater elevations

Date	Groundwater elevation (m)		
	P1	P2	P3
11/15/96	14.55	13.83	13.73
4/25/97	14.49	14.34	14.90
5/20/97	14.88	14.41	14.78
7/29/97	13.87	13.75	14.08

Plan View of Piezometers

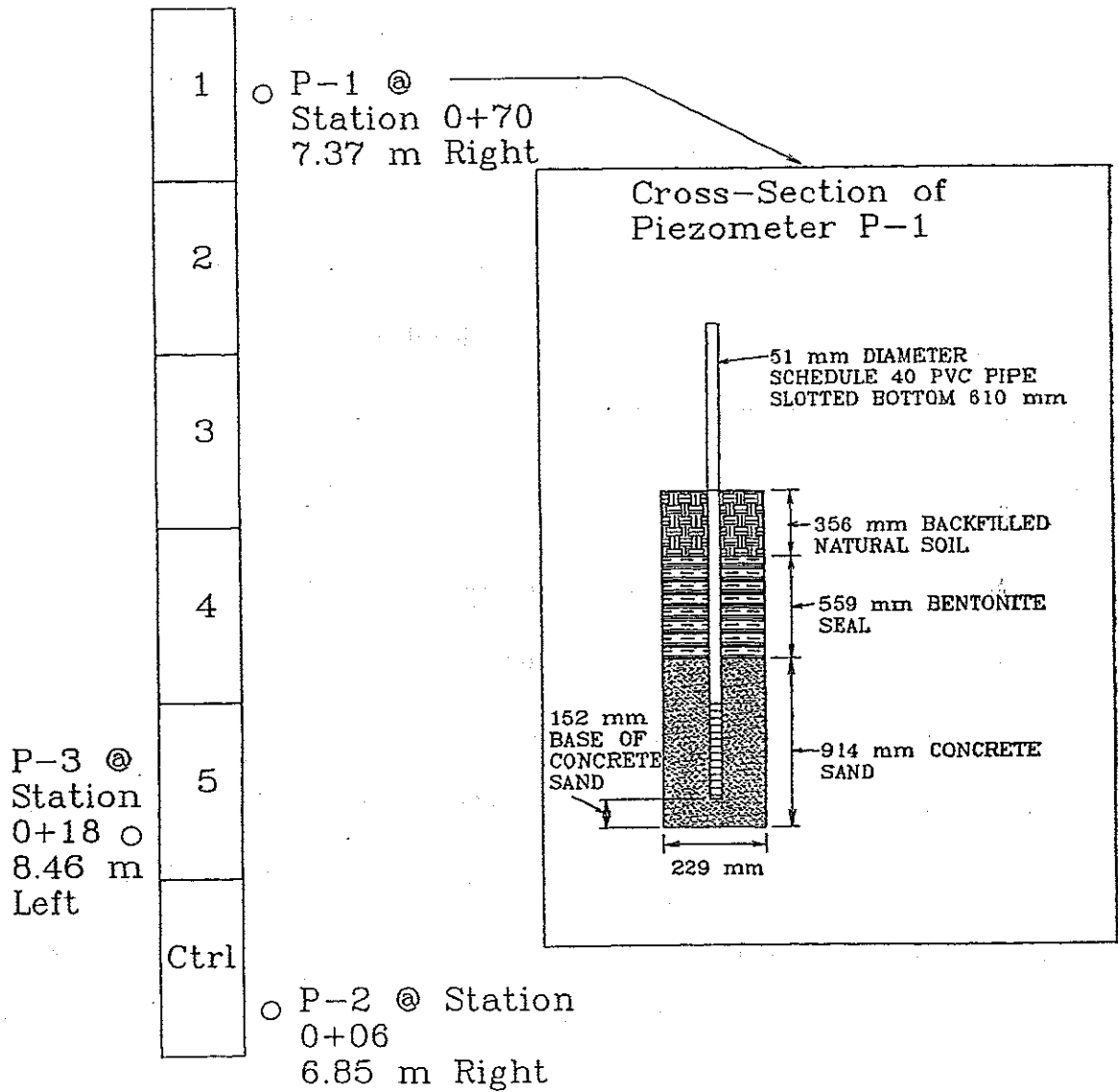


Figure 9.25 Plan location of piezometers and typical cross section

The test site consists of five 12.2-m (40-ft) long paved test sections and one 12.2-m (40-ft) long Control Section. Three sections contain tire chips, one section contains 67% tire chips/33% gravel, and one section contains 33% tire chips/67% gravel. Each tire chip and tire chip/soil layer is surrounded by geotextile. These sections contain from 152 to 305 mm (6 to 12 in.) of tire chips or tire chip/soil mixtures, 330 to 483 mm (13 to 19 in.) of gravel cover, and 13 mm (5 in.) of pavement. A 1.07-m (3.5 ft) deep edge drain is located on the left side of the road.

Type A tire chips with a maximum size of 76 mm (3 in.) were obtained from a stockpile on campus. Granular material for the edge drains and tire chip/soil mixtures was also obtained from a stockpile on campus. Aggregate for the subbase was obtained from a local contractor.

The roadbed and edge drain were excavated by a local contractor. Some of the granular material excavated from the roadbed was used to create a temporary vehicle bypass lane and some was stockpiled for later use in the shoulders. Geotextile was placed in the edge drain trench and the trench was filled and compacted. Next geotextile was placed on the exposed subgrade, the tire chip and tire chip/soil mixtures were placed, and then compacted by a smooth drum vibratory roller. The tire chip/soil mixtures, especially the 67% tire chips/33% gravel mixture, were difficult to mix and spread without causing segregation. The top of the tire chip and tire chip/soil layers were covered with geotextile. Next the gravel subbase was spread with a tractor and compacted with a smooth drum vibratory roller. Paving was performed by a local contractor.

Settlement plates were installed to record compression of the tire chip and tire chip/soil mixtures due to the weight of the overlying soil and pavement. Tire chip layers compressed from 11.9 to 17.8 percent. The 67% tire chips/33% gravel and 33% tire chips/67% gravel layers compressed 12.9 and 7.6 percent, respectively. A total of 96 thermocouples were installed to record subsurface temperatures. Fifty of these were recorded automatically every hour by a datalogger. Two frost free benchmarks were installed as reference elevations for heave measurements. Piezometers were installed to measure groundwater elevation.

10. FROST PENETRATION

10.1 INTRODUCTION

This chapter presents data on frost depth, frost heave, and backcalculated thermal conductivity for the winter of 1996-1997. The thermal conductivities of tire chips and tire chip/soil mixtures are backcalculated from the field measurements using both steady state and non-steady state conditions. Results of these calculations are then compared to values determined in the laboratory phase of this study as well as values reported in the literature.

10.2 FROST DEPTH

Subsurface temperatures were recorded and analyzed from December 3, 1996 to March 29, 1997, the day frost was undetectable in all sections. The temperature of the 53 thermocouples attached to the datalogger were recorded every hour. This data was stored in the datalogger and then retrieved with a laptop computer every 10 to 14 days. The average daily temperature of each thermocouple was computed and then used for subsequent analysis. The daily location of the zero degree Celsius isotherm was linearly interpolated from the thermocouple temperatures for each section. The zero degree isotherm was taken to be the freezing front.

Manual readings of some of the thermocouples were taken using an electronic thermometer (Omega Type 450 ATT) for the first several weeks of the project. This was intended to provide a check on the accuracy of the temperatures read by the thermocouples attached to the datalogger. The best way to measure the temperatures

would be to have the electronic thermometer in a heated space where it could be maintained at a constant temperature. However, manual readings were taken outside, so temperature variations of the electronic thermometer resulted in inaccurate readings and manual readings were discontinued.

Hourly air temperatures were taken from two thermocouples located on the back of the datalogger housing. These readings were in good agreement with temperatures measured with a mercury thermometer. The air temperatures measured by the thermocouples were used to compute the average daily air temperature and freezing degree days. Accurate average daily temperatures from the datalogger were available only after January 14, 1997. Readings from the University of Maine campus located approximately 1.6 km (1 mi) from the site were used to calculate average daily temperatures and freezing degree days before this date. Figures 10.1 and 10.2 depict cumulative freezing degree days versus date and average daily temperature versus date. Input parameters for calculation of frost depth were obtained from both of these plots.

The coldness of a winter is estimated by the freezing index, which is the difference between the maximum and minimum peaks in Figure 10.1. Freezing degree days were computed from December 19, 1996 to March 24, 1997 and totaled 461 °C-days (829 °F-days). The average freezing index for Orono is about 714 °C-days (1285 °F-days) (Bigelow, 1969). Thus, the winter of 1996-1997 was much warmer than an average winter. The length of the freezing season is the number of days between the maximum and minimum peaks. The length of the season was 96 days in 1996-1997.

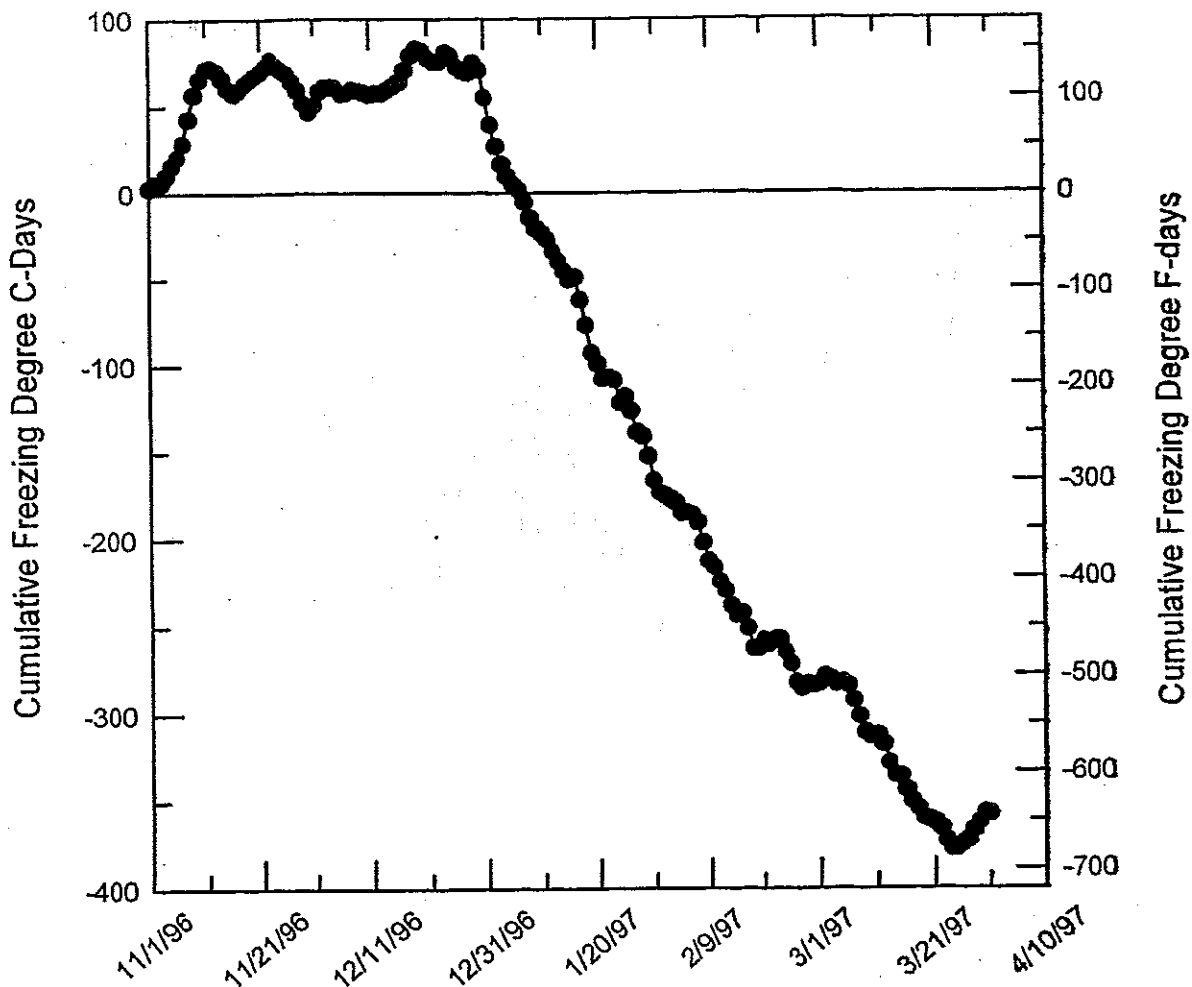


Figure 10.1 Cumulative freezing degree-days versus date

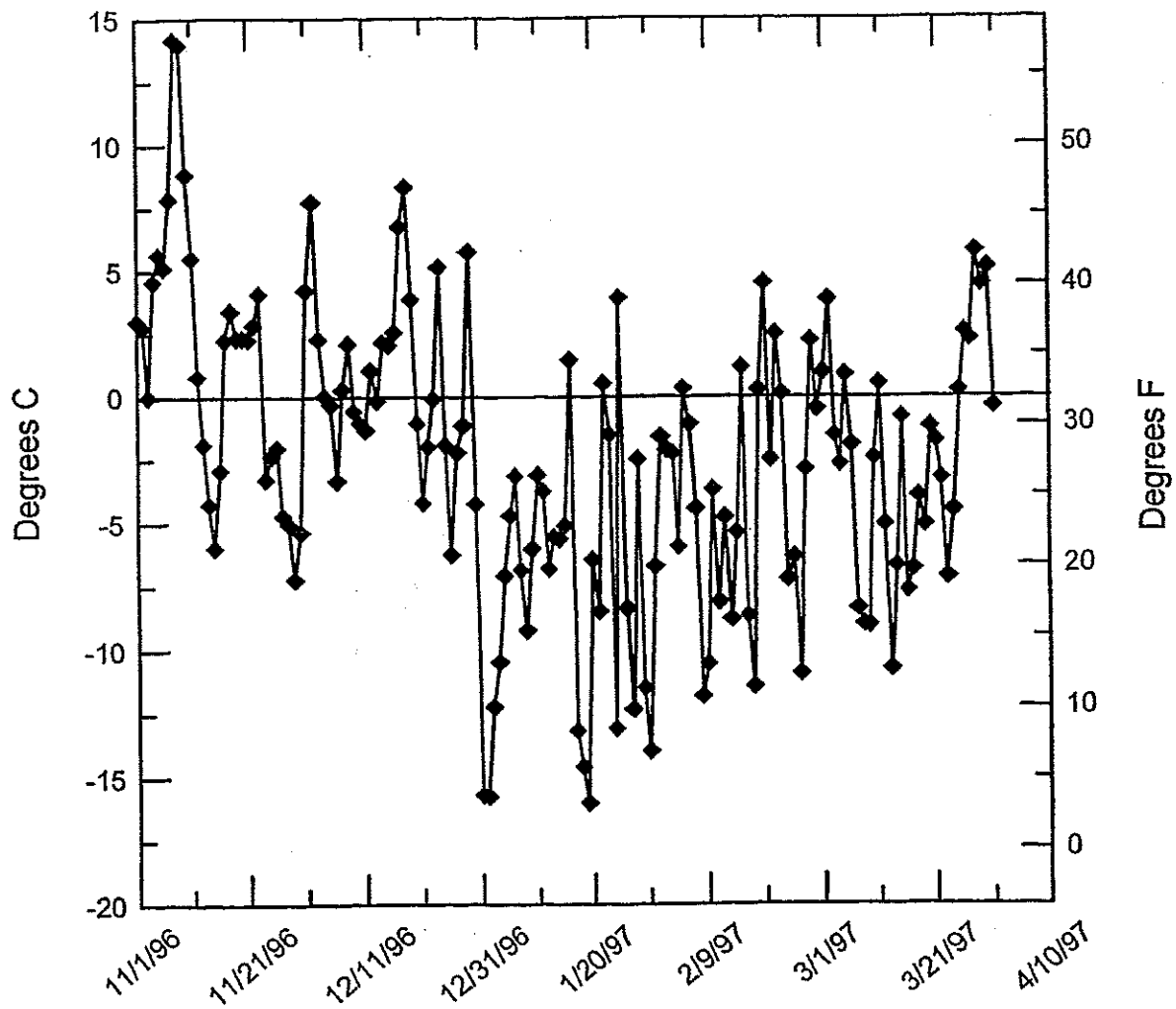


Figure 10.2 Average daily temperature versus date

10.2.1 Frost Depth Versus Date

Figures 10.3 through 10.5 show frost depth versus date for each section. Figure 10.3 shows frost depth versus date for the Control Section and Sections 1, 2, and 3. Section 1 contained 33% tire chips/67% soil, Section 2 contained 67% tire chips/33% soil, and Section 3 contained 100% tire chips. Each of these sections had 483 mm (19 in.) of soil and a 305 mm (12 in.) thick tire chip layer. The frost penetration behavior with time for Section 1 and the Control Section were similar. The frost penetration in these two sections was initially slower than the frost penetration in Sections 2 and 3. This could have been caused by the insulating value of the tire chips in Sections 2 and 3 preventing heat stored in the ground from warming the near surface granular soil above the tire chips. Since the Control Section had no insulation and Section 1 had the least insulation value of the tire chip/soil mixtures, heat from the ground flowed vertically to slow the initial frost penetration. However, this effect was short lived, and by mid-winter the Control Section and Section 1 had the greatest depth of frost penetration.

Freezing fronts of Sections 1, 2, and 3, and the Control Section passed through a depth of 610 mm (24 in.), which corresponds to the top of the tire chips or tire chip/soil mixtures, on nearly the same date. The freezing front in Section 3 diverged from the others at about mid-depth in the tire chip layer and remained in the tire chip layer for the entire winter. In Section 2 the freezing front diverged from Section 1 and the Control Section when it passed the bottom of the tire chip/soil layer. In Section 1 the freezing front diverged from the Control Section at a depth of about 1100 mm (43 in.).

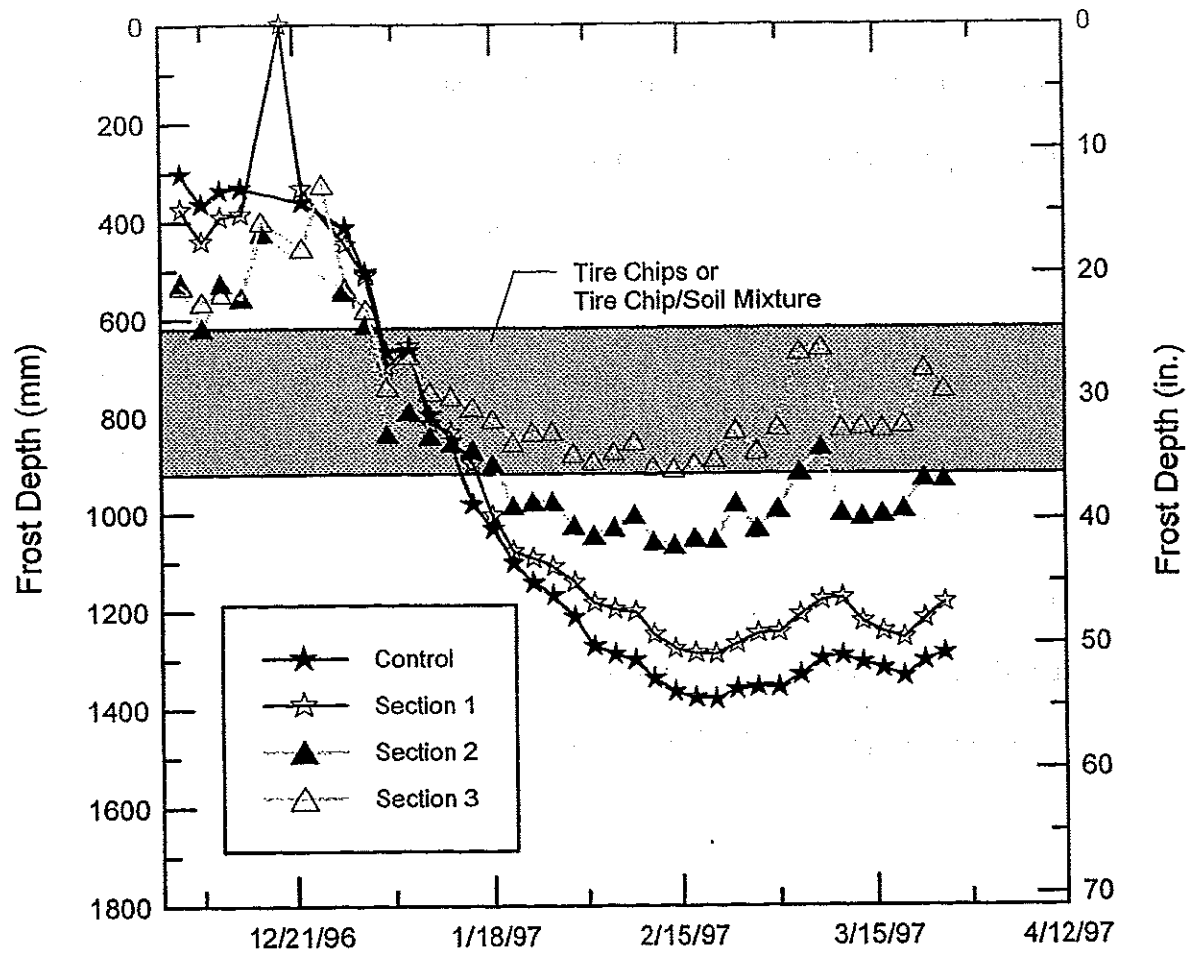


Figure 10.3 Depth of frost penetration vs. date, Sections 1 through 3

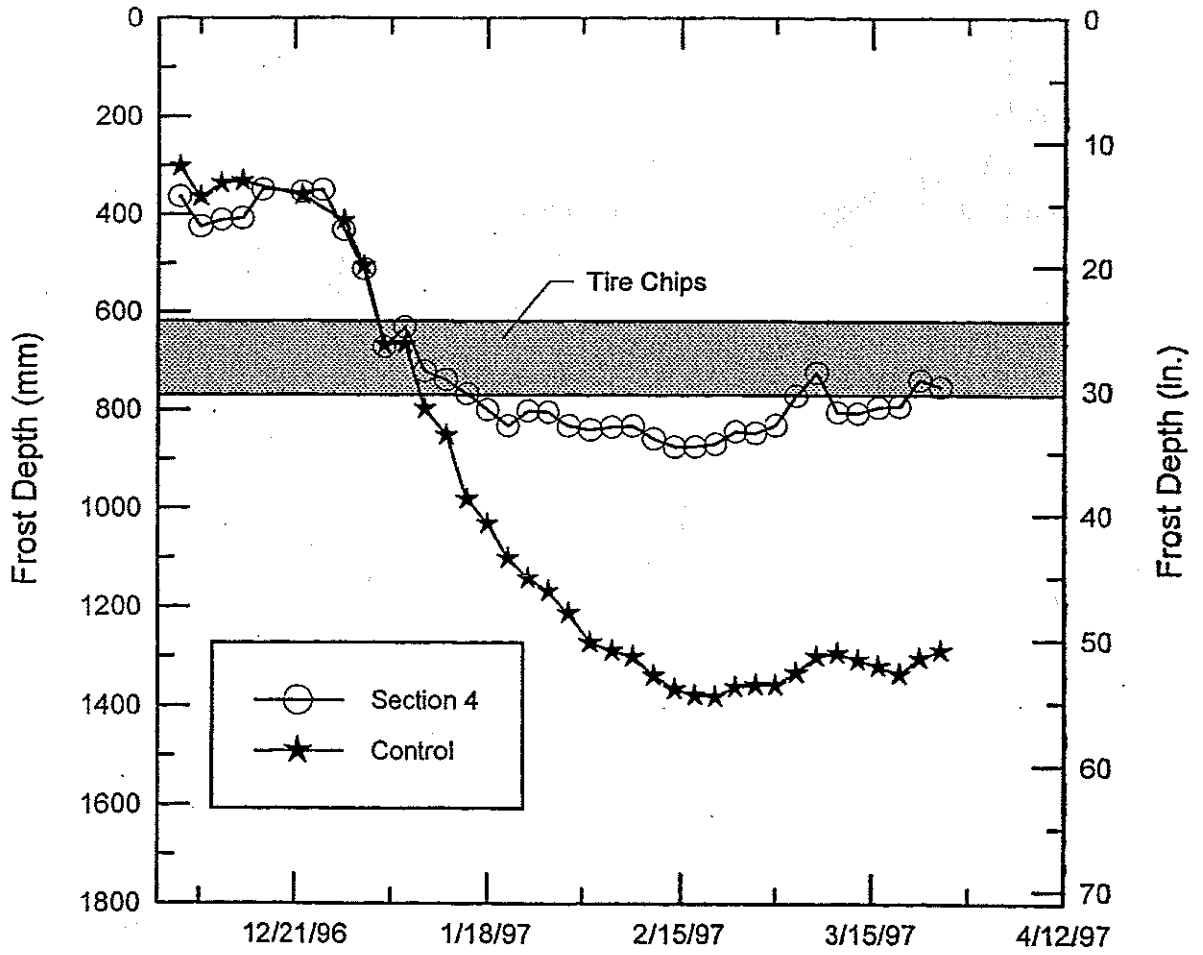


Figure 10.4 Depth of frost penetration vs. date, Section 4

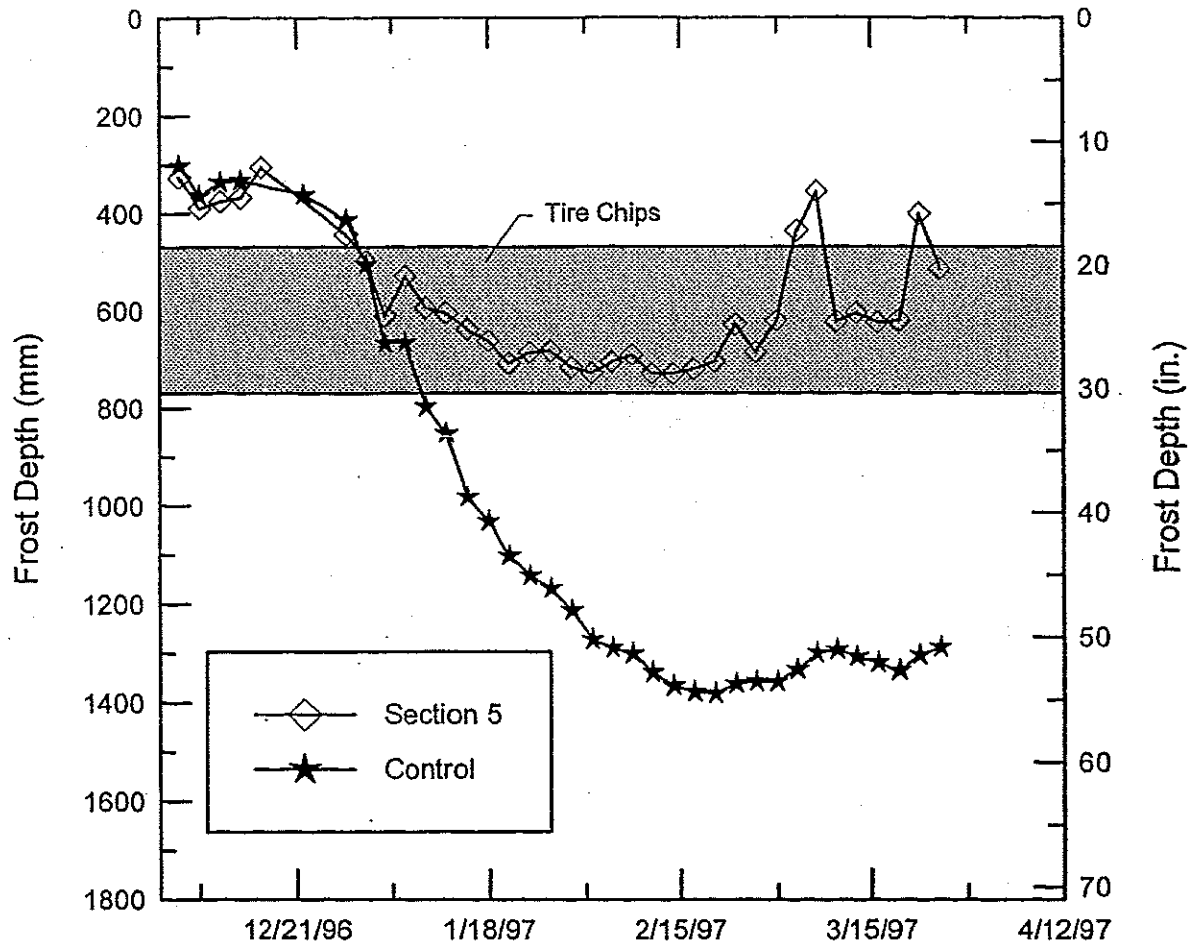


Figure 10.5 Depth of frost penetration vs. date, Section 5

Frost depth versus date for Sections 4 and 5 are shown in Figures 10.4 and 10.5, respectively. Section 4 contained 152 mm (6 in.) of tire chips with 483 mm (19 in.) of soil cover, and Section 5 contained 305 mm (12 in.) of tire chips with 330 mm (13 in.) of soil cover. The behavior of the freezing fronts in Sections 4 and 5 were nearly identical to that of the Control Section until they passed the top of their respective tire chip layers. The freezing front in Section 4 penetrated slightly into the subgrade soil and remained just below the bottom of the tire chip layer for the remainder of the winter. The freezing front in Section 5 did not reach the subgrade soil at any time during the winter.

10.2.2 Maximum Depth of Frost Penetration

Figure 10.6 shows the maximum depth of frost penetration by section as well as the location of the tire chip layers. Table 10.1 also summarizes the maximum depth of frost penetration and gives the percentage reduction in maximum frost depth for each section in comparison to the Control Section. Maximum frost depth was 1383 mm (54.4 in.) in the Control Section and 1290 mm (50.8 in.) in Section 1. Thus, the 33% tire chips/67% soil in Section 1 reduced the frost penetration by only 6.5 percent. The frost penetration in Section 2 was reduced 22.5 percent, Section 3 was reduced 34.0 percent, and Section 4 was reduced 36.2 percent. Section 5 had the smallest depth of frost penetration at 728 mm (28.7 in), which was a 47.1 percent reduction. Note that the frost did not penetrate into the subgrade in Sections 3 and 5.

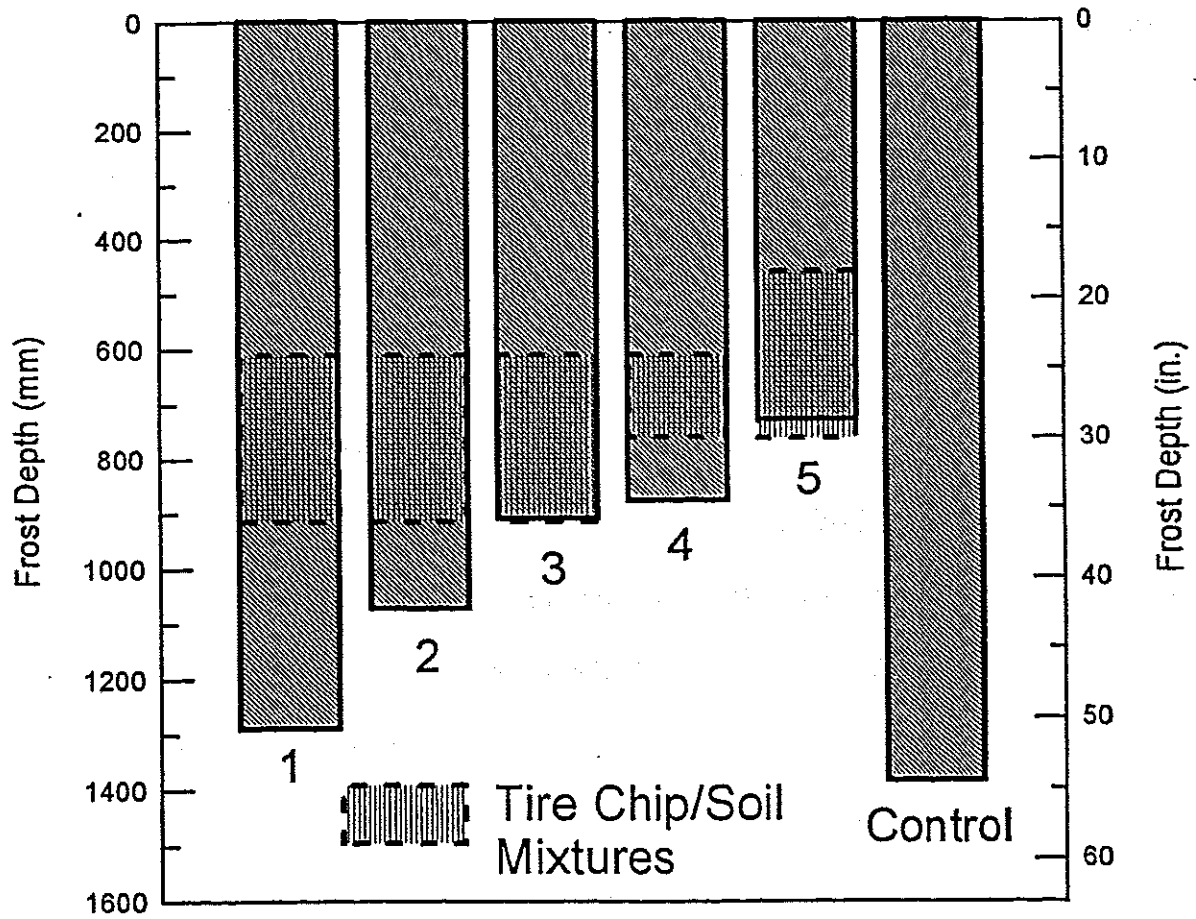


Figure 10.6 Maximum depth of frost penetration

Table 10.1 Summary of frost depths by section

Section	Percent Tire Chips (Volume)	Maximum Frost Depth (m)	Percent Reduction from Control
1	33	1.29	6.5
2	67	1.07	22.5
3	100	0.91	34.0
4	100	0.88	36.2
5	100	0.73	47.1
Control	----	1.38	----

The maximum depth of frost penetration was less than the elevation of the groundwater table, in every section except the Control. In Sections 1 through 5 the maximum depth of frost penetration was about 200 mm (8 in.) above the groundwater table. In the Control Section, however, the maximum depth of frost penetration was 510 mm (20 in.) below the groundwater table. Groundwater table elevations were interpolated at the center of each section based on readings taken in April and May, 1997 from the three standpipes located beyond the shoulders of the road.

10.2.3 Temperature Profiles

The profiles of temperature versus depth show the insulating effects of tire chips and tire chip/soil mixtures. The profiles in Figure 10.7 display temperature vs. depth on February 14, 1997. This date marks the end of a 47-day cold period from December 30, 1996 to February 14, 1997. This day was also on or close to the dates of maximum frost penetration for each section, as can be seen in Figures 10.3 through 10.5.

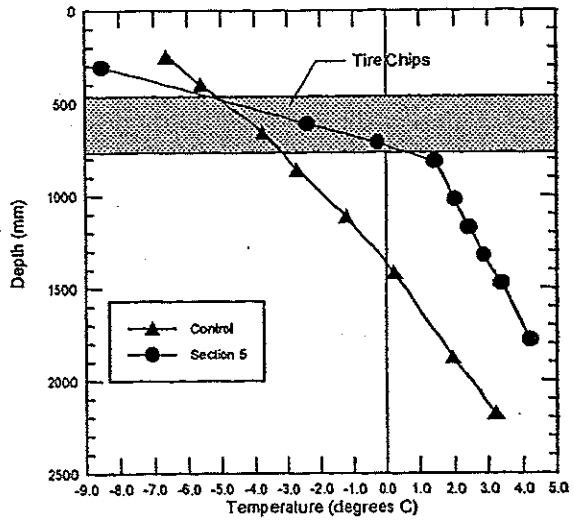
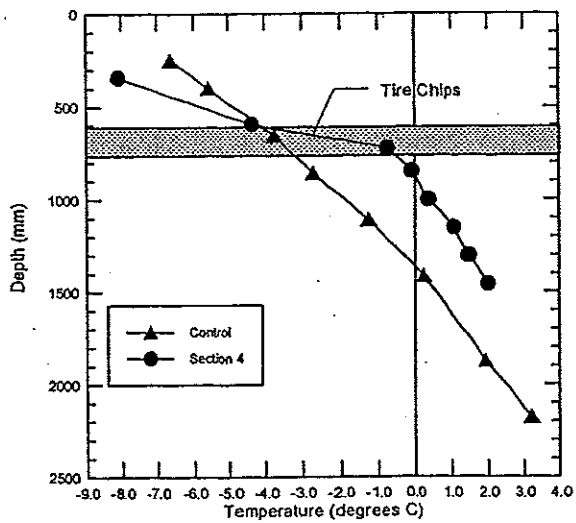
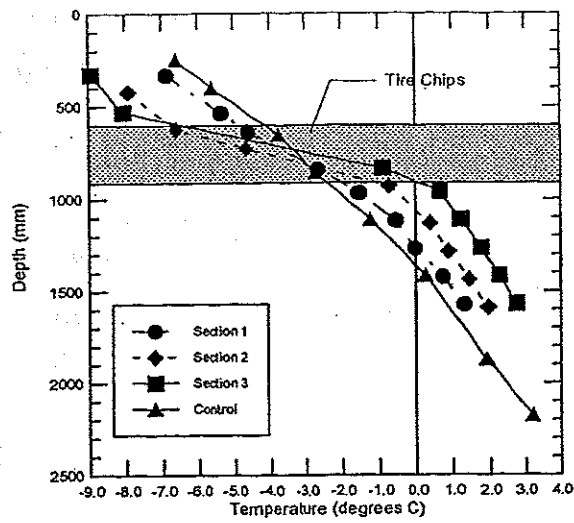


Figure 10.7 Temperature profiles on February 14, 1997

Figure 10.7 shows temperature versus depth on February 14, 1997 for all test sections and the Control. Figure 10.7 shows that there were sharp changes in the slopes of temperature lines as they crossed the top of the tire chip or tire chip/soil layers. Another sharp change in slope occurred as they crossed the bottom of the tire chip or tire chip/soil mixtures into the subgrade. The Control did not exhibit this drastic change in slope, but there was a slight change from above subgrade to below subgrade, which was at a depth of 762 mm (30 in.).

The temperature profiles of Sections 1, 2, and 3 show that temperatures above the tire chip or tire chip/soil mixtures decreased with an increase in the percentage of tire chips. This was due to the lower thermal conductivity of materials with higher proportions of tire chips. This impeded heat flow to the area above the tire chip/soil layers, resulting in lower temperatures in these regions. The reverse was true below the tire chip or tire chip/soil mixtures. Since heat flow was impeded, the temperatures in regions below the tire chip/soil layers were higher as the proportion of tire chips increased. Similar behavior was exhibited for tire chip Sections 4 and 5.

The difference in temperature from top to bottom of the tire chip and tire chip/soil mixtures increased as the percentage of tire chips increased. Table 10.2 shows that the smallest temperature difference for a tire chip or tire chip/soil mixture was 2.7°C (4.9°F) in the 33% tire chip/67% soil mixture (Section 1). The largest difference was 7.9°C (14.2°F) for the 305 mm (12 in.) tire chip layer at 610 mm (24 in.) below the top of pavement (Section 5).

Table 10.2 Temperature gradients of tire chip and tire chip/soil layers

Section	Percent Tire Chips Volume	Temperature Difference °C	Temperature Gradient °C/m
1	33	2.9	8.9
2	67	5.7	19.8
3	100	7.5	29.0
4	100	3.8	24.7
5	100	7.4*	24.3*
Control	-	2.0	6.6

* This is the estimated temperature difference and temperature gradient as described in the text

For comparison, there was a 2.0°C (3.6°F) difference in the Control for a 305 mm (12 in.) thick portion of granular subbase at the same depth as the tire chips in Section 5.

The data in Table 10.2 shows that the temperature gradient increases as the percentage of tire chips increase. Temperature gradients were determined from the slopes of temperature profile lines in Figure 10.7. To estimate these gradients, the temperature profile lines from the gravel base and subgrade were extended linearly to the interface with the tire chip or tire chip/soil mixture layers. The same was done within each tire chip or tire chip/soil layer which allowed the temperatures at the interfaces to be estimated. Temperature differences from top to bottom of each tire chip and tire chip/soil layer were divided by the thickness of each respective layer to obtain temperature gradients. The gradients determined for Sections 3 and 4 were 29.0 and 24.7°C/m (15.9 and 13.6°F/ft), respectively. These values are reliable since each of these sections had two thermocouples embedded in the overlying gravel, which could be used to find a temperature gradient. An accurate temperature gradient could not be determined in

Section 5 because it had only one thermocouple in the gravel base. Therefore, the temperature at the interface of tire chips and gravel in Section 5 were estimated using the slope of the temperature gradient for gravel in Section 3. Using this procedure, the best estimate of temperature gradient in Section 5 was $24.3^{\circ}\text{C}/\text{m}$ ($13.3^{\circ}\text{F}/\text{ft}$). The temperature gradients of the mixtures increased with an increase in percent tire chips. Thus, Table 10.2 shows that the tire chips effectively insulated the subgrade by reducing heat loss up through the tire chip or tire chip/soil layer and that an increase in the percentage of tire chips increased the insulating value of a tire chip/soil mixture.

10.3 FROST HEAVE

Frost heave was measured at 96 points. Each section contained sixteen survey points, arranged in a grid, four points longitudinally by four points transversely. The longitudinal spacing was 3.0 m (10 ft) and began 1.5 m (5 ft) from the border of each section. In each travel lane, the points were spaced laterally 0.6 m (2 ft) from the centerline and 0.9 m (3 ft) from the edges of the pavement. The surface heave of the road was the difference in road elevation between November 25, 1996 and the average of elevations on February 22 and March 26, 1997. The elevation of heave differed by about 6.0 mm (0.02 ft) between February and March readings, which is 15% of the magnitude of heave in the Control Section. This is probably due to inaccuracies in reading instruments rather than actual differences in heave since approximately half of the February readings were higher than the March readings. The reason for the month long delay between the readings was severe icing on the road that occurred in late February and early March, due to the colder surface temperatures in the insulated sections and shading from the adjacent woods. Some survey points were covered with approximately

50 to 75 mm (2 to 3 in.) of ice in the tire chip sections which made surveying these points difficult. The most severe icing occurred on the outer points nearest the shoulders, especially on the left side of the road, which was the most shaded and adjacent to the edge drain. Some of the survey points were covered with ice for the March survey, but the ice was removed.

Frost heave in each section is shown in Figure 10.8. Each section contains four bars, which correspond to readings taken in the approximate wheel paths of the road. Each bar, such as "left outside," is the average of four survey points taken in the left outside wheel path in a given section. In each section, the greatest heave occurred on the outside wheel paths. The inside wheel paths usually heaved much less. An explanation for this is that inside wheel paths were surrounded by tire chips or tire chip/soil mixtures, whereas the outside wheel paths were bordered by the natural ground which had a higher thermal conductivity. In addition the outside wheel paths had greater access to water from surface infiltration.

Frost heave was also greater on the left outside than on the right outside. There are three possible factors which would contribute to greater heave on the left side of the road. The first factor was the amount of exposure to sunlight. The left side of the road received almost no sunlight throughout the winter due to the woods on the left side of the road. The right side was shaded much of the day, but it usually received some sunlight, especially in the latter part of the winter. The second factor was the edge drain on the left side of the road. Although the edge drain was designed to reduce availability of

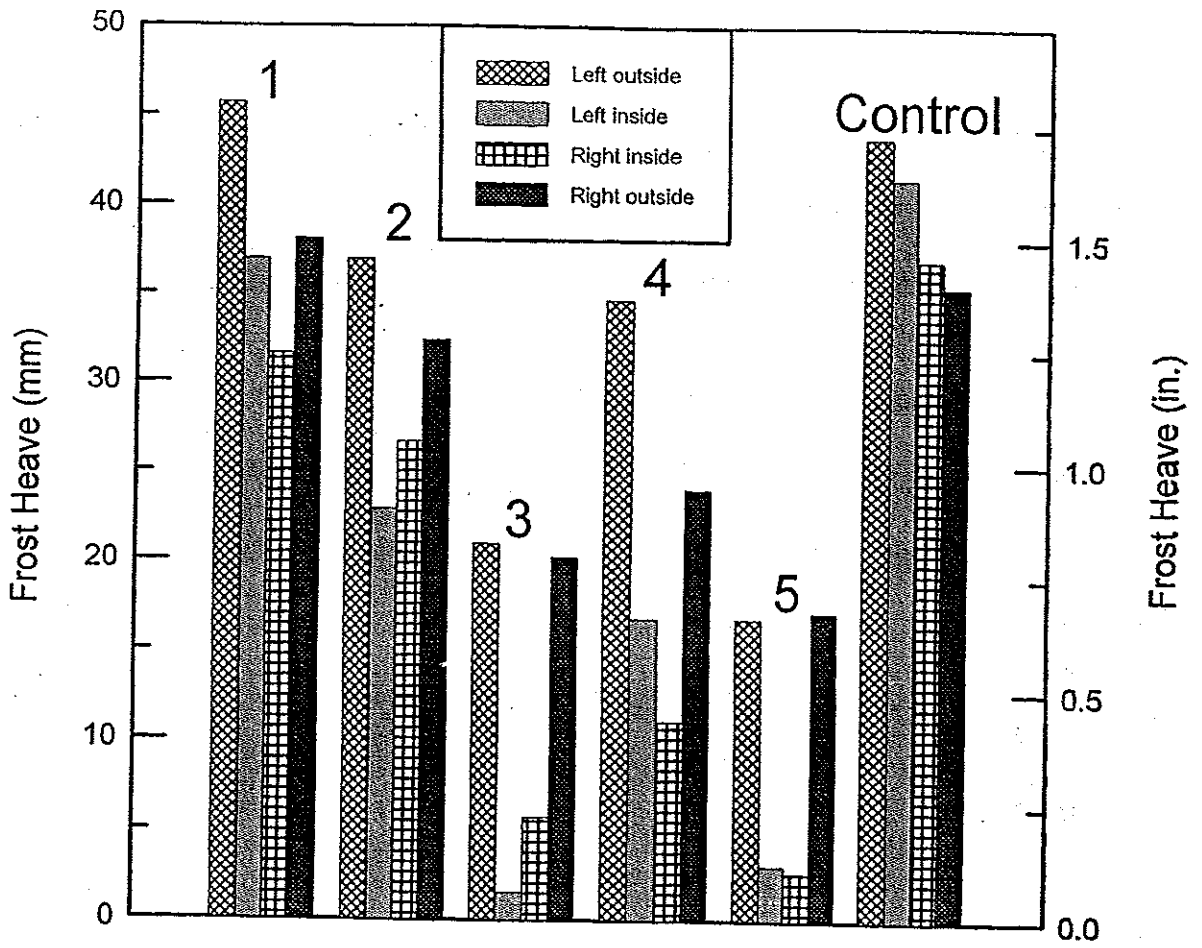


Figure 10.8 Average frost heave in individual wheel paths

water to the soils, the outlet of the drainage pipe became frozen during the winter. Thus, water may have accumulated in the edge drain and provided more water to the left side of the road. The third possible factor was better access to surface infiltration. A surface drainage ditch was located on the left side of the road, but not on the right, which drained to an adjacent field. Therefore, surface infiltration was more likely to be available on the left side. These factors probably contributed to more heave on the left side of the road.

10.3.1 Comparison of Heave Between Sections

Comparisons were made between the test sections to determine the effect on heave of percent tire chips, tire chip layer thickness, and depth to top of tire chip layer. Sections 1, 2, and 3 had the same layer thickness and depth to the top of the tire chip layer but different percentages of tire chips. Comparison of the average heave in Sections 1, 2, and 3 gives an approximate relationship between frost heave and percent tire chips as shown in Figure 10.9. The average heave in Section 1 and the Control were essentially the same, 38 mm (1.5 in.) and 39 mm (1.5 in.), respectively. This indicates that there is essentially no benefit in using 33% tire chips/67% gravel to reduce heave.

Sections 3 and 5 contained tire chips, but at different elevations. Section 3 was 610 mm (24 in.) from the surface, while Section 5 was 457 mm (18 in.) from the surface. Although moving tire chips 152 mm (6 in.) closer to the surface reduced maximum frost penetration by 20 percent, the average frost heave was essentially the same since frost did not penetrate into the subgrade in either section. The subgrade in Sections 4 and 5 were at the same depth, but frost heave was 55 percent lower in Section 5, with 305 mm

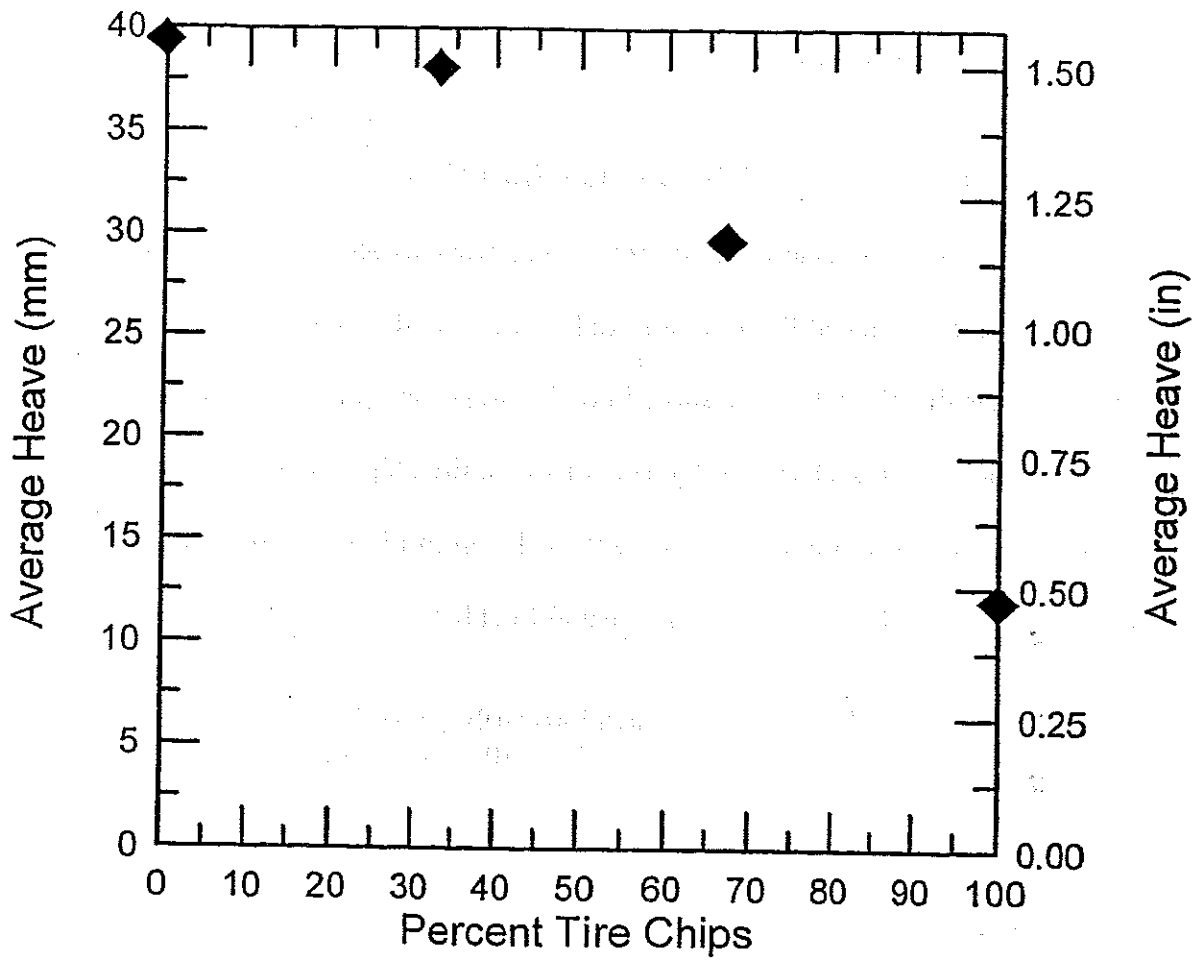


Figure 10.9 Average frost heave vs. percent tire chips, Sections 1, 2, and 3

(12 in.) of tire chips, than in Section 4, with 152 mm (6 in.) of tire chips. Therefore, increasing the thickness of tire chips seems to be more beneficial in reducing heave than reducing soil cover over tire chips.

10.3.2 Frost Penetration into Subgrade and Frost Heave

Frost-susceptible soils are necessary for frost heave to occur. The tire chips and tire chip/soil mixtures insulated the road and reduced the total depth of frost penetration, as well as the depth of frost penetration into the frost-susceptible subgrade soils. The relationship between frost heave in the sections with tire chips and tire chip/soil mixtures and frost penetration into the subgrade soils is shown in Figure 10.10. The relationship between frost penetration into the subgrade and frost heave was nearly linear.

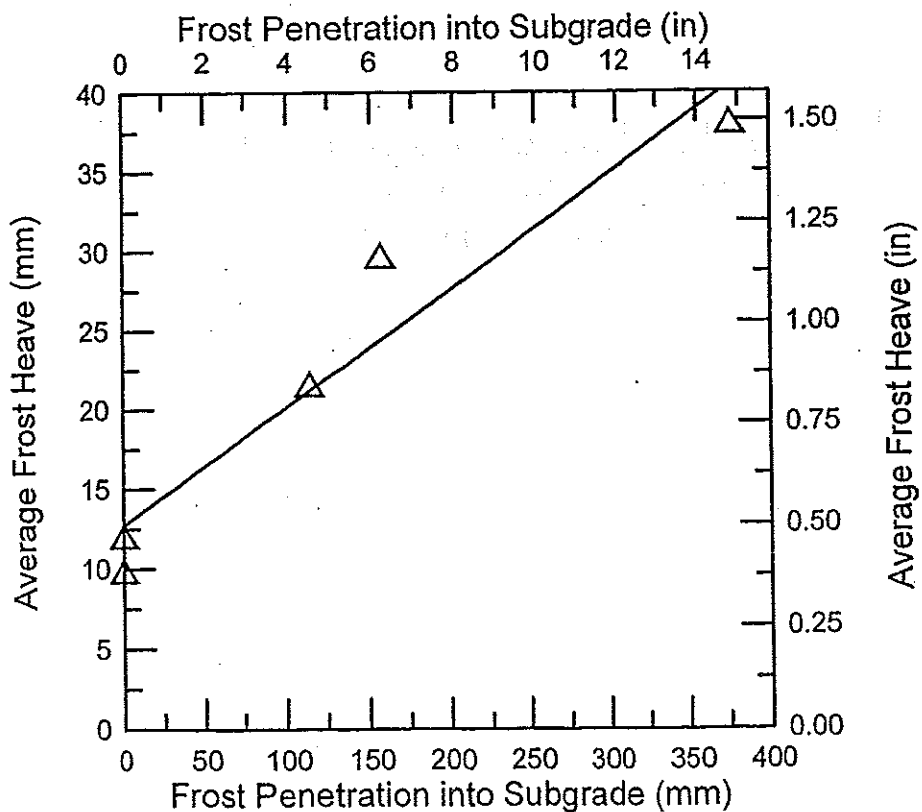


Figure 10.10 Average heave vs. frost penetration into subgrade

10.4 BACKCALCULATION OF THERMAL CONDUCTIVITY

The field thermal conductivity of tire chips and tire chip/soil mixtures was calculated using procedures given in Section 7.2. The first step was to calculate the volumetric heat capacity of tire chips and tire chip/soil mixtures. Then, the backcalculated thermal conductivities are presented.

10.4.1 Volumetric Heat Capacity of Tire Chips and Tire Chip/Soil Mixtures

The mass heat capacity of tire chips is 0.260 Cal/kg·°C (0.260 Btu/lb·°F), as determined by Equation 7.7. The mass heat capacity of tire chip/soil mixtures is then calculated as:

$$c_{m-mix} = \beta(c_{m-chip}) + (1-\beta)(c_{m-soil}) \quad (10.1)$$

where: $c_{m-soil} = 0.20$ Cal/kg·°C (0.20 Btu/lb·°F) (Jumikis, 1977)

β = percent tire chips by mass = 18.7% (33% volume) or 48.7% (67% volume)

The volumetric heat capacity of moist tire chips or tire chip/soil mixtures (c_{v-mix}) for use in calculation of frost penetration is generally taken as the average of the thawed and frozen values (Aldrich, 1956), which can be calculated as:

$$c_{v-mix} = [\rho_{d-mix} \cdot (c_{m-mix} + c_{mw} \cdot w/100) + \rho_{d-mix} \cdot (c_{m-mix} + c_{mi} \cdot w/100)]/2 \quad (10.2)$$

where: ρ_{d-mix} = dry density of tire chips or mixture in kg/m³ (lb/ft³)

c_{m-mix} = mass heat capacity of tire chips or mixture in Cal/kg·°C (Btu/lb·°F)

c_{mw} = mass heat capacity of water in Cal/kg·°C (Btu/lb·°F)

c_{mi} = mass heat capacity of ice in Cal/kg·°C (Btu/lb·°F)

w = water content in percent

The water content for tire chips was taken to be 4.0%, which is the approximate absorption capacity of tire chips (Humphrey, et al., 1992). Water contents for the other percentages of tire chips were linearly interpolated between a water content of 4.0% for tire chips to 5.0% for gravel based on the percentage by weight of each material. The dry densities were taken from the laboratory results in Table 6.1. The calculated values of c_v and c_m for tire chips and mixtures are listed in Table 10.3.

Table 10.3 Values of c_m and c_v for tire chips and tire chip/soil mixtures

Percent Chips - Volume	Percent Chips - Mass	Water Content	Density at Surchage of 12 kPa (250 psf)		Mass Heat Capacity c_m		Volumetric Heat Capacity c_v	
			Mg/m ³	pcf	Cal/kg·°C	Btu/lb·°F	Cal/m ³ ·°C	Btu/ft ³ ·°F
100	100	4.0	0.75	47	0.26	0.26	218	13.6
67	49	4.5	1.22	76	0.23	0.23	320	20.0
33	19	4.8	1.76	110	0.21	0.21	434	27.1

10.4.2 Backcalculation Methods

Two methods were used to backcalculate the thermal conductivity using temperature data collected at the University of Maine field trial. The calculation procedures are discussed in Section 7.2. In the first method, it was assumed that the heat flow had reached steady state conditions by February 14, 1997. This assumption is justified since the depth of frost penetration had stabilized by this date as shown in Figures 10.3 through 10.5. This means that the rate at which heat was removed from the freezing front was approximately equal to the rate at which heat was being supplied by the unfrozen subgrade. An assumed steady state relationship allows the thermal conductivity of the

tire chip or tire chip/soil mixtures to be calculated using Equation 7.3 if the thermal conductivity of the subgrade is estimated. Equation 7.3 is reproduced below:

$$K_2 = (i_3/i_2) \cdot K_3 \quad (7.3)$$

In this equation, layer 2 is taken to be the tire chip or tire chip/soil mixture layer and layer 3 is taken to be the subgrade. The value of K_3 was estimated from charts given by Kersten (1949). The subgrade soil is a silty clay, so the data for silt and clay soils was used. A typical water content of the subgrade soil at the site of the field trial was 18 percent (see Table 9.1) and a typical dry unit weight for the silty clay in this region (locally known as the Presumpscot Formation) is 1.52 Mg/m^3 (95 pcf). These properties were used with Kersten's (1949) charts to give a thermal conductivity of $1.19 \text{ W/m}\cdot^\circ\text{C}$ ($0.69 \text{ Btu/hr}\cdot\text{ft}\cdot^\circ\text{F}$) for the unfrozen condition and $1.47 \text{ W/m}\cdot^\circ\text{C}$ ($0.85 \text{ Btu/hr}\cdot\text{ft}\cdot^\circ\text{F}$) for the frozen condition. The unfrozen value was used for Sections 3 and 5 because the freezing front did not penetrate the subgrade, whereas the frozen value was used for the other sections because the freezing front did penetrate the subgrade. Temperature gradients for the tire chip and tire chip/soil mixture layers were listed in Table 10.2. For the subgrade soil, the temperature gradients were measured from the plots in Figure 10.7.

The steady state calculations yielded values of thermal conductivity for tire chip and tire chip/soil mixtures ($K_{tc/soil}$) as given in Table 10.4. The values of $K_{tc/soil}$ fall in a narrow range for Sections 3, 4, and 5 which have 100% tire chips. The average thermal conductivity of these three tire chip sections is $0.17 \text{ W/m}\cdot^\circ\text{C}$ ($0.10 \text{ Btu/hr}\cdot\text{ft}\cdot^\circ\text{F}$). The relationship between percent tire chips based on volume and K is shown in Figure 10.11. It shows a general trend of decreasing K with increasing percent tire chips.

Table 10.4 Estimated $K_{tc/soil}$

Section	Percent Tire Chips (Vol.)	Relation	Estimated K_3 (W/m·°C)	Estimated $K_{tc/soil}$	
				(W/m·°C)	(Btu/hr·ft·°F)
1	33	$0.46 \cdot K_3$	1.19	0.54	0.31
2	67	$0.18 \cdot K_3$	1.19	0.21	0.12
3	100	$0.11 \cdot K_3$	1.47	0.16	0.09
4	100	$0.14 \cdot K_3$	1.19	0.17	0.10
5*	100	$0.12 \cdot K_3$	1.47	0.18	0.10

* Using gradient as described in Section 4.4.2

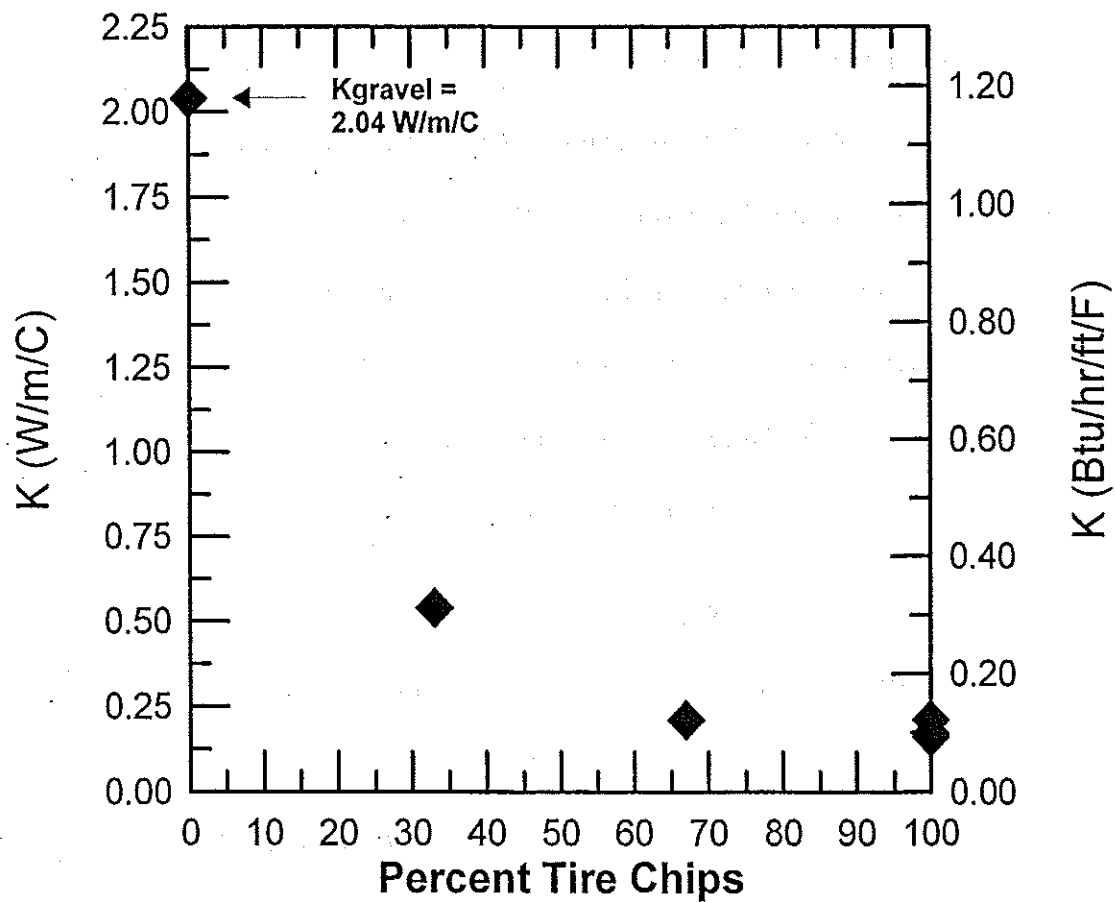


Figure 10.11 Thermal conductivity vs. percent tire chips

An independent method was used to evaluate the accuracy of the backcalculated values of thermal conductivity. This method was based on the modified Berggren equation, a non-steady state solution for the depth of frost penetration as described in Section 7.2. A thermal conductivity of 0.17 W/m·°C (0.10 Btu/hr-ft·°F) was used for tire chips in Sections 3, 4, and 5. The thermal conductivities of the two tire chip/soil mixtures listed in Table 10.4 were used in the modified Berggren equation. The following environmental factors were used in the equation:

- Air freezing index: 461 °C-days (829°F-days) measured for the winter of 1996-7
- Mean annual air temperature: 5.6 °C (42 °F) (from Linell, 1953)
- Duration of freezing period: 96 days, measured for the winter of 1996-97

The surface freezing index was taken to be equal to the air freezing index because the road was shaded for most of the winter so there would be no solar heating of the road surface. It was also on the edge of an open field, so conditions were very windy, and the high wind velocity would tend to equalize the air and pavement surface temperatures.

The input parameters used in the modified Berggren equation (Aldrich, 1956) are listed in Table 10.5. The layer "fill" refers to subbase material from previous construction which remained in thin layers over the silty clay subgrade after excavation. There was approximately 229 mm (9 in.) of this material in the Control Section, 178 mm (7 in.) in Section 5, 102 mm (4 in.) in Sections 3 and 4, and none in Sections 1 and 2. The calculation procedure was described in Section 7.2.

Table 10.5 Input parameters for modified Berggren equation

Layer Type	Dry Density Mg/m ³	Water Content %	c_v Cal/m ³ ·°C	K W/m·°C	Q_L Cal/m ³
Pavement	2.32	0	448	1.38	0
Gravel Base	2.08	5.0	494	2.04	8284
Tire Chips	0.75	4.0	173	0.17	2403
67% Tire Chips	1.22	4.2	282	0.22	4076
33% Tire Chips	1.76	4.5	411	0.55	6737
Fill	1.84	5.0	437	1.64	7343
Subgrade	1.60	18.0	509	1.73	21,796

Table 10.6 compares the measured and calculated depths of frost penetration. In Sections 3, 4, and 5, which had 100% tire chips, the calculated depth of frost penetration was between 9 and 14% greater than the measured value. This is reasonable agreement. In Section 1, the calculated frost penetration is 18% less than the measured value. This may be due to differences between the estimated and actual thermal properties of gravel or K of 33% tire chips/67% gravel could be higher than estimated using the steady state

Table 10.6 Comparison of measured and calculated frost penetration depth

Section	Measured (m)	Calculated (m) using $K_{tc/soil}$ from Table 10.4	% difference*
Control	1.38	1.22	-12%
1	1.29	1.06	-18%
2	1.07	0.97	-9%
3	0.91	1.01	+11%
4	0.88	0.96	+9%
5	0.73	0.83	+14%

* "-" indicates calculated depth less than measured depth; "+" indicates calculated depth greater than measured depth

method. In Section 2, there was better agreement, with the calculated depth of frost penetration being 9% less than the measured value.

Some of the differences in Table 10.6 could also be attributable to the mild winter with several freeze thaw cycles as shown in Figure 10.2. This could affect the actual frost depth, however, the modified Berggren equation does not take this into account.

10.4.3 Comparison of Laboratory and Field Thermal Conductivities

Laboratory thermal conductivities for moist samples were reported in Table 6.2. These results are plotted versus surcharge in Figure 10.12. This figure was used to obtain the laboratory thermal conductivity corresponding to the field surcharge. However, the laboratory tests were performed with temperature gradients ranging from 15°C/m (8.2°F/ft) for 33% tire chips/67% gravel to 32°C/m (17.6°F/ft) for 100% tire chips. As discussed in Section 6.4, the thermal conductivity of tire chips is a function of the temperature gradient, so it was necessary to correct the laboratory thermal conductivity to the field temperature gradient. The effect of temperature gradient was measured for air dried Pine State tire chips as shown in Figure 6.24. The laboratory test on moist tire chips was done with Palmer chips, however, it was necessary to assume that the relationship shown in Figure 6.24 could be used to correct the laboratory results to the field temperature gradient. This procedure was used for the comparisons in Sections 3, 4 and 5, which had 100% tire chips. However, Sections 1 and 2 had tire chip/gravel mixtures and a laboratory relationship between thermal conductivity and temperature gradient for mixtures was unavailable. Fortunately, the field gradient in Section 2 is almost the same

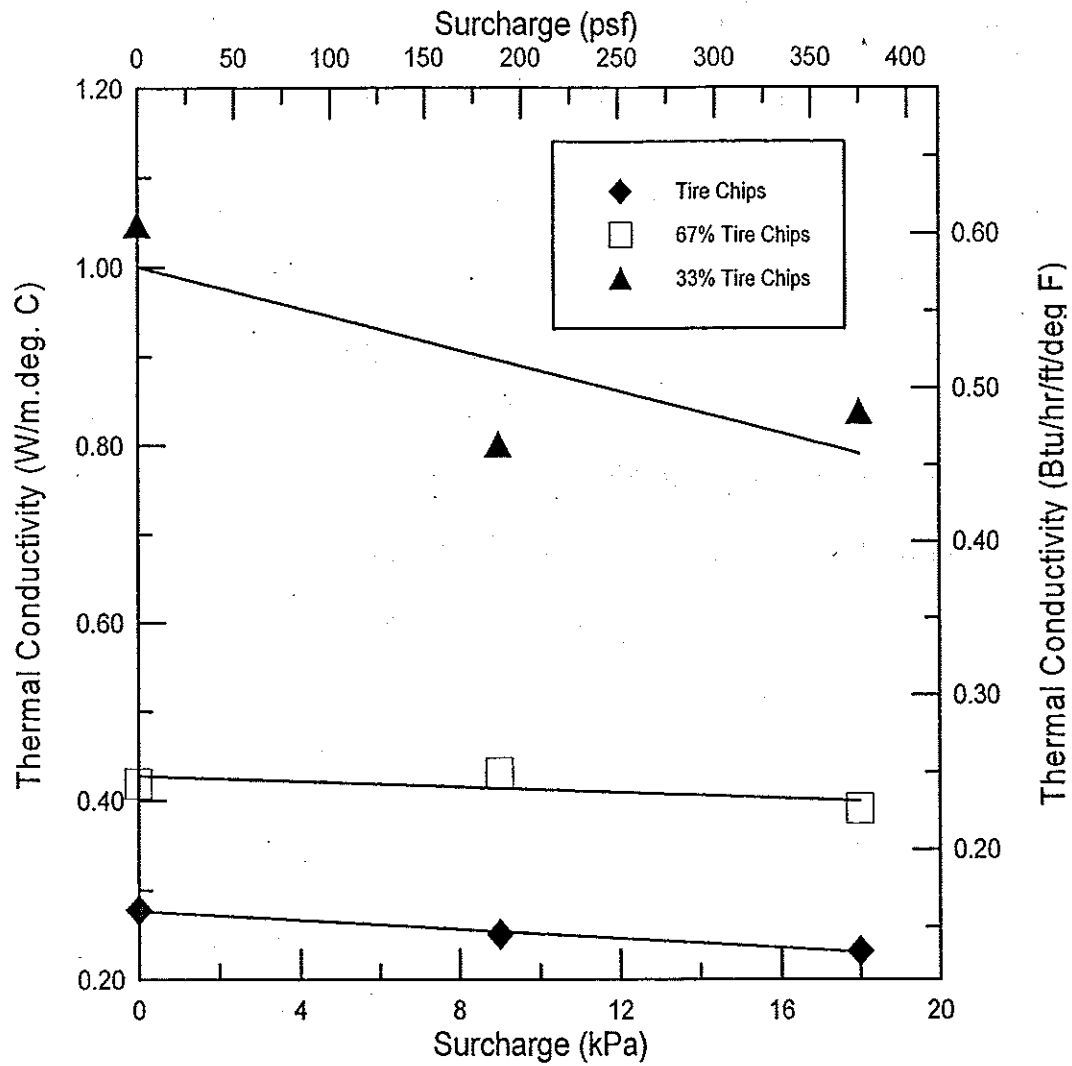


Figure 10.12 Laboratory thermal conductivity versus surcharge for moist tire chips and tire chip/soil mixtures

as the laboratory gradient, so no correction was necessary. In Section 1, it is likely that temperature gradient would have only a small effect for the 33% tire chips/67% gravel mixture since the smaller void ratio would limit circulation of air which is thought to be the main reason for the dependence of thermal conductivity on temperature gradient. Thus, no correction for temperature gradient was made in Section 1.

The results of the calculations are listed in Table 10.7. The thermal conductivities backcalculated in the field are consistently lower than those estimated from laboratory tests. In Section 3, 4, and 5, which have 100% tire chips, the difference ranges between 28% and 44%. There are several possible reasons for the difference. (1.) The thermal conductivity increases with increasing density and increasing water content. It is possible that the field density or water content was lower than in the moist laboratory tests. As discussed in Section 6.3.2.2, increasing the water content of Palmer chips from air dried to between 4.3% and 5.0%, increases the thermal conductivity by between 0.01 and 0.05 W/m·°C (0.006 and 0.03 Btu/hr-ft·°F). Figure 6.12 shows that a 0.05 Mg/m³ (3 pcf) difference in density can change the thermal conductivity by 0.02 W/m·°C (0.01 Btu/hr-ft·°F). (2.) As noted previously, the apparent thermal conductivity of tire chips is the combined effects of heat transfer by conduction and convection. It could be that tire

Table 10.7 Comparison of field and laboratory thermal conductivities

Section	Field surcharge (kPa)	Field gradient (°C/m)	Lab gradient (°C/m)	Lab K at field surcharge and lab gradient (W/m·°C)	K corrected to field gradient (W/m·°C)	K estimated from field measurements (W/m·°C)	Percent difference between lab and back-calculated K
1	13.4	8.9	15	0.84	0.84**	0.54	+56
2	13.4	19.8	20	0.41	0.41**	0.21	+95
3	13.4	29.0	32	0.24	0.23	0.16	+44
4	13.4	24.7	32	0.24	0.23	0.17	+35
5*	10.1	20.7	32	0.25	0.23	0.18	+28

* Using gradient determined as described in Section 10.4.2

** These values were not corrected as discussed in the text

chips placed in the field have a different particle arrangement than in the laboratory, leading to a different degree of heat transfer by either conduction or convection. (3.) Finally, it could be that some aspect of the laboratory test procedure or the assumptions made in backcalculating K from field measurements lead to the difference. In any event, it appears that the laboratory tests give a conservative estimate of the thermal conductivity of tire chips.

In Section 1, which was a mixture of 33% tire chips/67% gravel, the laboratory thermal conductivity was 56% greater than backcalculated from field measurements, and in Section 2, which was a mixture of 67% tire chips/33% gravel, the laboratory results were 95% greater than in the field. The differences could be due to the same reasons noted above for 100% tire chips. In addition, the field proportion of tire chips and gravel was very rough. It is possible that the field and laboratory proportions were different. Moreover, the mixture was subject to segregation in the field. This could also lead to different thermal properties.

10.4.4 Comparison with Richmond Field Trial

As discussed in Section 7.2, the best estimate of the thermal conductivity backcalculated from the Richmond Field Trial was $0.20 \text{ W/m}\cdot\text{°C}$ ($0.12 \text{ Btu/hr}\cdot\text{ft}\cdot\text{°F}$). This is very close to the thermal conductivities backcalculated for steady state conditions in the tire chip sections (Sections 3, 4, and 5) at the University of Maine Field Trial, which ranged from 0.16 to $0.18 \text{ W/m}\cdot\text{°C}$ (0.09 to $0.10 \text{ Btu/hr}\cdot\text{ft}\cdot\text{°F}$).

For the Richmond Field Trial, the depth of frost penetration predicted using the thermal conductivity backcalculated from that project (0.20 W/m·°C; 0.12 Btu/hr·ft·°F) ranged from 1% less to 15% greater than the actual depth of frost penetration, as summarized in Table 7.2. For the University of Maine Field Trial, the depth of frost penetration predicted using a backcalculated K of 0.17 W/m·°C (0.10 Btu/hr·ft·°F) ranged from 9% to 14% greater than the measured value. These are similar levels of agreement.

For the Richmond Field Trial, the laboratory thermal conductivity was 10% to 15% less than the field value as summarized in Table 7.3. In contrast, for the University of Maine Field Trial, the laboratory thermal conductivity was 28% to 44% greater than the field value. Thus, the laboratory and field thermal conductivities were in closer agreement for the Richmond project than for the University of Maine project.

10.5 SUMMARY

Six segments of road were monitored for temperature and heave for the winter of 1996-1997. The winter of 1996-1997 was warmer than average for the Orono, Maine area, recording 35% fewer freezing degree days than an average winter. The benefits of reducing frost depth with tire chips and tire chip/soil mixtures were seen in plots of frost penetration vs. time. Tire chips reduced the maximum depth of frost penetration by 34 to 47%. A mixture of 67% tire chips/33% gravel reduced frost penetration by 22%, while a mixture of 33% tire chips/67% gravel reduced frost penetration by only 7%. Overall, frost depth decreased with an increase in the percentage of tire chips, an increase in the thickness of tire chips, or a decrease in soil cover.

Temperature profiles showed that tire chips and tire chip/soil mixtures reduce heat flow up through the tire chip layers. The subgrade soil remained warmer in sections with tire chip and tire chip/soil mixtures, while the gravel above these insulating layers was colder than in the Control. Temperature gradients increased in the tire chip and tire chip/soil layers as the percentage of tire chips increased.

Frost heave was measured in the winter of 1996-1997. The outside wheel paths heaved more than the inside wheel paths in a given section, which is probably because the inside wheel paths were surrounded by tire chips or tire chip/soil mixtures, while the outside wheel paths were bordered by the higher thermal conductivity natural ground and had access to water from surface infiltration. The left outside wheel path experienced more heave than the right outside wheel paths in each section. This could be due to less exposure to sunlight, an edge drain whose outlet was frozen, or better access to water from surface infiltration. Heave was 55 percent smaller in Section 5 with 305 mm (12 in.) of tire chips compared to Section 4 with 152 mm (6 in.) of tire chips. It was also found that heave was roughly proportional to the depth of frost penetration into the subgrade. Frost heave was the same in the Control Section and Section 1, so there would be essentially no benefit in using 33% tire chips/67% gravel to reduce heave.

Two methods were used to calculate thermal conductivity. The first method was a steady state heat flow equation that was used to calculate the thermal conductivity of tire chip and tire chip/soil layers relative to the subgrade. The subgrade thermal conductivity was estimated from charts by Kersten (1949) and used as input for the second method which used the modified Berggren equation. Reasonable agreement was obtained between the measured and calculated frost depth which means that the backcalculated K

is reasonably accurate. The backcalculated field K was found to increase as the percentage of soil in the mixtures increased. The value of K backcalculated from the field trial was 0.16 W/m·°C (0.09 Btu/hr·ft·°F) for tire chips in Section 3 with 305 mm (12 in.) of tire chips and 483 mm (19 in.) of cover. The K of Section 4, with 152 mm (6 in.) of tire chips and 483 mm (19 in.) of cover was 0.17 W/m·°C (0.10 Btu/hr·ft·°F), and the K of Section 5, with 305 mm (12 in.) of tire chips and 330 mm (13 in.) of cover was 0.18 W/m·°C (0.10 Btu/hr·ft·°F). These values are relatively consistent. Moreover, they were similar to values backcalculated from the Richmond Field Trial. The K values of mixtures increased with a decrease in percent tire chips. Section 2, with 305 mm (12 in.) of 67% tire chips/33% gravel and 483 mm (19 in.) of cover, had a K of 0.21 W/m·°C (0.12 Btu/hr·ft·°F), and Section 1, with 305 mm (12 in.) of 33% tire chips/67% gravel and 483 mm (19 in.) of cover, had a K of 0.54 W/m·°C (0.31 Btu/hr·ft·°F).

Laboratory and field backcalculated thermal conductivities were compared. The laboratory values were higher than those calculated in the field. The range of differences was from 28% in Section 5 to 95% in Section 2. The differences could be due to differences between field and lab moisture contents or density, different particle arrangement between the lab and field which altered heat transfer by conduction or convection, and/or some aspect of the laboratory test procedure or the assumptions made in backcalculating K from field measurements. There is also the possibility that the many freeze-thaw cycles throughout the winter added uncertainty to backcalculation of thermal

conductivity. For design purposes, use of the laboratory K would give conservative estimates of frost penetration.

11. PAVEMENT PERFORMANCE

11.1 INTRODUCTION

Pavement deflections were measured in the field using two methods: Modified Benkelman Beam (MBB) and Heavy Weight Deflectometer (HWD) tests. The purpose of these measurements was to evaluate the effects of soil cover and percentage tire chips on pavement performance.

This chapter first discusses the test methodology for both deflection tests. The next section presents the results of the Modified Benkelman Beam tests. Data from these tests are compared to deflections predicted by KENLAYER, a computer program based on the solution for an elastic multilayer system under a circular loaded area. The solutions can be superimposed for to account for multiple wheels and applied iteratively for nonlinear layers (Huang, 1993). The next section presents the results of the HWD tests and back-calculation of Young's Modulus with the program MODCOMP4. The chapter concludes with a summary.

11.2 MEASUREMENT METHODS

11.2.1 Modified Benkelman Beam

Modifications to a standard Benkelman Beam were made by Nickels (1995) for a previous project using a tire chip layer beneath a paved road. This modified Benkelman Beam (MBB) measures the shape of the pavement deflection basin with dial gages

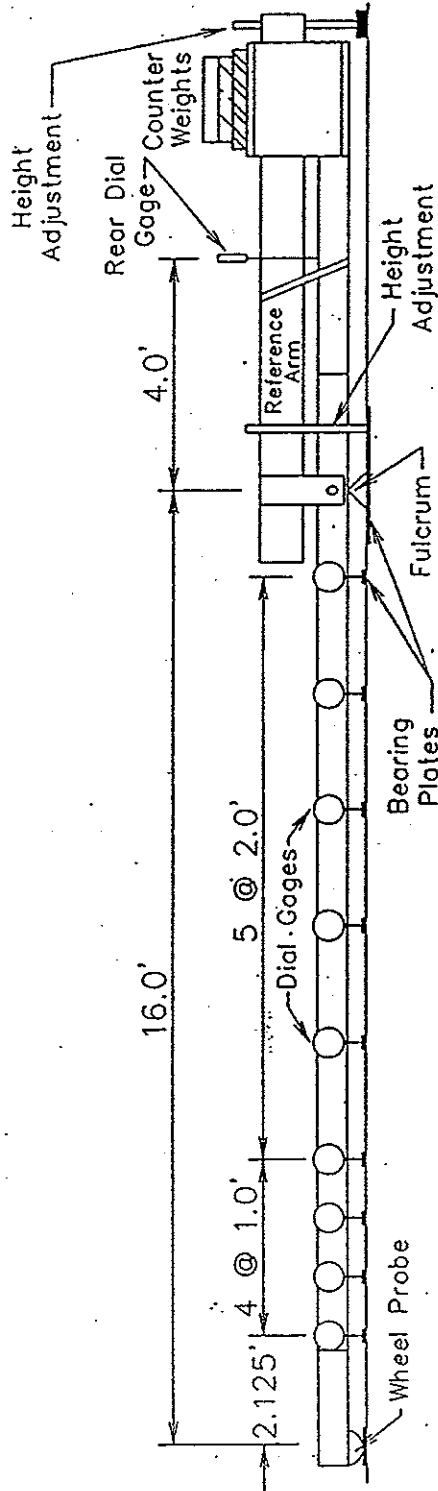
mounted on the arm of the beam. The beam length is 4.88 m (16 ft) in front of the fulcrum, with dial gages mounted as shown in Figure 11.1.

Each test section contained six locations for MBB measurements. The same locations were used for both MBB tests and HWD tests and are shown in Figure 11.2. To perform a test, one pair of dual wheels of a single rear axle dump truck that had been loaded to produce a rear axle load of 8165 kg (18,000 lb) was positioned directly over a test location. The MBB probe was inserted between the dual tires as shown in Figures 11.3 and 11.4. Next, the dial gages were zeroed. The truck then drove away, and the pavement was allowed to rebound for about one minute. More time was needed for sections with less soil cover over the tire chips. The dial gages were then read and recorded.

The maximum deflection occurs directly beneath the dual wheels. The deflection at this point, which is called the centerline deflection, is calculated as four times the deflection of the rear dial gage. To define the shape of the deflection basin, dial gage measurements were made at intermediate points on the beam. The measurements were corrected for beam rebound yielding the shape of the deflection basin.

11.2.2 Heavy Weight Deflectometer (HWD)

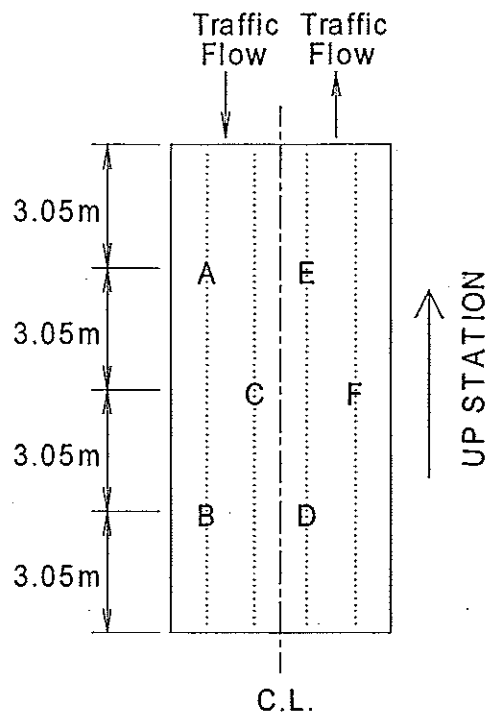
A Heavy Weight Deflectometer (HWD) is a nondestructive test method that was used to estimate Young's Modulus (E) for pavement layers. The HWD is a variation of the Falling Weight Deflectometer (FWD) and simulates higher vehicle loads than the FWD. The impulse force is controlled by varying the weight dropped or the height from



Note: Not to scale

(1.0 ft. = 0.305 m)

Figure 11.1 Modified Benkelman Beam used for pavement deflection measurements (after Nickels, 1995)



Measurement Locations for Sections 2, 4, & Control

- A - 1.83 m left of CL
- B and C - 0.61 m left of CL
- D - 0.61 m right of CL
- E and F - 1.83 m right of CL

Measurement Locations for Sections 1, 3, & 5

- A and B - 1.83 m left of CL
- C - 0.61 m left of CL
- D and E - 0.61 m right of CL
- F - 1.83 m right of CL

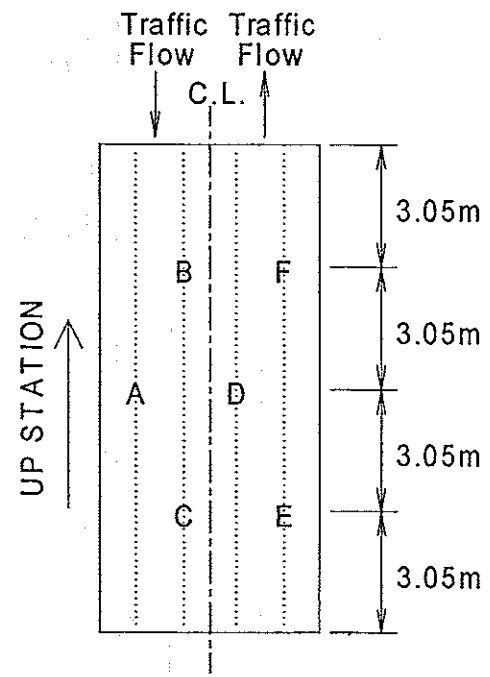


Figure 11.2 Plan view of test locations for Modified Benkelman Beam and HWD tests

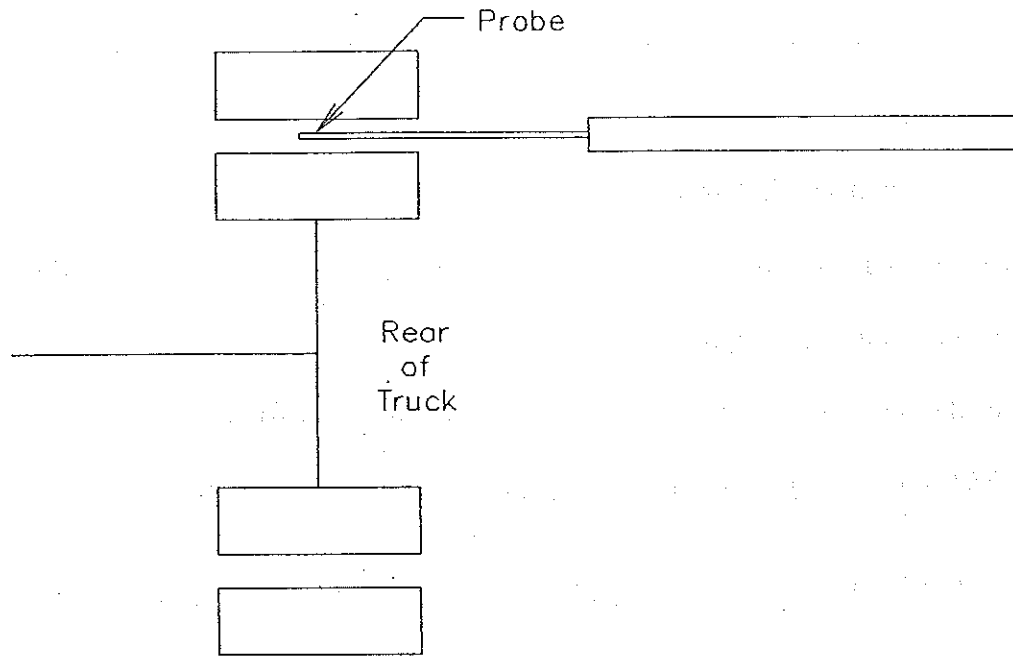


Figure 11.3 Plan location of MBB probe between dual truck tires (after Nickels, 1995)

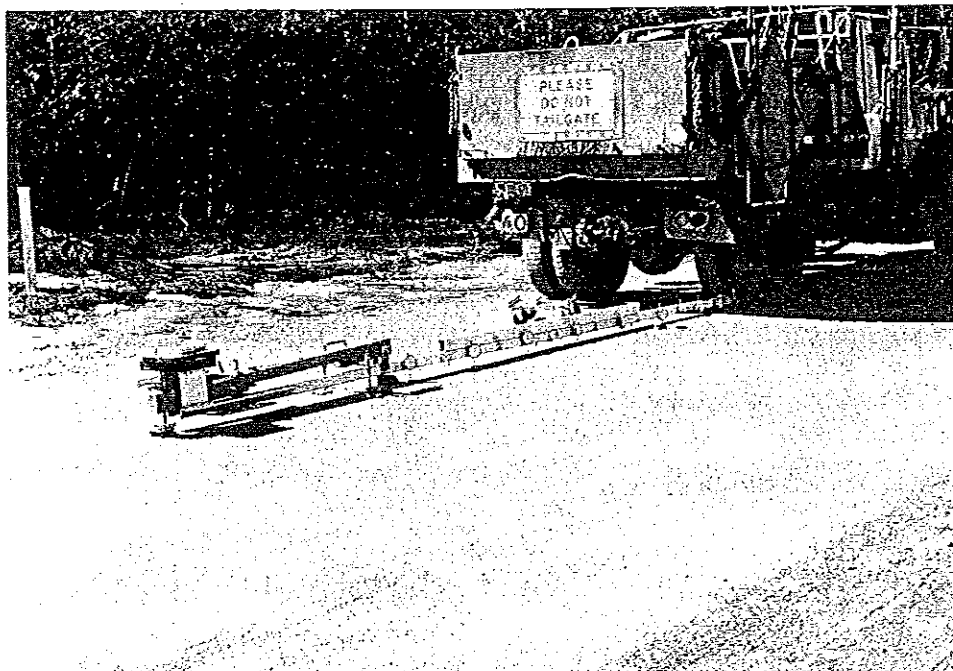


Figure 11.4 Photograph of MBB and dump truck on the test road

which it is dropped (Cosentino and Briaud, 1989). Figure 11.5 shows the HWD apparatus, which is carried on a trailer pulled by a van. Weights are dropped on a circular plate that is 305 mm (12 in.) in diameter and rests on the pavement. The trailer is outfitted with sensors that record the amount of downward vertical movement of the pavement as the weight strikes the pavement. Approximate sensor spacings relative to the center of the plate were: 0.00 m (at the center of the plate), 0.30 m (12.0 in.), 0.61 m (24.0 in.), 0.91 m (36.0 in.), 1.22 m (48.0 in.), 1.52 m (60.0 in.), and 1.83 m (72.0 in.).

At each test location, the HWD drops four different load levels four times each. The four load levels varied and were to some degree dependent on the pavement materials. Average load levels were approximately 2270 kg (5000 lb), 3630 kg (8000 lb), 4760 kg (10,500 lb), and 6350 to 6800 kg (14,000 to 15,000 lb). Total histories of pavement deflection with time can be recorded, but only the maximum deflections are used for modulus backcalculation. For each location and load level, the deflection basins of the four drops were averaged. This average was taken to represent the behavior at a particular drop location. For subsequent modulus backcalculation, the response at each of the six locations in each section were averaged. Thus, the average deflections at each of four load levels in each section were used in MODCOMP4 to backcalculate the modulus of the layers in the pavement system.

HWD tests were performed on November 19, 1996 and April 15, 1997. These tests were performed by the U.S. Army Cold Regions Research and Engineering Laboratory. An additional test with a Falling Weight Deflectometer (FWD) owned by the Maine Department of Transportation was performed on August 22, 1997. The sensor spacings

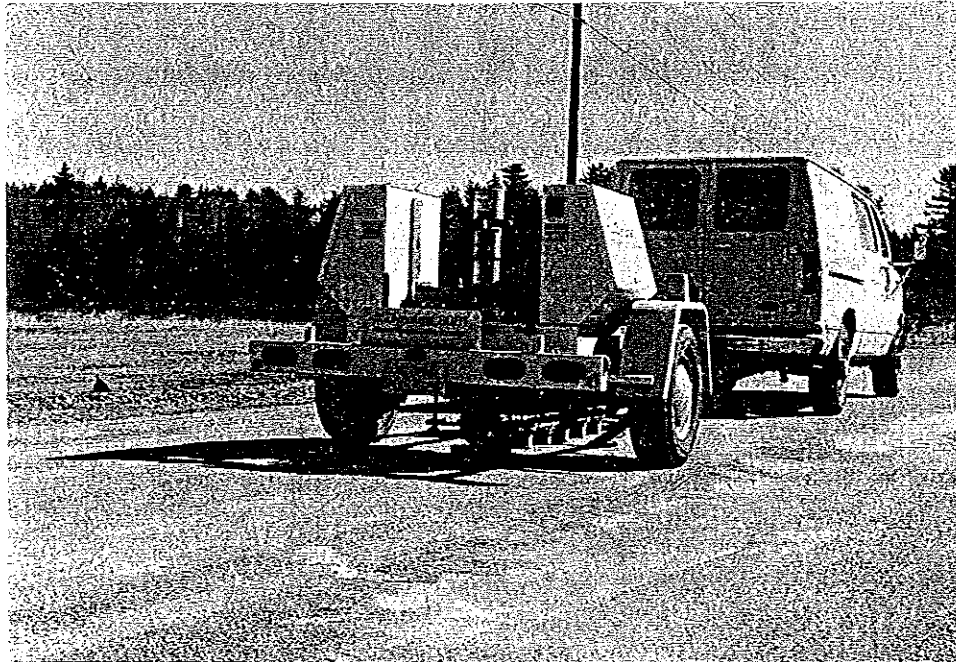


Figure 11.5 Photograph of Heavy Weight Deflectometer (HWD)

for these tests were 0 mm (0 in.), 203 mm (8 in.), 305 mm (12 in.), 457 mm (18 in.), 610 mm (24 in.), 914 mm (36 in.), and 1524 mm (60 in.) and the average load levels were about 2720 kg (6000 lb), 4080 kg (9000 lb), 5220 kg (11,500 lb), and 6580 kg (14,500 lb).

11.3 PAVEMENT DEFLECTIONS MEASURED WITH BENKELMAN BEAM

11.3.1 Results

Deflection measurements were taken on April 14 and 15, 1997, and August 18 and 19, 1997. Deflection basins were measured and plotted. A horizontal distance of 0 m corresponds to the centerline deflection. Deflections were plotted relative to the centerline deflection to facilitate direct comparison of the shape of the deflection basins from different trials.

Deflection basins for the April tests are shown in Figures 11.6 through 11.11. Sections 1, 2, 3, and Control have smaller scatter than Sections 4 and 5. The averages of centerline deflections for the April test are shown in Table 11.1.

Averages of the six deflections basins measured for each section are plotted in Figure 11.12. The average deflection basins of Sections 1 through 4 show an irregular displacement pattern near 1.25 m (4.1 ft). This is most likely due to a malfunctioning dial gage at this location. Figure 11.12 shows that the deflection data is grouped into three general magnitudes of deflection. There is little difference between Section 1 and the Control, which have average centerline deflections of 1.27 mm (0.05 in.) and 0.73 mm (0.029 in.), respectively. Both the shape and magnitude of these two deflection

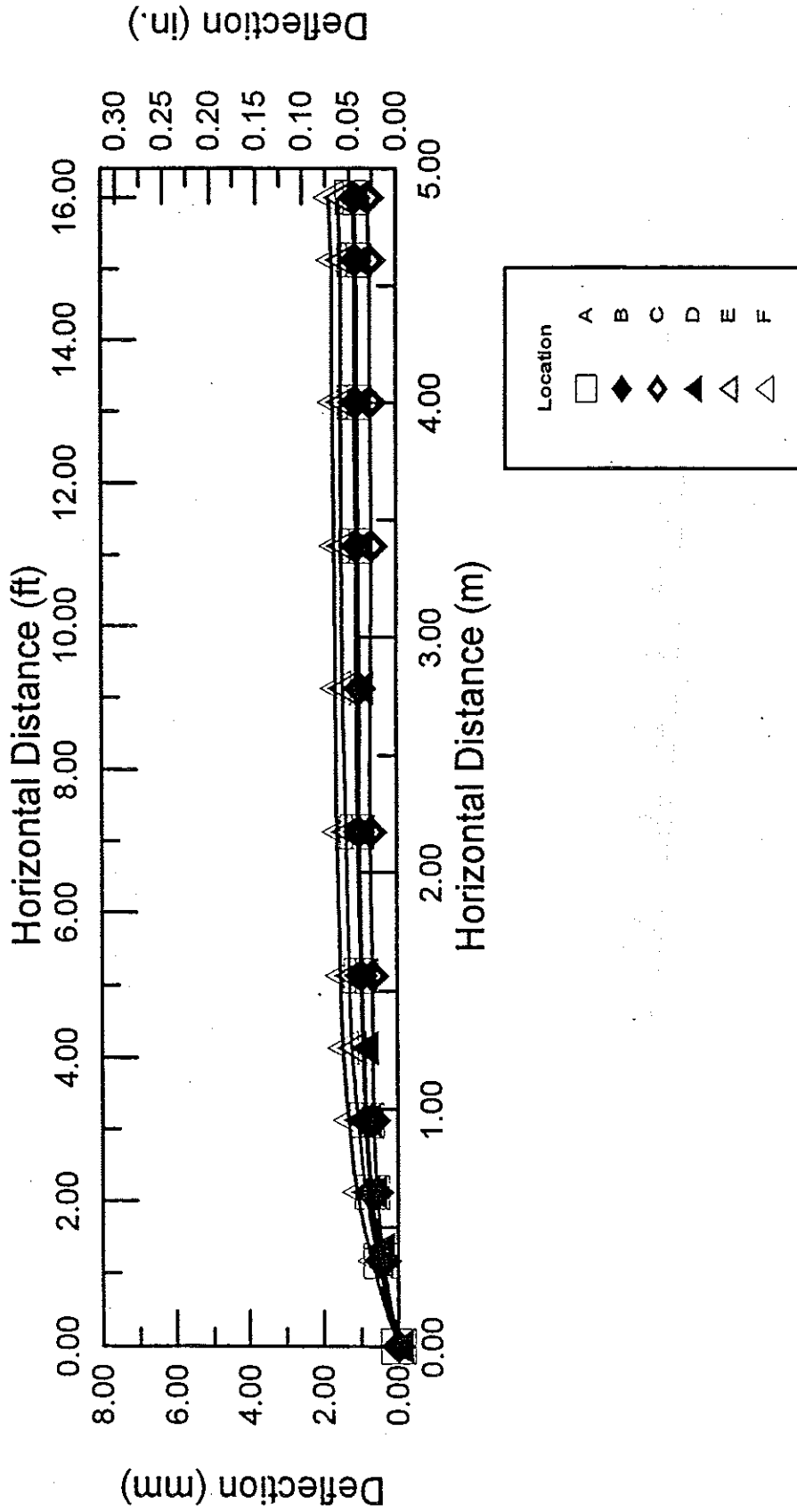


Figure 11.6 April pavement deflection basins for Section 1 with 483 mm (19 in.) of soil cover and 305 mm (12 in.) of 33% tire chip/67% soil

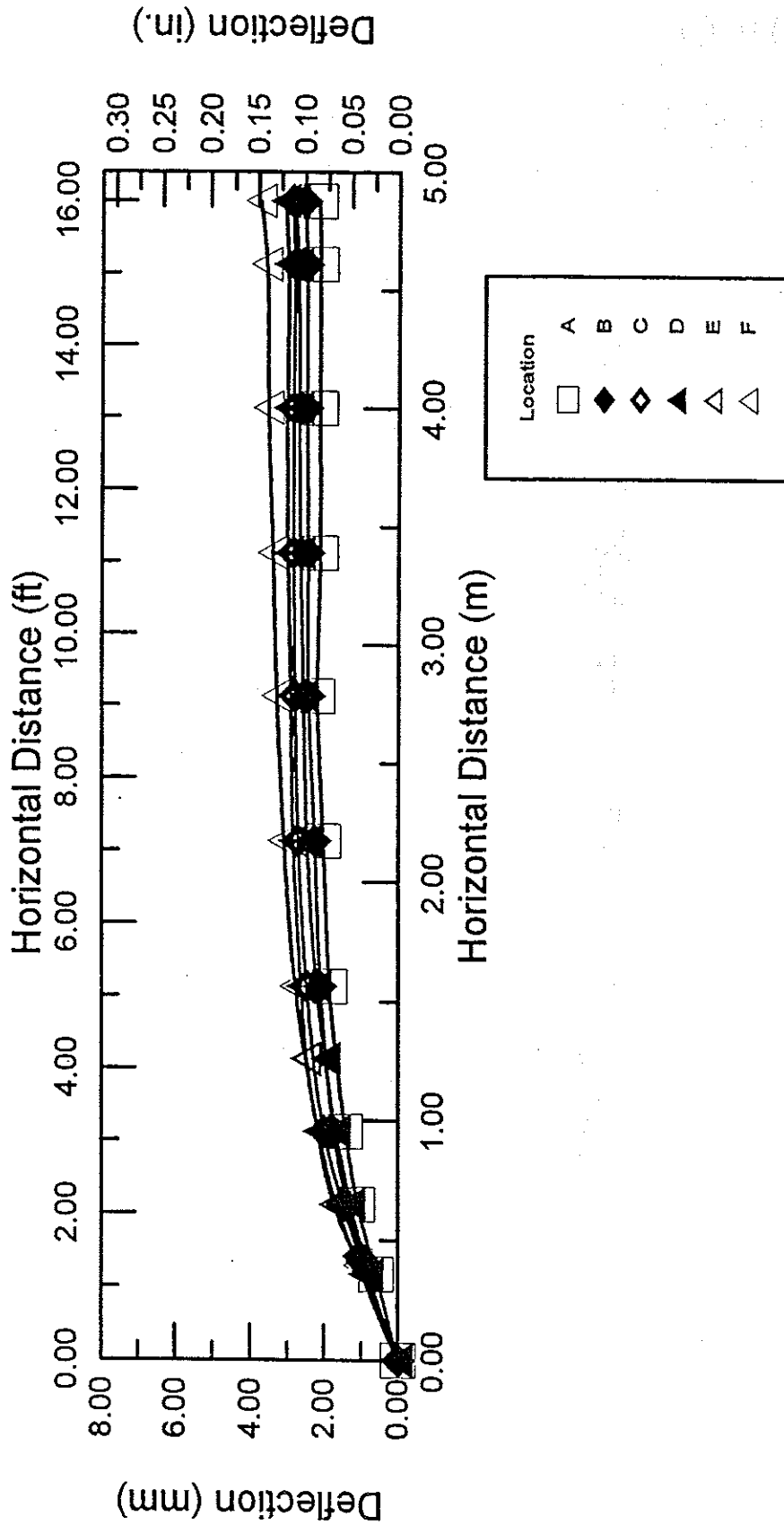


Figure 11.7 April pavement deflection basins for Section 2 with 483 mm (19 in.) of soil cover and 305 mm (12 in.) of 67% tire chip/33% soil

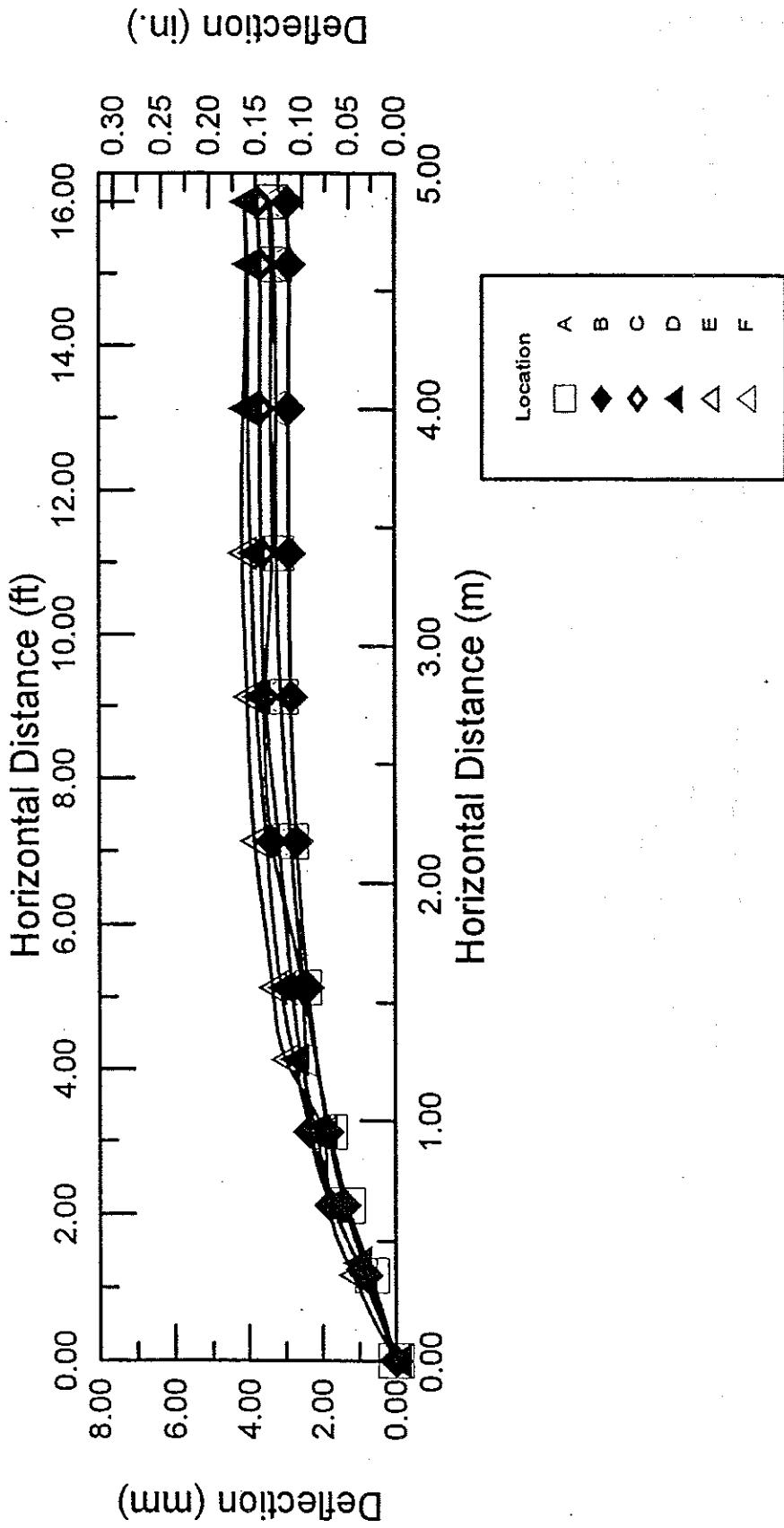


Figure 11.8 April pavement deflection basins for Section 3 with 483 mm (19 in.) of soil cover and 305 mm (12 in.) of tire chips

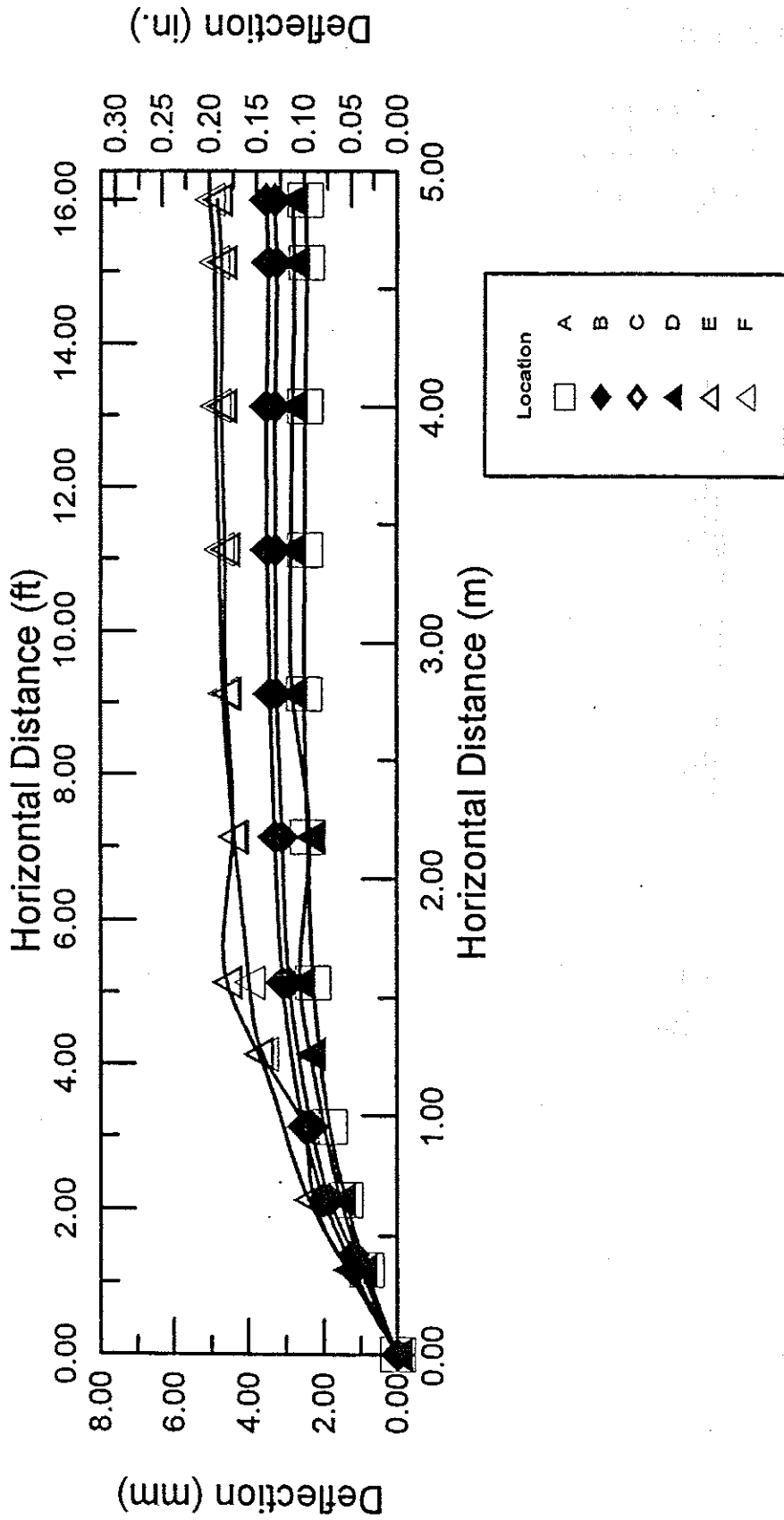


Figure 11.9 April pavement deflection basins for Section 4 with 483 mm (19 in.) of soil cover and 152 mm (6 in.) of tire chips

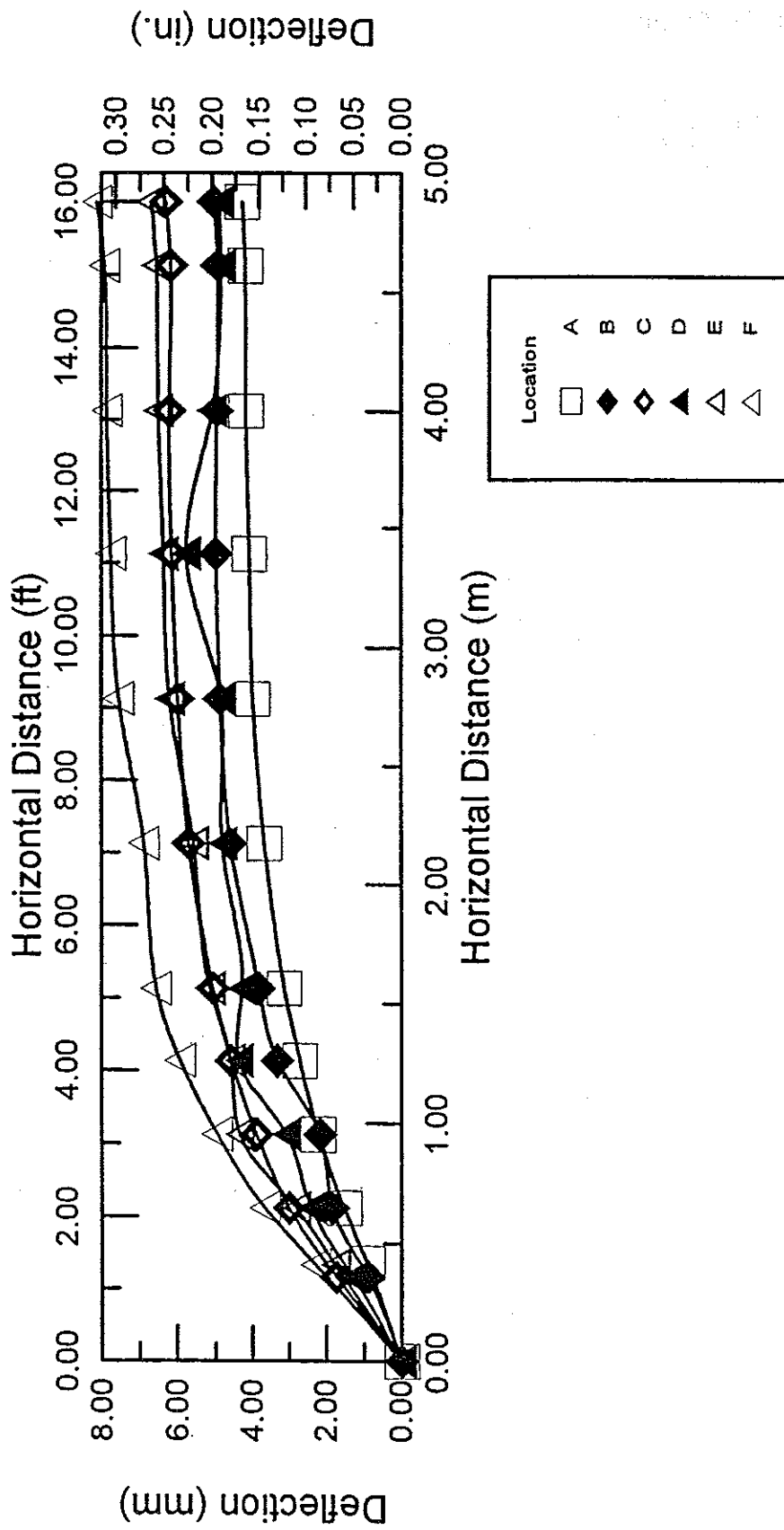


Figure 11.10 April pavement deflection basins for Section 5 with 330 mm (13 in.) of soil cover and 305 mm (12 in.) of tire chips

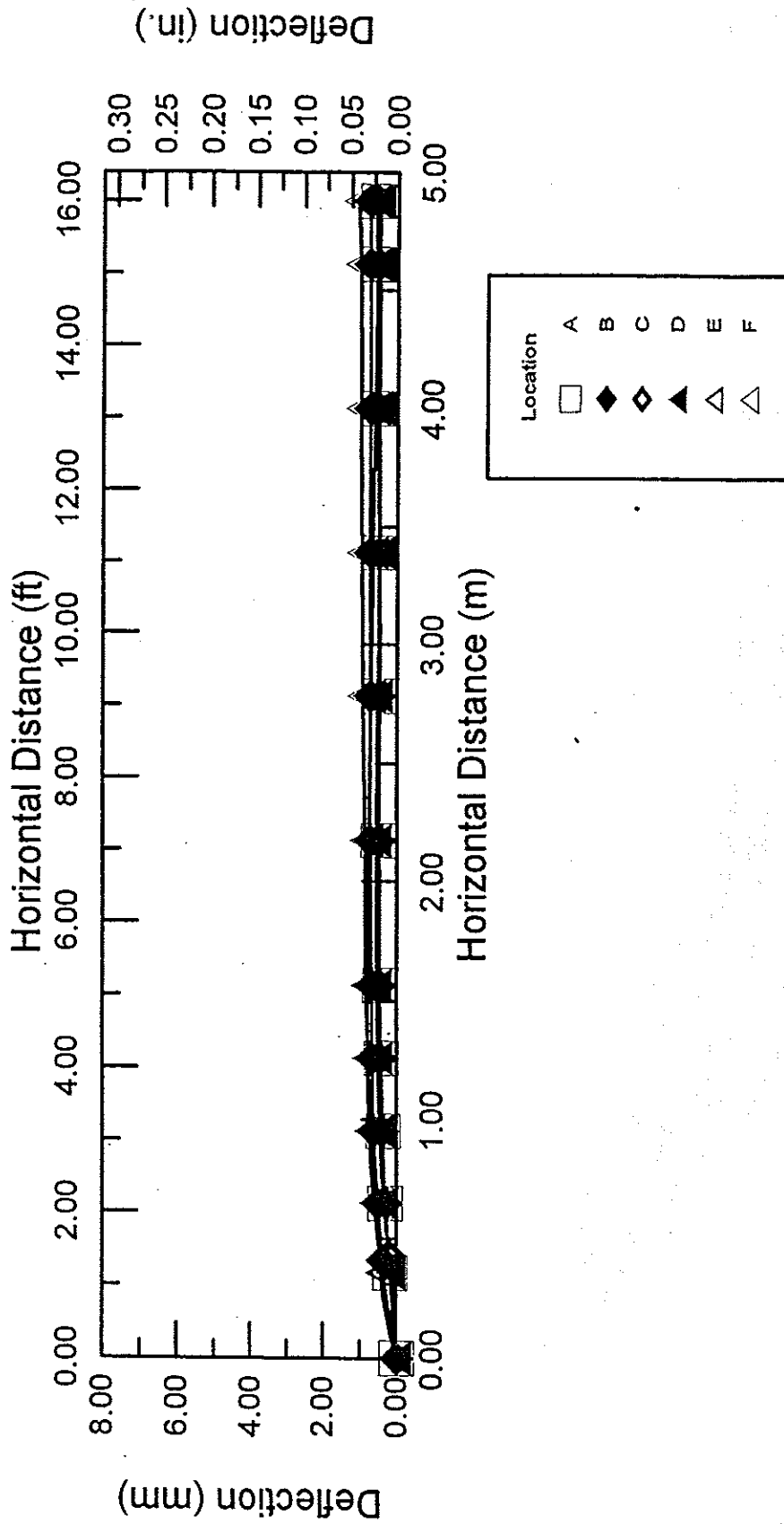


Figure 11.11 April pavement deflection basins for the Control Section with 635-mm (25-in.) thick aggregate subbase course

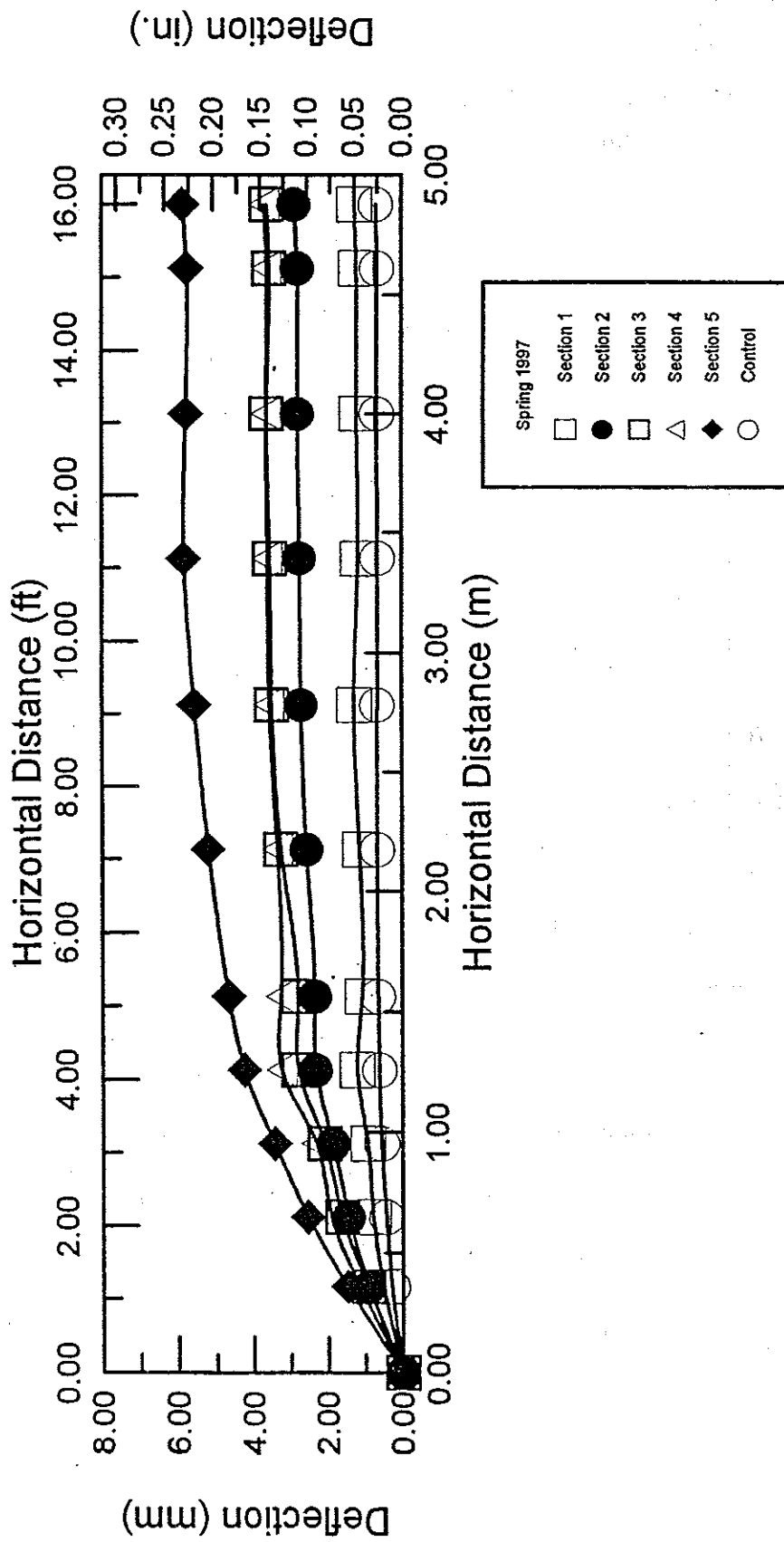


Figure 11.12 Average April pavement deflection basins for all sections

Table 11.1 Centerline pavement deflections, April 1997.

Section 1 305 mm 33% Tire Chips		Section 2 305 mm 67% Tire Chips		Section 3 305 mm Tire Chips		Section 4 152 mm Tire Chips		Section 5 305 mm Tire Chips		Control No Tire Chips	
Cover thickness = 483 mm								= 330 mm			
Loc.	C/L Def. mm	Loc.	C/L Def. mm	Loc.	C/L Def. mm	Loc.	C/L Def. mm	Loc.	C/L Def. mm	Loc.	C/L Def. Mm
A	1.17	A	2.20	A	3.37	A	2.52	A	4.27	A	0.57
B	1.13	B	2.57	B	2.95	B	3.33	B	5.03	B	0.78
C	0.77	C	2.90	C	3.76	C	3.56	C	6.30	C	0.56
D	1.15	D	2.85	D	4.13	D	2.88	D	5.77	D	0.57
E	1.57	E	3.10	E	4.18	E	4.88	E	6.71	E	0.81
F	1.83	F	3.76	F	3.53	F	5.07	F	8.13	F	1.09
Max.	1.83	Max.	3.76	Max.	4.18	Max.	5.07	Max.	8.13	Max.	1.09
Min.	0.77	Min.	2.20	Min.	2.95	Min.	2.52	Min.	4.27	Min.	0.56
Avg.	1.27	Avg.	2.89	Avg.	3.65	Avg.	3.71	Avg.	6.03	Avg.	0.73

basins are similar. Sections 2, 3, and 4 are clustered in the middle of Figure 11.12, with centerline deflections between 2.89 mm (0.114 in.) and 3.71 mm (0.146 in.). Section 5 shows the most deflection, with an average centerline deflection of 6.03 mm (0.237 in.). The radius of the deflection basins, as delineated by where the basin appears to flatten out, is different for each group. The radius of the deflection basins for Sections 1 and the Control are approximately 1.5 m (4.9 ft), Sections 2, 3, and 4 are approximately 2.5 m (8.2 ft), and Section 5 is approximately 3.5 m (11.5 ft).

The average temperatures in the gravel base course in each section are listed in Table 11.2 for the two Benkelman Beam test periods. Also listed are the number of days prior to the April test in which frost was no longer detectable in the test sections. The average temperatures were taken to be the average of the temperatures in the gravel base, with the exception of the Control, where the average in the upper 483-mm (19-in.) of the gravel base was used. The latter was equivalent the maximum thickness of gravel cover in the other test sections. The general trend was that the temperature in the gravel base decreased as the insulating value of the underlying material decreased. The temperatures listed for the April test and the time elapsed since frost was undetectable in each section clearly shows that the gravel base was in a thawed condition.

Figures 11.13 through 11.18 show results of the August tests. These show the same general trend of scatter as discussed above with the April measurements. The scatter was generally greater in April than in August, with the exception of Section 1 (Figure 11.13), which has about the same degree of scatter in both months, and Section 3 (Figure 11.15), where the August scatter was greater than the April scatter. The average deflection basin

Table 11.2 Gravel base temperature on Benkelman Beam test dates

Section	Gravel Base Temperature °C		April 14-15 Days Since No Frost
	April 14-15	August 18-19	
1	3.4	27.3	17
2	5.1	28.0	17
3	6.2	27.9	18
4	5.2	27.4	16
5	6.5	29.3	17
Control	3.9	27.9	18

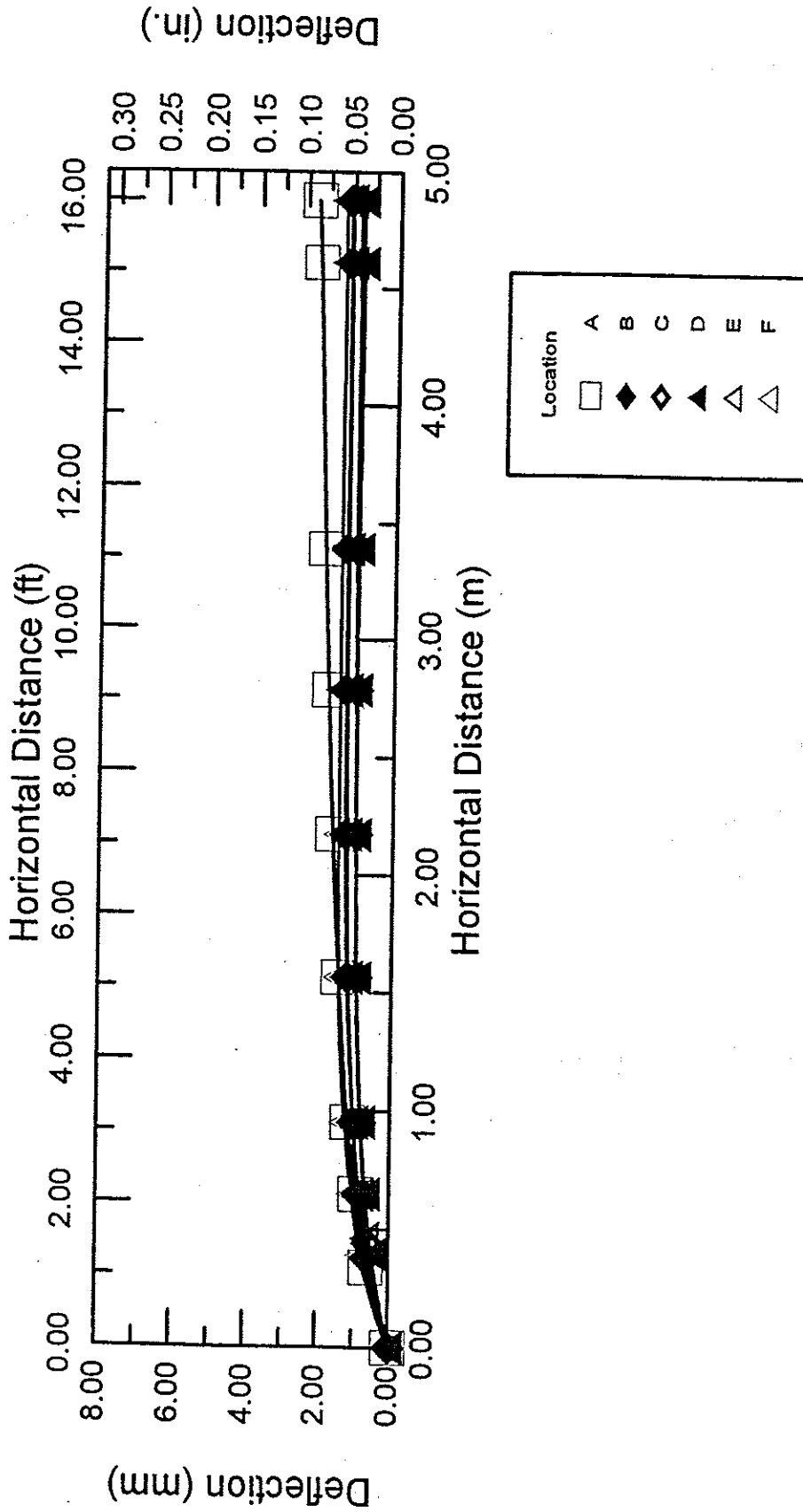


Figure 11.13 August pavement deflection basins for Section 1 with 483 mm (19 in.) of soil cover and 305 mm (12 in.) of 33% tire chip/67% soil

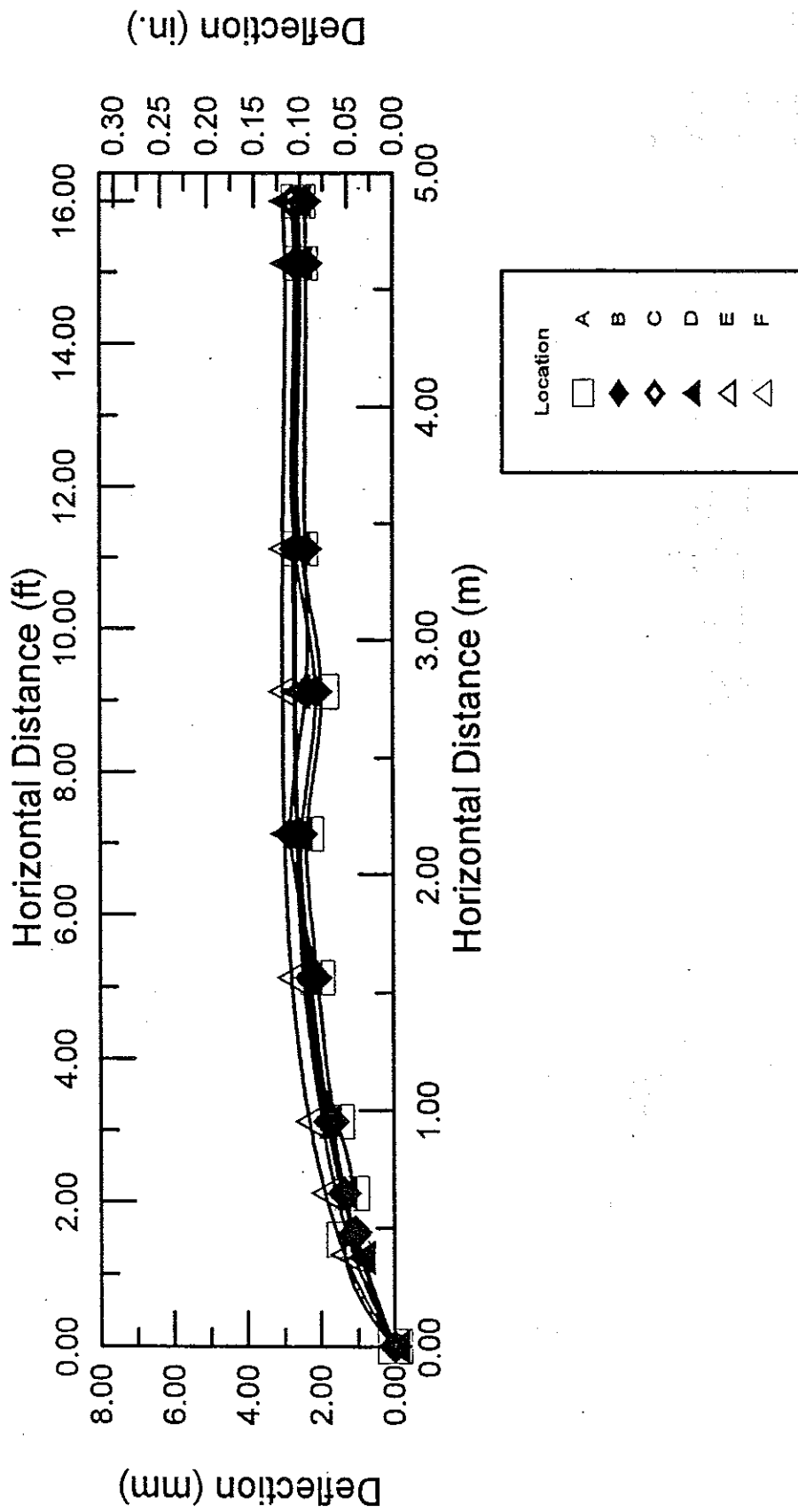


Figure 11.14 August pavement deflection basins for Section 2 with 483 mm (19 in.) of soil cover and 305 mm (12 in.) of 67% tire chip/33% soil

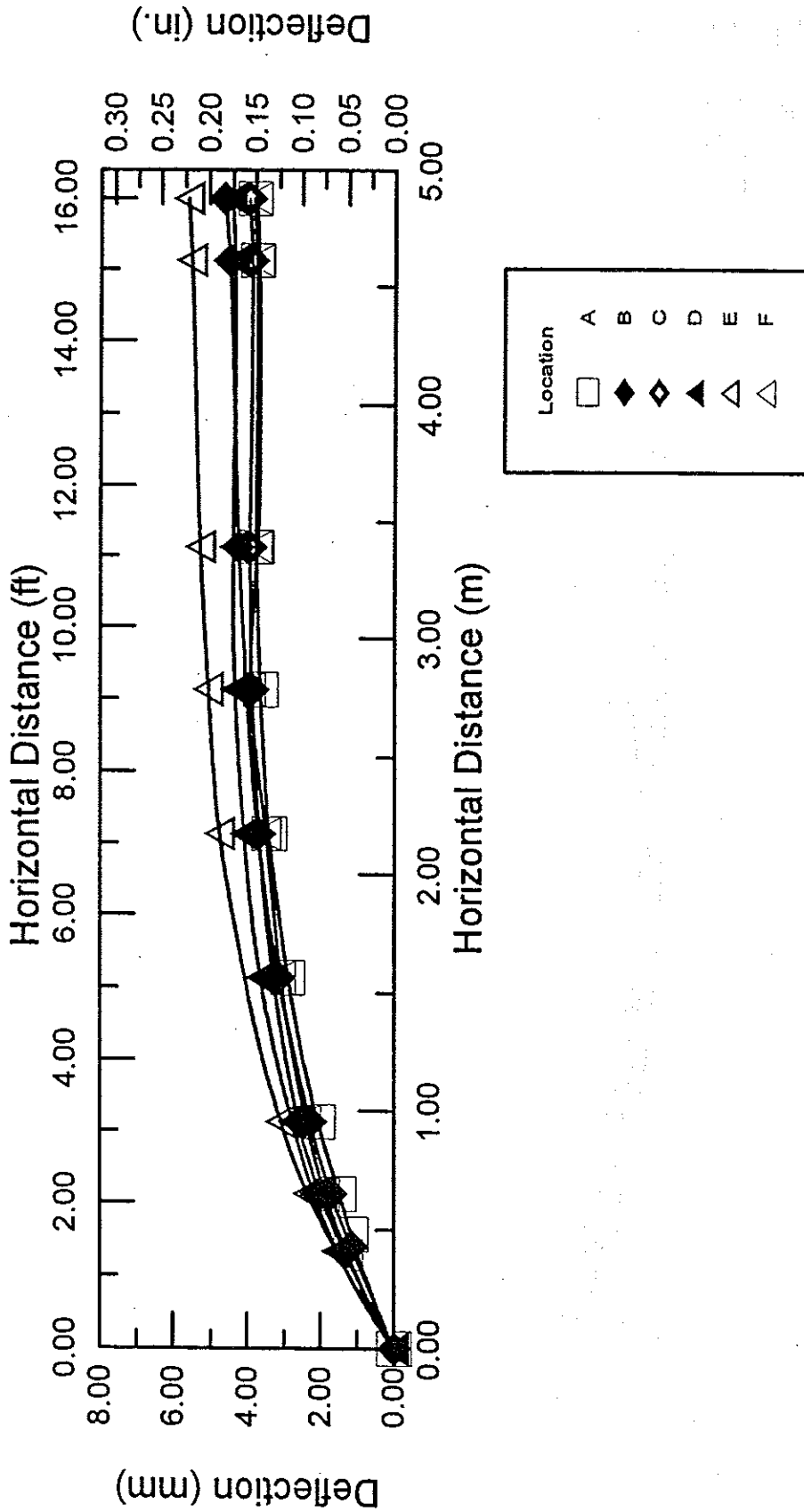


Figure 11.15 August pavement deflection basins for Section 3 with 483 mm (19 in.) of soil cover and 305 mm (12 in.) of fire chips

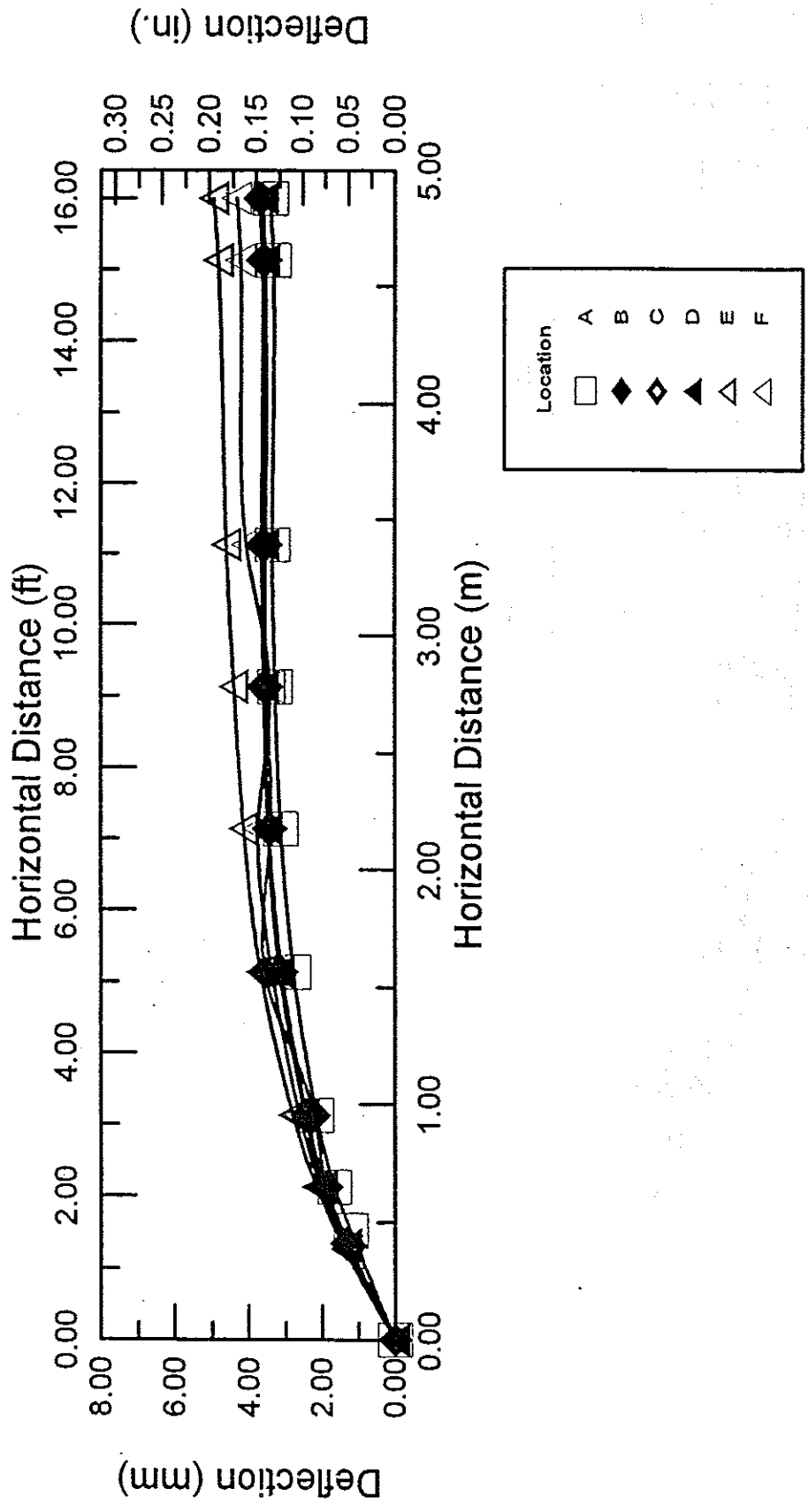


Figure 11.16 August pavement deflection basins for Section 4 with 483 mm (19 in.) of soil cover and 152 mm (6 in.) of tire chips

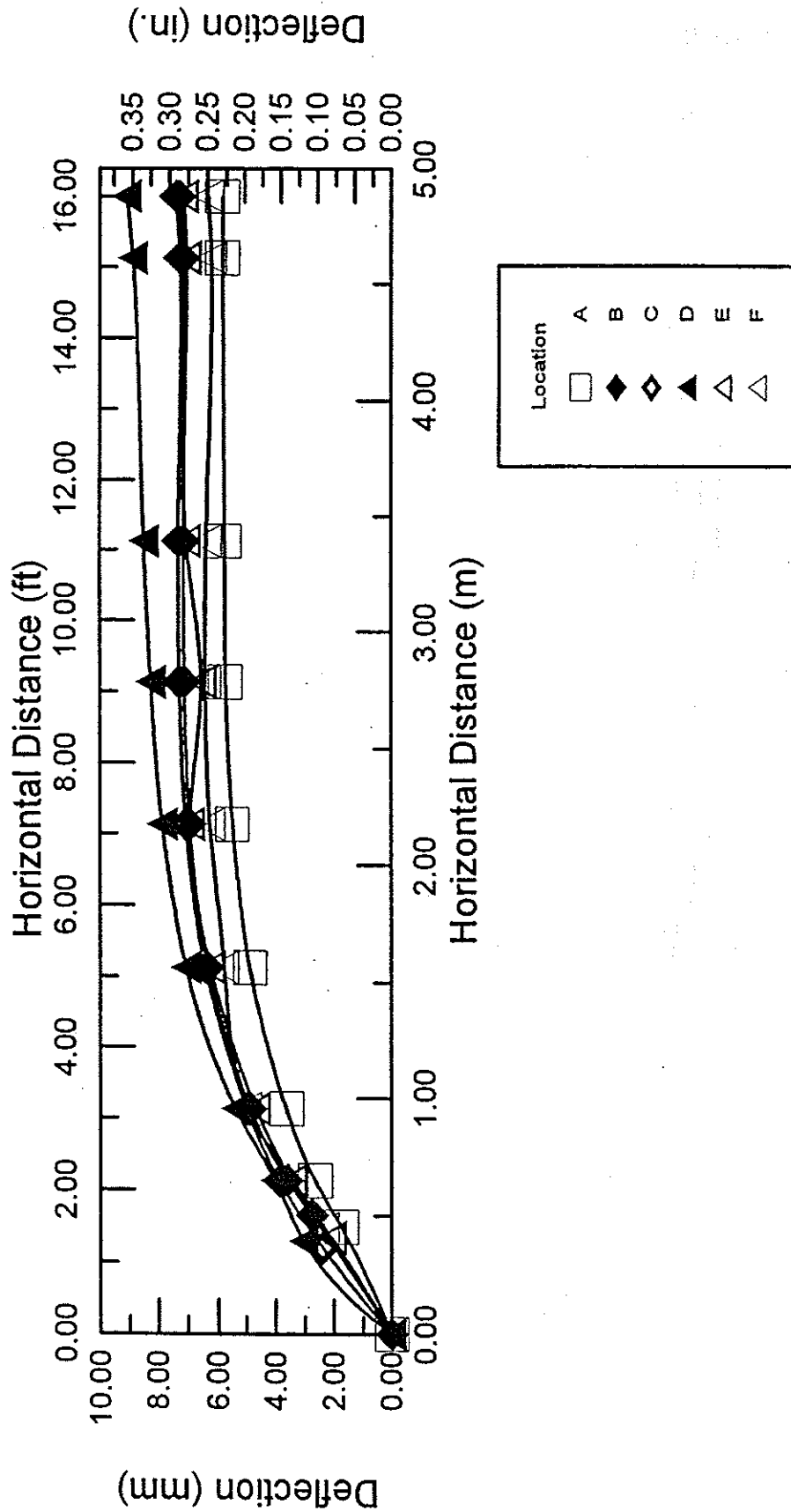


Figure 11.17 August pavement deflection basins for Section 5 with 330 mm (13 in.) of soil cover and 305 mm (12 in.) of tire chips

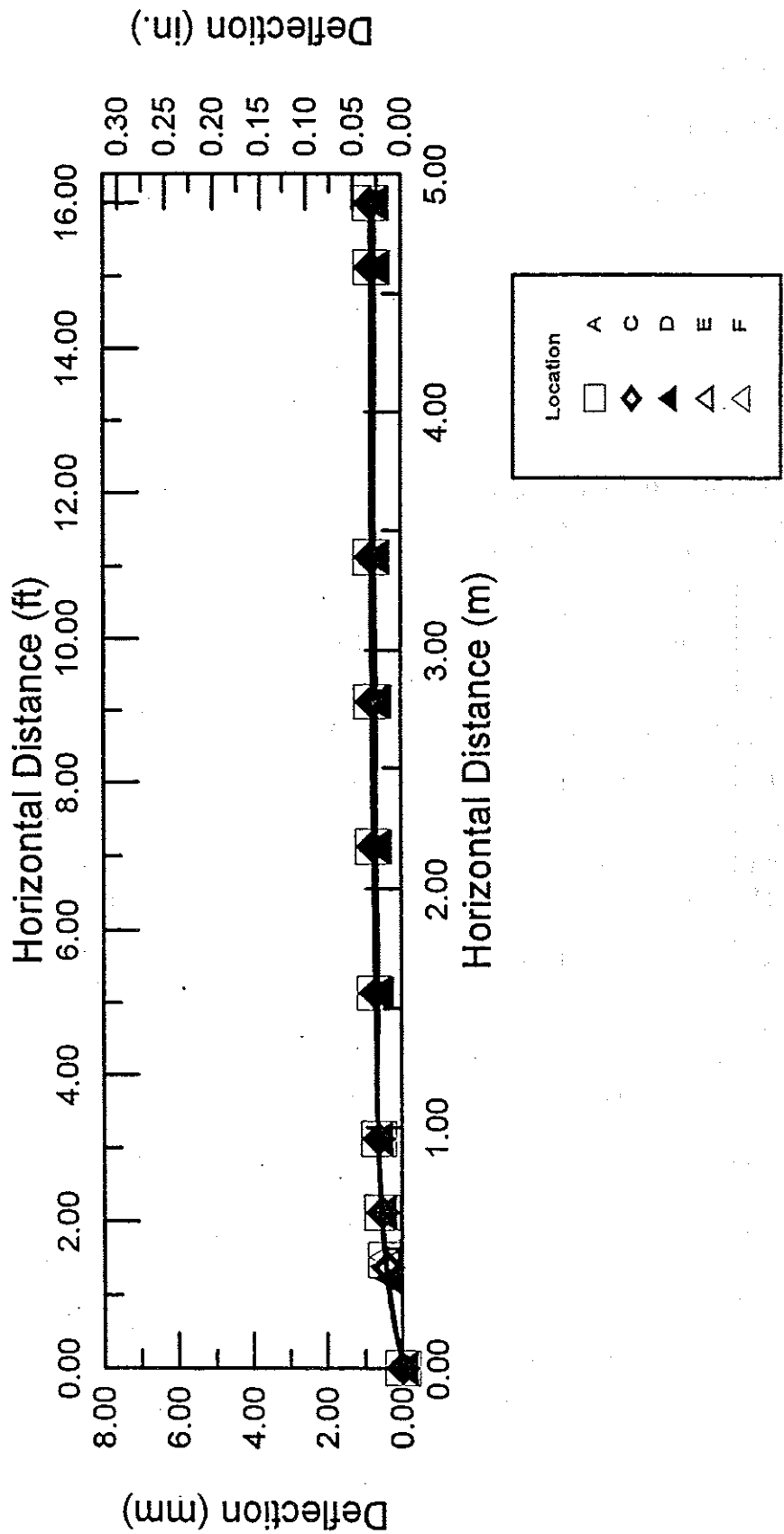


Figure 11.18 August pavement deflection basins for the Control Section with 635-mm (25-in.) thick aggregate subbase course

for August is shown in Figure 11.19. The general clustering of sections is the same as with the April readings, with the exception of Section 2, which seems to be midway between the lower and middle clusters. For the August readings, the average centerline deflections for each section are listed in Table 11.3.

Figures 11.20 through 11.25 compare average deflection basins in April and August. Deflection basins calculated by KENLAYER are also shown, however this will be

Table 11.3 Centerline pavement deflections, August 1997.

Section 1 305 mm 33% Tire Chips		Section 2 305 mm 67% Tire Chips		Section 3 305 mm Tire Chips		Section 4 152 mm Tire Chips		Section 5 305 mm Tire Chips		Control No Tire Chips	
Cover thickness = 483 mm								= 330 mm			
Loc.	CL Def. mm	Loc.	CL Def. mm	Loc.	CL Def. mm	Loc.	CL Def. mm	Loc.	CL Def. mm	Loc.	CL Def. Mm
A	2.26	A	2.58	A	3.85	A	3.42	A	5.85	A	0.81
B	1.37	B	2.83	B	4.67	B	3.65	B	7.30	B	--
C	1.10	C	2.77	C	3.98	C	3.72	C	7.42	C	0.83
D	1.02	D	2.66	D	4.47	D	3.63	D	9.09	D	0.73
E	1.33	E	3.03	E	5.64	E	4.97	E	7.15	E	0.72
F	1.51	F	2.73	F	3.93	F	4.35	F	6.43	F	0.77
Max.	2.26	Max.	3.03	Max.	5.64	Max.	4.97	Max.	9.09	Max.	0.83
Min.	1.02	Min.	2.58	Min.	3.85	Min.	3.42	Min.	5.85	Min.	0.72
Avg.	1.43	Avg.	2.77	Avg.	4.43	Avg.	3.96	Avg.	7.21	Avg.	0.77

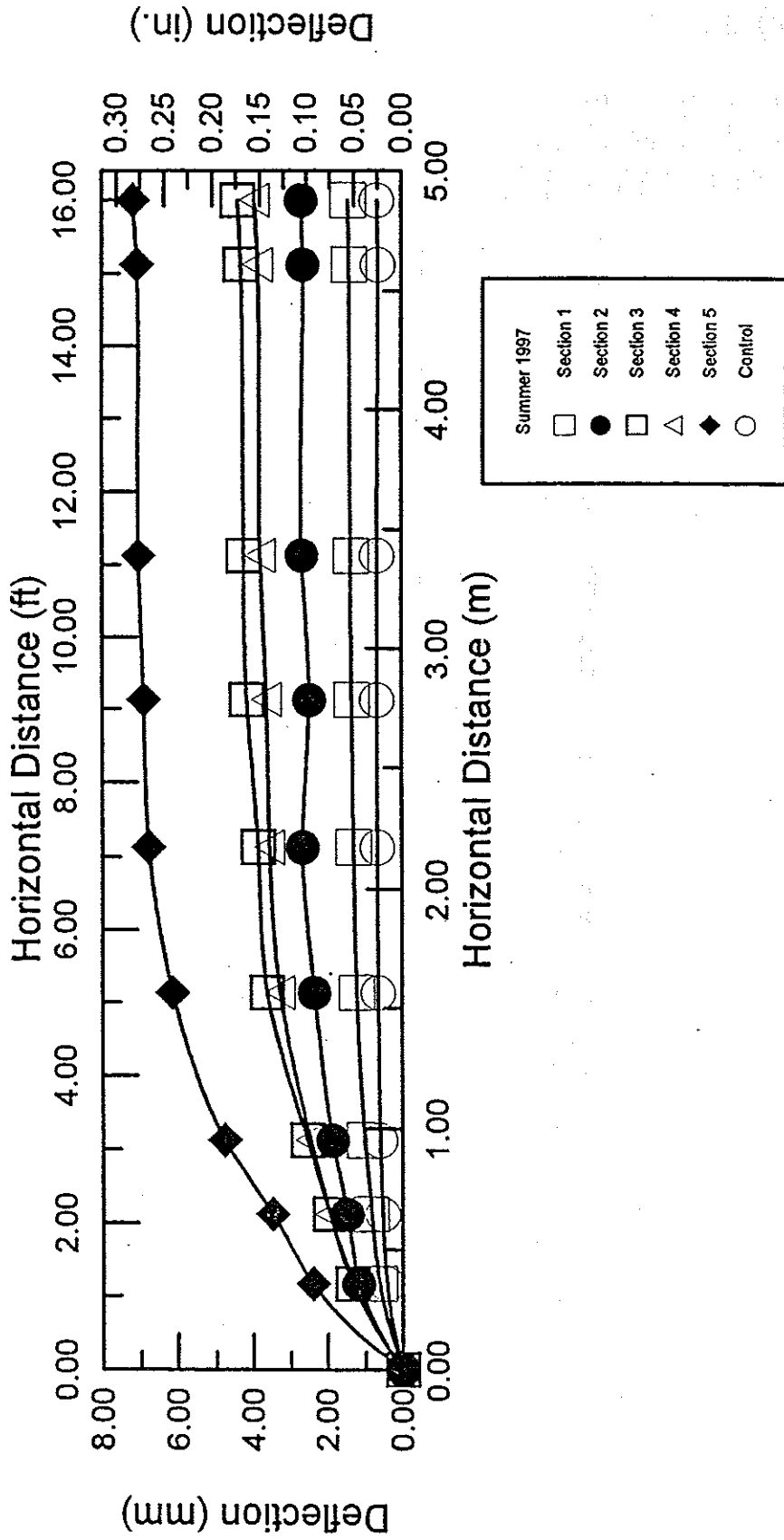


Figure 11.19 Average August pavement deflection basins for all sections

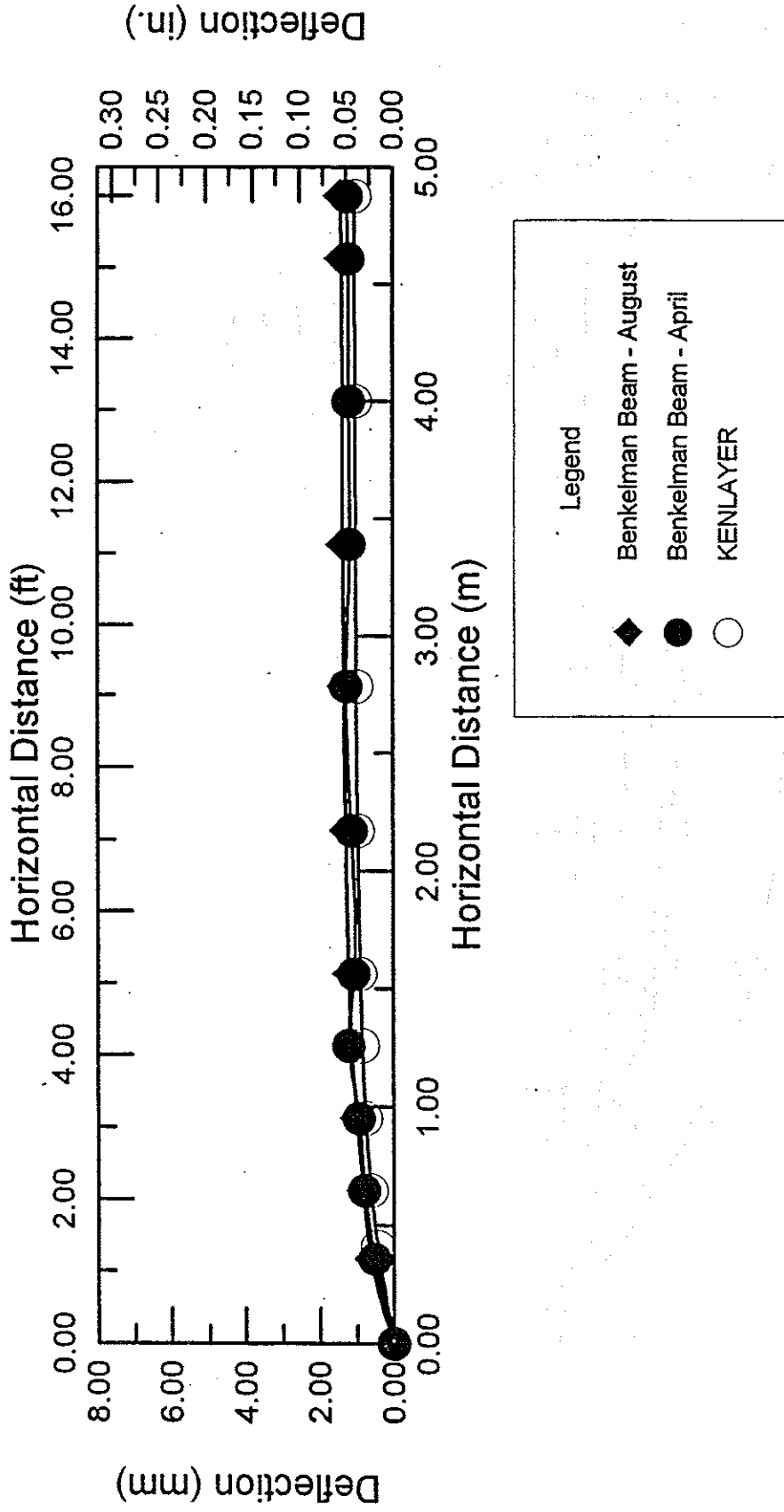


Figure 11.20 Comparison of measured April & August MBB deflection basins with deflection basins calculated by KENLAYER for Section I

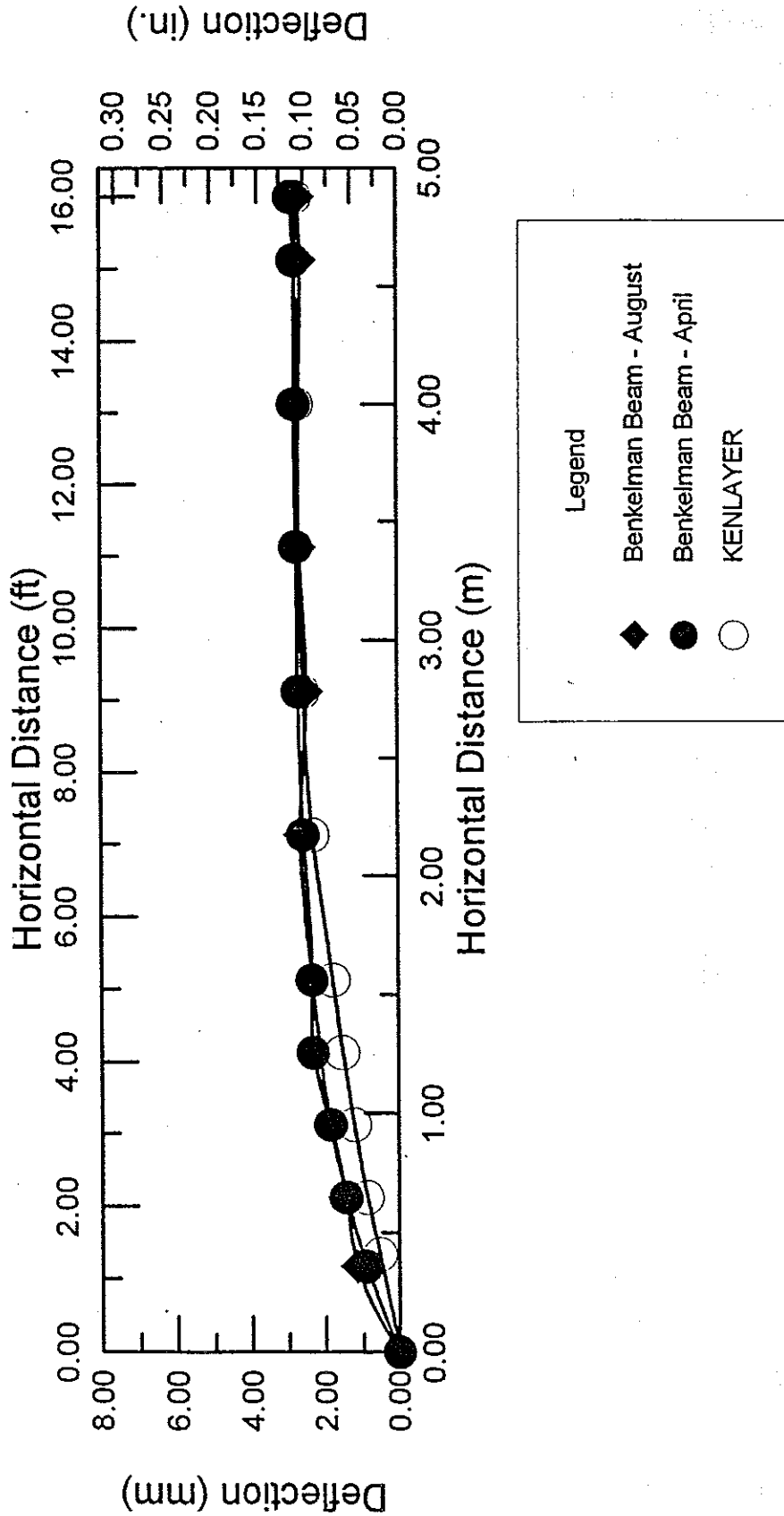


Figure 11.21 Comparison of measured April & August MBB deflection basins with deflection basins calculated by KENLAYER for Section 2

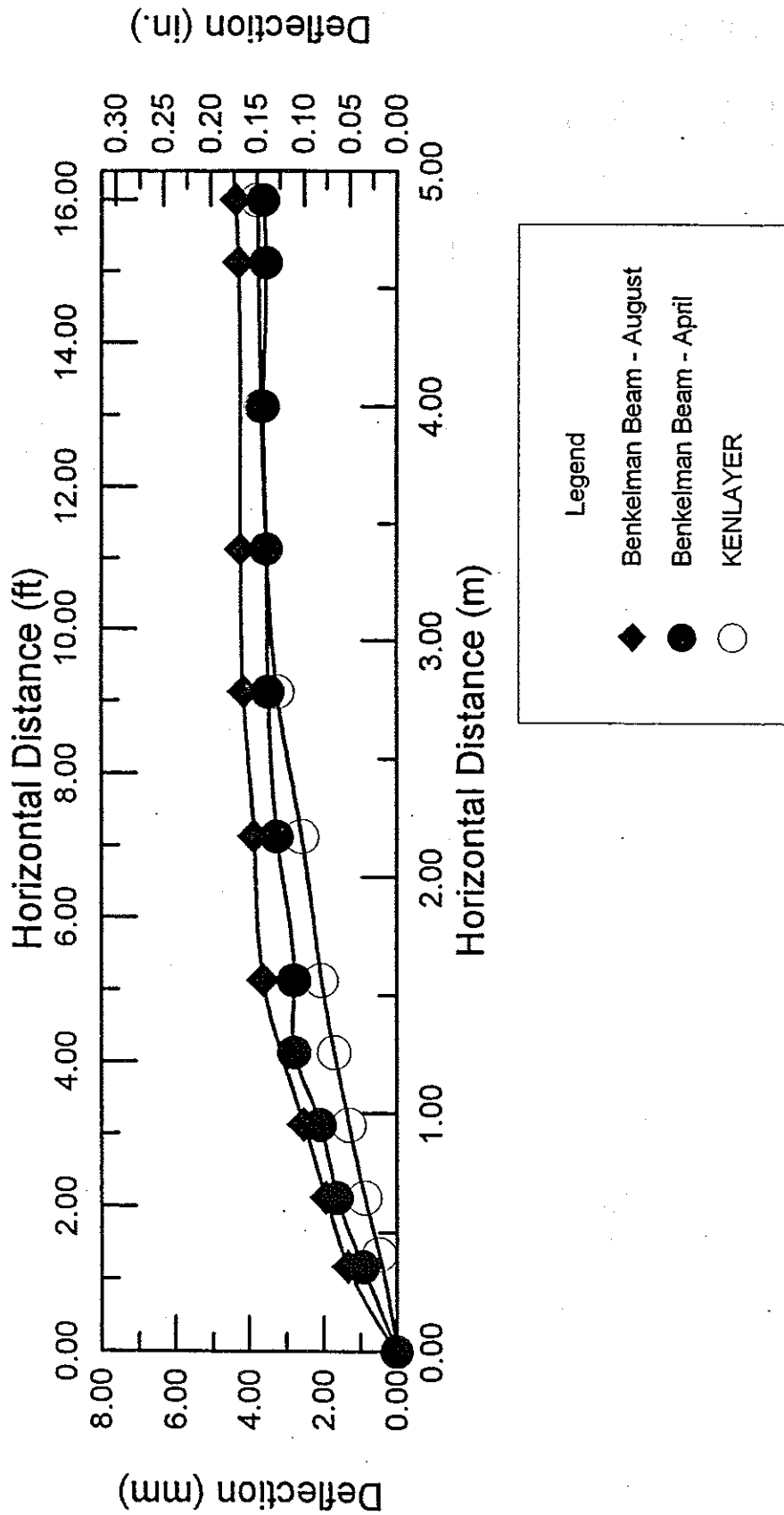


Figure 11.22 Comparison of measured April & August MBB deflection basins with deflection basins calculated by KENLAYER for Section 3

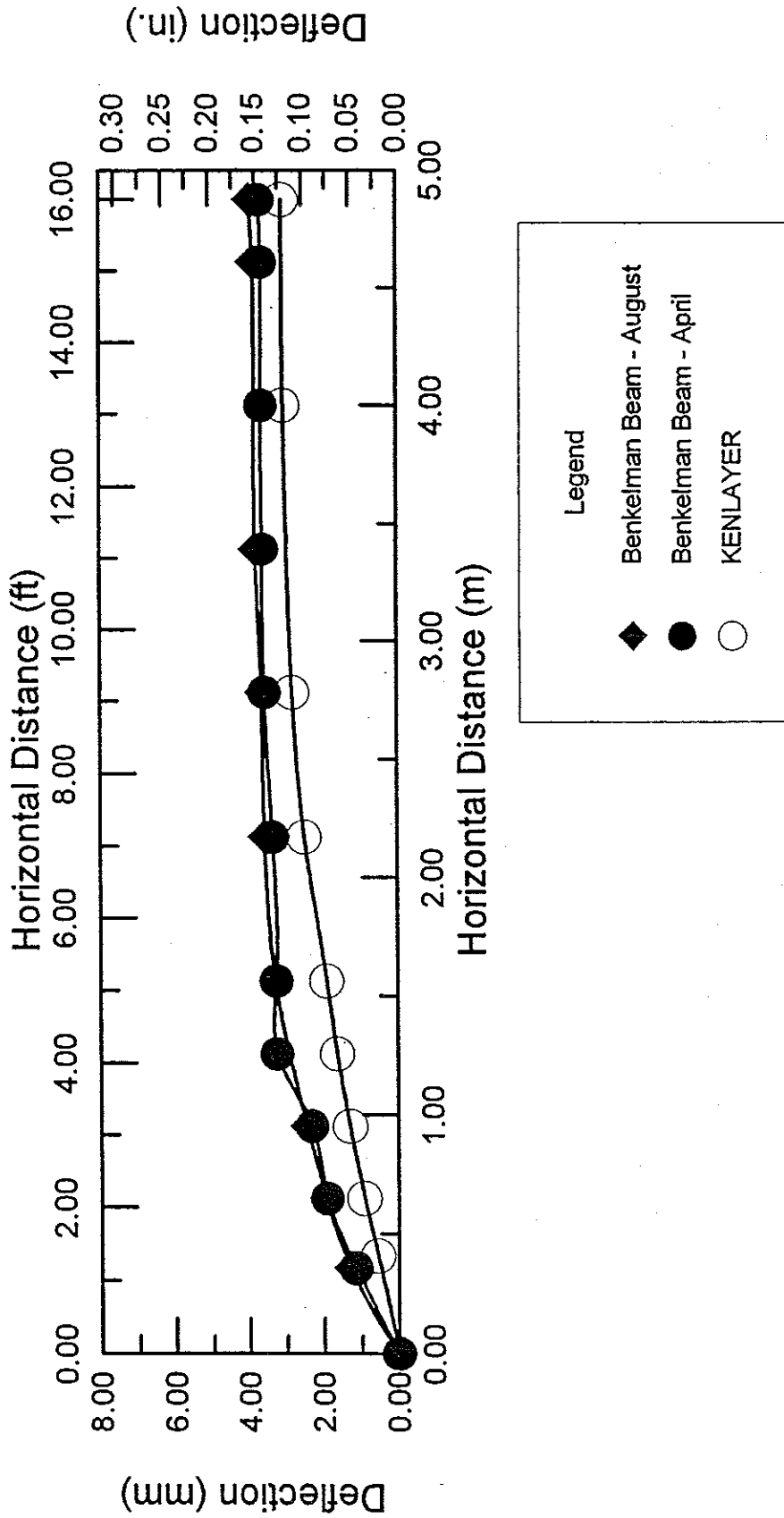


Figure 11.23 Comparison of measured April & August MBB deflection basins with deflection basins calculated by KENLAYER for Section 4

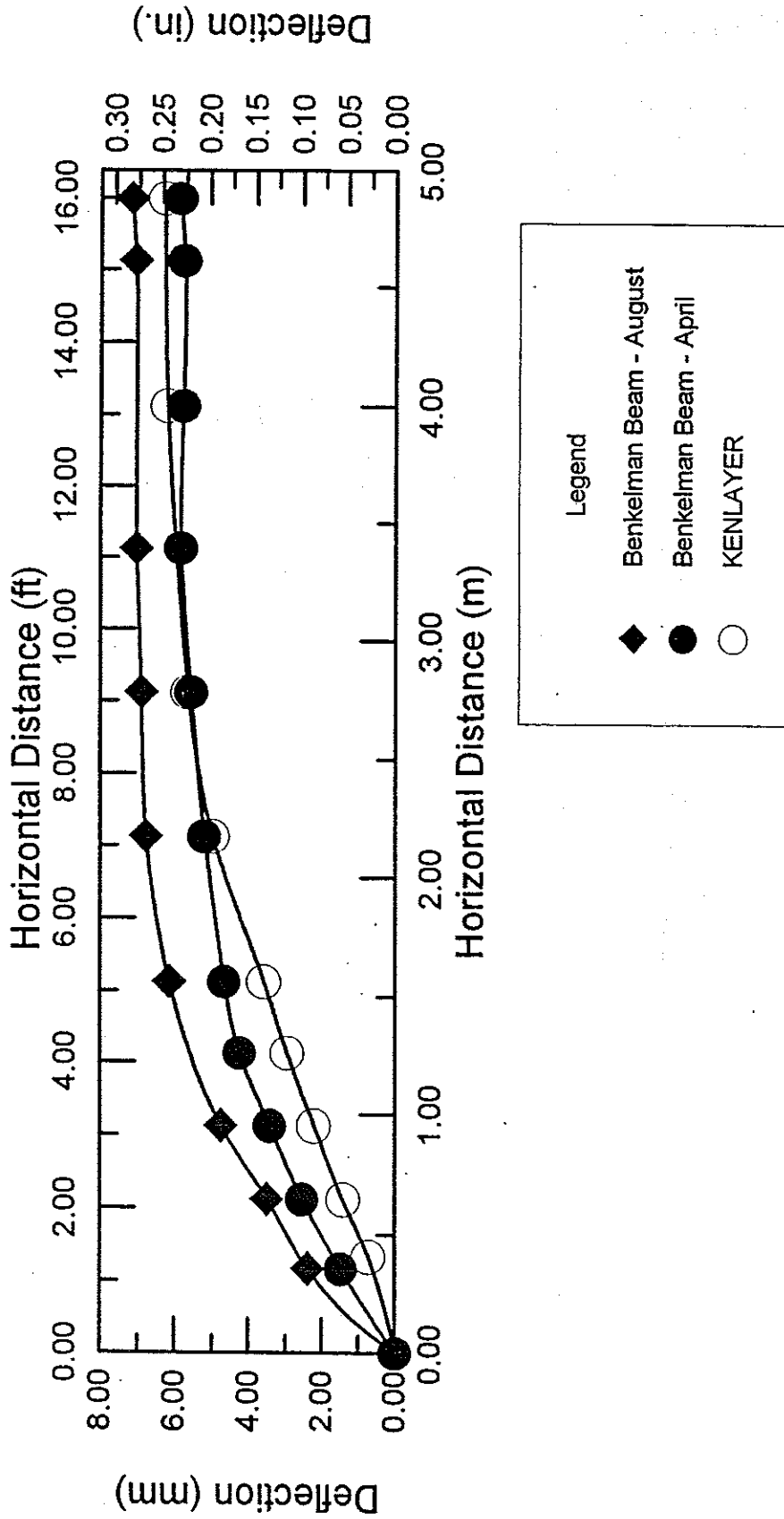


Figure 11.24 Comparison of measured April & August MBB deflection basins with deflection basins calculated by KENLAYER for Section 5

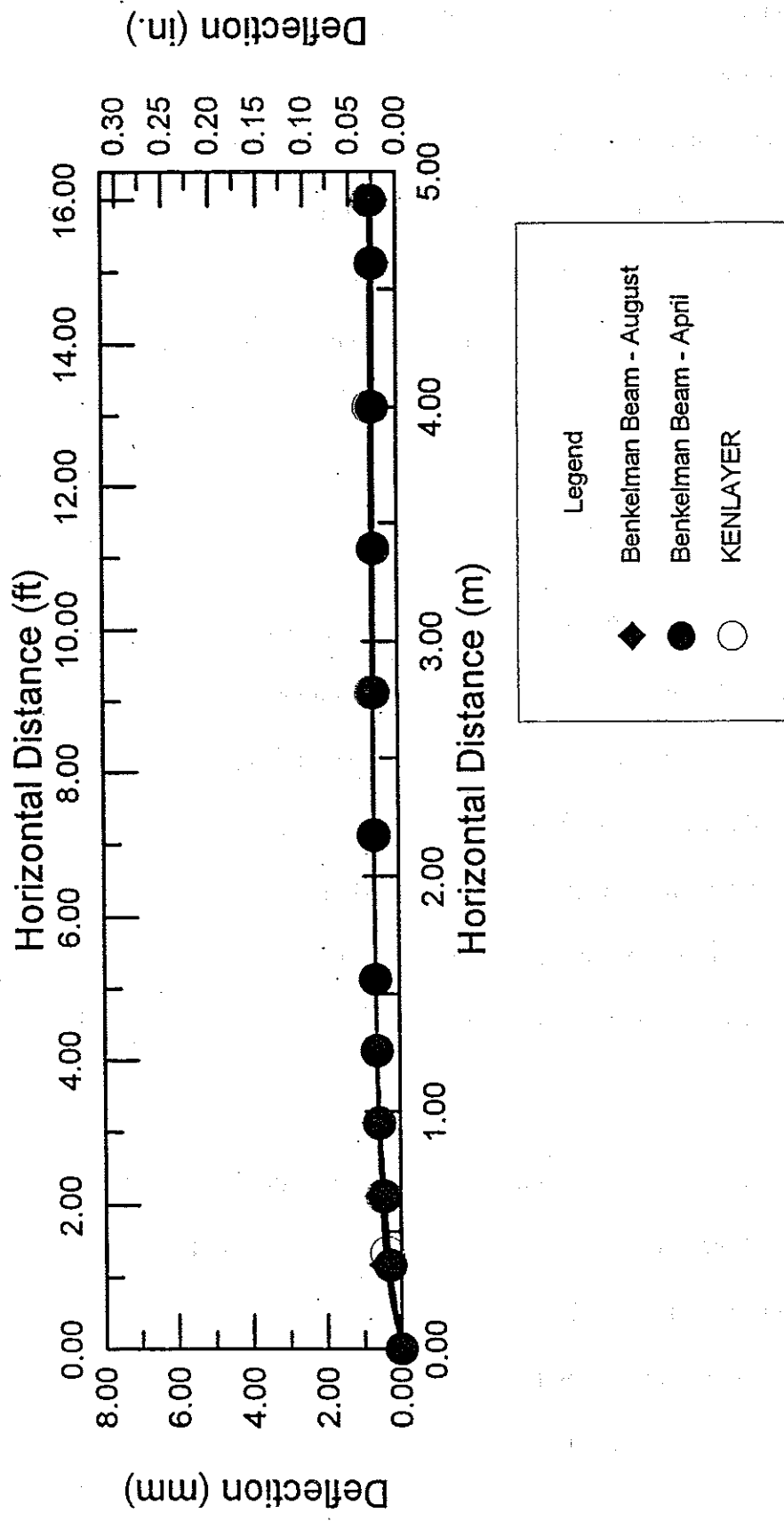


Figure 11.25 Comparison of measured April & August MBB deflection basins with deflection basins calculated by KENLAYER for the Control Section

discussed later in Section 11.3.2. Sections 1, 2, 4, and Control (Figures 11.20, 21, 23, and 25, respectively) show essentially the same deflections in August and April, however, deflections in August were greater than in April for Section 3 (Figure 11.22) and Section 5 (Figure 11.24). The largest difference between the April and August average deflection basins can be seen in Section 5. It could be that the combination of colder, and therefore stiffer, pavement in April combined with the good drainage provided by the tire chips in Sections 3 and 5 resulted in lower deflections in April. In total, comparison of the April and August deflections show that well drained pavement sections do not necessarily experience more deflection immediately following the spring thaw.

Average pavement centerline deflections from Tables 11.2 and 11.3 were plotted versus percent tire chips for Sections 1, 2, 3, and the Control in Figure 11.26. Sections 1 through 3 were chosen because the thickness of gravel cover and thickness of tire chip or tire chip/soil mixture are the same for these sections. Curves for April and August are similar. However, at 100% tire chips the August average is slightly higher than the April average. The relationship between percent tire chips and centerline deflection is linear and quite strong, with a coefficient of determination (r^2) of approximately 0.96 for both April and August.

The radius of the deflection basins in each section varied with the compressibility of the sections. The radius of the deflection basin for the Control appears to be about 0.75 m (2.5 ft). The radii of other sections are listed in Table 11.4. The radii were determined by visual inspection and were estimated as the distance at which the curves of Figures 11.20 through 11.25 became essentially horizontal. Observation of Sections 1

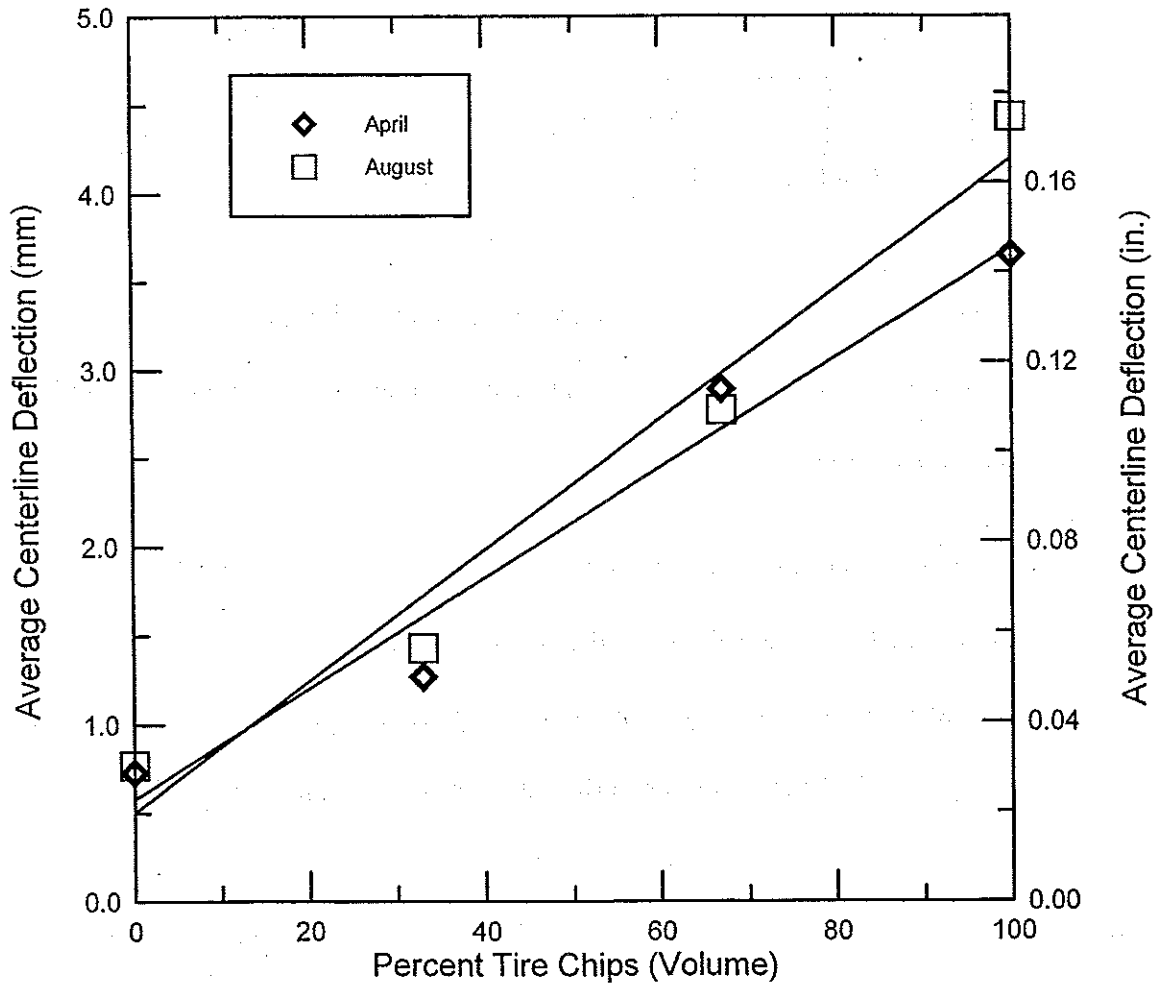


Figure 11.26 Average centerline deflections vs. percent tire chips, April and August, 1997

Table 11.4 Radius of deflection basins

Section	Percent Tire Chips by Volume (%)	Radius of Deflection Basin (m)
1	33	1.25
2	67	2.00
3	100	3.00
4	100	3.00
5	100	3.25
Control	0	0.75

through 3 reveal a trend of increasing deflection basin radius with increasing percent tire chips. Comparison of Sections 3 through 5 show an increase in deflection basin radius with a decrease in soil cover.

The pavement centerline deflections for the April and August MBB tests were plotted versus the distance from the edge drain (located on the left side of the road) in Figures 11.27 and 11.28, respectively. Although the relationships are not clearly defined, there is a general trend of increasing centerline deflection with increasing distance from the edge drain for the April measurements. The trend is most apparent in April for Sections 4 and 5. This suggests that the edge drain was providing beneficial drainage during the period immediately following the spring thaw. Of more importance, the results show that pavement deflections are not increased by the presence of the tire chip filled trench immediately adjacent to the roadway section. The August readings do not show such a trend or the trend is so weak that it is inconsequential, suggesting that the entire width of the section was well drained at this time.

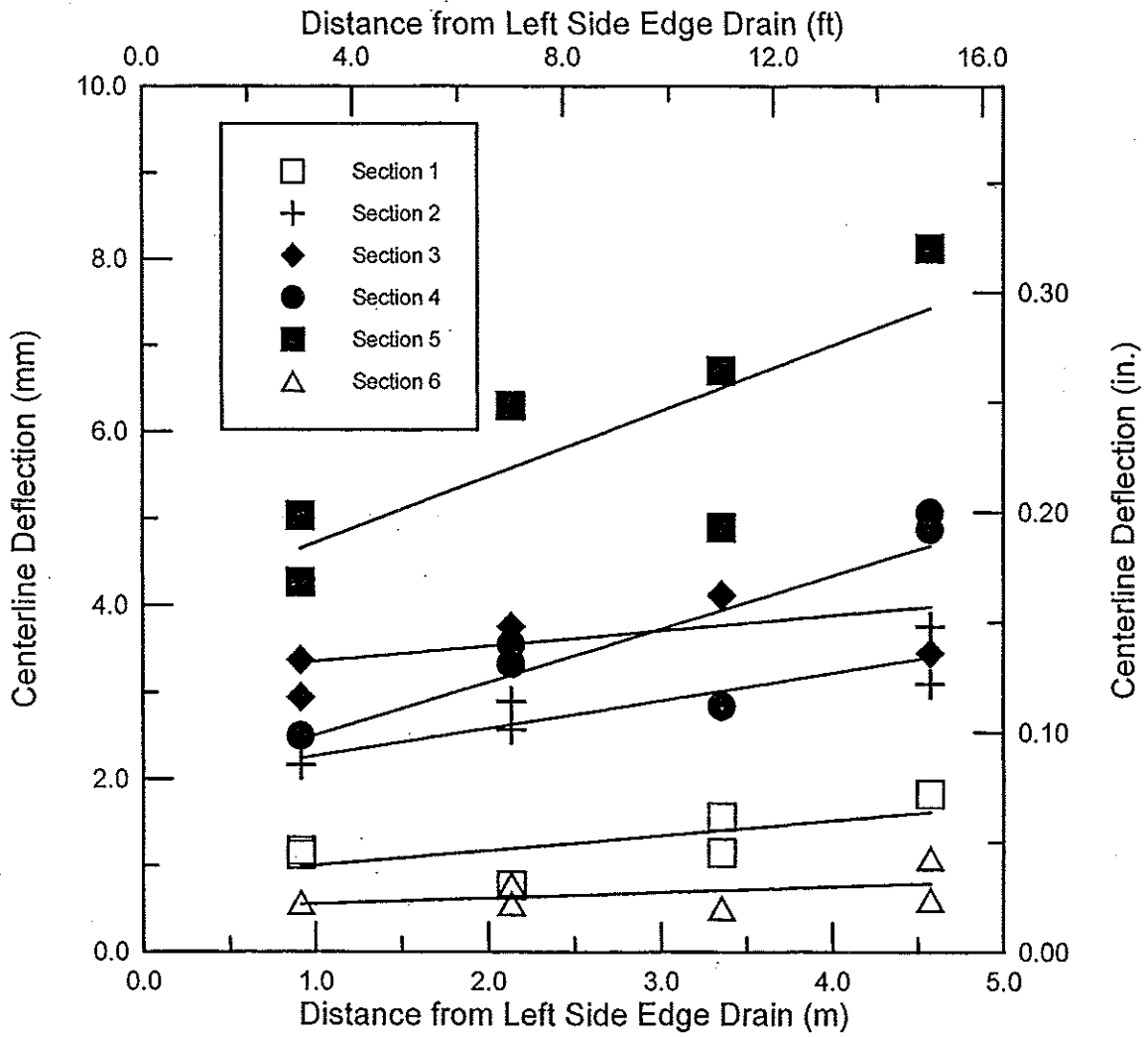


Figure 11.27 Centerline deflection versus distance from edge drain, April 1997

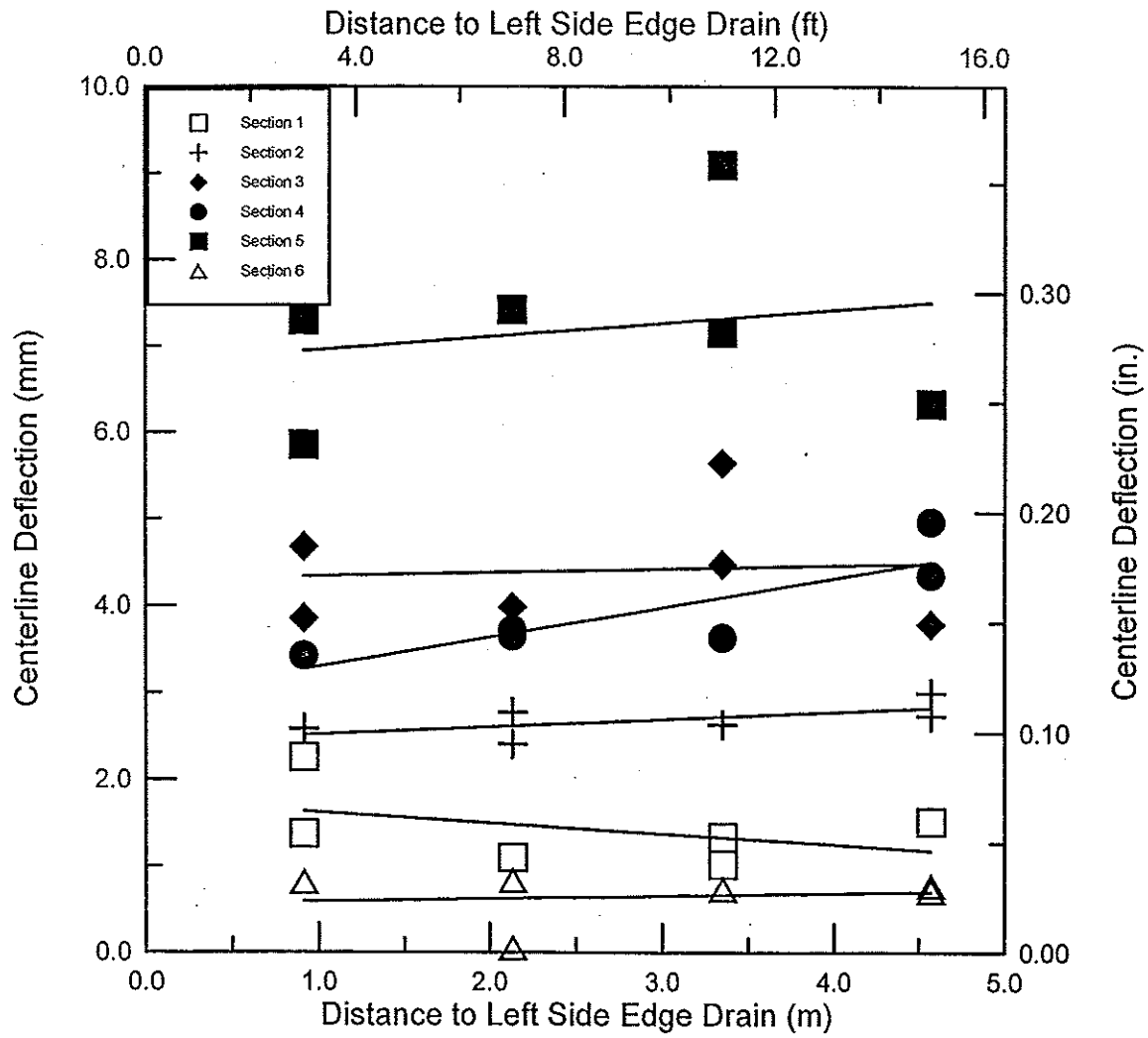


Figure 11.28 Centerline deflection versus distance from edge drain, August 1997

11.3.2 Model of Pavement Deflections with KENLAYER

Pavement deflections were modeled with KENLAYER, a program that calculates pavement deflections for up to 19 layers of underlying material (Huang, 1993). Pavement, gravel, tire chips, tire chip/soil mixtures, and subgrade were divided into layers ranging in thickness from 25 mm (1 in.) to 127 mm (5 in.). The program takes the lowest layer to be of infinite thickness. The loading type was a single axle with dual wheels. The dual wheel load was 4080 kg (9000 lb) and spacing between the dual wheels was 340 mm (13.5 in.). Additional input parameters are listed in Table 11.5.

KENLAYER computes the nonlinear moduli by using a first estimate of the moduli specified by the user and a method of successive approximation to iteratively solve for the moduli of the system. KENLAYER uses two nonlinear relationships, one for granular soil and one for fine grained soils. The resilient modulus increases with increasing stress levels for granular materials and decreases with increasing stress levels for fine grained soils. The relationship for granular materials is:

$$E = K_1 \theta^{K_2} \text{ (MPa or psi)} \quad (11.1)$$

where: $\theta = \text{bulk stress} = \sigma_x + \sigma_y + \sigma_z + \gamma z(1+2K_o)$ (MPa or psi)

$K_1 = \text{nonlinear parameter (MPa or psi)}$

$K_2 = \text{nonlinear parameter (unitless)}$

$\sigma_x = \text{normal stress in the x-direction due to loading (MPa or psi)}$

$\sigma_y = \text{normal stress in the y-direction due to loading (MPa or psi)}$

$\sigma_z = \text{normal stress in the z-direction due to loading (MPa or psi)}$

$\gamma z(1+2K_o) = \text{the weight of the layered system (geostatic stresses)}$

$K_o = \text{coefficient of earth pressure at rest}$

Table 11.5 KENLAYER input parameters

Properties	Material					
	Asphalt Concrete	Subbase	Tire Chips	67% Tire Chips	33% Tire Chips	Subgrade
Behavior	Linear Elastic	Nonlinear Elastic	Nonlinear Elastic	Nonlinear Elastic	Nonlinear Elastic	Nonlinear Elastic
K_1 (MPa)	---	431 MPa* (4480 psi)	13.4 MPa* (6.03 psi)	9.5 MPa* (20 psi)	92 MPa* (954 psi)	41.4 MPa (6000 psi)
K_2	---	0.53	1.16	0.85	0.53	43 (kPa)
K_3	---	---	---	---	---	1110
K_4	---	---	---	---	---	178
Poisson's Ratio	0.35	0.29	0.29	0.29	0.29	0.45
K_o	---	0.60	0.40	0.50	0.50	0.80
Unit Weight (Mg/m ³)	2.32	2.24	0.80	1.12	1.76	1.68

K_o = coefficient of lateral earth pressure at rest.

*Equation 11.1 is a unit specific equation so the conversion between K_1 in MPa and psi is

$$K_1(\text{MPa}) = K_1(\text{psi}) \cdot 0.006894757^{(1-K_2)}$$

For fine grained soils, the resilient modulus decreases with an increase in deviator stress.

The deviator stress is given by:

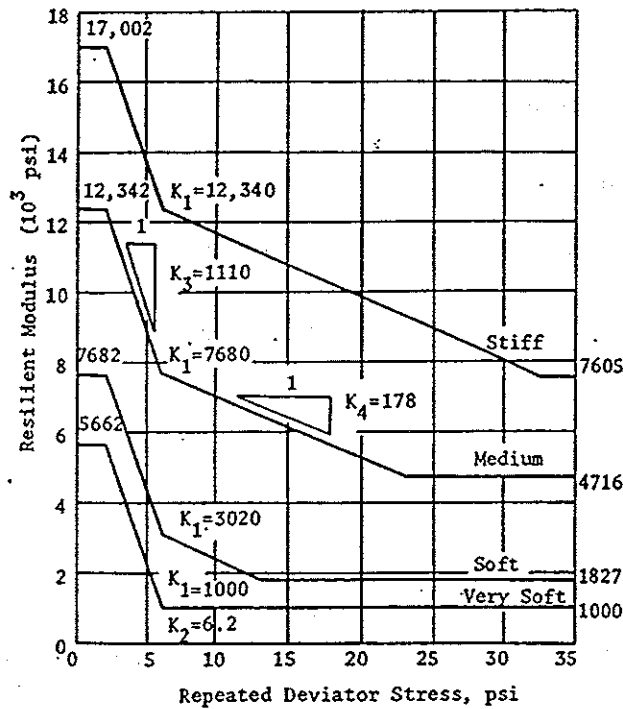
$$\sigma_d = \sigma_x - 0.5(\sigma_y + \sigma_z) + \gamma z(1 - K_o) \quad (11.2)$$

The equation used for fine grained soils by KENLAYER is:

$$E = K_1 + K_3(K_2 - \sigma_d) \quad \text{when } \sigma_d < K_2 \quad (11.3a)$$

$$E = K_1 - K_4(\sigma_d - K_2) \quad \text{when } \sigma_d > K_2 \quad (11.3b)$$

where: $K_1, K_2, K_3,$ and K_4 = material constants. Typical values are given in Figure 11.29.



1 MPa = 145 psi

Figure 11.29 Resilient modulus-deviator stress relationship for four types of subgrade (after Thompson and Elliot, 1985)

The nonlinear parameters K_1 and K_2 for tire chips were obtained from Nickels (1995). Values for subbase parameters were taken from typical values given by Huang (1993). The subbase K_1 of 31 MPa (4480 psi) and K_2 of 0.53 are within the ranges compiled by Shook (1982) of 20 to 53 MPa (2900 to 7750 psi) and 0.46 to 0.65, respectively. These values are for in service base and subbase materials. No compressibility data was available for tire chip/soil mixtures, so K_1 and K_2 parameters were estimated by interpolating between values for gravel and tire chips and adjusting the parameters as needed to obtain a reasonable fit with the deflection basin. Typical values of Poisson's ratio were used as recommended by Huang (1993).

Figure 11.29 shows typical relationships between resilient modulus and deviator stress for fine grained soils. This figure was used to estimate the K_1 , K_2 , K_3 , and K_4 factors for subgrade soils. K_1 was taken to be 41.4 MPa (6000 psi), which is slightly below the medium line in Figure 11.29. E_{MIN} and E_{MAX} were estimated as 27.6 and 76 MPa (4000 and 11,000 psi), respectively. K_2 , K_3 , and K_4 are the same for all soil types. The parameter K_o was obtained from Huang (1993), who recommends using K_o of 0.6 for granular layers and 0.8 for fine grained soils.

Figures 11.20 through 11.25 compare the average deflection basins measured in the field using the MBB with the deflection basin calculated by KENLAYER. The input pavement moduli were adjusted to 276 MPa (40,000 psi) to obtain a good fit to the MBB readings taken in April and August. This adjustment provided a good fit for the Control and reasonable deflection basin fits for the other sections. The MBB readings for April and August were in close agreement with the KENLAYER model deflection basin in Section 1 (Figure 11.20) and the Control (Figure 11.25). The basins differed in Sections 2, 4, and 5. In Sections 2 and 5, the maximum centerline deflection calculated by KENLAYER was between the April and August values, but the initial portion of the curve calculated by KENLAYER, up to about 2.25 m (7.4 ft) horizontally, was both lower in magnitude and had a flatter slope than the April and August MBB measured basins. In Section 4, the KENLAYER deflection basin had a smaller centerline deflection than the April and August measured deflections, and the initial slope of the KENLAYER curve was also flatter than the April and August MBB measured basins. The calculated basin in Section 3 was reasonably close to the MBB readings for April and

August. The deflection basin calculated by KENLAYER has less curvature in Sections 2, 3, 4, and 5 than from the MBB tests.

11.3.3 Layer Moduli

The pavement structure was divided into 19 layers, which were typically 76 to 102 mm (3 to 4 in.) thick. The modulus of each of these layers of a given material type was iteratively calculated by KENLAYER. The resulting moduli for each material were averaged and are listed in Table 11.6. The pavement modulus was fixed at 276 MPa (40,000 psi). The average modulus for gravel base was 77 MPa (11,170 psi). For all sections except the Control Section, the modulus of the subgrade was 76 MPa (11,000 psi), which corresponds to the value of EMAX specified as input. The Control Section had a modulus just below this upper limit of 76 MPa (11,000 psi), indicating that the modulus of this material may not be much greater than the preset upper limit.

The tire chip layers of Sections 3, 4, and 5 had an average modulus of between 0.21 and 0.25 MPa (30 and 36 psi). The mixture moduli fall between those of the tire chips and the gravel. The modulus of the 33% tire chip/67% gravel section was 12.4 MPa (1795 psi), which is about 1/6 that of the gravel base and subgrade, and the modulus of the 67% tire chip/33% gravel section was 0.59 MPa (85 psi), which is about 1/130 that of the gravel base and subgrade.

11.3.4 Pavement Strains

Minimum strain (i.e. tensile or minor principal strain) at the base of the pavement is one parameter calculated by KENLAYER. The minor principal strains are listed in

Table 11.6 Moduli calculated from KENLAYER

Section	Modulus					
	Gravel Base		Tire Chips or Mix		Subgrade	
	MPa	psi	MPa	psi	MPa	psi
1	83	12,090	12.4	1795	76	11,000
2	72	10,470	0.59	85	76	11,000
3	70	10,180	0.24	35	76	11,000
4	71	10,360	0.25	36	76	11,000
5	68	9870	0.21	30	76	11,000
Control	96	13,860	---	---	75	10,930

Table 11.7. The normalized strain is also calculated, which is the ratio of the strain in a given layer divided by the strain in the Control. The normalized strain of Section 5, at 1.323, was the highest of all tire chip layers. The normalized strain of Section 4, with 152 mm (6 in.) of tire chips, was approximately the same as Section 2, with 305 mm (12 in.) of 67% tire chips/33% gravel. Section 1, with 33% tire chips/67% gravel, had a normalized strain of 1.053. The lowest normalized strain was in Section 3 at 1.022. In

Table 11.7 Computation of strain at base of pavement in KENLAYER

KENLAYER Results				
Section	Soil Cover (mm)	Percent Tire Chips	Minor Principal Strain ($\times 10^{-2}\%$)	Normalized Strain
1	483	33	-5.149	1.053
2	483	67	-5.083	1.039
3	483	100	-4.998	1.022
4	483	100	-5.071	1.037
5	330	100	-6.473	1.323
Control	635	---	-4.891	1.000

Section 1 and the Control Section, the deflection basins were more accurately modeled by KENLAYER, so the normalized strains in these sections should be more reliable than normalized strains in other sections.

Pavement life is empirically related to modulus of elasticity of asphalt pavement and tensile strain at the base of the asphalt layer by the following exponential equation:

$$N_f = f_1 (\varepsilon_t)^{-f_2} (E_1)^{-f_3} \quad (11.4)$$

where: N_f = allowable number of load repetitions to prevent fatigue cracking

ε_t = tensile strain at the bottom of asphalt layer

E_1 = elastic modulus of asphalt layer

The factors f_1 , f_2 , and f_3 are constants determined from laboratory fatigue tests with f_1 modified to correlate with observed field performance (Huang, 1993). The Asphalt Institute recommends 0.0796, 3.291, and 0.854 for f_1 , f_2 , and f_3 , respectively. Shell Oil recommends 0.0685, 5.671, and 2.363 for f_1 , f_2 , and f_3 , respectively (Shook, et al., 1982). Equation 11.4 was used to calculate a normalized failure number that is useful for comparison of pavement life in tire chip and tire chip/soil mixture sections to the Control. Since E_1 , f_1 , and f_3 are constants for a given type of road at a given time and temperature, the normalized failure number will be related to the tensile strain in the base of the asphalt layer. Thus, Equation 11.4 can be used to form the ratio:

$$\frac{N_{f(tc)}}{N_{f(con)}} = \left(\frac{\varepsilon_{t(tc)}}{\varepsilon_{t(con)}} \right)^{-f_2} \quad (11.5)$$

where: $N_{f(tc)}$ = allowable number of load repetitions to prevent fatigue cracking in tire chip or tire chip/soil mixture section

$\epsilon_{l(tc)}$ = tensile strain at the bottom of the asphalt layer in tire chip or tire chip/soil mixture section

$N_{l(con)}$ = allowable number of load repetitions to prevent fatigue cracking in the Control Section

$\epsilon_{l(con)}$ = tensile strain at the bottom of the asphalt layer in the Control Section

The left hand side of the equation is a ratio that shows an approximate reduction in the number of load repetitions to failure of tire chip or tire chip/soil sections compared to the Control. This ratio considers only the effect of tensile strain on pavement life. The counterbalancing effect of improved drainage and reduced frost heave on increasing pavement life is discussed in the next paragraph. Table 11.8 shows the approximate failure ratio using $f_2 = 3.291$ and 5.671 . The ratios in Sections 1 through 4 range from 0.75 to 0.93. However, Section 5 has an extremely low ratio (0.20 to 0.40). Neglecting the possible increase in pavement life caused by improved drainage and reduced frost heave; this means that the expected number of repetitions to failure in this section would be only 20 to 40 percent of the number in the Control. Stated another way, the pavement life would be reduced by 60 to 80 percent. This number is very low and pavement performance in Section 5 would be unacceptable.

Table 11.8 Failure criterion ratios from normalized strains in tire chip and tire chip/soil mixture sections

Section	Pavement Life Ratio	
	Using $f_2 = 3.291$	Using $f_2 = 5.671$
1	0.84	0.75
2	0.88	0.80
3	0.93	0.88
4	0.89	0.81
5	0.40	0.20
Control	1.00	1.00

The AASHTO 1993 design equation for flexible pavements (AASHTO, 1993) was used to investigate the benefits that could be derived by improved drainage and reduced frost heave. The parameters shown in Table 11.9 were used in the equation. They are typical of those used by the Maine DOT. If the control section had fair drainage (drainage factor = 1.00) and was subjected to a heave rate of 1 mm/day for ten winters, the calculated service life of the road would be 8.5×10^6 equivalent single axle loads (ESAL's). However, improving the drainage to good (drainage factor = 1.25) and eliminating frost effects increases the service life to 3.1×10^7 ESAL's. Thus, improving the drainage and eliminating frost effects could increase the service life of the road by a factor of 3.7, more than compensating for the loss in service life caused by the compressibility of the tire chips in Sections 1 through 4. These results indicate that there is a net beneficial effect by using tire chips as a drainage and insulating layer.

Table 11.9 Parameters used in AASHTO 1993 design equation.

Parameter	Value
Reliability	90%
Standard deviation	0.45
Roadbed resilient modulus	64 Mpa (9000 psi)
Design serviceability loss	2
Layer coefficient for top 100 mm of asphalt	0.44*
Layer coefficient below 100 mm of asphalt	0.34*
Layer coefficient for subbase	0.1*

*assumes layer thickness is in inches.

This analysis is supported by visual inspection of the road surface. Within the first year of construction, the pavement in Section 5 showed signs of fatigue in the wheel paths while other sections did not show signs of fatigue. Reexamination of the pavement in the Springs of 1998 and 1999, after the second and third winters, confirmed this

observation. Minor cracking in the wheel path was noted in Section 5, but no signs of fatigue were evident in the remaining sections.

The performance predictions given above should be interpreted with caution as there are some uncertainties in the KENLAYER analysis and the AASHTO design equation. A pavement modulus of 275 MPa (40,000 psi) was necessary in KENLAYER to obtain a good deflection fit for the tire chip sections. Even though this is a static modulus, which would be expected to be lower than a dynamic modulus, this is still rather low for hot mix asphalt (HMA). A typical dynamic modulus given by Huang (1993) is about 2070 MPa (300,000 psi) for a temperature of 21 °C (70 °F) and a load frequency of 1 Hz. A higher pavement modulus would compare more favorably to those suggested by Irwin (1997), and those calculated in MODCOMP4, but the lower modulus was needed to create a better fit in the tire chip and tire chip/soil mixture sections.

In addition to the uncertainty in pavement modulus, the MBB measurements show a greater curvature in the vicinity of the wheel load compared to the computer model. The greater curvature in field measurements means that field strains in some sections are actually greater than calculated from the model. The deflection basins calculated by KENLAYER for Section 1 and the Control show similar curvature compared to MBB measurements within the first 1.00 m (3.28 ft), however the deflection basins of Sections 2, 3, 4, and 5 show much less curvature in the initial portion of the deflection basin. This indicates that tensile strains at the base of the pavement are higher than those calculated by KENLAYER for Sections 2, 3, 4, and 5.

Further research should be undertaken to find a pavement deflection analysis program that will better model tire chip and tire chip/soil sections. One factor that may be important is the effect of the 4080 kg (9000 lb) rear wheel load located at the other end of the truck axle. This does not need to be taken into account in typical pavements, but the compressibility of tire chips was shown to increase the deflection basin radius, raising the possibility that load imposed by one pair of dual wheels could affect the deflections at the other wheel.

11.4 HWD TESTS

HWD tests were performed on November 19, 1996, approximately one week after paving was complete. Another round was performed on April 15, 1997, at the approximate time when frost was no longer detectable in the test sections. An additional round of tests were performed with a Falling Weight Deflectometer (FWD) on August 22, 1997 by the Maine Department of Transportation.

11.4.1 Results

Results of November and April HWD data were input into MODCOMP4, Version 4.0H (Irwin, 1997), a modulus backcalculation program. The average deflections for each section are given in Appendix A. These tables report the average deflections at the six locations in each section. Each location, in turn, is the average of four drops at each of four load levels. Analysis of the HWD data is presented in the following sections. Also listed in Appendix A, are the average deflections for the August, 1997 FWD test. Analysis of the FWD data was attempted with MODCOMP4 but no reliable solutions could be calculated.

11.4.2 Backcalculation of Young's Modulus

Backcalculation of Young's Modulus was performed with MODCOMP4, Version 4.0H (Irwin, 1997). MODCOMP4 computes the modulus of each layer through an iterative approach in which the layer moduli are systematically varied until the desired fit of the surface deflection data is achieved (Irwin, 1994). Backcalculation was attempted with MODCOMP4 Version 4.0C, but it did not allow a modulus value less than 6.9 MPa (1000 psi) to be computed for any layer, however, this was greater than the expected modulus of tire chips. At the request of the investigators, Version 4.0C was altered by Dr. Lynne Irwin, Associate Professor and Director of the Cornell Local Roads Program, to allow a lower bound of 0.07 MPa (10 psi) to be computed for a given layer. This modified version is called MODCOMP4, Version 4.0H.

Input parameters for MODCOMP4 from November and April HWD tests are listed in Table 11.10. These parameters were chosen based on values reported in Manion and Humphrey (1992), MODCOMP4 help menus (Irwin, 1997), and parameters used in KENLAYER for the North Yarmouth field trial (Nickels, 1995). In addition to these parameters, seed moduli were necessary for MODCOMP4 to begin calculations. The backcalculated moduli are relatively insensitive to the seed moduli if the seed moduli were carefully chosen based on typical values or laboratory tests.

Table 11.10 Input parameters for MODCOMP4

Properties	Material					
	Asphalt Concrete	Subbase	Tire Chips	67% Tire Chips	33% Tire Chips	Subgrade
Behavior	Linear Elastic	Nonlinear Elastic	Nonlinear Elastic	Nonlinear Elastic	Nonlinear Elastic	Nonlinear Elastic
Poisson's Ratio	0.35	0.35	0.32	0.32	0.35	0.35
K_o	-	0.80	0.40	0.40	0.70	0.40
Unit Weight (Mg/m ³)	2.32	2.24	0.80	1.12	1.76	1.04

The resilient moduli calculated by MODCOMP4 are listed in Tables 11.11 and 11.12 for November and April measurements, respectively. For both tests the moduli of 33% tire chips/67% gravel was significantly lower than the moduli calculated for the gravel base. The moduli for 67% tire chips/33% gravel was only slightly greater than the moduli for 100% tire chips. The average modulus for tire chips from Sections 3, 4, and 5

Table 11.11 Backcalculated resilient moduli from MODCOMP4 for November test

Section	Pavement		Base		Tire Chips or Mix		Subgrade	
	x10 ³ psi	MPa	x10 ³ psi	MPa	x10 ³ psi	MPa	x10 ³ psi	MPa
1	1840	12700	21.9	151	2.36	16.3	8.3	57
2	2430	16800	12.0	83	0.53	3.7	15.0	103
3	1750	12100	27.8	192	0.41	2.8	6.8	47
4	2000	13800	16.6	114	0.39	2.7	4.3	30
5	2460	17000	27.7	191	0.44	3.0	4.8	33
Control	2000	13800	19.0	131	---	---	9.7	67

Table 11.12 Backcalculated resilient moduli from MODCOMP4 for April test

Section	Pavement		Base		Tire Chips or Mix		Subgrade	
	x10 ³ psi	MPa	x10 ³ psi	MPa	x10 ³ psi	MPa	x10 ³ psi	MPa
1	852	5880	25.8	178	1.68	11.6	9.3	64
2	1550	10700	14.0	97	0.65	4.5	6.7	46
3	1330	9170	13.8	95	0.36	2.5	8.7	60
4	1160	8000	12.2	84	0.25	1.7	5.7	39
5	1010	6970	23.4	161	0.30	2.1	5.7	39
Control	1100	7590	22.0	152	---	---	8.7	60

was 2.8 MPa (410 psi) in November and 2.1 MPa (300 psi) in April, with relatively little scatter in the data for both. This means that the modulus for 67% tire chips/33% gravel is approximately 2.2 times greater, and the modulus for 33% tire chips/67% gravel is approximately 5.6 times greater than the average modulus of 100% tire chips. The average gravel base modulus in November was 144 MPa (20,900 psi), which is 51 times greater than the average modulus of tire chips in November. The average gravel base modulus in April was 128 MPa (18,600 psi), which is 61 times greater than the average modulus of tire chips in April.

Laboratory moduli of tire chip/sand mixtures tested at the University of Wisconsin (Edil and Bosscher, 1992) ranged from approximately 2.8 MPa (400 psi) for a 70% tire chip/30% sand mixture to 10.3 MPa (1500 psi) for a 30% tire chip/70% sand mixture. These moduli were interpolated at a bulk stress of approximately 103 kPa (15 psi). Both of these values are very similar to those calculated by MODCOMP4 for 67% tire chips/33% gravel and 33% tire chips/67% gravel. The resilient modulus of rubber buffings from laboratory tests at the University of Alaska (Shao, et al., 1994) give moduli

from 0.65 to 1.3 MPa (94 to 185 psi) with minor principal stresses (σ_3) of 21 and 34 kPa (3 and 5 psi) and deviator stresses of 34, 69, and 103 kPa (5, 10, and 15 psi). This is slightly lower than the moduli of tire chips calculated in MODCOMP4, which ranged from an average of 2.8 MPa (410 psi) in November to 2.1 MPa (310 psi) in April.

11.4.3 Comparison with Typical Values of Moduli

The average modulus for the gravel base was 144 MPa (20,880 psi) in November and 128 MPa (18,560 psi) in April. These are in the typical range listed in Table 11.13.

Table 11.13 Typical values of Young's Modulus

MODCOMP4 Help Menus (Irwin, 1997)		Coduto (1994)		Bowles (1996)	
Material	E (MPa)	Material	E (MPa)	Material	E (MPa)
Asphalt	1,400 -				
Concrete	17,000				
Granular Base	200 - 500	Dense Sand	50 - 100	Dense Sand & Gravel	100 - 200
Granular Subbase	100 - 300	Medium - Dense Sand	20 - 60	Dense Sand	50 - 81
		Soft Clay	1.5 - 10	Soft Clay	5 - 25
		Medium Clay	5 - 50	Medium Clay	15 - 50
		Stiff Clay	15 - 75	Hard Clay	50 - 100

The average subgrade modulus was 56 MPa (8120 psi) in November and 51 MPa (7400 psi) in April. These moduli are between the values for medium and stiff clay listed in Table 11.13, which is reasonable for the subgrade soil at the site.

There is a significant difference between pavement moduli backcalculated in November and April (Tables 11.11 and 11.12). November pavement moduli were nearly double the April pavement moduli. Higher temperatures decrease the modulus of asphaltic concrete pavement. The pavement temperature on the day of the November test ranged from -8.9 to -3.3 °C (16 to 26 °F) and the average pavement modulus was 14,370 MPa (2,084,000 psi). The pavement temperature on the day of the April test ranged from -3.9 to 9.4 °C (25 to 49 °F) and the average pavement modulus was 8050 MPa (1,167,000 psi). Thus, temperature could be the cause of the difference in pavement modulus.

11.4.4 Comparison with KENLAYER Moduli

There are some differences between moduli calculated by MODCOMP4 and those used in KENLAYER. The first difference is the pavement modulus, which was calculated by MODCOMP4 to be between 5880 and 17,000 MPa (852,000 and 2,460,000 psi). This is an order of magnitude higher than the pavement modulus used in KENLAYER, which was set to 276 MPa (40,000 psi). As noted previously, this was necessary to improve the matches between KENLAYER results and measured field deflection basins. The MBB is a static test rather than a transient loading test. Thus, the static moduli of pavement used in KENLAYER would be expected to be less than the resilient moduli of pavement calculated by MODCOMP4.

The tire chip modulus backcalculated by MODCOMP4 (Sections 3 through 5) was also an order of magnitude higher than used in KENLAYER. MODCOMP4 backcalculated an average tire chip modulus of 2.5 MPa (360 psi) compared to an average of 0.23 MPa (34 psi) used in KENLAYER. The modulus used in KENLAYER was

based on quasi-static laboratory compressibility tests performed by Nickels (1995). Possible reasons for the large difference are that the resilient modulus of tire chips is much greater than the static modulus or that the laboratory tests did not accurately predict the modulus at the very low stress levels corresponding to the field conditions.

Similar to the results for tire chips, the average modulus for 67% tire chip/33% gravel mixtures (Section 2) backcalculated by MODCOMP4 (4.1 MPa; 590 psi) was a factor of 7 higher than used in KENLAYER (0.59 MPa; 85 psi). However, for 33% tire chips/67% gravel (Section 1), the average modulus backcalculated by MODCOMP4 (14.0 MPa; 2020 psi) was a factor of 1.1 higher than used in KENLAYER (12.4 MPa; 1795 psi). The moduli used in KENLAYER for the mixtures were interpolated from the compressibility of tire chips and gravel, thus there is considerable uncertainty in these values. Moreover, the differences could be due to the factors noted for tire chips in the preceding paragraph.

The average modulus for the gavel base backcalculated by MODCOMP4 (136 MPa; 19,600 psi) was a factor of 1.8 higher than used in KENLAYER (77 MPa; 11,100 psi). However, the average subgrade modulus backcalculated by MODCOMP4 (54 MPa; 7,800 psi) was 0.7 times the value used in KENLAYER (76 MPa; 11,000 psi). It is recalled that the moduli used in KENLAYER were based on typical values reported in the literature, which could account for the differences.

11.5 SUMMARY

Modified Benkelman Beam (MBB) tests were performed in April 1997 and August 1997, and Heavy Weight Deflectometer (HWD) tests were performed in November 1996

and April 1997. An additional set of Falling Weight Deflectometer Tests (FWD) was done in August, 1997. August pavement deflections measured by the MBB were significantly higher than April deflections in Sections 3 and 5, which both have 305-mm (12-in.) thick tire chip layers. The MBB deflection basins for section with tire chip/soil mixtures, 152-mm (6-in.) tire chip layer, and the Control were about the same in April and August. A possible explanation is that the colder, and therefore stiffer, pavement in April combined with the good drainage provided by the tire chips in Sections 3 and 5 resulted in lower deflections in April. Overall, MBB deflection basins responded as expected, with the centerline deflection and radius of the deflection basin increasing as the percentage of tire chips increased and/or the amount of soil cover decreased.

The computer program KENLAYER was used to estimate the effect of the compressible tire chip layer on deflection basins and strains at the base of the pavement. The counterbalancing effect of improved drainage and reduced frost action was then addressed using the AASHTO 1993 design equation for flexible pavements. KENLAYER is a computer program based on the solution for an elastic multilayer system under a circular loaded area. A pavement modulus of 276 MPa (40,000 psi) was needed to obtain a reasonable approximation of the actual MBB field basins. This is very low compared to resilient moduli normally used for pavement analysis. However, the MBB is a static rather than a transient loading test. The static modulus of pavement would be expected to be less than its resilient modulus. The centerline deflections calculated by KENLAYER were similar to field measurements, however, KENLAYER calculated basins that were flatter in slope than the field measurements for the radii up to 2.0 to 2.5 m (6.6 to 8.2 ft) in Sections 2 through 5. KENLAYER closely modeled the

centerline deflection and the slope of the initial portion of the basins in Section 1 and the Control Section.

Tensile strains at the base of the pavement were computed by KENLAYER. The strain in each section was divided by the strain in the Control Section to give normalized strains. Normalized strains ranged from 1.022 in Section 3 to 1.323 in Section 5. Using an empirical formula designed to predict the effect of tensile strain on pavement life, a pavement life ratio was calculated for each section. This ratio is the pavement life of a section divided by the pavement life of the Control Section. This ratio does not consider the benefits provided by improved drainage and reduced frost action, which is discussed in the next paragraph. The lowest ratios were in Section 5 and ranged from 0.20 to 0.40 while the highest ratios were in Section 3 and ranged from 0.88 to 0.93. Thus, Section 3, which has 483 mm (19 in.) of soil cover and 305 mm (12 in.) of tire chips, the increased tensile strain would cause very little loss of pavement life compared to Section 5, which has 330 mm (13 in.) of soil cover and 305 mm (12 in.) of tire chips. In Section 5 the significant effect of tensile strains on pavement life renders this configuration unacceptable for most traffic loadings. Since the deflection basins calculated by KENLAYER displayed less curvature than the field, the actual strains in the field may be greater than that calculated in KENLAYER. Still, the calculated reduction in pavement life gives a qualitative sense of the performance of pavement in tire chip and tire chip/soil mixture sections. This is supported by visual inspection of the road surface, which exhibited minor fatigue cracking in Section 5 within 1 year of construction. Other sections have not yet (through June, 2000) shown visible signs of fatigue.

The AASHTO 1993 design equation for flexible pavement was used to examine the counterbalancing effect that improved drainage and reduced frost heave would have on pavement life. This equation indicated that pavement life could be increased by a factor of 3.7 if the drainage was improved from fair to good and frost heave was eliminated. Thus, the net effect of a tire chip insulation and drainage layer would be beneficial except for thin soil covers over the top of the tire chip layer, such as the 330 mm (13 in.) of soil cover in Section 5.

HWD test results were analyzed with MODCOMP4 to backcalculate the moduli and the nonlinear parameters, K_1 and K_2 , of tire chips and tire chip/soil mixtures. Moduli values for 100% tire chips (Sections 3 through 5) ranged from 1.7 to 3.0 MPa (250 to 440 psi). For 67% tire chips/33% gravel (Section 2) the moduli ranged from 3.7 to 4.5 MPa (530 to 650 psi) and for 33% tire chips/67% gravel (Section 1) they ranged from 11.6 to 16.3 MPa (1680 to 2360 psi). Seasonal variation of moduli in the pavement was evident, with higher moduli in November due to the colder pavement temperature. Moduli of pavement, subbase, and subgrade calculated in MODCOMP4 fall in or near the range of typical values listed in several sources.

12. SUMMARY, CONCLUSIONS, AND RECOMMENDATIONS

12.1 SUMMARY

In the United States 253 million waste tires are discarded annually, with an estimated 850 million scrap tires stockpiled throughout the country (Associated Press, 1996). In Maine alone, there are some 30 to 60 million scrap tires piled up in stockpiles. In 1996, 15 million scrap tires were used in the United States for civil engineering applications including: artificial reefs, breakwaters, lightweight fill, retaining wall backfill, landfill cell daily cover, septic system leach fields, and leachate collection systems (Zimmer, 1996). Tire chips have also been used as subgrade insulation on a gravel surfaced road (Humphrey and Eaton, 1993a, 1993b; Humphrey and Eaton, 1994; Humphrey and Nickels, 1994; Humphrey and Eaton, 1995).

The objectives of this study were to investigate the insulation and drainage qualities of tire chips and tire chip/soil mixtures in the laboratory and a full scale paved field trial. The following tasks were accomplished:

1. A literature review was conducted of laboratory studies and construction projects where tire chips or tire chip/gravel mixtures were used as subgrade insulation or drainage.
2. An apparatus was designed and constructed to measure the apparent thermal conductivity⁷ of tire chips and tire chip/gravel mixtures.

⁷ Apparent thermal conductivity includes the combined effects of heat transfer by conduction and convection (air circulation through the voids) and is the appropriate parameter to use for field calculations of frost penetration.

3. The apparent thermal conductivity of tire chips, gravel, and tire chip/gravel mixtures was measured. The influence of density (or void ratio), moisture content, steel or glass belt content, temperature gradient, and gravel content on the apparent thermal conductivity of tire chips and tire chip/gravel mixtures was investigated.
4. The laboratory thermal conductivity results were compared with the Richmond field trial that was constructed in 1992.
5. The permeability of tire chips and tire chip/gravel mixtures was measured in an apparatus constructed as part of a previous NETC project.
6. A full scale field trial using tire chips and tire chip/gravel mixtures as subgrade insulation and drainage was designed and constructed.
7. The field trial was monitored throughout the winter of 1996-97. The influence of percent tire chips, thickness of gravel cover, and thickness of tire chip or tire chip/gravel layers on maximum frost depth, frost heave, and overall frost behavior was investigated. Thermal conductivity was also calculated from field measurements and compared to laboratory and other field trial values.
8. Pavement deflection basins were measured with a modified Benkelman Beam (MBB), Heavy Weight Deflectometer (HWD), and Falling Weight Deflectometer (FWD). A computer model was used to estimate the tensile strain at the base of the pavement. Deflection basins were also generated by KENLAYER, a computer program based on the solution for an elastic multilayer system under a circular loaded area, and compared to the MBB

deflection basins. Moduli were backcalculated from the results of the HWD tests.

The literature review included a laboratory study of the thermal conductivity of crumb rubber and tire chips performed at the University of Alaska Fairbanks (Shao, et al., 1995). Tire chip thermal conductivities ranged from 0.1227 W/m·°C (0.071 Btu/hr·ft·°F) for unwetted frozen tire chips with low compaction to 0.1707 W/m·°C (0.0988 Btu/hr·ft·°F) for wetted frozen tire chips with high compaction. Other tests were performed in Quebec (Dore, et al., 1995), which showed that the thermal conductivity of tire chips was 0.38 W/m·°C (0.22 Btu/hr·ft·°F).

Three case histories were found in the literature using tire chips as subgrade insulation or drainage. These were a field trial in Richmond, Maine, a test site in Saint-Joachim, Quebec, Canada, and a town highway in Georgia, Vermont. Tire chips were found to significantly reduce the depth of frost penetration and improve drainage. The results of two field trials that examined the effect of tire chips on pavement performance were also reviewed.

A one-sided mode insulated-hot-plate apparatus was built for to measure the thermal conductivity of tire chips. The apparatus uses two steel plates to create parallel isothermal surfaces: a hot plate maintained at a constant temperature by a heater and a cold plate at room temperature which acted as a heat sink. Tire chips or tire chip/gravel mixtures were placed between these two plates. Under steady state heat flow, a constant heat flux was created across the sample. A second heater and two backflow plates were used beneath the hot plate to force the heat introduced at the hot plate to go through the

test sample. This was done by adjusting the lower heater to maintain the two backflow plates at the same temperature, resulting in no heat exchange between these two plates. The dimensions of the sample were 0.9 m×0.9 m×0.3 m (3 ft×3 ft×1 ft). Three surcharges were used to simulate compression of the sample under the weight of overlying soil and pavement: none, 9 kPa (188 psf), and 18 kPa (375 psf). By measuring the energy input at the hot plate, the temperatures at the top and bottom of the sample, and the sample thickness, the apparent thermal conductivity of the sample was computed.

Five types of tire chips were tested: F&B steel belted, F&B glass belted, Palmer steel belted, Pine State steel belted, and Sawyer with partial removal of steel belts. Six tire chip/gravel mixtures were tested. They are 33% tire chip/67% gravel mixture and 67% tire chip/33% gravel mixture for F&B glass belted chips, F&B steel belted chips and Palmer chips. The mixture ratios were based on volume. Each of the preceding samples was tested under air-dried conditions. In addition, five tire chip and tire chip/gravel mixtures were tested at water contents typical of field conditions. The apparent thermal conductivity of the air-dried and moist gravel was also tested.

The test results for air dried samples show that the apparent thermal conductivity (K) of gravel increases from 0.522 to 0.608 W/m·°C (0.302 to 0.352 Btu/hr·ft·°F) as the dry density (ρ) increases from 1.88 to 1.97 Mg/m³ (118 to 123 pcf). For tire chips, the overall results show that the K of steel belted tire chips decreases from about 0.32 to 0.20 W/m·°C (0.18 to 0.11 Btu/hr·ft·°F) as the ρ increases from 0.58 to 0.79 Mg/m³ (36.0 to 49.6 pcf). The K of glass belted tire chips decreases slightly from about 0.21 to 0.20 W/m·°C (0.12 to 0.11 Btu/hr·ft·°F) as the ρ increases from 0.62 to 0.73 Mg/m³ (38.5 to

45.4 pcf). The pattern of K versus ρ for a given test on tire chip/gravel mixtures is similar to that of tire chips. The K of the mixtures falls between that of gravel and tire chips. The K of tire chip/gravel mixtures increases as the percent gravel in the mixture increases.

Moisture increased the thermal conductivity of gravel by a factor of about 2.5. However, for steel belted tire chips, the effect was small with moisture increasing the thermal conductivity by between 0.01 and 0.05 W/m·°C (0.006 and 0.03 Btu/hr·ft·°F). Overall, the results for air dried and moist steel belted chips fell in the same range. The effect was larger for F&B glass belted chips with moisture increasing the thermal conductivity to the approximate range for steel belted chips, thereby, negating the insulating advantage shown by air-dried glass belted chips.

The influence of temperature gradient was investigated for Pine State tire chips under full surcharge. The apparent thermal conductivity increased from 0.161 to 0.226 W/m·°C (0.093 to 0.131 Btu/hr·ft·°F) as the temperature gradient increased from 22.3 to 68.5°C/m (12.2 to 37.6°F/ft). Thus, the temperature gradient used in the laboratory tests should be the same as anticipated in the field or a correction should be made for the difference between the laboratory and field temperature gradient.

Thermal conductivity of Pine State tire chips were estimated from the results of the Richmond field trial using a steady state heat transfer method and confirmed by the Modified Berggren equation (Aldrich, 1956). The procedure was to estimate the K of tire chips based on an estimated K of the underlying gravel and the $K_{\text{tire-chip}}/K_{\text{gravel}}$ ratio which was backcalculated from subsurface temperature measurements. The estimated

$K_{\text{tire-chip}}$ was then used to calculate the frost penetration depth using the modified Berggren equation. The difference between the steady state and modified Berggren methods is that the latter considers the effect of volumetric heat of the soils and latent heat of fusion of the water as the frost penetrates into the ground. The backcalculated $K_{\text{tire-chip}}$ was $0.20 \text{ W/m}\cdot\text{C}$ ($0.12 \text{ Btu/hr}\cdot\text{ft}\cdot\text{F}$), which is slightly higher than the value measured in the laboratory. The frost penetration depths calculated using $K_{\text{tire-chip}} = 0.20 \text{ W/m}\cdot\text{C}$ ($0.12 \text{ Btu/hr}\cdot\text{ft}\cdot\text{F}$) in the modified Berggren method were close to the measured values.

Permeabilities of tire chips, tire chip/gravel mixtures, and gravel were found using a constant head apparatus. A vertical stress was applied to simulate compression of the sample under the weight of overlying material. For the tire chip samples, Palmer chips showed the highest permeability, ranging from 26.3 cm/s for an uncompressed sample to 6.5 cm/s for a compressed sample. F&B glass belted chips showed the lowest permeability, ranging from 7.6 cm/s for an uncompressed sample to 1.5 cm/s for a compressed sample. Compression decreased the permeability by less than one order of magnitude. The permeability of tire chips, even when compressed, is greater than most drainage aggregate used in construction applications. There was a significant trend of decreasing permeability with increasing percentage of gravel. The permeability of a mixture of 33% Palmer chips/67% gravel was more than four orders of magnitude less than for 100% Palmer chips. For comparison, the Federal Highway Administration (FHWA) recommends a minimum permeability of 0.35 cm/s (FHWA, 1990). A study conducted for MDOT found that the in-situ permeability of subbase aggregate at six sites ranged from 6×10^{-6} to $1.7 \times 10^{-2} \text{ cm/s}$ (Manion, et al., 1995).

A full scale field trial using tire chips and tire chip/gravel mixtures as subgrade insulation and drainage layer beneath a paved road was constructed at the University of Maine in the fall of 1996. Five 12.2-m (40-ft) long test sections were designed, three containing tire chips, one containing 67% tire chips/33% gravel, and one containing 33% tire chips/67% gravel. Soil cover was either 330 mm (13 in.) or 483 mm (19 in.) and tire chip and tire chip/gravel mixture layers were either 152 mm (6 in.) or 305 mm (12 in.) thick. Tire chip and tire chip/gravel mixtures were enclosed with geotextile. A 12.2-m (40-ft) long Control Section containing 635 mm (25 in.) of gravel was also constructed. All sections were overlain with 127 mm (5 in.) of bituminous pavement. A 1.07-m (3.5-ft) deep edge drain was constructed on the left side of the road. Ninety-six thermocouples, ten settlement plates, two benchmarks, and three piezometers were installed. Compression of the tire chips due to the weight of the overlying soil and pavement ranged from 11.9 to 17.8 percent. The 67% tire chip/33% gravel and 33% tire chip/67% gravel layers experienced 12.9 and 7.6 percent compression, respectively.

Subsurface and air temperatures were recorded at the site for the winter of 1996-97. Based on the on-site air temperatures, the freezing index was 35% warmer than an average winter. Tire chips reduced frost penetration up to 47%. Mixtures of 67% tire chips/33% gravel and 33% tire chips/67% gravel reduced frost penetration by 22% and 7%, respectively. Temperatures in the subgrade below the tire chip and tire chip/soil layers were higher than those in the Control Section and temperatures in the gravel above tire chip and tire chip/soil layers were lower than those in the Control Section. This shows that tire chips and tire chip/soil mixtures were effective in providing insulation to

restrict heat flow from the subgrade. Subgrade temperatures increased with an increase in percent tire chips and an increase in tire chip thickness.

Frost heave was reduced by up to 74% in tire chip sections and by 23% in the 67% tire chip/33% gravel section. Frost heave was essentially the same in the 33% tire chip/67% gravel section as in the Control. For all the sections, heave was greater on the outside wheel ruts than on the inside wheel ruts. This is probably due to the inside locations being surrounded by tire chips or tire chip/soil mixtures, while the outside wheel paths were bordered by the higher K natural ground which allowed some frost penetration under the edge of the road. More infiltration on the outside edges may also have contributed to increased heave.

Steady state and non-steady heat flow equations were used to estimate the thermal conductivity of tire chip and tire chip/soil mixtures from field temperature measurements. The backcalculated K in the sections with 100% tire chips ranged from 0.16 W/m²·°C (0.09 Btu/hr·ft²·°F) to 0.18 W/m²·°C (0.10 Btu/hr·ft²·°F). In Section 2, with 305 mm (12 in.) of 67% tire chips/33% gravel, the K was 0.21 W/m²·°C (0.12 Btu/hr·ft²·°F) while in Section 1, with 305 mm (12 in.) of 33% tire chips/67% gravel, the K was 0.54 W/m²·°C (0.31 Btu/hr·ft²·°F). Laboratory and field backcalculated thermal conductivities were compared. The laboratory values were greater than the field values by between 28% and 44% in the sections with 100% tire chips. Tire chip/soil mixtures showed greater differences: 95% in Section 2 and 56% in Section 1. The differences may be due to differences between field and lab moisture contents or densities, different particle arrangement that lead to altered heat transfer by conduction or convection, laboratory test

methods, assumptions made in backcalculating K or, for Sections 1 and 2, differences between percent gravel in the laboratory tests and used in the field.

Pavement deflections were measured in April and August of 1997 with a Modified Benkelman Beam (MBB), two sets of Heavy Weight Deflectometer (HWD) tests (November 1996 and April 1997), and a Falling Weight Deflectometer (FWD) test (August 1997). August pavement deflections measured by the MBB were significantly higher than April deflections in Sections 3 and 5, which both have 305-mm (12-in.) thick tire chip layers. The MBB deflection basins for section with tire chip/soil mixtures, 152-mm (6-in.) tire chip layer, and the Control were about the same in April and August. A possible explanation is that the colder, and therefore stiffer, pavement in April combined with the good drainage provided by the tire chips in Sections 3 and 5 resulted in lower deflections in April. Overall, MBB deflection basins responded as expected, with the centerline deflection and radius of the deflection basin increasing as the percentage of tire chips increased and/or the amount of soil cover decreased.

The computer program KENLAYER was used to estimate the effect of the compressible tire chip layer on deflection basins and strains at the base of the pavement. The counterbalancing effect of improved drainage and reduced frost action was then addressed using the AASHTO 1993 design equation for flexible pavements. KENLAYER is a computer program based on the solution for an elastic multilayer system under a circular loaded area. A pavement modulus of 276 MPa (40,000 psi) was needed to obtain a reasonable approximation of the actual MBB field basins. This is very low compared to resilient moduli normally used for pavement analysis. However, the MBB is a static rather than a transient loading test. The static modulus of pavement

would be expected to be less than its resilient modulus. The centerline deflections calculated by KENLAYER were similar to field measurements, however, KENLAYER calculated basins that were flatter in slope than the field measurements for the radii up to 2.0 to 2.5 m (6.6 to 8.2 ft) in Sections 2 through 5. KENLAYER closely modeled the centerline deflection and the slope of the initial portion of the basins in Section 1 and the Control Section.

Tensile strains at the base of the pavement were computed by KENLAYER. The strain in each section was divided by the strain in the Control Section to give normalized strains. Normalized strains ranged from 1.022 in Section 3 to 1.323 in Section 5. Using an empirical formula designed to predict the effect of tensile strain on pavement life, a pavement life ratio was calculated for each section. This ratio is the pavement life of a section divided by the pavement life of the Control Section. This ratio does not consider the benefits provided by improved drainage and reduced frost action, which is discussed in the next paragraph. The lowest ratios were in Section 5 and ranged from 0.20 to 0.40 while the highest ratios were in Section 3 and ranged from 0.88 to 0.93. Thus, Section 3, which has 483 mm (19 in.) of soil cover and 305 mm (12 in.) of tire chips, the increased tensile strain would cause very little loss of pavement life compared to Section 5, which has 330 mm (13 in.) of soil cover and 305 mm (12 in.) of tire chips. In Section 5 the significant effect of tensile strains on pavement life renders this configuration unacceptable for most traffic loadings. Since the deflection basins calculated by KENLAYER displayed less curvature than the field, the actual strains in the field may be greater than that calculated in KENLAYER. Still, the calculated reduction in pavement life gives a qualitative sense of the performance of pavement in tire chip and tire chip/soil

mixture sections. This is supported by visual inspection of the road surface, which exhibited minor fatigue cracking in Section 5 within 1 year of construction. Other sections have not yet (through June, 2000) shown visible signs of fatigue.

The AASHTO 1993 design equation for flexible pavement was used to examine the counterbalancing effect that improved drainage and reduced frost heave would have on pavement life. This equation indicated that pavement life could be increased by a factor of 3.7 if the drainage was improved from fair to good and frost heave was eliminated. Thus, the net effect of a tire chip insulation and drainage layer would be beneficial except for thin soil covers over the top of the tire chip layer, such as the 330 mm (13 in.) of soil cover in Section 5.

HWD test results were analyzed with MODCOMP4 to backcalculate the moduli and the nonlinear parameters, K_1 and K_2 , of tire chips and tire chip/soil mixtures. Moduli values for 100% tire chips (Sections 3 through 5) ranged from 1.7 to 3.0 MPa (250 to 440 psi). For 67% tire chips/33% gravel (Section 2) the moduli ranged from 3.7 to 4.5 MPa (530 to 650 psi) and for 33% tire chips/67% gravel (Section 1) they ranged from 11.6 to 16.3 MPa (1680 to 2360 psi). Seasonal variation of moduli in the pavement was evident, with higher moduli in November due to the colder pavement temperature. Moduli of pavement, subbase, and subgrade calculated in MODCOMP4 fall in or near the range of typical values listed in several sources.

12.2 CONCLUSIONS

12.2.1 Thermal conductivity of tire chips

1. The apparent thermal conductivity of air dried tire chips varies from about 0.20 to 0.32 W/m·°C (0.11 to 0.18 Btu/hr·ft·°F), and that of air dried gravel varies from about 0.51 to 0.60 W/m·°C (0.30 to 0.35 Btu/hr·ft·°F). The apparent thermal conductivity of air dried tire chip/gravel mixtures were between that of tire chips and gravel: 0.37 to 0.58 W/m·°C (0.21 to 0.34 Btu/hr·ft·°F) for 33% tire chip/67% gravel mixtures, and 0.30 to 0.51 W/m·°C (0.17 to 0.29 Btu/hr·ft·°F) for 67% tire chip/33% gravel mixtures. The thermal conductivity increases as the percent gravel in the mixture increases.
2. The apparent thermal conductivity of air dried gravel increases as the density increases. The K of gravel increases about 18%, from 0.51 to 0.60 W/m·°C (0.30 to 0.35 Btu/hr·ft·°F), as the density increases only 5%, from 1.88 to 1.97 Mg/m³ (117.6 to 123.0 pcf). This is probably caused by the decrease of the volume of air voids as the density increases.
3. There is an overall trend that the apparent thermal conductivity of tire chips decreases as density increases. For steel belted tire chips, the apparent thermal conductivity decreases from about 0.32 to 0.20 W/m·°C (0.18 to 0.11 Btu/hr·ft·°F) as the dry density increases from 0.58 to 0.79 Mg/m³ (36.0 to 49.6 pcf). This corresponds to K decreasing by about 38% as dry density increases by 20%. The K of glass belted tire chips also decreases as the density increases. However, it is much less significant than for steel belted chips.

4. The effect of water content on the K of tire chips is small. Increasing the water content from air dried to 5% increased K by less than $0.05 \text{ W/m}\cdot\text{C}$ ($0.03 \text{ Btu/hr}\cdot\text{ft}\cdot\text{F}$). Water content has a larger effect on the K of gravel and tire chip/gravel mixtures.
5. Air dried tire chips with steel belts have higher apparent thermal conductivity than tire chips with glass belts. Comparing F&B steel belted chips with F&B glass belted chips, the K of the glass belted chips is about 14% lower than the K of the steel belted chips at the same density. The reason is because glass fabric has a much lower thermal conductivity than steel belt. However, the K of moist steel belted and glass belted tire chips is about the same.
6. The apparent thermal conductivity of tire chips increases as the temperature gradient increases. The K of tire chips increases by about 40% from 0.16 to $0.23 \text{ W/m}\cdot\text{C}$ (0.09 to $0.13 \text{ Btu/hr}\cdot\text{ft}\cdot\text{F}$) as the temperature gradient increases from 22.3 to 68.5C/m (12.22 to 37.6F/ft). A possible reason is an increase in the free heat convection within the sample as the temperature gradient increases.

12.2.2 Permeability of tire chips

1. The permeability of tire chips, even when compressed under the weight of simulated overburden, is greater than 1 cm/s . However, the permeability of tire chip/gravel mixtures decreases significantly with increasing percentage of gravel. Adding 33% gravel decreases the permeability by a factor of 10 to 20 and 67% gravel decreases the permeability by 3 to 4 orders of magnitude.

Thus, tire chip/gravel mixtures should not be used in applications where very high permeability is desired.

12.2.3 Field performance of tire shreds

1. Tire chips are effective in limiting the depth of frost penetration beneath paved roads. The maximum depth of frost penetration was reduced by up to 47% in tire chip sections. A mixture of 67% tire chips/33% gravel reduced frost penetration by 22% and a mixture of 33% tire chips/67% gravel reduced frost penetration by 7%. Overall, frost penetration decreased with increasing percent tire chips, increasing thickness of tire chips, or decreasing thickness of soil cover.
2. Tire chip layers are effective in reducing frost heave beneath paved roads. In sections with 100% tire chips, heave was reduced by up to 74%. However, frost heave was reduced by only 23% in the 67% tire chip/33% gravel section. Frost heave was essentially the same in the 33% tire chips/67% gravel section as in the Control Section. Thus, there would be no benefit to use 33% tire chips/67% gravel to reduce frost heave.
3. The thermal conductivity of tire chips backcalculated from the Richmond field trial was about 0.20 W/m·°C (0.12 Btu/hr·ft·°F). This value agrees well with the laboratory results of 0.22 to 0.29 W/m·°C (0.13 to 0.17 Btu/hr·ft·°F) for the same type of tire chips. The difference between these values can be explained by the conditions in the laboratory tests not exactly duplicating field conditions and small differences between assumptions made in the backcalculation and actual field conditions.

4. The thermal conductivity of tire chips backcalculated from the Witter Farm Road field trial varied from 0.16 W/m·°C (0.09 Btu/hr-ft·°F) to 0.18 W/m·°C (0.10 Btu/hr-ft·°F). The backcalculated K of the 67% tire chip/33% gravel mixture was 0.21 W/m·°C (0.12 Btu/hr-ft·°F) and that of 33% tire chips/67% gravel was 0.54 W/m·°C (0.31 Btu/hr-ft·°F).
5. The laboratory values of K for tire chips and tire chip/soil mixtures were equal to or greater than the values backcalculated from the Richmond and Witter Farm field trials. Thus, use of the laboratory K would give conservative estimates of frost depth for both tire chips and tire chip/soil mixtures.
6. The deflection basin radius increased from 0.75 m for the control section to 3.25 m for Section 5, which had 330 mm (13 in.) of gravel over 305 mm (12 in.) of tire chips. Overall, the radius of the deflection basin increased as the percentage of tire chips increased and as the thickness of soil cover decreased.
7. The average moduli of the three tire chip sections calculated by MODCOMP4 was 2.8 MPa (406 psi) in November and 2.1 MPa (305 psi) in April.
8. The modulus of the 67% tire chip/33% gravel section was 3.7 MPa (530 psi) in November and 4.5 MPa (650 psi) in April. The modulus of 33% tire chips/67% gravel was 16.3 MPa (2360 psi) in November and 11.6 MPa (1680 psi) in April. Therefore, the 67% tire chip/33% gravel mixture showed a marginal increase in modulus over tire chips, while the 33% tire chip/67% gravel mixture modulus was more than 5 times greater than that of tire chips.

12.3 DESIGN RECOMMENDATIONS

The material properties listed in Table 12.1 are recommended for design of tire chip insulation/drainage layers. The recommended properties were chosen based on a conservative interpretation of the results of the laboratory and field study. These recommendations are applicable to tire chips and gravel with gradations similar to those tested in this study. Thus, Table 12.1 is applicable to tire chips with 100% passing a 75-mm (3-in.) sieve and, when mixed with gravel, the gravel is assumed to will be a well-graded mixture of gravel and sand with less than 7% passing the No. 200 (0.075 mm) sieve.

Table 12.1 Tire chip properties recommended for design.

Property	100% tire chips	67% tire chips/33% gravel	33% tire chips/67% gravel
Thermal conductivity	0.32 W/m·°C (0.18 Btu/hr-ft·°F)	0.51 W/m·°C (0.29 Btu/hr-ft·°F)	1.0 W/m·°C* (0.60 Btu/hr-ft·°F)
Permeability	1.0 cm/s	0.1 cm/s	0.0005 cm/s*

*Not recommended for insulation or drainage applications.

When used for insulation, it is recommended that the modified Berggren method be used to calculate the required thickness of the insulation layer (see example calculation on pages 131 to 134). For preliminary design of an insulation layer with 100% tire chips, a 300 mm (12 in.) thick tire chip layer should be assumed in Maine, New Hampshire, Vermont, and western Massachusetts. For the remainder of New England a 150-mm (6-in.) thick layer should be assumed. When used for drainage, the tire chip layer thickness should be a minimum of 150 mm (6 in.) to facilitate construction.

The thickness of the overlying pavement and base/subbase course should be based on local practice or AASHTO 1993 design procedures for flexible pavement used with the anticipated traffic loading (ESALs), and the resilient modulus of subgrade soils in the area. The results of this research suggest that the benefits of improved drainage and reduced frost heave could allow for overlying base/subbase course thicknesses as low as 480 mm (19 in.), however, at this time it is recommended that the base/subbase course should be at least 600 mm (24 in.) thick. Moreover, it is recommended that the initial applications of tire chips as insulation/drainage layers beneath state highways be limited to projects with annual average daily traffic counts (AADT) less than about 6000. As additional experience is gained it may be possible to extend this application to higher traffic loadings.

The tire chip layer should be completely enclosed in geotextile to minimize the infiltration of soil into the chips over time. If possible, the tire chip layer should be allowed to settle for about 30 days after placement of the overlying base/subbase course prior to final grading and paving.

12.4 RECOMMENDATIONS FOR FURTHER RESEARCH

The University of Maine field trial should be monitored for an additional winter to compare backcalculated thermal conductivities from two winters. An attempt should also be made to find a program which would more accurately model tire chip and tire chip/soil deflection basins, whether that means working with KENLAYER or using another program.

13. REFERENCES

- AASHTO (1986), Standard Specifications for Transportation Materials and Methods of Sampling and Testing, Part II: Methods of Sampling and Testing, 14th ed., American Association of State Highway and Transportation Officials, Washington, DC., pp. 1275.
- Ahmed, I. (1993), "Laboratory Study on Properties of Rubber Soils," FHWA/IN/JHRP-93/4, Purdue University, West Lafayette, Indiana, 47907, 348 pp. + appendices.
- Ahmed, I., and Lovell, C.W. (1993), "Rubber Soils as Lightweight Geomaterial," Transportation Research Record, No. 1422, pp. 61-70.
- Aldrich, H.P., Jr. (1956), "Frost Penetration Below Highway and Airfield Pavements," Highway Research Board Bulletin 135, National Academy of Sciences, National Research Council, Washington, pp. 124-149.
- ALGOR (1989), ALGOR Reference Manual, Pittsburgh, Pennsylvania.
- Andersland, O.B., and Ladanyi, B. (1994), An Introduction to Frozen Ground Engineering, Thomson Publishing Company, New York, NY, p. 53.
- Associated Press (1996), "A Big Pile of Tires is a Huge Problem in a Small State," 21 Sept., 1996, p. 2.
- ASTM (1992), "C1044-90, Standard Practice for Using the Guarded-Hot-Plate Apparatus in the One-Sided Mode to Measure Steady-State Heat Flux and Thermal Transmission Properties," Annual Book of ASTM Standards, American Society for Testing and Materials, Philadelphia, PA, Vol. 04.06, pp. 534-536.
- ASTM (1992), "C168-90, Standard Terminology Relating to Thermal Insulating Materials," Annual Book of ASTM Standards, American Society for Testing and Materials, Philadelphia, PA, Vol. 04.06, pp. 14-19.
- ASTM (1992), "C177-85, Standard Test Method for Steady-State Heat Flux Measurements and Thermal Transmission Properties by Means of the Guarded-Hot-Plate," Annual Book of ASTM Standards, American Society for Testing and Materials, Philadelphia, PA, Vol. 04.06, pp. 20-31.
- ASTM (1992), "C518-91, Standard Test method for Steady-State Heat Flux Measurement and Thermal Transmission Properties by Means of the Heat Flow Meter Apparatus," Annual Book of ASTM Standards, American Society for Testing and Materials, Philadelphia, PA, Vol. 04.06, pp. 153-164.
- Benda, C.C. (1995), "Engineering Properties of Scrap Tires Used in Geotechnical Applications," Report 95-1, Materials and Research Division, Vermont Agency of Transportation, Montpelier, Vermont.
- Benson, C. H., Olson, M. A., and Bergstrom, W. R. (1996), "Temperatures of an Insulated Landfill Liner," preprint for Transportation Research Board 75th Annual Meeting, Washington D.C., 15 pp.

- Bigelow, N., Jr. (1969), "Freezing Index Maps of Maine," Technical Paper 69-5R, Materials and Research Division, Maine State Highway Commission, Augusta, Maine.
- Bowles, J.E. (1996), Foundation Analysis and Design, McGraw-Hill, Inc., p.125.
- Bressette, T. (1984), "Used Tire Material as an Alternative Permeable Aggregate," Report No. FHWA/CA/TL-84/07, Office of Transportation Laboratory, California.
- Brownell, D. L. (1989), "Part 2: Thermophysical Properties of Selected Engineering Materials," Handbook of Applied Thermal Design, C. Eric and D. L. Brownell, eds., New York, NY, pp. 2-1 to 2-12.
- Chamberlain, E.J. (1981), "Frost Susceptibility of Soil - Review of Index Tests," U.S. Army Cold Regions Research and Engineering Laboratory, Monograph 81-2, December, 121 pp.
- Coduto, D.P. (1994), Foundation Design: Principles and Practices, Prentice-Hall, Inc., Englewood Cliffs, NJ, p. 63.
- Columbia University Press (1995), The Concise Columbia Encyclopedia, New York.
- Cosentino, P.J., and Briaud, J.-L. (1989), "FWD Backcalculated Moduli Compared with Pavement Pressuremeter Moduli and Cyclic Triaxial Moduli," Nondestructive Testing of Pavements and Backcalculation of Moduli, ASTM Special Technical Publication 1026, ASTM, Philadelphia, PA, pp. 323-340.
- Cosgrove, T.A. (1995), "Interface Shear Strength Between Tire Chips and Geomembrane for Use as a Drainage Layer in a Landfill Cover," Geosynthetics'95, Industrial Fabrics Association, St. Paul, Minnesota, Vol. 3, pp. 1157-1168.
- Cosgrove, T.A. (1998), "Field Trials Using Tire Shreds as Bridge Abutment Backfill," M.S. Thesis, University of Maine, Orono, ME.
- Dore, G., Konrad, J.M., Roy, M., and Rioux, N. (1995), "The Use of Alternative Materials in Pavement Frost Protection: Material Characteristics and Performance Modeling," Transportation Research Record No. 1481, Transportation Research Board, Washington, D.C., pp. 63-74.
- Edil, T.B., and Bosscher, P.J. (1992), "Development of Engineering Criteria for Shredded or Whole Tires in Highway Applications," Report No. WI 14-92, Department of Civil and Environmental Engineering, University of Wisconsin, Madison, Wisconsin, November.
- Edil, T.B., and Bosscher, P.J. (1994), "Engineering Properties of Tire Chips and Soil Mixtures," Geotechnical Testing Journal, Vol. 17, No. 4, December, pp. 453-464.
- Eldin, N.N., and Senouci, A.B. (1992), "Use of Scrap Tires in Road Construction," Journal of Construction Engineering and Management, ASCE, Vol. 118, No. 3, Sept. 1992, pp. 561-576.
- EPA (1993), "State Scrap Tire Programs: A Quick Reference Guide," EPA 530-B-93-001, US Environmental Protection Agency, Washington D.C., April, 53 pp.

- EPA (1991), "Summary of Markets for Scrap Tires," Report No. EPA/530-SW-90-0748B, US Environmental Protection Agency, Washington D.C., pp. 1-12.
- FHWA (1990), "Technical Guide Paper on Subsurface Pavement Drainage," Technical Paper 90-01, Federal Highway Administration, Office of Engineering, Pavement Division, Washington, D.C.
- Frascoia, R.I., and Cauley, R.F. (1995), "Tire Chips in the Base Course of a Local Road," Proceedings of the Sixth International Conference on Low-Volume Roads, Vol. 2, Transportation Research Board, Washington, D.C., pp. 47-52.
- Gebhart, B. (1961), Heat Transfer, McGraw-Hill, New York, NY, pp. 251-282.
- Geisler, E., Cody, W.K., and Niemi, M.K. (1989), "Tires for Subgrade Support," Annual Conference on Forest Engineering, Coeur D'Alene, ID, 5 pp.
- Gharegrat, H. (1993), "Finite Element Analysis of Pavements Underlain by a Tire Chip Layer and of Retaining Walls with Tire Chip Backfill," M.S. Thesis, Department of Civil Engineering, University of Maine, Orono, Maine, 222 pp.
- Gilman, G.D. (1964), "The Freezing Index in New England," Special Report 63, U.S. Army Engineer Cold Regions Research and Engineering Laboratory, Hanover, N.H.
- Hall, T.J. (1990), "Reuse of Shredded Waste Tire Material for Leachate Collection Systems at Municipal Solid Waste Landfills," for Iowa Department of Natural Resources Waste Management and Authority Division, by Shive-Hattery Engineers and Architects, Inc.
- Holtz, R.D., and Kovacs, W.D. (1981), An Introduction to Geotechnical Engineering, Prentice-Hall, Englewood Cliffs, New Jersey.
- Huang, Y.H. (1993), "Kenlayer Computer Program," Chapter 3 in Pavement Analysis and Design, Prentice-Hall, Inc., Englewood Cliffs, NJ, pp. 100-167.
- Humphrey, D.N. (1996), "Tire Chips – A New Road-Building Geomaterial," TR News, No. 184, May-June, pp. 17.
- Humphrey, D.N., Cosgrove, T., Whetten, N.L., and Hebert, R. (1997), "Tire Chips Reduce Lateral Earth Pressure Against the Walls of a Rigid Frame Bridge," Proceedings of the Conference on Renewal, Rehabilitation and Upgrades in Civil and Environmental Engineering, 1997 Maine Section ASCE Technical Seminar, 11 pp.
- Humphrey, D.N., and Eaton, R.A. (1993a), "Tire Chips as Insulation Beneath Gravel Surfaced Roads," Proceedings of the International Symposium on Frost in Geotechnical Engineering, Anchorage, Alaska, A.A. Balkema Publishers, Rotterdam, Netherlands, pp. 137-149.
- Humphrey, D.N., and Eaton, R.A. (1993b), "Tire Chips as Subgrade Insulation - Field Trial," Proceedings of the Symposium on Recovery and Effective Reuse of Discarded Materials and By-Products for Construction of Highway Facilities, Federal Highway Administration, Washington, D.C., pp. 5-55 to 5-68.

- Humphrey, D.N., and Eaton, R.A. (1994), "Performance of Tire Chips as an Insulating Layer Beneath Gravel Surface Roads," Proceedings of the Fourth International Symposium on Cold Region Development, Espoo, Finland, pp. 125-126.
- Humphrey, D.N., and Eaton, R.A. (1995), "Field Performance of Tire Chips as Subgrade Insulation for Rural Roads," Proceedings of the Sixth International Conference on Low-Volume Roads, Transportation Research Board, Washington, D.C., Vol. 2, pp. 77-86.
- Humphrey, D.N., Katz, L.E., and Blumenthal, M. (1997), "Water Quality Effects of Tire Chip Fills Placed Above the Groundwater Table," Testing Soil Mixed with Waste or Recycled Materials, ASTM STP 1275, Mark A. Wasemiller and Keith B. Hoddinott, Eds., American Society for Testing and Materials, pp. 299-313.
- Humphrey, D.N., and Manion, W.P. (1992), "Properties of Tire Chips for Lightweight Fill," Proceedings of the Conference on Grouting, Soil Improvement, and Geosynthetics, ASCE, New Orleans, Louisiana, Vol. 2, pp. 1344-1355.
- Humphrey, D.N., and Nickels, W.L., Jr. (1994), "Tire Chips as Subgrade Insulation and Lightweight Fill," Proceedings of the 18th Annual Meeting of the Asphalt Recycling and Reclaiming Association, Asphalt Recycling and Reclaiming Association, Annapolis, Maryland, pp. 83-105.
- Humphrey, D.N., and Nickels, W.L., Jr. (1997), "Effect of Tire Chips as Lightweight Fill on Pavement Performance," Proceedings of the Fourteenth International Conference on Soil Mechanics and Foundation Engineering, Balkema, Vol. 3, pp. 1617-1620.
- Humphrey, D.N., and Sandford, T.C. (1993), "Tire Chips as Lightweight Subgrade Fill and Retaining Wall Backfill," Proceedings of the Symposium on Recovery and Effective Reuse of Discarded Materials and By-Products for Construction of Highway Facilities, Federal Highway Administration, Washington, D.C., pp. 5-87 to 5-99.
- Humphrey, D.N., Sandford, T.C., Cribbs, M.M., Gharegrat, H.G., and Manion, W.P. (1992), "Tire Chips as Lightweight Backfill for Retaining Walls - Phase I," A Study for the New England Transportation Consortium, Department of Civil Engineering, University of Maine, Orono, Maine, 137 pp. + appendices.
- Humphrey, D.N., Sandford, T.C., Cribbs, M.M., and Manion, W.P. (1993), "Shear Strength and Compressibility of Tire Chips for Use as Retaining Wall Backfill," Transportation Research Record No. 1422, Transportation Research Board, Washington, D.C., pp. 29-35.
- Irwin, L.H. (1994), Instructional Guide for Back-Calculation and the Use of MODCOMP3 (Version 3.6), CLRP Publication No. 94-10, Cornell University Local Roads Program, 55 pp.
- Irwin, L.H. (1997), MODCOMP4, Version 4.0C, Computer Program, Cornell University Local Roads Program.
- Jumikis, A.R. (1977), "Physical Properties of Unfrozen Soils," Thermal Geotechnics, Rutgers University Press, New Brunswick, NJ, pp. 61-105.

- Kersten, M.S. (1949), "Thermal Properties of Soils," Bulletin No. 28, Engineering Experiment Station, University of Minnesota, 225 pp.
- Kreith F., and Dreider, J.F. (1978), Principles of Solar Engineering. Hemisphere Publishing Corporation, WA, 778 pp.
- Linell, K.A. (1953), "Frost Design Criteria for Pavements," Highway Research Board, Washington, D.C., Bulletin 71.
- Maine Department of Environmental Protection (DEP) (1989), Bureau of Solid Waste Management, report to Maine State Legislature on Tires, White Goods and Demolition Debris, May.
- Manion, W.P., and Humphrey, D.N. (1992), "Use of Tire Chips as Lightweight and Conventional Embankment Fill, Phase I - Laboratory," Technical Paper 91-1, Technical Services Division, Maine Department of Transportation, May, 186 pp.
- Manion, W.P., Humphrey, D.N., and Garder, P.(1995), "Evaluation of Existing Aggregate Base Drainage Performance," Technical Paper 94-2, Technical Services Division, Maine Department of Transportation, Augusta, Maine, 56 pp.
- McQuinston, F.C., and Parker, J.D. (1977), Heating, Ventilating, and Air Conditioning Analysis and Design. John Wiley & Sons, pp. 140-181.
- Nickels, W.L., Jr. (1995), "The Effect of Tire Chips as Subgrade Fill on Paved Roads," M.S. Thesis, Department of Civil and Environmental Engineering, University of Maine, Orono, Maine, 215 pp.
- Peavy, B., and Rennex, B. (1986), "Circular and Square Edge Effect Study for Guarded-Hot-Plate and Heat-Flow-Meter Apparatus," Journal of Thermal Insulation, Vol. 9, pp. 254-300.
- Rioux, N. (1994) "Etude Comparative de Materiaux Pour Fins de Protection Contre le Gel Incorporant la Reutilisation de Pneus," Communication presentee au Congres 1994 de l'IRF, Calgary (Alberta), Canada, pp. A105-A128.
- Ryan, J.V. (1990), "Characterization of Emissions from the Simulated Open Burning of Scrap Tires," U.S. Environmental Protection Agency, Air and Energy Engineering Research Laboratory, Research Triangle Park, North Carolina.
- Scrap Tire News (1997), "A New Generation of Materials Use," Scrap Tire News, Vol.11, No. 8, August, pp. 1-3.
- Shao, J., Zarling, J. P., and Esch, D. (1995), "Thermal Conductivity of Recycled Tire Rubber for Insulation Beneath Roadways", preprint for Transportation Research Board Annual Meeting, Washington, D.C.
- Shook, J.F., Finn, F.N., Witzak, M.W., and Monismith, C.L. (1982), "Thickness Design of Asphalt Pavements-The Asphalt Institute Method," Proceedings, 5th International Conference on the Structural Design of Asphalt Pavements, Vol. 1, pp. 17-44.
- Strawberry Tree Computers, Inc. (1987), Instruction Manual - Analog Connection PC, San Jose, CA, 225 pp.

Strawberry Tree, Inc. (1993), Data Acquisition Systems User Manual, Sunnyvale, CA, 141 pp.

Thompson, M.R. and Elliot, R.P. (1985), "ILLI-PAVE-Based Response Algorithms for Design of Conventional Flexible Pavements, Transportation Research Record 1043, Transportation Research Board, pp. 50-57.

Tweedie, J.J., Humphrey, D.N., and Sandford, T.C. (1998), "Tire Chips as Lightweight Backfill for Retaining Walls - Phase II, Field Trial," A Study for the New England Transportation Consortium, Department of Civil Engineering, University of Maine, Orono, Maine.

Whetten, N.L., Weaver, J., Humphrey, D.N., Sandford, T.C. (1997), "Rubber Meets the Road in Maine," Civil Engineering, Vol. 67, No. 9, September, pp.60-63.

Zimmer, J. (1996), "Scrap Tire Recovery: an Analysis of Alternatives," Texas Scrap Tire Market Development Conference, Texas Natural Resource Conservation Commission, Austin, Texas, pp. 63-87.

APPENDIX A
FWD AND HWD TEST RESULTS

Average Deflections, in Mils,
for All Load Levels for November 1996
Heavy Weight Deflectometer (HWD) Test

Load, lb.	Sensor Spacing, in.						
	0	12	24	36	48	60	
Section 1							
5000	9.581	7.816	5.691	4.083	2.913	2.114	1.531
8100	15.865	13.032	9.523	6.836	4.835	3.489	2.530
10819	21.153	17.472	12.786	9.168	6.492	4.630	3.381
14127	27.717	22.944	16.820	12.035	8.453	6.005	4.376
Section 2							
4839	14.051	12.372	10.044	8.007	6.324	5.016	3.983
7894	22.738	20.018	16.194	12.870	10.016	7.838	6.163
10466	29.903	26.460	21.411	16.968	13.149	10.224	7.975
13659	38.716	34.219	27.646	21.860	16.845	12.994	10.089
Section 3							
5000	14.293	12.585	10.386	8.524	7.011	5.776	4.766
8147	23.962	21.176	17.493	14.392	11.748	9.687	8.005
10749	31.684	28.112	23.210	19.053	15.502	12.713	10.471
13747	41.226	36.536	30.102	24.625	19.893	16.138	13.190
Section 4							
4703	15.007	13.194	10.723	8.638	6.903	5.542	4.433
7574	24.723	21.708	17.571	14.088	11.115	8.809	7.007
10287	32.890	28.975	23.395	18.685	14.683	11.556	9.169
13473	42.864	37.664	30.326	24.131	18.834	14.702	11.566
Section 5							
4833	17.444	15.858	13.471	11.190	9.203	7.445	6.099
7914	29.417	26.923	22.967	19.290	15.888	13.066	10.731
10518	38.403	35.233	30.010	25.113	20.578	16.818	13.732
13675	49.545	45.374	38.619	32.293	26.378	21.467	17.492
Control							
5091	6.728	5.239	3.505	2.306	1.534	1.103	0.828
8237	11.202	8.774	5.934	3.945	2.645	1.890	1.440
10962	14.895	11.758	8.001	5.328	3.580	2.550	1.951
14206	19.556	15.443	10.559	7.057	4.729	3.343	2.534

1 in. = 25.4 mm
1 lb. = 0.454 kg
1 mil = 0.0254 mm

Average Deflections, in Mils,
for All Load Levels for April 1997
Heavy Weight Deflectometer (HWD) Test

Load, lb.	Sensor Spacing, in.						
	0	12	24	36	48	60	72
Section 1							
4957	11.311	8.909	6.092	4.013	2.680	1.864	1.353
7989	18.422	14.630	10.070	6.677	4.454	3.072	2.235
10750	24.948	19.859	13.698	9.078	6.053	4.146	3.021
15073	35.259	28.043	19.364	12.770	8.441	5.724	4.136
Section 2							
4814	15.850	13.668	10.657	8.051	6.037	4.564	3.523
7804	25.663	22.271	17.393	13.126	9.788	7.343	5.623
10532	34.549	30.050	23.475	17.660	13.080	9.738	7.411
14729	48.162	41.878	32.702	24.478	17.943	13.192	9.917
Section 3							
4827	18.526	15.929	12.592	9.748	7.554	5.832	4.625
7829	30.635	26.635	21.170	16.486	12.835	10.078	7.920
10561	41.027	35.715	28.333	21.975	16.942	13.183	10.268
14725	57.155	49.717	39.388	30.383	23.196	17.759	13.693
Section 4							
4956	20.252	17.310	13.334	9.962	7.437	5.539	4.220
8039	32.915	28.250	21.779	16.299	12.118	9.035	6.830
10774	44.136	37.917	29.240	21.831	16.104	11.929	8.959
14961	61.514	52.673	40.521	30.011	21.919	15.967	11.833
Section 5							
4753	23.605	20.841	16.805	13.059	9.970	7.490	5.797
7715	38.328	34.293	27.786	21.739	16.731	12.870	9.804
10367	50.740	45.411	36.713	28.575	21.730	16.403	12.376
14351	70.153	62.595	50.593	39.229	29.609	22.132	16.550
Control							
4876	7.738	5.933	3.877	2.415	1.533	1.047	0.785
7868	12.507	9.683	6.398	4.035	2.570	1.750	1.353
10561	17.036	13.249	8.815	5.567	3.522	2.404	1.830
14992	24.448	19.052	12.743	8.068	5.104	3.445	2.645

1 in. = 25.4 mm

1 lb. = 0.454 kg

1 mil = 0.0254 mm

Average deflections, in Mils,
for All Load Levels for August 1997
Falling Weight Deflectometer (FWD) Test

Load, lb.	Sensor Spacing, in.						
	0	8	12	18	24	36	60
Section 1							
6212	15.770	12.158	10.067	8.320	5.483	3.902	2.586
9109	23.693	18.438	15.300	12.668	8.363	5.875	3.824
12062	31.552	24.627	20.509	17.008	11.241	7.878	5.117
15136	39.366	30.748	25.634	21.235	13.997	9.783	6.342
Section 2							
6017	24.224	20.145	17.494	15.221	11.052	8.530	5.913
8798	37.645	31.754	27.717	24.305	17.800	13.911	9.763
11518	48.975	41.340	36.098	31.633	22.968	17.763	12.254
14516	61.130	51.530	45.098	39.589	28.685	22.079	15.258
Section 3							
6030	31.700	26.852	23.932	21.414	16.647	14.059	10.742
8753	43.096	36.515	32.143	28.603	21.523	17.372	12.675
11508	60.094	51.311	45.437	40.776	30.965	25.465	18.718
14440	72.761	61.923	54.779	49.015	36.716	29.612	21.339
Section 4							
5902	29.822	24.540	21.268	18.488	13.413	10.520	7.384
8602	45.912	38.355	33.461	29.367	21.485	16.780	11.876
11270	59.517	49.654	43.173	37.835	27.282	21.043	14.545
14215	74.225	62.220	54.249	47.686	34.291	26.362	18.171
Section 5							
5857	44.308	38.569	35.125	31.867	24.927	20.682	15.539
8528	57.019	49.274	43.670	39.040	29.130	23.135	15.857
11196	79.617	69.763	62.752	56.978	43.363	35.150	25.248
14260	96.408	85.965	76.920	69.988	52.475	42.207	29.517
Control							
6158	9.282	6.738	5.366	4.281	2.655	1.862	1.237
8964	13.700	10.012	8.050	6.415	4.026	2.756	1.825
11816	18.192	13.345	10.786	8.615	5.435	3.744	2.469
15326	23.575	17.338	14.094	11.265	7.129	4.919	3.278

1 in. = 25.4 mm

1 lb. = 0.454 kg

1 mil = 0.0254 mm